# Experimental characterization and modeling of airflow and heat transfer in a closed refrigerated display cabinet

Nattawut Chaomuang

NNT: 2019IAVF0017

# THÈSE DE DOCTORAT

préparée à l'Institut des sciences et industries du vivant et de l'environnement (AgroParisTech)

pour obtenir le grade de

## Docteur de l'Institut agronomique, vétérinaire et forestier de France

**Spécialité : Génie des procédés**

École doctorale n°581
Agriculture, alimentation, biologie, environnement et santé (ABIES)

*par*

**Nattawut CHAOMUANG**

# Caractérisation expérimentale et modélisation des écoulements d'air et transferts thermiques dans un meuble frigorifique fermé

Directrice de thèse : **Onrawee LAGUERRE**
Codirecteur de la thèse : **Denis FLICK**

**Thèse présentée et soutenue à Paris, le 16 septembre 2019**

**Composition du jury:**

| | |
|---|---|
| **M. Jocelyn BONJOUR**, Professeur, INSA de Lyon, France | Président |
| **M. Giovanni CORTELLA**, Professeur, University of Udine, Italie | Rapporteur |
| **M. Pedro Dinis GASPAR**, Professeur associé, University of Beira Interior, Portugal | Rapporteur |
| **Mme Onrawee LAGUERRE**, Directrice de recherche, Irstea, France | Directrice de thèse |
| **M. Denis FLICK**, Professeur, AgroParisTech, France | Codirecteur de thèse |
| **M. Alexandre MISKIZAK**, Responsable R&D, EPTA, France | Membre invitée |

**UR FRISE - IRSTEA**
1 rue Pierre-Gilles de Gennes
CS 10030 92761 Antony cedex

NNT: 2019IAVF0017

# DOCTORAL THESIS

submitted to Paris Institute of Technology for Life, Food and Environmental Sciences

(AgroParisTech)

in fulfilment of the requirements for the degree of Doctor of Philosophy in

## Institute of Agricultural, Veterinary and Forestry of France

**Specialty: Process Engineering**

Doctoral school No. 581:
Agriculture, Food, Biology, Environment and Health (ABIES)

*By*

## Nattawut CHAOMUANG

# Experimental characterization and modeling of airflow and heat transfer in a closed refrigerated display cabinet

Thesis director: **Onrawee LAGUERRE**

Thesis co-director: **Denis FLICK**

**Thesis presented in Paris, September 16, 2019**

**Thesis committee**

| | |
|---|---|
| **Mr. Jocelyn BONJOUR**, Professor, INSA de Lyon, France | Chairman |
| **Mr. Giovanni CORTELLA**, Professor, University of Udine, Italy | Reviewer |
| **Mr. Pedro Dinis GASPAR**, Assistant professor, University of Beira Interior, Portugal | Reviewer |
| **Mrs. Onrawee LAGUERRE**, Senior researcher, Irstea, France | Thesis director |
| **Mr. Denis FLICK**, Professor, AgroParisTech, France | Thesis codirector |
| **Mr. Alexandre MISKIZAK**, R&D Manager, EPTA, France | Invited member |

**UR FRISE - IRSTEA**

1 rue Pierre-Gilles de Gennes

CS 10030 92761 Antony cedex

# Acknowledgement

Firstly, I gratefully acknowledge the financial support provided by the King Mongkut's Institute of Technology Ladkrabang (KMITL, Thailand), the National Research Institute of Science and Technology for Environment and Agriculture (Irstea, France) and the Embassy of France in Thailand through the Franco-Thai scholarship program. The completion of my PhD would not have been possible without this support.

I would like to express my deep and sincere gratitude to both of my thesis directors, Dr. Onrawee Laguerre and Prof. Dr. Denis Flick, for their advice and guidance throughout this research. They have been supportive both academically and morally. Their profound scientific knowledge, expertise and excellent practical abilities have inspired me to do my utmost to finish this project. It has truly been a privilege to be supervised by them. In the future, I wish to continue our collaborations and create mutual research projects together. Likewise, I would like to express my heartfelt gratitude to Asst. Prof. Dr. Maradee Phongpipatpong. Without her, I would not have had the opportunity to pursue my PhD in the first place.

I would like to express my great appreciation to my thesis defense committee, Prof. Dr. Jocelyn Bonjour, Prof. Dr. Giovanni Cortella, Asst. Prof. Dr. Pedro Dinis Gaspar and Mr. Alexandre Miskizak, for sacrificing their valuable time to review and assess the thesis. I would also like to thank all members of my thesis committee as a whole for keeping my research progress on schedule. I genuinely appreciate their honest and insightful feedback on the research.

I also recognized the support and friendships of my colleagues. It has been a great pleasure to be a part of the team at Refrigeration Process Engineering Research Unit of Irstea. Special thank is given to Dr. Steven Duret for always sharing many useful ideas concerning simulation works. I also acknowledge the help offered by the technicians for their help in handling of the experiments. Administrative assistance provided by the unit's secretary was also greatly appreciated.

I am also indebted to Dr. Judith Vatteville for her advice concerning Particle Image Velocimetry system. Likewise, I am immensely grateful for the staffs of EPTA (France) for both their valuable insights on retail refrigeration industry and for allowing me to visit their factory.

I would like to express my deepest gratitude to my parents for their constant supports. I also would like to thank my girlfriend for her love, patience and understanding. Regards are also given to my relatives and friends for their encouragement and friendships. This thesis is dedicated to them all.

Above all, praise be to the God and Father of the Lord Jesus Christ… (1 Peter 3) for making these past three years in France an incredible and memorable experience.

**Nattawut Chaomuang** Paris, September 16th, 2019

# Contents

# List of Figures

# List of Tables

# Chapter I

# General introduction

## 1.1. Background

World population is predicted to increase from 7.3 billion in 2015 to 9.7 billion in 2050 (United Nations, 2017). This population growth would drive up food demand by approximately 59% to 98% (Valin et al., 2014). Global food production therefore needs to increase to keep up with a rising demand (Hunter, 2017).

A cold chain is an essential part of production chains where several refrigeration facilities are used to keep food products, from production to consumption, at their good quality and low risk to consumer (Badia-Melis et al., 2018). Temperature is a main determining factor of the food quality deterioration (Mercier et al., 2018). A failure in temperature control at any cold chain stage can markedly compromise the quality and safety of food products (Ndraha et al., 2018). High temperature accelerates the physiological changes of food, the growth of spoilage/pathogenic microorganisms, and eventually shortens the product shelf life (Nunes et al., 2009; Rediers et al., 2009). Therefore, effective temperature control along the cold chain is of paramount importance.

Governments and/or public authorities in various countries have established legislation and regulations regarding temperature control in the cold chain (Carson and East, 2018; Mercier et al., 2018). In practice, product temperature is well controlled at the early stages e.g. production, storage, distribution and transport (Baldera Zubeldia et al., 2016). However, with the exception of household practices, the temperature control at retail display appears to be problematic (Evans, 2010; Derens-Bertheau et al., 2015; Derens et al., 2006). In addition, food waste at supermarkets can be as high as 55% due to poor temperature conditions (Nunes et al., 2009).

Open refrigerated display cabinets are widely used by retailers and account for almost half of the refrigerating equipment use in a typical supermarket (ASHRAE, 2010). The open display cabinets prove to be popular among retailers as they provide customers with almost unrestricted access to products (Evans, 2014), whilst maintaining good product attractiveness (Alzuwaid et al., 2015). Nevertheless, their major limitations concern the thermal performance.

In open display cabinets, an air curtain creates a non-physical barrier between the cold air inside and the warm air outside. However, the air curtain cannot completely prevent the warm and humid ambient air infiltration (Foster et al., 2005), which leads to the increase of temperature and energy consumption (Amin et al., 2008; Evans, 2014; Laguerre et al, 2012b). Several studies indicated that the ambient air infiltration has contributed approximately to 66-77% of total heat load of the open refrigerated display cabinets (Faramarzi, 1999; Gaspar et al., 2011; Tassou et al., 2011). It also causes internal temperature heterogeneity (Laguerre et al, 2012b). Temperature differences of more than 5 °C was observed on cabinet shelves (Willocx et al., 1994), with the higher temperature commonly located at the front of the cabinets, and the lower temperature at the back (Evans et al., 2007).

Due to an increasing concern for energy efficiency and food safety, the issues of ambient air infiltration in open display cabinets have been subjects of attention. Numerous experimental investigations and numerical simulations have been carried out with the attempt to maximize the air curtain efficiency, thereby improving the overall performance of open display cabinets (Chen, 2009; Chen and Yuan, 2005; Cortella et al., 2001; D'Agaro et al., 2006; Foster et al., 2005; Gaspar et al., 2012; Hadawey et al., 2012; Jouhara et al., 2017; Laguerre et al., 2012; Marinetti et al., 2012; Moureh and Yataghene, 2016; Navaz et al., 2005; Wu et al., 2015; Yu et al., 2008). Hammond et al. (2016) proposed a novel short air curtain design, instead of a conventional single long air curtain, to improve temperature homogeneity and energy efficiency. In this study, despite multiple short air curtains were created to provide enclosure at the front of every shelf, they cannot eliminate the air infiltration.

Installation of doors on open-front display cabinets has become an alternative design to address the air infiltration issue. It has been proven that the closed display cabinets show several favorable outcomes including potential energy savings (Faramarzi, 1999; Fricke and Becker, 2010; Kauffeld, 2015; Navigant Consulting Inc., 2009), reductions in internal temperature heterogeneity (Evans and Swain, 2010; Lindberg et al., 2010), and improved food quality (Atilio de Frias et al., 2015). Additionally, doors can also provide better thermal comfort in retail stores due to less cold air spillage from the display cabinet (Lindberg et al., 2017). In view of these benefits, some major retailers in Europe have made closed display cabinets

a default specification for their new and renovated stores (EIA, 2017). This trend is especially notable in France where the authorities and the supermarket stakeholders have signed an agreement to replace open display cabinets with closed ones. The country aims to increase the installation of closed display cabinets to 75% by 2020 (RPF, 2016).

Energy savings of closed display cabinets demonstrated in various studies **(Figure 1.1)** could be explained by a reduction in the entrainment of warm and moist ambient air into the cabinets. However, a wide variation of energy saving percentages among studies, ranging from 23-73% could be attributable to the difference of cabinet configurations and test conditions used in each study. This difference can be, for example, door integrity (retrofitted/factory-built), door type (hinged/sliding), door material (single/double/triple glazing windows with/without low emissivity coating), use of anti-sweat heaters, LED lightings, night covers, frequency and duration of door openings (Evans, 2014). The last one (frequency of door openings) is pointed out as one of the main factors contributing to an increased energy consumption due to the air entrainment (Li et al., 2007). The energy consumption of closed display cabinet during stable night condition was approximately 10% lower than that operating under periodical door openings (Vallée, 2015). Lindberg et al. (2010) showed that the heat extraction rate of the evaporator increased by 16% when the opening frequency increased from 10 to 30 openings per hour. Door openings appeared to be the largest contributor to the total heat load of closed display cabinet when the frequency reached 60 openings per hour (Orlandi et al., 2013).

Unlike energy consumption, the temperature performance of closed refrigerated display cabinets is less studied, only the internal temperature and its heterogeneity were reported. Lindberg et al. (2010) observed that an overall air temperature reduction of at least 2 °C was achieved in the cabinet retrofitted with doors. Atilio de Frias et al. (2015) reported that the temperature difference within the closed cabinet was 6 °C lower than that within the open one.

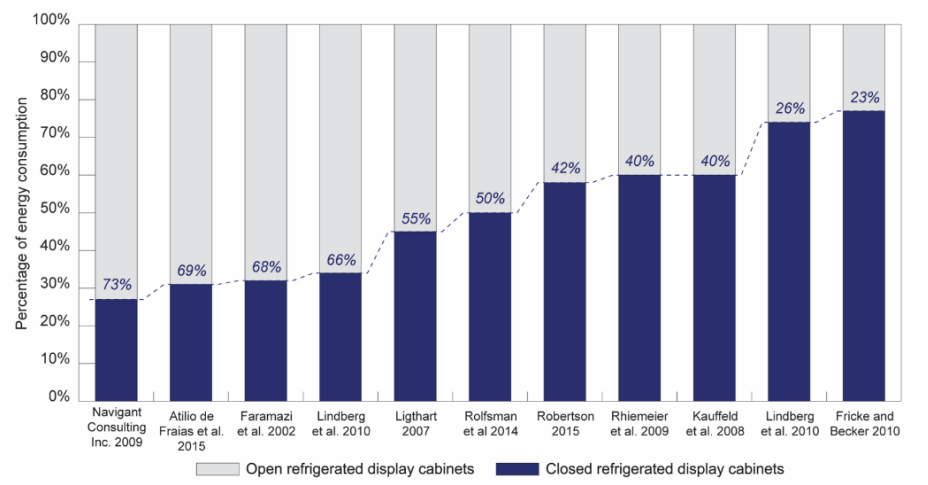


**Figure 1.1** Comparison of energy consumption between open and closed refrigerated display cabinets (source: Laguerre and Chaomuang, 2019).

## 1.2. Research interests

The growing trend of closed refrigerated display cabinet use has contributed to the necessity to expand research in this field. However, to the author's knowledge, current literature only addresses the benefits of closed display cabinets over open ones. Studies on the mechanism of heat transfer and airflow within closed display cabinets are still limited. In fact, the airflow pattern influences the heat exchange between air and product, thus, product temperature. Faramarzi et al (2002) found that installing doors caused a reversal variation in product temperatures – product temperature at the front upper shelf became warmer than that at the bottom shelf. To accommodate door openings, doors fitted to display cabinets often have gaps at the edges; however, these gaps allow ambient air infiltration (Evans, 2014). The advanced techniques of air velocity measurements, such as Particle Image Velocimetry (PIV), Laser Doppler Velocimetry (LDV), together with Computational Fluid Dynamics (CFD) simulations would provide an insight into the transport phenomena in closed refrigerated display cabinets.

Complex phenomena take place when door is open during which the disrupted air curtain causes the entrainment of warm and humid ambient air. A further investigation into the effects of frequency and duration of door openings on food temperature increase and energy consumption is therefore important.

A simplified heat transfer model based on a zonal approach should also be developed to obtain complementary knowledge of the mechanisms of heat transfer in a closed display cabinet. This model would be linked with the other well-established models for processing plant (Lecoq et al., 2016), refrigerated vehicle (Hoang et al., 2012), cold room (Laguerre et al., 2015), open refrigerated display cabinets (Laguerre et al., 2012a) and household refrigerator (Laguerre & Flick, 2004). These models allow the prediction of product temperature in each equipment in short calculation time compared to CFD simulation. The closed display cabinets will soon be an additional component of the series of refrigeration equipment in the food cold chain. In conjunction with other equipment models, the closed display cabinet model would enable the prediction of time-temperature history of food products of the entire cold chain. Accordingly, the evaluation tool of consumer risk exposition can be constituted by integrating the proposed models with predictive microbial and/or quality models (Duret et al., 2015).

## 1.3. Aim and scope

Following the previous reasoning, the present thesis was conducted with the two main objectives.

Firstly, it aims to develop an experimental methodology to identify the thermal transport phenomena in a closed refrigerated display cabinet. Evolutions of spatial and temporal air/product temperatures and air velocity are the main parameters taken into investigations. The influence of different operating conditions on these parameters was then studied. These conditions include ambient air temperature, product-occupied volume, door-opening frequency and duration. Internal airflow pattern was characterized by both a hot-wire anemometer and PIV technique. The results obtained from these experiments were further used for the estimation of model input parameters and for the model validation purposes.

Secondly, it aims to develop numerical tools by both CFD simulation and simplified heat transfer model base on a zonal approach.

The CFD simulation allows the better understanding of airflow and heat transfer phenomena in the closed display cabinet, which cannot be observed by the experiments. However, the main objective is not to represent precisely all the flow

and transfers details. Instead, the aim is to examine the capability of a 2D-CFD k-ε model to reproduce the main phenomena and to predict the product temperatures in the cabinet with acceptable accuracy. Although it is not in the scope of the thesis, after its validation with the experimental data, the model could be used to study the influence of unexplored operating conditions and design parameters.

The simplified model in both static and dynamic regimes permits, respectively, the predictions of both time-averaged air and product temperatures and the temperature fluctuations according to the on/off working cycles of the compressor regulation. The model in the dynamic regime was solved with a spectral approach, thus the influence of different parameters on the damping of the temperature fluctuations can be identified with quick calculation.

## 1.4. Structure of the thesis

The structure of manuscript presented in **Figure 1.2** includes 8 chapters, which are described briefly below:

**Chapter I General introduction** describes the background, research interests, aim/scope and structure of the thesis as well as list of publications.

**Chapter II Literature review** provides the state of the art of the investigations involving experimental (carried out in fields and in laboratories) and numerical research studies on open and closed retail refrigerated display cabinets. The current usage situation of display cabinets and the problem of temperature control at retail display based on field investigations were presented. Studies aiming to improve the performance of the display cabinets were explored and the influencing factors were then analyzed in terms of temperature distribution and energy consumption. The growing trend of closed refrigerated display cabinet use in Europe was also highlighted. More detail is presented in Article 1 (published).

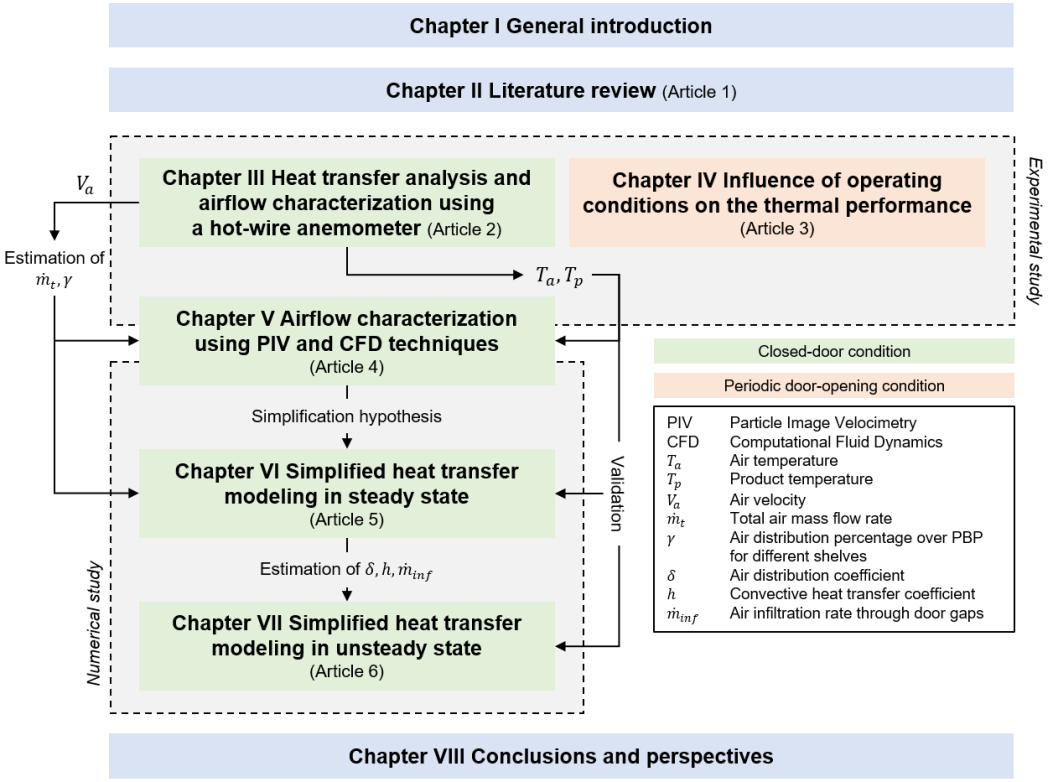


**Figure 1.2** Structure of the thesis

**Chapter III Heat transfer analysis and airflow characterization using a hot-wire anemometer.** In spite of the potential of energy savings of closed display cabinets, the literature review *(Chapter II)* shows the lack of knowledge on heat transfer and airflow compared to the open ones. This chapter presents the experimental investigations of heat transfer and airflow in a closed refrigerated display cabinet (an integral type equipped with a single band air curtain and two double-glazing doors) under closed-door condition in a controlled-temperature test room. First, the overall thermal transmission coefficient of the studied closed display cabinet was determined by measuring heat loss through all cabinet doors/walls. The heat loss contribution of different components (walls, doors, door gaps and thermal bridges) was then estimated. Second, the air temperature was measured in the unloaded closed display cabinet using calibrated T-type thermocouples (40 thermocouples). The result made it possible to gain an insight into the temperature fluctuation and the mean temperature at different positions in the cabinet, thus, the warm and cold positions were identified. Effect of room temperature (15, 19 and 24 °C) on the internal air temperature distribution was also examined. The result revealed that the room temperature had an almost linear

influence on the internal air temperature, and it had a significant effect on the compressor working cycles. Third, the influence of loading was studied by putting test packages made of methylcellulose on the shelves (60% occupied volume). Additional thermocouples (40 thermocouples) were inserted/attached to the core/surface of the test packages. It was observed that the trend of temperature distribution in the unloaded and loaded cabinet was the same (the highest temperature position at the front-top shelf and the lowest temperature position at the rear-bottom shelf). Finally, the benefit of door installation was studied by doing experiment using the unloaded cabinet with doors completely removed. Without doors, the mean air temperatures in the storage compartment were higher at all positions (minimum increase 0.4 °C and maximum increase 3.1 °C) compared to the case without doors. In addition to the temperature measurements, the air velocity was measured at the front of the closed-door and unloaded display cabinet for different heights from the discharge to return air grilles using a hot-wire anemometer. The shape of the air velocity in the curtain was presented (the air curtain was deviated towards the doors due to a Coanda effect with maximum air velocity of about 0.6 $m \cdot s^{-1}$ near the discharge grille). In the storage compartment, the air velocity was low, varying from 0.01 to 0.2 $m \cdot s^{-1}$. The air velocity measurement in the rear duct was also carried out and the airflow distribution over the perforated back panel of different shelves was then quantified. More detail is presented in Article 2 (published). Because the precision of the velocity measurement using the hot-wire anemometer was limited, particularly for low velocity application (< 0.5 $m \cdot s^{-1}$), Particle Image Velocimetry (PIV) technique was used and presented in *Chapter V*.

**Chapter IV Influence of operating conditions on the thermal performance**. The thermal performance of the closed refrigerated display cabinet was presented under permanently closed-door condition in *Chapter III (heat transfer analysis and airflow characterization using a hot-wire anemometer)*. This chapter continues to present the temperature performance under periodic door openings. An automatic door opening system developed and used in experiments enabled the investigation of effects of different door Opening frequencies Per Hour (OPH) on the air and product temperature variations. The studied frequencies were 0 (permanently closed), 10, 20, 40, 60 OPH, and ∞ (permanently open – doors completely removed)

and the studied opening duration was 15 s and 30 s. The frequency of 10 OPH with 15 s duration and 90° opening angle was programed with respect to the one prescribed in the standard test (EN ISO 23953-2, 2015), and this opening procedure was set to a baseline. Based on data available in the literature (Fricke and Becker, 2010) and information provided by a display cabinet manufacturer, the opening frequency in supermarkets is averagely 6.3 OPH (12 s duration) and 12.1 OPH (13 s duration), respectively. Effects of ambient air temperature (14.6, 19.4, 24.3 and 29.2 °C) and product-occupied volume (half-loaded and full-loaded) on the air and product temperature distribution were experimentally investigated. It was observed that the product located at the front of mid-height of display cabinet was more influenced by the door opening frequency. However, the air and product temperatures in the cabinet with doors (whatever the frequency of door openings) remained lower, compared to the case without doors. More detail is presented in Article 3 (published).

**Chapter V Airflow characterization using PIV and CFD techniques.** Due to the precision limitation of the hot-wire anemometer for low velocity applications, the PIV technique was used to characterize the airflow pattern in the closed display cabinet. A Computational Fluid Dynamics (CFD) simulation was also developed in parallel due to the difficulties to implement the PIV technique experimentally at some areas in the cabinet. This chapter presents the air velocity measurement using a 2D-PIV system in a display cabinet with two configurations: closed and open doors (doors were open with 90° angle). In the closed configuration, experiments were conducted under two conditions: refrigeration system turned "off" or "on" so that its influence on the airflow pattern is highlighted. A zone of air recirculation was identified where ambient air infiltration was also observed through the door gaps, leading to an increase in the air curtain temperature). Because of the technical constraints, only the experiment with the refrigeration system turned "off" was carried out in the open configuration. The air curtain characteristics (mean velocity and velocity fluctuations) of the closed and open configurations were then compared and the implications on the internal temperature distribution was addressed. A cabinet with doors yields better thermal performance because the air curtain is more stable compared to the case without. Without doors, large unsteady eddies developed in the mixing layers, thereby promoting greater external air

infiltration. Finally, a 2D-CFD model was developed to investigate the airflow and its influence on the temperature distribution in the closed display cabinet. The model showed the ability to reproduce the main flow phenomena observed in the experiment and allowed the prediction of product temperatures with acceptable accuracy. The experimental data of *Chapter III (Heat transfer analysis and airflow characterization using a hot-wire anemometer)* were used for the model input and validation. More detail is presented in Article 4 (under review, first submission).

**Chapter VI Simplified heat transfer modeling in steady state.** Because of the calculation time-consuming using the CFD simulation, this chapter presents the development of a simplified heat transfer model in steady state based on the zonal approach. The model allows the prediction of time-averaged air and load temperatures at various positions in the closed display cabinet. Details of overall model conceptualization, static model development, determination of model input parameters as well as model validation by comparing with experimental data were described. In addition, the model was further used to estimate the frost formation on the evaporator surface due to the air infiltration through the door gaps. Suggestions were also provided to generalize the model for other closed display cabinets and to take into account the air infiltration due to door openings in simple or more realistic manners. Like *Chapter V (Airflow characterization using PIV and CFD techniques)*, some experimental data of *Chapter III (Heat transfer analysis and airflow characterization using a hot-wire anemometer)* were used for the model input and the model validation which showed a good agreement. More detail is presented in Article 5 (under review, second submission). Moreover, all input parameters determined in this chapter were further used in *Chapter VII*.

**Chapter VII Simplified heat transfer modeling in unsteady state.** This chapter presents the development of the simplified heat transfer model in transient state, which allows the prediction of the air and load temperature fluctuations according to the on/off working cycles of the compressor operation and the defrosting operation during which the compressor is "off". This dynamic model was solved with a spectral method by using Fourier transform and transfer functions. With this solving method, the model showed the influence of different parameters on the damping of the temperature fluctuations with quick calculation time. The estimation of the equivalent load thickness at which the temperature fluctuation was the same

order as at the surface was also proposed. Some experimental data of *Chapter III (Heat transfer analysis and airflow characterization using a hot-wire anemometer)* were used for the model input and the model validation which showed a good agreement. More detail is presented in Article 6 (under review, second submission).

Finally, the conclusions and perspectives are provided in **Chapter VIII Conclusions and perspectives**.

A list of literature cited throughout the thesis is summarized in **Reference**.

## 1.5. List of publications

*In peer-reviewed journals*

- **Chaomuang, N.**, Flick, D., & Laguerre, O. (2017). Experimental and numerical investigation of the performance of retail refrigerated display cabinets. Trends in food science & technology, 70, 95-104. (Article 1)
- **Chaomuang, N**., Flick, D., Denis, A., & Laguerre, O. (2019). Experimental analysis of heat transfer and airflow in a closed refrigerated display cabinet. Journal of Food Engineering, 244, 101-114. (Article 2)
- **Chaomuang, N.**, Flick, D., Denis, A., & Laguerre, O. (2019). Influence of operating conditions on the temperature performance of a closed refrigerated display cabinet. International Journal of Refrigeration, 103, 32-41. (Article 3)
- **Chaomuang, N**., Flick, D., Denis, A., & Laguerre, O. (n.d.). Characterization of airflow in a closed refrigerated display cabinet using PIV and CFD techniques. Journal of Food Engineering (submitted). (Article 4)
- **Chaomuang, N.**, Laguerre, O., & Flick, D. (n.d.). Simplified heat transfer modelling of a closed refrigerated display cabinet: Part I - Static model development and validation. Applied Thermal Engineering (submitted). (Article 5)
- **Chaomuang, N.**, Laguerre, O., & Flick, D. (n.d.). Simplified heat transfer modelling of a closed refrigerated display cabinet: Part II - Dynamic model development and application. Applied Thermal Engineering (submitted). (Article 6)

*In book chapter*

※ Laguerre, O., & **Chaomuang, N.** (2019). Close refrigerated display cabinet: Is it worth it for food quality? In P. D. Gaspar & P. D. Silva (Eds.), Handbook of Research on Technologies and Systems for Food Preservation. IGI Global (In-press). (Article 7)

*Technical paper under preparation*

※ Denis, A., **Chaomuang, N.**, Flick, D., & Laguerre, O. (n.d.). Caractérisation expérimentale des champs de vitesse d'air dans un meuble frigorifique fermé par la Vélocimétrie Imagerie des Particules. Revue Générale du Froid. (Article 8)

*In conference paper*

※ **Chaomuang, N.**, Laguerre, O., & Flick, D. (2019, August 24-30). A simplified heat transfer model of a closed refrigerated display cabinet. Paper presented at the 25th IIR International congress of refrigeration (ICR2019), Montreal, Canada. (Article 9)

# Chapter II

# Literature review

# Experimental and numerical investigation of the performance of retail refrigerated display cabinets

**Nattawut Chaomuang**, Denis Flick and Onrawee Laguerre

Published in *Trends in Food Science & Technology* (2017), 70 (Supplement C), pages 95-104

---

**Abstract**

Refrigerated display cabinets are widely used to preserve chilled and frozen food products in retail food stores. Storage temperatures must be efficiently controlled to ensure that the product temperature is maintained below the recommended value. Numerous surveys have demonstrated that refrigerated display cabinets, seem to be a weak link in the food cold chain, and household practices also constitute weak links. A great deal of effort has been devoted to the investigation and improvement of the performance of cabinets in terms of both temperature homogeneity and energy efficiency.

In this review article, an investigation of refrigerated display cabinet performance, from basic experimental field and laboratory studies to advanced numerical simulation, is presented. Field investigation enables knowledge of real-use conditions to be acquired and identifies problems encountered during food storage. However, such investigation is usually costly and time-consuming. The Computational Fluid Dynamics (CFD) approach is becoming a promising alternative used to study the influence of various design parameters and operating conditions on the cabinet performance.

Ambient air infiltration across air curtains is the most significant factor indicating the performance of open display cabinets. This issue is still problematic in many research and development contexts. The application of closed doors becomes an alternative solution which has been proven that it can provide several advantages. As little research involving this type of refrigeration equipment is available, thus further investigation is required in order to obtain additional data.

***Keywords:*** Refrigerated display cabinets, retail food stores, storage temperatures, energy consumption, Computational Fluid Dynamics (CFD)

## 2.1. Introduction

About a half of food products in retail food stores are presented in refrigerated display cabinets (Bertrand, 1993). Typically, for chilled products, vertical multi-deck display cabinets are often preferred because the limited space available in the stores can be utilized effectively. Food quality and consumer safety strongly depend on temperature control. Even though a great deal of legislation and regulations are extensively imposed, several surveys show that food products presented in retail cabinets encounter temperature abuse: this problem has been demonstrated in the UK (Evans et al., 2007), and in France (Derens et al., 2006). Around 360 million tons of food are lost annually worldwide because of the insufficient use of refrigeration (IIR, 2009).

Open-front refrigerated display cabinets are the most commonly used equipment, since they allow customers to access the products without any barriers. Despite good design of the air curtain, warm and humid air infiltration inevitably leads to temperature heterogeneity within the cabinets. This heterogeneity can cause food quality deterioration and high electrical energy consumption. In order to address these issues, numerous wide-ranging studies have been carried out with a view to improve the performance of display cabinets, particularly in terms of air curtain design, using both experimentation and numerical simulation. Nevertheless, infiltration can be limited using display cabinets with doors. Due to a possible reduction in product sales, customer interviews were carried out in supermarkets in England, and these interviews showed that half of the customers surveyed would prefer to purchase products from cabinets without doors (Grocery Trader, 2013). On the contrary, Fricke and Becker (2010) indicated that the utilization of closed display cabinets had no effects on product sales in the USA. As it is difficult to reach a clear conclusion regarding the influence of the presence of doors in terms of sales volume, and given the large amount of energy that can be saved, the use of closed refrigerated display cabinets is becoming more and more widespread, and closed cabinets will account for 75% of all display cabinets in retail stores by the end of 2020 in France (RPF, 2016).

This review article is divided into two main sections based on the type of refrigerated display cabinets: open or closed. Each section aims to present the state of the art of the investigations involving both field and laboratory studies on the air temperature evolution in the display cabinets and the food products inside the cabinets. These investigations were carried out by experimental and numerical approaches in order to study the heat and mass transfer, the airflow and the energy consumption of the cabinets. The objective of this review is to provide information on the current usage situation and to examine attempts to improve the performance of the display cabinets in terms of both temperature distribution and efficient energy consumption. Future trends in the field of refrigerated display cabinets are also highlighted.

## 2.2. Open display cabinets

Since energy saving has become a major concern worldwide during the past two decades, the performance of retail refrigeration systems must be optimized. Several experimental and numerical investigations have been carried out to determine the factors which have the greatest effects on system performance. These factors can be design parameters, operating conditions or ambient conditions. The knowledge acquired makes it possible to control the food temperature, to reduce temperature fluctuations and to achieve energy savings in refrigerated display cabinets.

### *2.2.1. Field investigation*

A retail display cabinet constitutes the last stage in the food cold chain prior to purchase of food products by consumers. Effective temperature control is needed, as the quality of the products on the shelves can be adversely affected by inappropriate control and inadequate temperature levels (Mariquele, 2012). Field surveys have been carried out in various countries in order to investigate and identify the ongoing situation of cabinet operation. Most surveys produced the same results: chilled food products available in retail stores are subjected to temperature abuse as shown in **Table 2.1**.

A field study was carried out in France. The temperatures of three types of food products (dairy, prepared and packed meat products, with a total of 307 samples) throughout the entire food cold chain were monitored (Derens et al., 2006). The results showed that around 30% of the products were stored at temperatures that

were at least 2 °C higher than the recommended values. Almost a decade later, a similar study within the framework of the European FRISBEE project was performed using a ham product (Derens-Bertheau et al., 2015). It was demonstrated that food preservation in display cabinets tends to take place under better temperature conditions than in the past due to a decrease in the mean product temperature and a lower percentage of products in which the temperature is higher than the specified temperature. However, the authors noted that the results should be interpreted carefully, given that only a small number of samples (83 samples) was considered in this study.

The position in which food products are placed inside the cabinet is also important. Temperature differences of more than 5 °C were observed on the cabinet shelves by Willocx et al. (1994). When examining the effect of operating duration, they found that the temperature at one position increased by 4 °C towards the end of the day and by almost 7 °C towards the end of the week due to an increase in the store temperature. They also noticed that the top shelf had the highest temperature and that the opposite was true for the bottom shelf. This is quite different from Gill et al. (2003) who monitored the temperatures of beef products stored in open display cabinets in ten Canadian retail stores. The packages on the top and bottom shelves were similar and warmer than the packages on the middle shelves, while the packages at the front were warmer than the packages at the back. The results also showed that the maximum temperature of the selected product packages (5389 samples) from all stores was above 4 °C. Further investigation of this issue was performed in detail in a laboratory by Evans et al. (2007). **Table 2.1** summarizes the field studies conducted in several countries.

**Table 2.1** Field investigations on chilled food products at retail displays in various countries

| Country | Sample | Temperature (°C) | | | % of samples at specified temperature | Reference |
|---|---|---|---|---|---|---|
| | | Min. | Mean | Max. | | |
| Canada | Beef | -2.0 | 2.6 | 10.6 | 18% > 4 °C | Gill et al. (2003) |
| | Fresh-cut lettuce | | 4.1 | | | McKellar et al. (2014) |
| Denmark | Chilled product | | | 14.0 | 50% > 5 °C | Bøgh-Sorensen (1980) |
| France | Yogurt | -2.1 | 4.2 | 9.8 | 18% > 6 °C | Derens et al. (2006) |
| | Processed meat | -1.1 | 3.3 | 10.2 | 36% > 4 °C | |
| | Ham | 0.2 | 2.8 | 7.0 | 12% > 4 °C | Derens-Bertheau et al. (2015) |
| | Bakery, pock and dairy | | | 16.0 | 70% > 7 °C | Morelli et al. (2012) |
| Finland | Fish | 0.3 | 3.5 | 8.6 | 53% > 5 °C | Lundén et al. (2014) |
| | Minced meat | 0.1 | 3.1 | 6.9 | 10% > 7 °C | |
| Germany | Chilled product | | | 11.0 | 87.9% > 4 °C; 39.4% > 7 °C | Murmann and Kuhlung (1987) |
| Greece | Pasteurized milk | 0 | 4.9 | 11.7 | 35% > 6 °C | Koutsoumanis et al. (2010) |
| | Smoked sliced turkey | | 4.0 | | | Gogou et al. (2015) |
| Ireland | Cooked sliced ham | 1.5 | 5.7 | 12.7 | 14% > 5 °C | FSAI (2003) |
| Slovenia | Meat | 0 | 3.8 | 10.5 | | Likar and Jevšnik (2006) |
| | Dairy | 0 | 5.6 | 16.0 | | |
| Spain | Meat | -1.8 | 4.3 | 9.9 | 43% > 4 °C | Baldera Zubeldia et al. (2016) |
| | Fish | 2.9 | 6.2 | 10.0 | 75% > 4 °C | |
| | Dairy | 1.2 | 6.4 | 15.3 | 57% > 8 °C | |
| Sweden | Chilled product | -1.0 | 4.9 | 16.0 | 36% > 5 °C | Bøgh-Sørensen and Olsson (1990) |
| UK | Cooked meat | | | | 28% > 5 °C | Sagoo et al. (2007) |
| | Chilled products | | | | 55% > 5 °C | Evans (2010) |
| USA | Leafy green salad | | | | 40% > 7.2 °C | Brown et al. (2016) |
| | Meat, fish and dairy | -10.0 | 5.4 | 21.1 | 47% > 5 °C; 22% > 7 °C | Audits International (1999) |
| | Meat | | | 20.0 | 38% > 4 °C | Rogers and Althen (1980) |

### *2.2.2. Experimental study conducted in a laboratory*

Evans et al. (2007) and Evans and Swain (2010) performed extensive studies on the performance of different types of refrigerated display cabinets in terms of both temperature performance and energy consumption. These cabinets included well freezers, chest freezers, frozen and chilled door cabinets (solid or glass door) and open-front (chilled) display cabinets. The performance was analyzed under EN 441 test standard conditions (or more recent EN ISO 23953). For all cabinet types, the maximum temperatures of the test packages were generally in the areas the most exposed to ambient, whereas the minimum temperatures were located in the least exposed packages. For 135 open-front display cabinets, these authors observed that most of the packages at the maximum temperature (97% of observed display cabinets) were at the front, and 60% of them were at the cabinet front base or on the bottom shelf. Meanwhile, most of the packages at the minimum temperature (98%) were located at the back of the cabinets. These findings match those obtained in a study conducted by Bøgh-Sørensen and Olsson (1990).

To gain an insight into the evolution of air and product temperatures in an open refrigerated display cabinet under unsteady conditions, Laguerre et al. (2012b) performed an experimental study. The air and product temperature fields in the cabinet and the temperature and velocity profiles of its air curtain were mapped using the Particle Image Velocimetry (PIV) technique. The results showed that the on/off compressor cycle promoted variations in the temperature of the air stream. The air temperature varied readily, but the product temperature varied only slightly because of the thermal inertia of the products. The air temperature increased about 2.8 °C when the air flowed upwards along the back of the cabinet because of heat conduction through the wall. A temperature of 3.9 °C was observed at the supply air duct and the air temperature rose to 11.8 °C when the air reached the return air duct. As observed by Evans et al. (2007), the product position in the cabinet is a determining factor of its temperature. For this reason, the products located at the front of the cabinet had higher temperatures than those at the back of the cabinet. The product with the highest temperature was located at the front base of the cabinet and had a mean surface temperature of 9.5 °C, whereas at the back of this level, the lowest product temperature (0.9 °C) was observed. Based on the velocity profile mapped by PIV, the temperature fluctuations in the air curtain were affected by the

introduction of ambient air via transient vortices which accelerate the infiltration rate. To determine the influence of operating conditions on the cabinet performance, a simplified heat transfer model was developed in a later study (Laguerre et al., 2012a), and these experimental results were used for the model validation.

### *2.2.3. The effect of ambient conditions*

Howell et al. (1999a) monitored the relative humidity in eight supermarkets in the Tampa, Florida, area throughout the year (November 1997 to October 1998). This study aimed to evaluate the existing levels of relative humidity in a retail store. Overall, an annual average store relative humidity of 45% was observed: the lowest average relative humidity of 37% occurred in March and the highest average value of 57% was recorded in September. Howell et al. (1999b) demonstrated the influence of store relative humidity on display cabinet performance. These authors indicated that the performance based on energy requirements in the three components (cabinet refrigeration, defrost system and anti-sweat heaters) was strongly affected by the ambient relative humidity. Based on the results, the total energy demand of display cabinets was reduced by 10% when the store relative humidity was reduced by 5%, and consequently a 5% reduction in the total energy consumption of the entire store could be achieved. This can be explained by less frost formation on evaporator coils and less anti-sweat heat operation, and thus a lower latent heat load requirement. This observation is in agreement with that reported by Tassou et al. (2001).

Axell and Lindberg (2005) conducted field measurement of temperature variations in refrigerated display cabinets in three supermarkets in Sweden. They found that the outdoor climatic conditions influenced the indoor conditions of the supermarkets, given that the total electrical power consumed by chilled display cabinets increased 55% during summer. This variation was mainly caused by variations in the ambient humidity. In the supermarkets, the mean air temperature in the cabinets during daytime operation was 4.1 °C in summer and 1.9 °C in winter. The mean air temperature difference between the top and the bottom of the cabinets was 3.3 °C in winter and 6.7 °C in summer. A difference of more than 2 °C could be observed between daytime and night operation when a night cover was applied. Regarding this observation, the authors pointed out that night covers should be placed on display cabinets during closing hours because 50% energy savings can

be achieved. Moreover, the authors concluded that the vicinity of open display cabinets has provided poor thermal comfort to supermarket customers due to cold air spillage from the cabinets (a so-called cold leg effect). The recent study confirmed this finding by comparing the ambient temperature measurement with supermarket customers/staffs responses to the questionnaires (Lindberg et al., 2017).

An experimental study was carried out in a laboratory by Chen and Yuan (2005). These authors found that room temperature and humidity caused an increase in the air temperature and heat gain in the cabinet refrigeration system. The temperature increase in the cabinet is mainly due to the increase in the room temperature, but this increase is also to some extent due to the humidity. However, higher humidity exerts effects on the latent heat gain, which in turn leads to higher energy demand. The effect of Reynolds (*Re*) numbers (based on the supplied air velocity and the width of the air curtain) on the air temperature distribution and total heat gain was also shown. When the *Re* increased from 4100 to 5000, the temperature inside the cabinet decreased 1.0-1.5 °C approximately. When the *Re* increased from 5000 to 5700, the temperature changed only slightly. The authors proposed the thermal entrainment factor to characterize the air curtain performance; this factor is correlated to the Reynolds and Richardson (*Ri*) numbers. This study also showed the benefits of the application of night covers, which enable more homogeneous inside air temperatures to be achieved. It should be borne in mind that the Reynolds number characterizes flow regimes for forced convection (laminar or turbulent flow) and the Richardson number characterizes the importance of natural convection relative to forced convection.

In accordance with the results obtained by Gaspar et al. (2011), the ambient climate exerts a great impact on the total heat transfer rate and infiltration rate. The latent heat transfer rate component increased 42% when the humidity rose from 35% to 60%. The heat transfer rate due to air infiltration was the individual component with the greatest increase (from 67% to 77%). As humidity has an immediate impact on the latent heat transfer rate, the authors emphasized that the influence of humidity should be taken into account when calculating the thermal entrainment factor.

Heidinger et al. (2013) studied the influence of ambient conditions on the performance of the evaporators of refrigerated display cabinets. The climate classes

3 (25 °C, 60%RH) and 6 (27 °C, 70%RH) according to ISO 23953:2005 were compared in this study. A total heat load increase of 25% was observed when the climate changed from Class 3 to Class 6. This also caused thicker frost formation on the evaporator and led to less efficient heat exchange with air due to a reduction in the air velocity. Thus, the electrical energy demand of the display cabinets became higher.

By gaining an insight into the effect of ambient conditions, the design of display cabinets can be optimized, thus promoting energy savings and food safety.

### *2.2.4. The effect of design parameters and operating conditions*

The infiltration between the refrigerated compartment of an open display cabinet and the ambient surroundings across its air curtain represents almost 67-77% of the total refrigeration load (Faramarzi 1999; Gaspar et al., 2011; Tassou et al., 2011). Many researchers have endeavored to improve air curtain design in order to enhance the cabinet performance.

Gray et al. (2008) experimentally studied the effect of the proportion of holes in the perforated back plate on the performance of refrigerated display cabinets. The arrangement and the number of holes exerted a marked influence on the discharge airflow rate. These authors reported that a ratio of 70% airflow rate at the supply air duct and 30% at the perforated plate allows good cabinet performance. This condition allowed a higher Reynolds number (from 3740 to 4100) and a lower Richardson number (from 0.13 to 0.11) compared with the original design. In this manner, the air temperature at the supply air duct decreased from -0.5 to -0.85 °C. This *Re* number range, however, is lower than that reported by Chen and Yuan (2005) due to the different designs.

The influence of the width of return air duct of an open display cabinet performance was studied by Hammond (2011). He studied the influence of the return air duct width in the range of 35 to 145 mm on the infiltration coefficient $I$ defined as $I = (T_{ra} - T_{sa})/(T_{amb} - T_{sa})$ where $T_{ra}$, $T_{sa}$ and $T_{amb}$ are the return air, supply air and ambient temperatures, respectively. It was found that the optimal return air duct width was 70 mm (for a 300-mm high curtain with a jet velocity of 0.9 $m \cdot s^{-1}$). The author concluded that the effect of the width is relatively small on the cabinet performance; however, excessive width can cause poorer performance.

The temperature stability in the air curtains of open display cabinets is difficult to control because many parameters play simultaneous roles. Hammond et al. (2016) proposed a new air curtain design to replace the conventional one, the so-called short air curtain. With this innovation, the front of the cabinet is enclosed by multiple short air curtains provided for each shelf rather than a single long air curtain. The experimental results showed that the cabinet with the short air curtain generated higher energy savings and greater temperature distribution uniformity. The cooling load was reduced from 4.24 kW to 3.04 kW (reduction of 28.3%), and this represented a 35.9% reduction in electrical energy consumption. The range of maximum and minimum product temperatures was also narrower (a difference of 9.5 °C for the conventional design and 3.1 °C for the short air curtain). These results can assist display cabinet manufacturers or engineers when designing and manufacturing high-performance display cabinets.

Yu et al. (2009b) proposed an alternative design to maximize air curtain performance by supplying cold air from a central unit located outside the display cabinet. This system was then compared with a conventional display cabinet with an integrated cold production system. Based on the experimental results obtained by these authors, many benefits were obtained in the case of cold air supplied from the central unit, i.e. a better-controlled air curtain, longer intervals between defrost cycles (extended from once every 6 h to once every 9 h) due to less frost formation and lower maximum product temperature during defrosting periods. Moreover, these authors found that the optimal velocity of the air curtain for this cabinet type is 0.7-0.8 $m \cdot s^{-1}$, corresponding to a *Re* number of 4350-5000.

Kou et al. (2015) studied the influences of thermostat settings (at -0.5 °C and -2.2 °C with the same defrosting interval of 12 h and duration of 30 min) on the product temperature and quality of packaged baby spinach products at various locations. With the -2.2 °C thermostat temperature, the products located on the top shelf at the front of the display cabinet had the highest temperature (a mean temperature of 6.5 °C) and the temperature decreased subsequently towards the back of the cabinet. The lowest mean temperature was below zero (-0.6 °C), and the product located in this zone was thus subjected to freezing damage. To overcome this thermal problem, the warmer temperature of the thermostat was set at -0.5 °C. However, the products in the front rows then undergo temperature abuse. This represents the

situation in supermarkets and the controlling of such temperature abuse to ensure that all products are preserved at suitable temperatures without freezing problems is becoming a major challenge. These results were confirmed by Laguerre et al. (2012b): a warmer product temperature at the front and a cooler product temperature at the rear of the same shelf.

The temperatures of products preserved in display cabinets can rise several degrees during defrost operation and will take an hour to reach the correct temperature once again. Under such fluctuating temperature conditions, temperature-sensitive food products can deteriorate at rates that are different from those of products stored under normal conditions (Wells and Singh, 1989). The application of a heat pipe and phase-change materials (PCM) installed in the cabinet shelves was introduced to deal with this issue by Lu et al. (2010). Two cabinet prototypes, a shelf retrofitted with a heat pipe and combined heat pipe and PCM, were experimentally tested in their study. Based on their results, the authors claimed that the use of a heat pipe and PCM provides several benefits: a reduction in the core product temperatures (3.0 to 5.5 °C lower with a heat pipe alone), improved temperature distribution homogeneity (a small range of max.-min. temperatures during normal operation) and a reduction in the temperature rise occurring during the defrost process (0.3 °C rise with the combined structure) with no change in energy consumption. These findings are in corresponding with Wu et al. (2017) who reported that the temperature fluctuation of food packages is reduced by 53.3 - 83.3% during defrosting of a vertical open display cabinet equipped with such a composite shelf (heat pipe and PCM) and the average temperature of food packages is reduced by 13.7 - 32%.

### *2.2.5. Development of numerical models*

A field investigation and laboratory experimentation are necessary in order to determine the operating conditions and problems occurring within a refrigerated display cabinet. However, such investigation is both costly and time-consuming. For this reason, a numerical approach is complementary. Modelling of refrigeration systems can be applied to practical use in real situations. The model allows the operator to observe and predict the thermal phenomena under various conditions, and the knowledge acquired will allow the operator/engineer to find solutions designed to improve the performance. Thanks to recent advances in computer

technology, modelling has become more reliable, and increasingly detailed and complex models can be developed. Computational Fluid Dynamics (CFD) is a tool that enables simulation of fluid flow problems by solving differential equation systems (mass, momentum, and energy equations). It is being successfully implemented for many applications worldwide, including refrigeration applications, as highlighted by Smale et al. (2006). This review aims to further expand more recent developments in the area of refrigerated display cabinets. **Table 2.2** summarizes the numerical studies conducted on open display cabinets using the CFD approach.

In earlier numerical studies related to the refrigerated display cabinet application, CFD codes based on the finite element method (Cortella, 2002; Cortella et al., 2001) and finite difference method (Ge and Tassou, 2001) were developed individually in the authors' laboratories. Since computer technology is now more advanced and more reliable commercial CFD codes have been developed, many researchers tend to adopt them in their studies. The most common codes include FLUENT and CFX in which discretization is based on the finite volume method. CFD is proving to be a very useful tool at the design stage of refrigerated display cabinets as it enables knowledge of airflow and thermal phenomena to be acquired.

Among the typical thermal load contributions in an open display cabinet, the contribution of infiltration is responsible for the greatest thermal load (Tassou et al., 2011). Reducing infiltration into the food preservation zone of the display cabinet is becoming the main priority in most studies. With validated CFD models, the efficiency of cabinet air curtains is quantified on the basis of the heat transfer rate across the air curtains (Chen 2009; Gaspar et al., 2012; Ge and Tassou, 2001; Madireddi and Agarwal, 2005), or in terms of thermal entrainment (D'Agaro et al 2006; Moureh and Yataghene, 2016; Navaz et al, 2005). Considering this defined factor as a benchmark, researchers can then numerically modify cabinet design parameters and vary operating conditions so that optimal conditions can be obtained.

The findings of various studies provide a common principle even though different types of display cabinets were examined in the studies. The insulating ability of the air curtain can be maintained by selecting appropriate jet characteristics. To ensure that less ambient warm air is introduced, the jet must not generate a high turbulence

intensity but must be able to reach the return air duct with minimum spillage to the external surroundings so that the open front is totally sealed, and customer comfort is ensured. The air curtain can be scientifically described by two dimensionless variables: the Reynolds number (*Re*) and the Richardson number (*Ri*). Reducing the *Re* of the curtain can achieve this characteristic. However, there is no specific optimum value as each particular cabinet establishes its own value. The *Re* in the range of 3200-3400 were recommended by Navaz et al. (2005), while Field and Loth (2006) reported that for conventional display cabinets, the *Re* range of 4200-8000 was typically found.

To represent the most accurate prediction of the real situation, a CFD model has to take into account many aspects. Some significant parameters to be taken into account for model development were underlined by several researchers. These parameters include ambient radiative heat transfer (Laguerre et al., 2012a; Madireddi and Agarwal, 2005) and geometric dimensions (2D or 3D) (D'Agaro et al., 2006). Moreover, some authors have introduced new modelling techniques to predict the performance of display cabinets: the integration of refrigeration devices in calculation domains (Gaspar et al., 2012; Ge et al., 2010), calculation based on normal or modified two-fluid (TF or MTF) models in which the flow regime is assumed to consist of two fluids (turbulent and non-turbulent fluids) (Cao et al., 2010; Yu et al., 2007, 2008). Most of developed CFD models for display cabinet considered the flow regime at the exit of heat exchangers as an input model boundary. However, airflow maldistribution in the heat exchangers and cooling air ducts can cause an aggravated evolution of velocity profile at the discharge air grille of display cabinets. To obtain an insight of the transport phenomena in this region, numerical studies have been performed by Marinetti et al. (2014). After validation with the experimental results (Marinetti et al. 2012), the obtained results notified that there was a maldistribution of mass flow rate in the duct – higher velocity at the exit of cooling coils was observed on the right part. The study of Rossetti et al. (2015) showed that this air velocity has a great relationship with its temperature. Due to the residual time inside the evaporator, higher air outlet temperatures were in the higher velocity areas whereas lower air outlet temperatures were in lower velocity area. With all obtained knowledges, a better model development can be promoted.

Several correlation models have been developed in order to assess the performance of refrigerated display cabinets in a rapid manner. Based on the results obtained using CFD models, simplified correlation models for the total heat transfer across the air curtain and the return air temperature were established and introduced by Ge and Tassou (2001). Using an approach similar to that of Yu et al. (2009a), these authors developed correlation formulae describing the thermal entrainment factor (TEF) for typical open display cabinets with single and double air curtains. By using these TEF formulae, the return air temperature can be also calculated. By comparing these data with published experimental data, the authors indicated that the developed model is sufficiently accurate for engineering applications.

Unlike the previous studies which built models based on simulation results, Laguerre et al. (2012a) developed another simplified model based on a zonal or compartmental approach. The objective of their model is to enable rapid prediction of air and product temperatures in open display cabinets. The results obtained in their previous study (Laguerre et al., 2012b) were employed for the model validation. A comparison showed that the calculated values of both temperatures were slightly below the predicted values due to the simplification hypotheses. Finally, the authors mentioned that the product time-temperature evolution throughout the entire food cold chain can be monitored by integrating this developed model with similar models that have already been developed for domestic refrigerators and refrigerated vehicles (Laguerre et al., 2014).

**Table 2.2** Numerical studies on heat transfer and airflow in open display cabinets

| CFD codes | Turbulence models | Display cabinet schemes | Studied parameters | Main observations | References |
|---|---|---|---|---|---|
| SOFIE<br>(2D and 3D[(1)]) | Standard k-ε | VORDC<br>Single curtain<br>5 shelves<br>Loaded | ➢ Load arrangement<br>➢ Hole characteristics of a perforated plate | ➢ Velocity profile | Axell et al. (1999) |
| In-house<br>(2D) | LES | VORDC<br>Double curtain<br>6 shelves<br>Loaded | ➢ Air velocities of both inner and outer jets | ➢ Temperature profile<br>➢ Velocity profile<br>➢ Flow pattern<br>➢ Air curtain efficiency | Cortella et al. (2001) |
| In-house<br>(2D) | n/a | VORDC<br>Single curtain<br>5 shelves<br>Empty | ➢ Ambient enthalpy<br>➢ Temperature difference between the jet and the air in a cabinet<br>➢ Jet initial temperature<br>➢ Jet initial velocity<br>➢ Jet thickness<br>➢ Air curtain height | ➢ Total heat transfer<br>➢ Return air temperature | Ge and Tassou (2001) |
| In-house<br>(2D) | LES | VORDC<br>Double curtain<br>6 shelves<br>Loaded<br>HORDC<br>Loaded | ➢ Cabinet configurations: vertical and horizontal dimensions | ➢ Temperature profile<br>➢ Velocity profile<br>➢ Flow pattern<br>➢ Load temperature (separate code) | Cortella (2002) |

**Table 2.2** Numerical studies on heat transfer and airflow in open display cabinets

| CFD codes | Turbulence models | Display cabinet schemes | Studied parameters | Main observations | References |
|---|---|---|---|---|---|
| In-house, ROYA (2D) | Cebeci-Smith (algebraic model) Low-Re k-ε | VORDC Single curtain | ➢ Discharge air velocity<br>➢ Discharge air temperature | ➢ Infiltration rate<br>➢ Velocity profile | Navaz et al. (2002) |
| CFX (3D) | Standard k-ε | VORDC Single curtain 5 shelves Loaded | ➢ A number of design parameters:<br>➢ Size and position of the cooling coils (evaporator)<br>➢ The presence of a baffle plate within a back panel | ➢ Temperature profile<br>➢ Flow pattern<br>➢ Product temperature | Foster et al. (2005) |
| FLUENT (3D) | Standard k-ε | VORDC Single curtain 5 shelves Loaded | ➢ Radiation (based on discrete-ordinates radiation model)<br>➢ Inlet mass flow rate | ➢ Product temperature<br>➢ Sensible heat load | Madireddi and Agarwal (2005) |
| FLUENT (2D) | n/a | VORDC Single curtain 4 shelves Empty | ➢ Reynolds numbers (based on supply duct width)<br>➢ Turbulence intensity<br>➢ Presence of a perforated back plate | ➢ Infiltration rate<br>➢ Temperature profile<br>➢ Velocity profile | Navaz et al. (2005) |
| CFX (2D and 3D) | Standard k-ε RNG k-ε | VORDC Triple curtain 5 (inclined) shelves | ➢ 3D effect (cabinet length)<br>➢ Warm air curtain temperature (the 3rd curtain exposed to ambient) | ➢ Temperature profile<br>➢ Flow pattern<br>➢ Induction factor<br>➢ Return air temperature | D'Agaro et al. (2006) |

**Table 2.2** Numerical studies on heat transfer and airflow in open display cabinets

| CFD codes | Turbulence models | Display cabinet schemes | Studied parameters | Main observations | References |
|---|---|---|---|---|---|
| | | Loaded | ➢ Longitudinal ambient air velocity | ➢ Refrigerating capacity | |
| In-house, FORTRAN (2D) | Standard k-ε, (TF and MTF) | VORDC<br>Double curtain<br>No shelf<br>Empty | ➢ Comparison of turbulence and two-fluid models<br>➢ Internal and external air curtain velocities | ➢ Temperature profile | Yu et al. (2007, 2008) |
| FLUENT (2D) | Standard k-ε | VORDC<br>Single curtain<br>6 shelves<br>Empty | ➢ Length-width ratio<br>➢ Discharge angle of air curtains<br>➢ Height-depth of the cabinet<br>➢ Dimensions and positions of internal shelves | ➢ Stability of air curtain (based on temperature distribution and sensible cooling load) | Chen (2009) |
| In-house, FORTRAN (2D) | Standard k-ε (TF) | VORDC<br>Single curtain<br>6 shelves<br>Double curtain<br>5 shelves<br>Empty | ➢ Velocity and temperature of supply air (inner and outer in case of dual curtains)<br>➢ Air curtain width and height<br>➢ Central distance between supply and return air ducts<br>➢ Ambient temperature and humidity<br>➢ Perforated back panel airflow ratio and its temperature | ➢ Thermal entrainment factor<br>➢ Return air temperature | Yu et al. (2009a) |

**Table 2.2** Numerical studies on heat transfer and airflow in open display cabinets

| CFD codes | Turbulence models | Display cabinet schemes | Studied parameters | Main observations | References |
|---|---|---|---|---|---|
| FLUENT<br>TRNSYS<br>(2D) | Standard k-ε | VORDC<br>Single curtain<br>5 shelves<br>Loaded | ➢ Ambient temperature<br>➢ Ambient air humidity<br>➢ Cabinet air flow rate | ➢ Temperature profile<br>➢ Flow pattern<br>➢ Refrigerant mass flow rate<br>➢ Cooling capacity<br>➢ Product temperature | Ge et al. (2010) |
| FLUENT<br>(2D) | RNG k-ε | VORDC<br>Single curtain<br>5 shelves<br>Loaded | ➢ Integration of air flow in the duct into simulation domain | ➢ Temperature profile<br>➢ Velocity profile<br>➢ Relative humidity field<br>➢ Mass flow and heat transfer rate across air curtain | Gaspar et al. (2012) |
| In-house<br>(2D) | n/a | VORDC<br>Single curtain<br>5 shelves<br>Loaded | ➢ Ambient temperature<br>➢ Radiation<br>➢ Internal infiltration rate<br>➢ External infiltration rate | ➢ Air temperature<br>➢ Product temperature | Laguerre et al. (2012) |
| n/a<br>(2D) | Standard k-ε | VORDC<br>Single curtain<br>6 shelves<br>Loaded | ➢ Lighting<br>➢ Air velocity at evaporator outlet<br>➢ Ambient temperature and relative humidity | ➢ Product temperature | Zhijuan et al. (2013) |
| CFX<br>(3D) | Standard k-ε | Mock-up model of cooling air bottom duct | ➢ One study condition | ➢ Velocity profile on different three heights | Marinetti et al. (2014) |

**Table 2.2** Numerical studies on heat transfer and airflow in open display cabinets

| CFD codes | Turbulence models | Display cabinet schemes | Studied parameters | Main observations | References |
|---|---|---|---|---|---|
| FLUENT (2D) | n/a | VORDC<br>Single curtain<br>6 shelves<br>Loaded | ➢ Percentage of porosity on a perforated back plate<br>➢ Location of perforations on a plate | ➢ Temperature profile<br>➢ Flow pattern<br>➢ Air curtain velocity | Wu et al. (2014) |
| CFX (3D) | Two-equation eddy-viscosity | Mock-up model of cooling air bottom duct | ➢ The presence of cooling coils in the bottom duct | ➢ Velocity profile in laminar and turbulent flow regimes in the duct<br>➢ Velocity profile on a single fin of cooling coils | Rossetti et al. (2015a) |
| CFX (3D) | Two-equation eddy-viscosity | Mock-up model of cooling air bottom duct | ➢ One study condition | ➢ Velocity profiles in the duct and on a single fin of cooling coils<br>➢ Temperature profiles in the duct and on a single fin of cooling coils | Rossetti, et al. (2015b) |
| FLUENT (2D) | Standard k-ε | VORDC<br>Single curtain<br>6 shelves<br>Loaded | ➢ The application of a phase-change material (PCM) | ➢ Temperature profile<br>➢ Defrost cycle<br>➢ On/off compressor cycle<br>➢ Compressor working time<br>➢ Product temperature | Alzuwaid et al. (2016) |
| In-house (2D) | n/a | VORDC<br>Single curtain<br>5 shelves | ➢ The application of PCM | ➢ Air temperature<br>➢ Product temperature | Hoang et al. (2016) |

**Table 2.2** Numerical studies on heat transfer and airflow in open display cabinets

| CFD codes | Turbulence models | Display cabinet schemes | Studied parameters | Main observations | References |
|---|---|---|---|---|---|
| | | Loaded | | | |
| FLUENT (3D) | Standard k-ε RSM | Mock-up model Single curtain | ➢ External lateral flow velocity | ➢ Air curtain flow pattern<br>➢ Jet deflection<br>➢ Jet characteristics<br>➢ Thermal entrainment | Moureh and Yataghene (2016) |

(1) 3D modelled for one shelf only.

n/a – not available; LES – Large Eddy Simulation; RNG – Reynolds Normalization Group; RSM – Reynolds Stress Model; TF – normal two-fluid model; MTF -modified two-fluid model (turbulent fluid calculated based on Standard k-ε); VORDC – vertical open refrigerated display cabinet; HORDC – horizontal open refrigerated display cabinet

As previously mentioned in **Section 2.2.4**, defrosting has a negative impact on the food shelf life of food products in display cabinets as well as energy consumption. One notably solution using phase-change materials (PCM) has been proposed by many researchers. It was experimentally and numerically proven that the positive responses using PCM can be achieved including higher energy efficiency and more stabilization of air and product temperatures during defrosting (Alzuwaid et al., 2016; Hoang et al., 2016). Another technology to improve the performance is to apply a desiccant to refrigeration system to remove moisture in return air before entering to an evaporator (Zhang et al., 2017). Through theoretical analysis, the proposed system of a frost-free (open) refrigerated display cabinet can provide high coefficient of performance (COP) of 3.2. The authors noticed that the humidity and the temperature of return air have a significant effect on the COP. They reported that COP increased by 35% when humidity decreased from 80% to 50% and by 115% when return air temperature decreased from 14 to 8 °C.

## 2.3. Closed display cabinets

Ambient air infiltration is a major drawback in open-front display cabinets. In spite of efforts to provide better design, two problems are often observed in practice: temperature control and energy efficiency. In addition, more tighten regulations are imposed i.e. the Food Code by the U.S. Food and Drug Administration (FDA). It requires all refrigerated food products need to be stored at the temperature at 5 °C or below (FDA, 2013). These technical issues bring more challenges to both manufactures and retailer to develop new design of display cabinet. An alternative is the installation of doors. It has been proven that energy savings of up to 70% can be achieved with this solution (Fricke and Becker, 2010; Rhiemeier et al., 2009; Rolfsman and Borgqvist, 2014) as well as the better temperature homogeneity (Atilio de Frias et al. 2015; Lindberg et al. 2010). Given these findings, the thermal performance of closed refrigerated display cabinets is attracting more and more attention.

Moreover, the use of doors by retrofitting an open fronted display cabinet can also provide environmental and economic benefits as highlighted in the review of Evans (2014). The thermal comfort of supermarket customers has been improved since around 2 K of mean temperature of air in front of the cabinet retrofitted with doors

was increased (Lindberg et al., 2008). The prediction of annual financial saving of supermarkets by fitting doors to cabinets varies due to the store sizes (about 50,000-300,000 € for 2,500 to 18,000 $m^2$) and a payback period for door retrofitting was about 16 months. Nevertheless, the author (Evans, 2014) noted that there were some limitations of the reported data, i.e. limitation of cabinet numbers, neglect of some significant factors (net demand of cooling capacity in stores, maintenance, labors, etc.) in cost estimation.

### *2.3.1. Field and laboratory investigations*

Many comparisons of the performance of refrigerated display cabinets with and without doors have been performed by a number of researchers. The potential energy savings are usually taken into consideration in most studies, as shown in **Table 2.3**. Such savings are mainly achieved through a reduction in the entrainment of ambient warm and moist air into the preservation space, which leads to less frost formation on cooling coils and less compressor energy demand (Faramarzi et al., 2002). However, findings published by Evans and Swain (2010) demonstrated that the energy consumption based on the mean total energy consumption per unit display area was slightly different between the two cabinet types: 10.01±0.40 (open) and 10.81±1.41 (closed) $kWh \cdot m^{-2}$ per day. This evidence suggests that closure with doors on the cabinets may not always consume less energy. Moreover, the frequency and duration of door openings are the other important factors which can cause higher demand of energy consumption (Li et al., 2007). As indicated by Vallee (2015), the refrigeration energy consumption was approximately 15% higher when the display cabinet was operated under periodically opening condition.

Only a few studies on the performance in terms of temperature variation and homogeneity have been conducted. For instance, a decrease in the overall air temperature of at least 2 °C in display cabinets retrofitted with doors was reported by Lindberg et al. (2010). Evans and Swain (2010) conducted a comprehensive study which demonstrated that the temperature distribution within closed display cabinets also varied according to product positions. As in open-type cabinets, 94% of the products with the highest temperature were located at the front of the chilled display cabinet, and nearly half of them (49%) were located on the bottom shelf. Conversely, most often, the products with the lowest temperatures were located at the rear of the cabinet and about 70% were on the top shelf. In addition, the

comparative results obtained with open and closed display cabinets revealed that the temperature variation within closed cabinets is lower than that within open cabinets.

Similarly, Atilio de Frias et al. (2015) also affirmed that the temperature heterogeneity in the closed cabinet was less compared to the open one due to the decrease of spatial temperature differences almost by 6 °C (**Table 2.3**). As the quality of chilled/frozen food products is sensitive to storage temperature, the improvement on temperature homogeneity in display cabinets is expected to provide better food quality during preservation. In the demonstration by this research team, it proved that higher visual quality and lower decay rate of minimally processed vegetables can be achieved by the installation of doors on display cabinets.

**Table 2.3** Comparison of the performance of open and closed display cabinets

| Country | Study nature | Potential savings | Temperature distribution | | Reference |
|---|---|---|---|---|---|
| | | | Open | Closed | |
| Germany | Review of literature | 40% | | | Rhiemeier et al. (2009) |
| UK | Laboratory | | $T_a$ = 2.7±2.1 °C<br>ΔT = 8.6±4.5 °C | $T_a$ = 3.7±1.2 °C<br>ΔT = 5.1±1.6 °C | Evans and Swain (2010) |
| USA | Laboratory | 68% | | | Faramarzi et al. (2002) |
| | Review of literature | 73% | | | Navigant Consulting Inc. (2009) |
| | In the field | 23% | | | Fricke and Becker (2010) |
| | Laboratory | 69% | $T_p$ = 4.6-8.1 °C | $T_p$ = 2.0-4.8 °C | Atilio de Frias et al. (2015) |
| Sweden | In the field | 26% | $T_a$ = 6.7-7.2 °C (D)<br>$T_a$ = 4.5-6.7 C (N) | $T_a$ = 3.6-4.7 °C (D)<br>$T_a$ = 1.5-3.4 °C (N) | Lindberg, et al. (2010) |
| | Laboratory | 66% | $T_a$=3.3-3.5 °C<br>ΔT=7.8-8.3 °C | $T_a$=6.0-6.6 °C<br>ΔT=2.7-3.1 °C | |
| | In the field | 50% | | | Rolfsman and Borgqvist (2014) |
| New Zealand | In the field | 42% | $\Delta T^* \approx$ 0.6-3.0 °C | $\Delta T^* \approx$ 0.4-0.7 °C | Robertson (2015) |

$T_a$ – mean air temperature; $T_p$ - mean product temperature; ΔT – max.-min. temperature difference of products; $\Delta T^*$ – return and discharge air temperature difference; D – daytime operation; N – night operation

The advantages of the implementation of refrigerated display cabinets closed with doors compared with conventional open-type cabinets in terms of energy consumption, temperature variation as well as the food quality still constitute an issue which is generating discussion. Thus, further investigation is required in order to obtain additional data.

### *2.3.2. Development of numerical models*

In order to understand the mechanism of transport phenomena occurring in a closed display cabinet, particularly when its doors are open, both experimental and numerical investigations are required. A review of the literature shows that little research involving extensive studies has been conducted, as shown in **Table 2.4**.

To the authors' knowledge, the only detailed numerical study applied to this type of cabinet is that performed by Orlandi et al. (2013). The incoming energy was numerically quantified during the door opening procedure (opening, holding and closing). In their study, two three-door cabinets were considered: one was equipped with sliding doors and the other one was equipped with hinged doors, and only the central door openings were analyzed. The comparative results showed that the internal temperatures were relatively similar for both door types during the holding step. However, during the opening and closing steps for the cabinet with sliding doors, the air temperature at the return air duct was markedly lower than in the case of the cabinet with hinged doors. For this reason, the display cabinet closed with sliding doors consumed 17% less energy than the other cabinet.

Moreover, the research team also highlighted the impact of the door opening frequency on energy consumption. According to ISO 23953 (10 openings, each with a duration of 15 seconds, per hour per door), the energy contribution due to door openings was responsible for 12% of the total heat extraction rate on evaporator coils, while the contribution of lights was greater (25%). Nevertheless, when a higher frequency was applied (60 openings per hour for each door), the contribution of openings became significant. It accounted for 44% of the total heat extraction rate. This very high frequency may not happen in real life situations. Fricke and Becker (2010) found that the most frequent door opening duration was only 5 seconds and the daily mean door opening frequency was only 6.3 openings per hour, which means that one door is opened every 9.5 minutes. These data would

indicate that the standard door opening cycle is more demanding than the most common situation in practice. Another numerical model of a closed display cabinet was used by D'Agaro et al. (2006). In this study, a model of the misting and demisting process in the glass doors of a closed frozen product display cabinet was developed. The main objective of this study was only to gain an insight into the physical mechanism of the thermo-fluid phenomena of fogging and defogging taking place during the door opening, as this is a very important issue for this type of cabinet. The high fogging level leads to poor transparency of the glass, thus influencing the visibility of the products from the customer's point of view. Defogging with a heater is then required, and this process leads to higher energy demand and cooling load. However, no case study was shown to demonstrate the influence of these phenomena on the cabinet performance in terms of both energy efficiency and temperature distribution.

## 2.4. Conclusions

Many studies on retail refrigerated display cabinets have been carried out over the past two decades, and awareness of food product quality and energy efficiency is rising continuously. Many researchers have made an effort to investigate and identify the key factors which influence the cabinet performance by means of both experimental (field-based and laboratory-based) and numerical (in-house code and commercial code) approaches. The knowledge acquired will provide an opportunity to optimize this equipment in terms of both temperature homogeneity and energy consumption. The thermal entrainment factor of air curtains seems to be the main performance indicator in the case of open display cabinets as it directly represents the amount of entrained ambient air. This issue still poses problems in many research and development contexts. The application of closed doors is becoming an alternative solution and several studies have demonstrated that closed doors can provide several advantages. Since there is no conclusion on the loss of sales of products due to the use of doors, many researchers are conducting investigations on the influence of doors. Nevertheless, most of these studies focused on the energy consumption perspective alone. The impact of temperature variations on food quality, particularly the effect of ambient operating conditions and door openings, requires further elucidation.

**Table 2.4** Numerical studies conducted on closed display cabinets

| CFD code | Turbulence model | Display cabinet scheme | Studied parameters | Main observations | Reference |
|---|---|---|---|---|---|
| Commercial code (3D)<br>Open-source code (3D) | Realizable k-ε | CRDC<br>3 doors<br>6 shelves<br>Loaded | ➢ Types of doors (hinged and sliding doors)<br>➢ Operation time (day and night)<br>➢ The frequency of door openings | ➢ Temperature profile<br>➢ Velocity profile<br>➢ Flow pattern<br>➢ Return air temperature<br>➢ Incoming thermal loads through a door<br>➢ Heat extraction rate | Orlandi et al. (2013) |
| CFX<br>In-house<br>(2D and 3D) | n/a | CRDC<br>5 shelves<br>Empty | ➢ Fogging (condensation) and defogging (with electric heaters) processes due to opening doors | ➢ Temperature profile on a glass surface<br>➢ Water layer height | D'Agaro et al. (2006) |

CRDC – a closed refrigerated display cabinet

# Chapter III

# Heat transfer analysis and airflow characterization using a hot-wire anemometer

# Experimental analysis of heat transfer and airflow in a closed refrigerated display cabinet

**Nattawut Chaomuang**, Alain Denis, Denis Flick and Onrawee Laguerre

Published in *Journal of Food Engineering* (2019), 244, pages 101-114.

**Abstract**

This study presents the experimental investigations on heat transfer and airflow in a closed refrigerated display cabinet. Air and product temperatures and air velocity were measured with thermocouples and a hot-wire anemometer, respectively. Temperature variation in the cabinet depends on the positions. The front areas contributed to higher temperature, whereas the rear areas were at a lower temperature. Benefits of doors were also examined by comparing the results of air and product temperatures with the case without doors. The cabinet with doors provided less temperature heterogeneity ($\Delta T_{\max}$= 2.1 °C) compared to the case without door ($\Delta T_{\max}$= 4.9 °C). The maximum air velocity in the air curtain of 0.6 $m \cdot s^{-1}$ was observed at the discharge grille. The horizontal air velocity from the perforated plate was low (< 0.2 $m \cdot s^{-1}$) for all shelves. The loading percentage in the cabinet did not significantly affect the airflow rate through the perforated plate.

***Keywords:*** Closed refrigerated display cabinet; Heat transfer; Temperature; Airflow; Velocity; Experimental study

**Nomenclature**

| | |
|---|---|
| A | area [$m^{-2}$] |
| $D_h$ | hydraulic diameter $= \frac{4A}{P}$ [m] |
| Q | power supply [W] |
| P | perimeter [m] |
| Re | Reynolds number [-] |
| T | temperature [°C or K] |
| $\bar{T}$ | mean temperature [°C or K] |
| $T^*$ | dimensionless temperature [-] |
| ΔT | mean temperature difference between front and back positions [°C or K] |
| U | overall heat transfer coefficient [$W \cdot m^{-2} \cdot K^{-1}$] |
| UA | overall thermal transmittance [$W \cdot K^{-1}$] |
| $v$ | velocity [$m \cdot s^{-1}$] |
| | |
| *Greek letters* | |
| $\rho$ | density [$kg \cdot m^{-3}$] |
| $\mu$ | dynamic viscosity [$kg \cdot m^{-1} \cdot s^{-1}$] |
| | |
| *Subscripts* | |
| a | air |
| amb | ambient |
| cf | cabinet fan |
| ext | external |
| h | heater |
| hf | heater fan |
| $i$ | index for a given position |
| int | internal |
| th | thermostat |
| | |
| *Abbreviations* | |
| DAG | Discharge Air Grille |
| PBP | Perforated Back Panel |
| RAG | Return Air Grille |
| PPA | Percentage of Perforated Area |

## 3.1. Introduction

A refrigerated display cabinet is typically employed to display food products in retail stores. It is the last storage stage in the cold chain prior to purchasing by consumers. Product temperature control plays a vital role in maintaining food quality. Various studies have demonstrated that food products at this stage are

subjected to temperature abuse despite extensively imposed legislation and regulations. A field investigation conducted in France showed that around 30% of monitored products were stored at temperatures above their recommended values (Derens et al., 2006). Even if the situation tends to improve, and products have been maintained under better temperature conditions during the past decade (Derens-Bertheau et al., 2015), insufficient temperature control remains problematic.

Vertical open refrigerated display cabinets are the most common refrigerated equipment adopted in many retail stores because they enable customers to have free access to food products. Regarding this open design, the food products stored inside the display cases are isolated from the external ambient environment only by one or more cold air curtains. Although the air curtain is well designed, warm and humid air infiltration is unavoidable. It is the greatest drawback of this type of display cabinet because it causes very high energy consumption: air infiltration contributes to approximately 66-77% of heat gain (Faramarzi, 1999; Gaspar et al., 2011; Tassou et al., 2011) and it results in temperature heterogeneity inside the cabinets. As reported by Willocx et al. (1994), temperature differences of more than 5 °C were observed on the cabinet shelves. Evans et al. (2007) indicated that the maximum temperatures in cabinets were generally in the front areas which is the most exposed to ambient whereas the minimum temperatures were located in the back. These authors reported that for 135 investigated display cabinets, 97% of the packages of the maximum temperature were at the front of the cabinets (60% of them were on the bottom shelves), and 98% of the packages at the minimum temperature were at the back. These findings match those obtained in an experimental study conducted by Laguerre et al. (2012). The product with the highest temperature with a mean surface temperature of 9.5 °C was located at the front and at the bottom of the cabinet, while the lowest product temperature (0.9 °C) was observed at the back, on the same level.

Many studies have been conducted on open and closed display cabinets and were reviewed by Chaomuang et al. (2017). Between them, experimentation (Amin et al., 2009; Chen and Yuan, 2005; Gaspar et al., 2011) and numerical simulation (Cortella, 2002; D'Agaro et al., 2006; Moureh and Yataghene, 2016) were carried out with a view to improve the performance of display cabinets. In these studies, the influence of significant factors on the display cabinet performance has been

pointed out: ambient conditions, design parameters and operating conditions. Nevertheless, the issue of air infiltration remains unsolved and is still attracting a lot of attention, and therefore a lot of research is being conducted on this issue.

The installation of doors on open display cabinets is becoming an alternative and has proven to provide many advantages including the achievement of energy savings (Faramarzi et al., 2002; Fricke and Becker, 2010), reduced temperature fluctuations (Evans and Swain, 2010; Lindberg et al., 2010) and improved food quality (Atilio de Frias et al., 2015). These results encourage many retailers to replace their conventional open-front display cabinets with closed cabinets fitted with doors. Particularly in France, according to a voluntary convention signed between the government and the main retailer groups, it is expected that both new and refurbished closed display cabinets will account for up to 75% of all display cases in retail stores by 2020 (RPF, 2016). This transition is generating a new research trend. The energy consumption of the refrigeration system of closed display cabinets has been widely studied, but few studies focused on the temperature performance (airflow and its corresponding temperature distribution), which impacts food quality.

The present study was an attempt to bridge this research gap and was designed to investigate the air and product temperatures and airflow in a closed refrigerated display cabinet. With the acquired knowledge, real-life conditions and possible problems of food preservation in this equipment can be identified, thereby enabling design improvements and operating practices to be addressed.

## 3.2. Material and methods

### *3.2.1. Description of the closed refrigerated display cabinet*

A closed refrigerated display cabinet (Costan, Offlip 2 Eco 125S) with external and internal dimensions (width × length × height) of 650 mm × 1310 mm × 1980 mm and 525 mm × 1250 mm × 1345 mm, respectively, was employed (**Figure 3.1**). It is equipped with two hinged doors (22 mm double-glazing window made of 2 panes of tempered glass, each pane with a thickness of 4 mm, a 14 mm air gap filled with 90% argon gas). The glass panes are coated with a low-emissivity coating material to avoid the transmission of infrared radiation. There is an 8-mm gap between doors and lateral glass walls to facilitate door openings. There are five shelves from the

top (Shelf 1) to bottom (Shelf 5). The space above Shelf 1 to 4 (dimension of a shelf 350 mm × 1250 mm) is 225 mm, while the one above Shelf 5 (475 mm × 1250 mm) is 345 mm. These spaces between shelves represent the total storage volume of about 0.60 $m^3$ for this display cabinet. The rear edge of the shelves is designed to have a 10-mm gap which allows products to have better cold exchange with the air from the PBP and reduce the potential of product freezing.

The food temperature inside the display cabinet is preserved by two cold air streams. The first one is the air flowing downward from a discharge air grille (DAG, 50 mm in width) equipped with a honeycomb at the top of the display cabinet and forms an air curtain. The second cold air stream is the air instantly penetrating from the back through the perforated back panel (PBP) towards the front where the two air streams are mixed. These air streams descend to a return air grille (RAG) by 2 propeller fans, and they are driven through the cooling coils (a finned-tube evaporator, heat exchange surface area of about 5 $m^2$) to decrease the temperature, and then return to the display cabinet.

The closed display cabinet was installed in a test room in which the ambient temperature was maintained at 19 °C. The room temperature was homogenized by 2 fans. To avoid the influence of airflow in the room on the measured value inside the cabinet, the rear of the display cabinet was located against these fans (**Figure 3.1**)

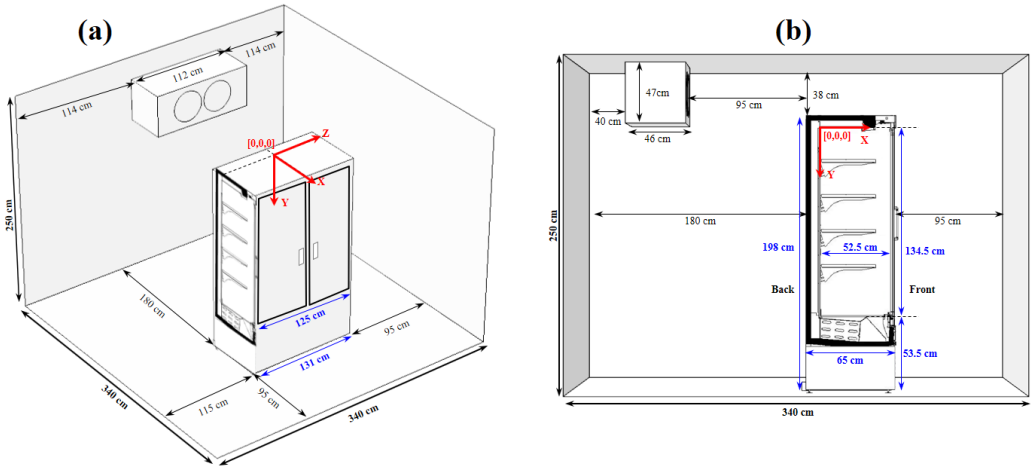


**Figure 3.1** Location of the closed display cabinet in the climate-controlled room: (a) perspective view (b) side view

To determine the benefit of the doors on the temperature performance, an experiment was also carried out with an open configuration of the display cabinet (doors were completely removed). The results of closed and open display cabinet configurations were then compared. Experiments at ambient temperatures of 15 °C and 24 °C were also carried out in the same manner as that conducted at a temperature of 19 °C in order to study the influence of the ambient temperature on the air temperature in the food storage domain of the closed display cabinet.

The air temperature and air velocity can be controlled in the test room, but it is technically not possible to control the air humidity. The measurement of the air characteristics ($T_a$ and %RH) was undertaken with a hygrometer (Testo 174H, accuracy ±3%RH) and the air humidity ratio (kg of water vapor/kg of dry air) was then calculated using a psychrometric chart. It was found that the value of air humidity ratio in the test room was in the range of 0.003-0.004 kg of water vapor/kg of dry air for all room temperatures. This level of humidity is two times lower than that of EN 23953 testing condition (0.006-0.007 kg of water vapor/kg of dry air for a room temperature of 20 °C). As higher air humidity would accelerate frost formation on the evaporator, on one hand, this could affect the refrigeration load. On the other hand, a large amount of frost on the evaporator could decrease the air flow rate due to an increase of pressure drop and it could also cause higher temperature of the supply air due to less heat exchange efficiency. So, strictly speaking, the obtained results correspond to stores in relatively dry climate conditions. Nevertheless, for a given air flow rate and a given air temperature after the evaporator, the air and product temperatures should be the same for other air humidity values since there was no condensation observed in the cabinet during the experiments. The experimental results reported by Chen and Yuan (2005) affirmed that the variations in air humidity have only a moderate effect on the temperature rise inside the display cabinet (open type in their study). These authors observed that the refrigeration load increases when the humidity ratio increases.

### *3.2.2. Determination of the overall thermal transmission*

The overall thermal transmission ($UA$) of the closed display cabinet (a low value indicates high insulating capacity) was evaluated by means of reverse heat loss rate measurement. The display cabinet, of which the refrigeration unit was switched off,

was installed in a climate-controlled room in which the ambient temperature ($T_{ext}$) was maintained at 5 °C. The internal temperature in the cabinet ($T_{int}$) was maintained at about 30 °C, by adjusting the power supplies of two electric heaters, placed on the left and right sides of the cabinet. In addition, small fans were installed at the end of each heater, and the cabinet ventilating fans were turned on to ensure a homogeneous air temperature inside the display cabinet. The temperature difference ($T_{int} - T_{ext}$) between the inside and the outside of the display cabinet (25 °C) is of the same order of magnitude that under real operating conditions in a supermarket. Temperatures at various positions inside (7 points) and outside (5 points) of the cabinet were measured with calibrated thermocouples (T-type, accuracy ±0.2 °C). Temperatures were recorded every minute until the cabinet temperatures reached a steady state (after 6 h), during which the power supplies of the heaters ($Q_h$), small fans ($Q_{fh}$) and cabinet fans ($Q_{fc}$) were also recorded using digital wattmeters (Digiwatt, accuracy ±1% of the reading). The internal and external air temperatures and total power supplies were then averaged over a period of 5 h of steady state, and the overall thermal transmission of the display cabinet was calculated using the following equation:

$$UA = \frac{Q_h + Q_{fh} + Q_{fc}}{T_{int} - T_{ext}} \tag{3.1}$$

According to the equipment accuracies, the relative accuracy of $UA$ was estimated of which the value was about 3%.

### *3.2.3. Air temperature measurement*

**Figure 3.2a** depicts the experimental setup for air temperature measurement at various positions in the display cabinet using T-type thermocouples. Each thermocouple was calibrated in the temperature range of -5 °C to 30 °C with a high precision thermostatic oil bath (Fluke, model 7340) and the precision of ±0.2 °C was determined. The measurement was divided into three planes: at z = 0 m (middle), z = -0.525 m (left) and z = +0.525 m (right). On each plane, the air temperature was measured at three height levels (top, middle and bottom shelves) and three positions on each shelf (5, 30, and 44 cm from the PBP). The air temperatures at the DAG, RAG and the middle of the vertical rear duct at the same levels (3 cm behind the PBP) were also measured. The display cabinet was switched

on, and the air temperatures were recorded every 10 seconds for at least 24 hours using two data loggers (Agilent 34970A). The mean values were then calculated at each measurement point during quasi-steady state (temperature fluctuations during defrost cycles were excluded from the calculation). Replications were also run in order to check repeatability.

Another experiment was performed in the display cabinet loaded with test product packages (60% of total storage volume). The package was made of methylcellulose (dimensions in width × height × length: 100 × 50 × 200 mm; thermophysical properties at 0 °C: density = 1100 $kg \cdot m^{-3}$, thermal conductivity = 0.49 $W \cdot m^{-1} \cdot K^{-1}$, specific heat = 3372 $J\ kg^{-1} \cdot K^{-1}$). Thermocouples were positioned at the geometric center and the surface of some test packages as well as at 2 cm from the package surface as shown in **Figure 3.2b**.

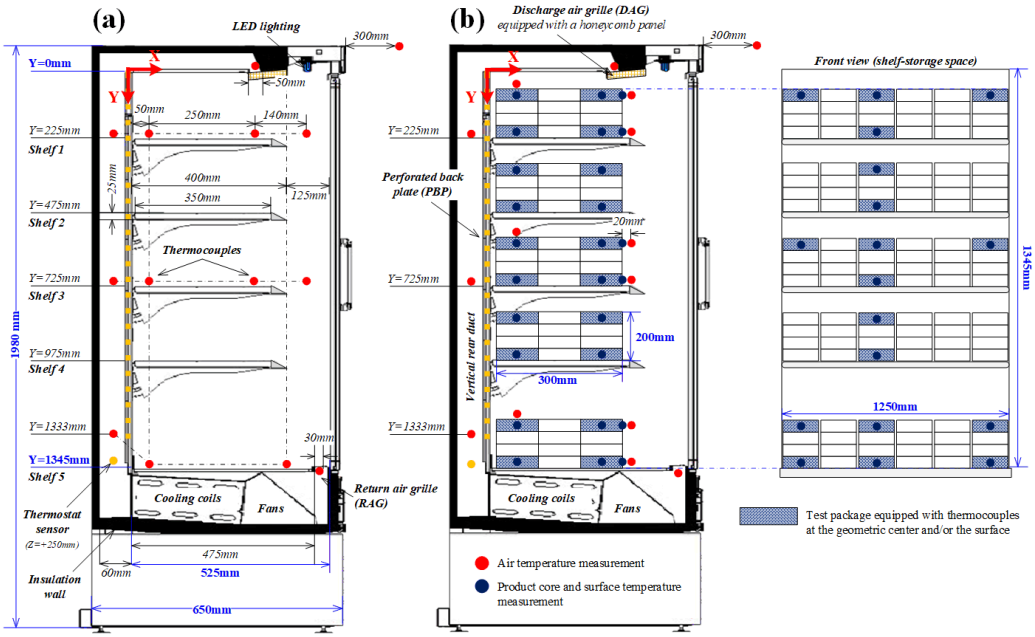


**Figure 3.2** Schematic view of the experimental setup for temperature measurement in the closed display cabinet: (a) unloaded and (b) loaded conditions

### *3.2.4. Air velocity measurement*

There are two cold air streams in the display cabinet. One is an air curtain flowing vertically from the DAG to the RAG and the other stream flows horizontally from the PBP to the front. A hot-wire anemometer (Testo 435-4) fixed on a height adjustable support device (**Figure 3.3b**) was used to measure air velocity profiles

in the display cabinet. This anemometer was previously calibrated in the range of 0-2 $m \cdot s^{-1}$ (the air velocity range often observed in display cabinets) of which the uncertainty was between 0.02 $m \cdot s^{-1}$ and 0.06 $m \cdot s^{-1}$. The velocity profiles on the cabinet middle plane (z = 0 m) and right plane (z = +0.26 m, aligned with the center of right fan located under the bottom shelf) were measured. The device used to support the hot-wire anemometer was placed 300 mm away from the measurement position to minimize perturbation (**Figure 3.3b**). The sensor is small compared to the space between two shelves. **Figure 3.3a** shows the measurement positions on each plane. There were 27 air velocity measurement positions from the PBP to the front, with 1 cm intervals between 2 positions in the air curtain region (Zone 2) and 2 cm in the other regions (Zones 1 and 3). The measurements were performed 16 cm above the top and intermediate shelves and at 21 cm above the bottom shelf. In Zone 1, the airflow was mostly dominated by the air supply from the PBP, and the anemometer was oriented against the horizontal flow direction (x-axis). Both vertical and horizontal flow directions (x- and y-axes) were measured for Zones 2 and 3. To take into account the air velocity fluctuations with time, the air velocity at each position was averaged from 300 measurements (every second for 5 min). The measurement began after 1 min since doors were closed to minimize the influence of door movement on flow perturbation. In fact, some preliminary tests had been run previously for different durations (3, 5, 7 and 10 min) and it was found that the measurement duration should be at least 5 min. to ensure the reliability of the mean air velocity.

### *3.2.5. Airflow rate in the vertical rear duct*

To quantify the distribution of the airflow rate discharged through the PBP at various heights, measurement of the air velocity inside the vertical rear duct of the display cabinet was performed (**Figure 3.4a**). Six height levels, H1 (y = 0.015 m), H2 (y = 0.215 m), H3 (y = 0.465 m), H4 (y = 0.715 m), H5 (y = 0.965 m) and H6 (y = 1.335 m) were considered, and at each height three holes were drilled in the back wall of the cabinet (at z = -0.26, 0, and +0.26 m). In each hole, the air velocity at three positions across the rear duct was measured using the hot-wire anemometer. As mentioned in **Section 3.2.4**, the air velocity was recorded every second for 5 min and its mean value at each position was then calculated. As the cross-section of rear duct is known, it is possible to calculate the airflow rate at each height. The

influence of the occupied volume of the load in the display cabinet on the airflow rate distribution was also studied: 0, 36% and 52% of total storage volume. **Figure 3.4b and c** show the loading arrangement of test packages for each occupied volume, with 1-cm spaces between each stack of packages and between the back stacks and the PBP.

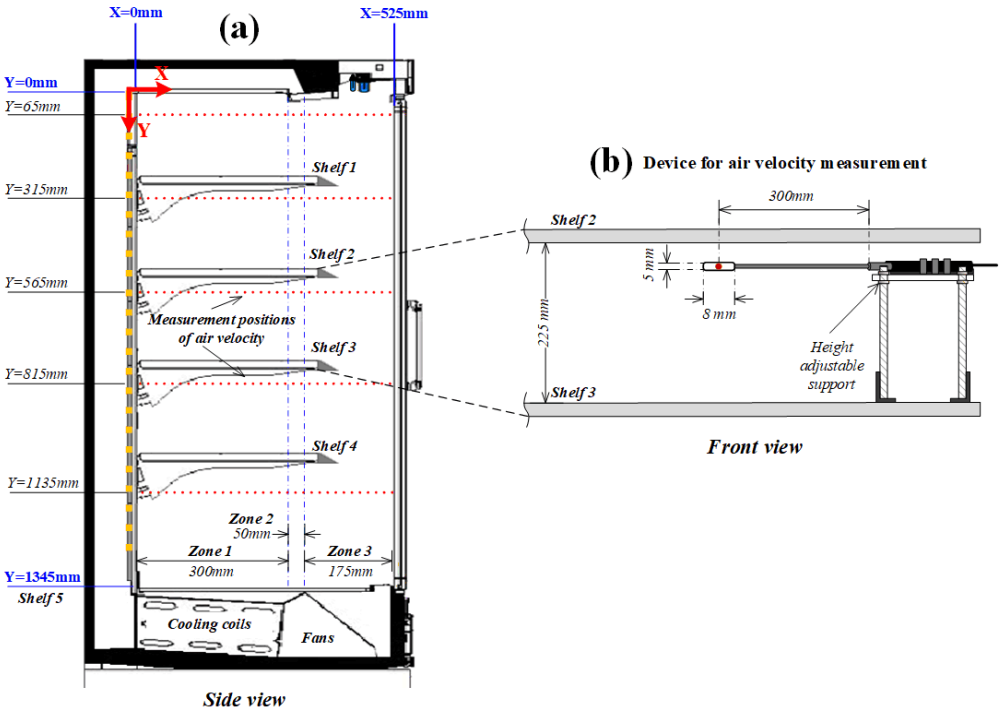


**Figure 3.3** Schematic view of the experimental setup for velocity measurement: (a) measurement positions on middle (z = 0 m) and right (z = +0.26 m) planes (b) position of a hot-wire anemometer and its support on a shelf

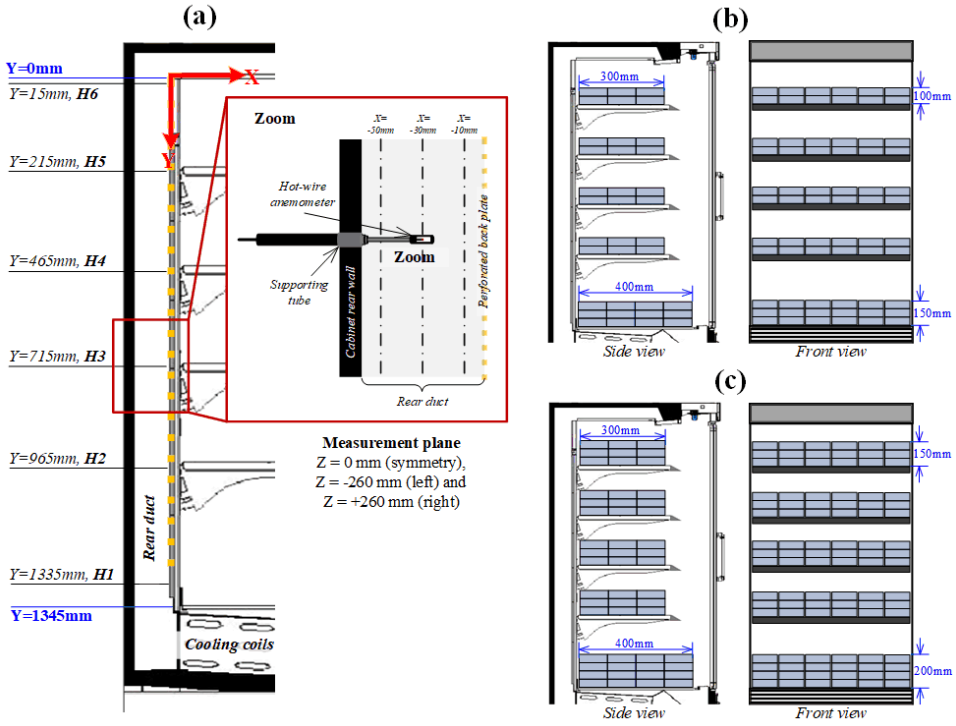


**Figure 3.4** Velocity measurement in the vertical rear duct with three percentages of test package-occupied volumes in the display cabinet: (a) 0% (b) 36% and (c) 52% of total storage volume

**Figure 3.5** illustrates the perforation patterns of the back plate at different levels. The perforation patterns over the cabinet shelves are different; the percentages of perforated area (PPA) are shown in **Table 3.1**. The back plate over Shelf 1 had no perforations in the middle part (**Figure 3.5a**), thus providing a minimum percentage of perforated area of 2.3%, while the maximum of 8.3% was on Shelf 5 (**Figure 3.5c**) and the same value of 3.8% applied to Shelves 2 to 4. Considering the total plate area, the percentage of perforated area was about 4.4%.

**Table 3.1** Percentage of perforated area (PPA) on different shelves

| Shelves | Plate area ($m^2$) | Percentage of perforation (%) |
|---|---|---|
| Shelf 1 (top) | 0.28 | 2.3 |
| Shelf 2-4 | 0.28 | 3.8 |
| Shelf 5 (bottom) | 0.44 | 8.3 |
| Total plate | 1.68[(a)] | 4.4 |

[(a)]Total plate area includes the area covered by shelf thickness (0.03 $m^2$)

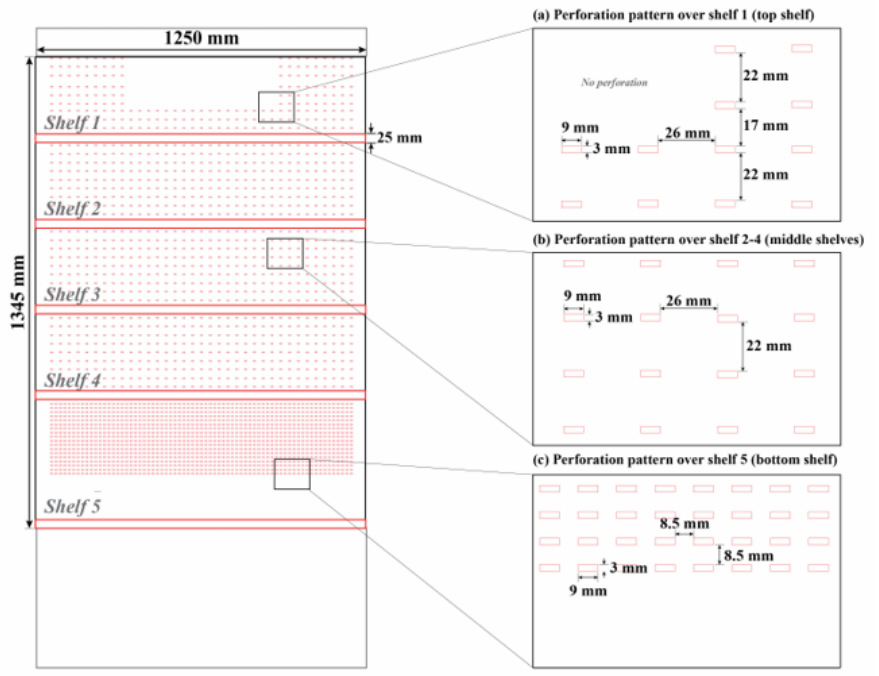


**Figure 3.5** Perforation patterns on the back panel at different levels

## 3.3. Results and discussion

### *3.3.1. Overall thermal transmission of the display cabinet*

There were apparently three main heat loss paths in the display cabinet: through glass walls (doors and side walls), through insulated walls (rear, top and bottom walls, conductive heat transfer coefficient of about 0.77 $W \cdot m^{-2} \cdot K^{-1}$), and through the gaps (about 8 mm) along the door frame where air can flow out and be replaced by ambient air. The overall thermal transmission of the closed display cabinet was found to be 21.3 $W \cdot K^{-1}$. This value corresponds to an overall average heat transfer coefficient of about 2.74 $W \cdot m^{-2} \cdot K^{-1}$, considering that the mean surface area of the display cabinet was 7.8 $m^2$. To the authors' knowledge, the thermal transmission of closed display cabinets is not available in the literature. The value of the overall average heat transfer coefficient of the studied closed display cabinet was 5 – 10 times higher than those of domestic refrigerators of which the value was about 0.28 $W \cdot m^{-2} \cdot K^{-1}$ (Laguerre, 2010) and 0.53 – 0.56 $W \cdot m^{-2} \cdot K^{-1}$ (Melo et al., 2000). The poor insulating capacity of the display cabinet compared with that of domestic refrigerators can be mainly explained by greater heat transfer rate through the doors and side walls (made of double-glazing glass, with an conductive heat transfer coefficient of 1.13 $W \cdot m^{-2} \cdot K^{-1}$) which are less insulated than those of domestic

refrigerators (0.67 $W \cdot m^{-2} \cdot K^{-1}$) (Laguerre and Flick, 2004), and by convective losses through the gaps around the doors and through thermal bridges i.e. the connections between the internal and external components (evaporator, expansion valve and compressor) of the refrigeration system. Based on our estimation of heat losses through the walls and the doors (by knowing the thermal conductivity and thickness of wall and door materials as well as by estimating the convective resistances), gaps and thermal bridges were responsible for approximately 70% of the overall thermal transmission of the display cabinet. According to our estimation of room lighting with fluorescent tubes (~600 lux), transmission of visible radiation corresponds to less than 7% of the total transmission of conduction and convection through the glass doors and sides walls (about 25 $W \cdot m^{-2}$).

### *3.3.2. Temperature profiles*

#### *3.3.2.1. Empty closed display cabinet*

**Figure 3.6** presents the air temperature evolution under closed-door conditions, at three different positions (DAG, front of the top shelf, and at the back of the bottom shelf) with the refrigeration system turned on, under ambient temperature conditions of 19 °C. The cooling duration of the system varied according to the positions in the display cabinet. The air temperature at the DAG took about 30 min to cool down from the onset of the quasi-steady state during which the min./max. temperature variation was between -4.0 °C and 1.3 °C (**Figure 3.6a**). Two temperature fluctuation cycles were observed: small and large fluctuations. The former (during the quasi-steady state) was due to the regulation of the on/off compressor working cycle which is automatically conducted by the thermostat sensor. The latter fluctuation was due to a time/temperature-based defrosting cycle, which occurred every 6 h with duration of about 25 min. An electric defrost system is used in this display cabinet. The compressor is switched off during defrosting and warm air heated by the electric strip heater is blown over the evaporator by the fans. This explains a rapid increase of temperature with a peak of 6.0 °C. Defrost termination is when either temperature threshold (6.0 °C) or maximum duration (30 min.) is reached. As depicted in **Figure 3.6b and c**, the air temperature takes about 58 min to cool down at the front of the top shelf (min./max. temperature variation of -0.3/+2.3 °C), while it requires a shorter cooling duration about 26 min at the

back of the bottom shelf (min./max. temperature variation of -2.8/+1.3 °C). This obtained information suggests that a closed refrigerated display cabinet should be run at least an hour for temperature stabilization before placing products.

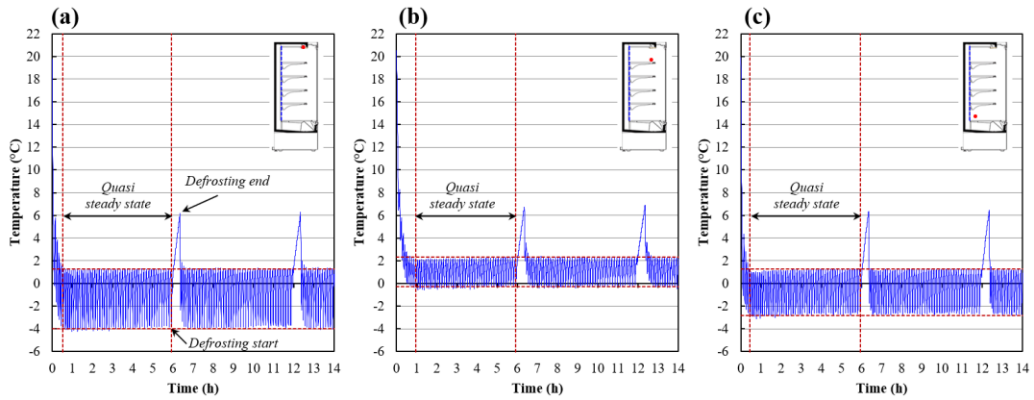


**Figure 3.6** Evolution of air temperatures (on the middle plane, z = 0 m) at various positions in the closed display cabinet for a room temperature of 19 °C: (a) discharge air grille, (b) front of top shelf, and (c) back of the bottom shelf

**Figure 3.7** presents the temperature evolution at different positions on the middle plane (z = 0 m) of the display cabinet together with mean temperatures and standard deviations during the quasi-steady state. It can be noticed that the min./max. temperature variations varied from one position to another with the same frequencies due to the regulation of the on/off cycle of the compressor as previously mentioned. The air temperature variation curve at the bottom of the vertical rear duct (**Figure 3.7a**), near the thermostat sensor (x = -0.03 m, y = +0.05 m, z = +0.25 m), provided information on the compressor working cycle. The compressor was turned on when the air temperature reached its maximum threshold value of 2.0 °C, resulting in a rapid decrease in the air temperature to about -7.0 °C at which point the compressor was then turned off. The on/off cycle for the closed display cabinet lasted about 380 seconds: 90-second "on", 290-second "off".

Apparently, air temperature fluctuations in the vertical rear duct had greater amplitudes than in the other positions. At these positions (a, b and c in **Figure 3.7**), an increase in the minimum temperature was observed (-7 °C at "a" to -6 °C at "c") while the maximum temperature was relatively similar in all positions (about 2 °C). The heat loss through the cabinet walls explained a slight increase in the mean

temperature of 0.3 °C (-1.3 °C at “a” and -1.0 °C at “c”). The standard deviation, however, became slightly lower (2.5 °C at “a” and 2.1 °C at “c”). This can be explained by stabilization due to the thermal inertia of the wall of the rear duct. The same phenomena were observed in the upper horizontal duct (ceiling) from “c” to “d”: an increase in the mean temperature (-1.0 °C at “c” and -0.6 °C at “d”) due to heat losses and a lower standard deviation (2.1 °C at “c” and 1.6 °C at “d”) due to exchanges with duct walls and the honeycomb of the DAG.

In the area in which food products are stored (positions e, f, g, h, i and j in **Figure 3.7**), the air temperature was below 2 °C, which is the recommended temperature for perishable foods (meat and fish). The lowest air temperature value was observed at the back of the bottom shelf (position “i”): mean temperature of -0.6 °C, standard deviation of 1.3 °C. This could cause freezing damage to foods with high moisture content like fruit and vegetables. A great deal of attention should be paid to the selection of the types of foods to store in such positions inside display cases.

The mean temperatures at the front of the shelves (positions f, h and j in **Figure 3.7**: 1.1 °C, 0.6 °C and -0.2 °C, respectively) were higher than at the DAG (-0.6 °C at “d”). This is because the air curtain exchanges heat with doors, through which heat is transferred from the external ambient (19 °C) and because of the infiltration of external air through the gaps. The mean temperatures at the back of the shelves (positions e, g and i in **Figure 3.7**: 0.5 °C, 0.3 °C and -0.6 °C, respectively) were lower than those at the front, especially on the bottom shelf. This is because of the air flowing through the PBP at an initial temperature of around -1.0 °C, particularly on the bottom shelf where the percentage of perforated area was the highest (8.3%). Mixing of air coming from the back and from the air curtain probably occurred on each shelf as shown schematically in **Figure 3.7**.

In the area in which food products are stored, with the exception of the back of the bottom shelf (position “i”), the standard deviations were lower than 1 °C in spite of the large temperature fluctuations just after the evaporator (standard deviation of 2.5 °C, position “a”). The fluctuations in this zone are acceptable, and thus, a reduction in the amplitude of the regulation (-7 °C/ 2 °C) is not necessary for this display cabinet. In fact, such regulation would increase the number of on/off cycles, thus reducing the lifespan of the compressor. The ratio of high-low compressor

pressure used for this display cabinet was 5 to 1 and the average evaporating temperature was about -7.5 °C.

The reduction in the standard deviation of the air temperature on the shelves in comparison with that at the DAG is due to heat exchange between air and the wall, door and shelves for which the thermal inertia damps the fluctuations. At the back of the bottom shelf, the standard deviation was the highest (1.3 °C) in the storage zone because a large amount of air came from the rear duct where the standard deviation was also high (2.5 °C) through the PBP which is perforated to a large extent (8.3%) at this level.

**Figure 3.8a** presents the mean air temperature and standard deviation calculated based on the measurement on the three planes (z = -0.525, 0 and +0.525 m) for the storage zone of the closed display cabinet. It shows that, from the rear duct upstream to the DAG, the air temperature after flowing across the cooling coils rose from -1.0 ± 2.2 °C to -0.3 ± 1.5 °C. This is very similar to the observation in the middle plane (**Figure 3.7**). In the storage zone (**Table 3.2**), the mean temperatures were slightly higher (about 0.5 °C) than at the middle plane (**Figure 3.7**) because there were additional heat losses near the lateral glass walls, but the trends are similar. The temperature at a distance of 4 cm from the edge of the top shelf (position "k") was significantly higher than that at the DAG. This is because this position was located outside the air curtain as observed by air velocity measurements presented in the following section (Section 3.3). **Figure 3.8a** also shows the temperature at the RAG (1.0 ± 1.3 °C), which is important for compressor energy consumption: the higher the value (compared to the one at the DAG), the higher the refrigerating power. For this closed display cabinet $\bar{T}_{DAG} - \bar{T}_{RAG}$ is only 1.3 °C.

**Table 3.2** Mean temperature and standard deviation (°C) during quasi-steady state at various positions within the food storage zone on the left, middle and right planes for a room temperature of 19 °C

| Planes | Positions | | | | | | |
|---|---|---|---|---|---|---|---|
| | e | f | g | h | i | j | All |
| **Left** | 0.9±0.6 | 1.8±0.5 | 0.4±0.5 | 0.9±0.6 | -0.6±1.1 | 0.1±1.2 | 0.6±1.1 |
| **Middle** | 0.5±0.7 | 1.1±0.8 | 0.3±0.6 | 0.6±0.6 | -0.6±1.3 | -0.2±1.0 | 0.3±1.0 |
| **Right** | 0.8±0.5 | 2.0±0.4 | 0.6±0.6 | 1.6±0.7 | -0.1±0.9 | 1.1±1.1 | 1.0±1.0 |
| **All** | 0.7±0.6 | 1.6±0.7 | 0.4±0.6 | 1.0±0.7 | -0.4±1.1 | 0.3±1.2 | 0.6±1.1 |

To ensure that food products are stored at appropriate temperature in the display cabinet, a temperature is generally displayed on a monitoring screen (Baldera Zubeldia et al., 2016). The display value corresponds to the instantaneous air temperature at a given position. In fact, air temperature depends on the positions in the cabinet. It should be preferable to display the temperature at the warmest and coldest positions: position "f" and "i" in our case, respectively.

*3.3.2.2. Benefits of door installation*

Doors of the studied display cabinet were removed to investigate the influence of the presence of doors on the temperature performance. **Figure 3.8a and b** show the mean air temperature calculated from the three planes (z = -0.525, 0 and +0.525 m) and the standard deviations in the display cabinet with and without doors, respectively. The temperature profile in these two cases has the same trend: the highest temperature at the front of the top shelf (position "f") and the lowest temperature at the back of the bottom shelf (position "i"). Without doors, the mean air temperatures in the storage zone increase in all positions with a minimum increase of 0.4 °C (from -0.4 °C to 0.0 °C at position "i") and a maximum increase of 3.1 °C (from 1.0 °C to 4.1 °C at position "h") compared to the case with doors. The comparison of the air temperature at 4 cm from the shelf edges (positions "k" and "ℓ") shows a large increase: 8.2 °C (from 5.7 °C to 13.9 °C) at the top and 9.5 °C (from 2.4 °C to 11.9 °C) at the mid-height.

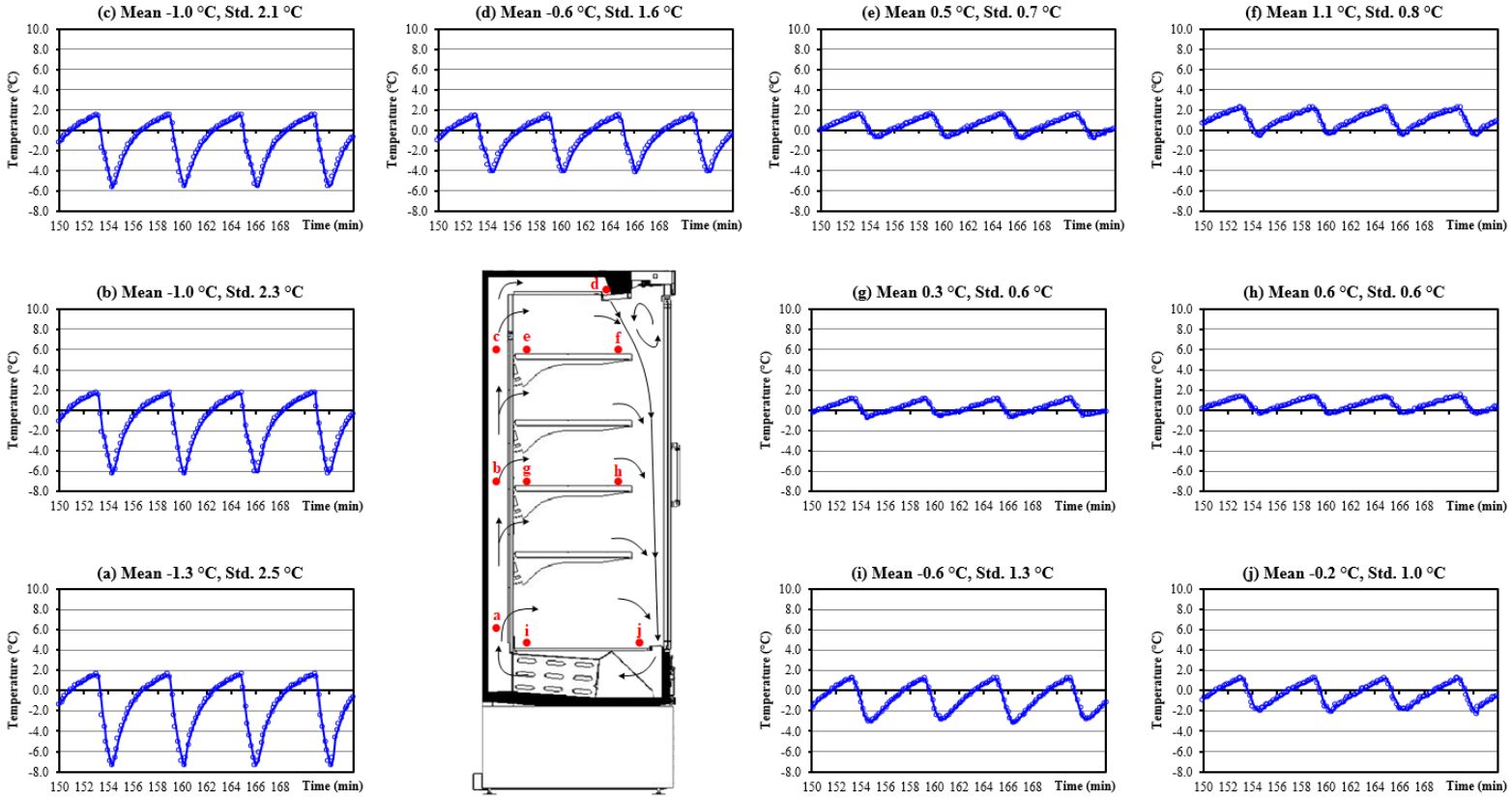


**Figure 3.7** Evaluation of air temperature during quasi-steady state in various positions (on the middle plane) in the closed display cabinet for a room temperature of 19 °C

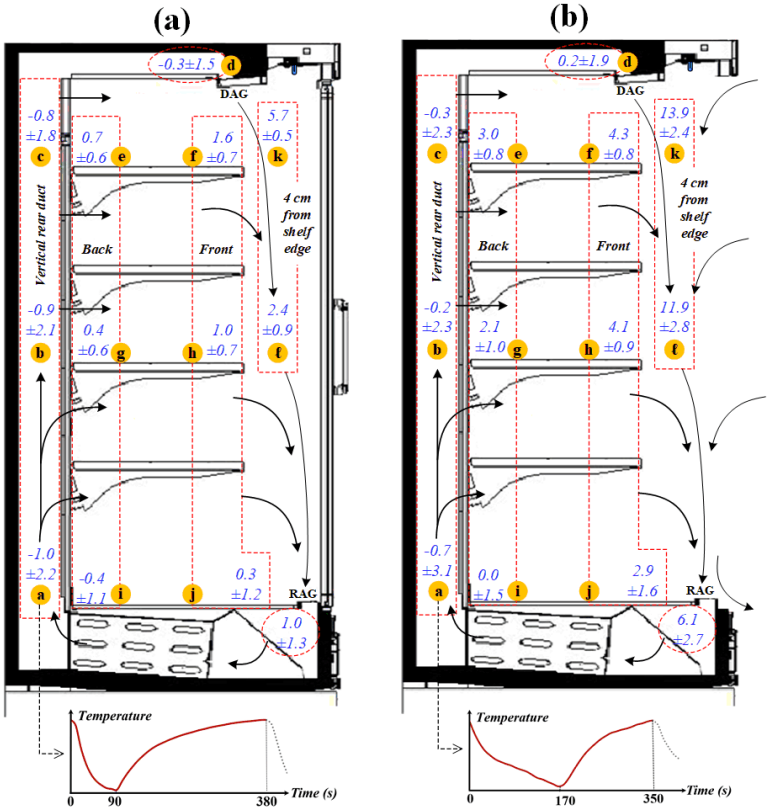


**Figure 3.8** Mean air temperature and standard deviation (°C) during quasi-steady state (average of the measurements on the three planes: z = -0.525, 0 and +0.525 m) of the display cabinet (a) with doors and (b) without doors for a room temperature of 19 °C

This can be explained by the mixing of the cold air from DAG with the warm air (from outside) and along the turbulent air curtain. The higher temperature at the RAG (6.1 °C without doors instead of 1.0 °C with the doors) leads to higher heat loads on the evaporator: $\bar{T}_{DAG} - \bar{T}_{RAG}$ increased from 1.3 °C (with doors) to 5.9 °C (without doors). The on/off compressor working cycle for the open display cabinet lasted about 350 seconds: 170-second "on" and 180-second "off". The time fraction during the compressor is "on" increased from 24% with the doors to 49% without them. The amplitude of the temperature variation just after the evaporator (position "a") also increased (standard deviation from 2.2 to 3.1 °C, **Figure 3.8**). As a consequence, a slight increase of mean air temperature in the vertical rear duct (position a-d, **Figure 3.8b**) as well as at the back of the shelves (position e, g and i, **Figure 3.8b**) was observed. An increase of the standard deviation of air temperature was also observed at all positions in the cabinet without doors.

For empty and same room conditions, the temperature performance of the closed display cabinet is better compared to the open one due to lower mean air temperature and less temperature heterogeneity in the storage zone. The mean temperature differences between the front and the back positions were less than 1 °C in the case with the doors whereas thereabout 2-3 °C in the case without.

*3.3.2.3. Influence of ambient temperature*

**Table 3.3** shows the influence of the ambient temperature (15 °C, 19 °C and 24 °C) on the air temperature in the food storage zone (mean value and standard deviation over 5 h of quasi steady state periods). The mean temperature at the thermostat position ($T_{th}$) was slightly different for these three different ambient temperatures. To compare the results obtained under several ambient temperatures, temperature difference ($T - T_{th}$) was shown in **Table 3.3**. Averagely for all the positions $T - T_{th}$ increases from 1.1 to 2.0 °C when $\bar{T}_{amb} - T_{th}$ rises from 15.2 to 25.4 °C. In order to determine if the influence of the ambient temperature is linear, a dimensionless temperature was also calculated defined as $T_i^* = \frac{T_i - T_{th}}{\bar{T}_{amb} - T_{th}}$ where $i$ is a given position. It appears that $T_i^*$ is almost independent of $\bar{T}_{amb} - T_{th}$. This is due to the linearity (between $T_{amb}$ and $T_i$) since the forced convection and conduction are predominant heat transfer modes. In the closed configuration, free convection is negligible because of the rather high velocities at the DAG and PBP. Radiation is also limited because the glass doors shield the radiation from the external walls in opposite to the open configuration. The highest value of $T^*$ is at the position f (the front of the top shelf) where $T_f - T_{th}$ is about 12% of $\bar{T}_{amb} - T_{th}$. The lowest value of $T^*$is at the position i (the back of the bottom shelf) where the temperature is slightly higher than to the thermostat one.

An increase in ambient temperature causes also an increase in the frequency of compressor working cycles (shorter "off" period) in order to maintain the desired thermostat temperature. The number of compressor "on" cycles over a 5-hour period rose from 36 (for 15 °C) to 52 (for 24 °C). This implies an increase in the energy consumption of the display cabinets installed in stores without air-conditioning systems in summer. It should be borne in mind that these experiments were carried out under closed conditions, with less ambient air infiltration into the cabinet than for an open cabinet.

**Table 3.3** Effect of ambient temperatures on the internal air temperature of the closed display cabinet

| **Ambient temperature** | **Temperature difference** | **Number of compressor "on" cycles/5h** | | **Temperature difference and time-averaged dimensionless temperature at a given position** | | | | | | **All positions** |
|---|---|---|---|---|---|---|---|---|---|---|
| $T_{amb} \pm SD$ [°C] | $T_{amb}-T_{th}$ [°C] | | | **e** | **f** | **g** | **h** | **i** | **j** | |
| 15 ± 0.5 | 15.2 | 36 | $T-T_{th}$ [°C] | 1.1 | 1.7 | 1.0 | 1.4 | 0.3 | 0.8 | 1.1 |
| | | | $T^*$ [-] | 0.07 | 0.11 | 0.06 | 0.09 | 0.02 | 0.06 | 0.07 |
| 19 ± 0.4 | 20.3 | 44 | $T-T_{th}$ [°C] | 1.5 | 2.4 | 1.2 | 1.8 | 0.4 | 1.1 | 1.4 |
| | | | $T^*$ [-] | 0.08 | 0.12 | 0.06 | 0.09 | 0.02 | 0.06 | 0.07 |
| 24 ± 0.3 | 25.4 | 52 | $T-T_{th}$ [°C] | 2.3 | 3.7 | 1.6 | 2.4 | 0.6 | 1.5 | 2.0 |
| | | | $T^*$ [-] | 0.09 | 0.14 | 0.06 | 0.09 | 0.02 | 0.06 | 0.08 |
| **All ambient temperatures** | | | **$T^*$** [-] | **0.08** | **0.12** | **0.06** | **0.09** | **0.02** | **0.06** | **0.07** |

*3.3.2.4. Closed display cabinet under loaded condition*

The obtained results of the temperature profiles in the closed display cabinet under unloaded condition enable an insight into the thermal mechanism occurring in the equipment. To further investigate the temperature performance of this cabinet under real use condition, test product packages were placed in the cabinet with an occupied volume of about 60% of total storage volume. As reported in **Figure 3.9a**, the averages and standard deviations of product (core and surface) and air temperatures on the middle plane (z = -0.105 m) of the cabinet with doors were calculated during quasi-steady state. As expected, the temperature profiles of the closed display cabinet under loaded and unloaded conditions were consistent. The products placed at the front of the top shelf had the highest temperature (core 2.4 °C and surface 3.3 °C) whereas the products placed at the back of the bottom shelf had the lowest temperature (core -0.5 °C).

The incident of high temperature on the top shelf can be explained by interdependencies among various influencing factors. The products located at this position were mainly subject to heat exchanges with the air curtain and heat losses through the glass doors because less cooled air supplies from the back due to low percentage of perforation area (2.3%) on this shelf. In the vicinity of cabinet lighting, there was additional heat generation due to (visible) light absorption in the products. It can be noticed (**Figure 3.9a**) that product surface temperature was higher than that of the surrounding air (maximum difference of 2.6 °C) and was slightly higher than that of its core temperature (maximum difference of 0.9 °C).

At the lower shelves, more cooled air from the back instantly supplies to the storage space according to higher percentage of perforation areas. As a consequence, product temperature at the front gradually decreased from the top (core 2.4 °C and surface 3.3 °C) to the bottom (core 0.4 °C and surface 0.8 °C).

A temperature variation of products between the front and the back was also observed, of which the highest variation was on the top shelf (maximum difference of 2.1 °C). This results from a combination of convection between product and cold air coming from the PBP and conduction within and between the products.

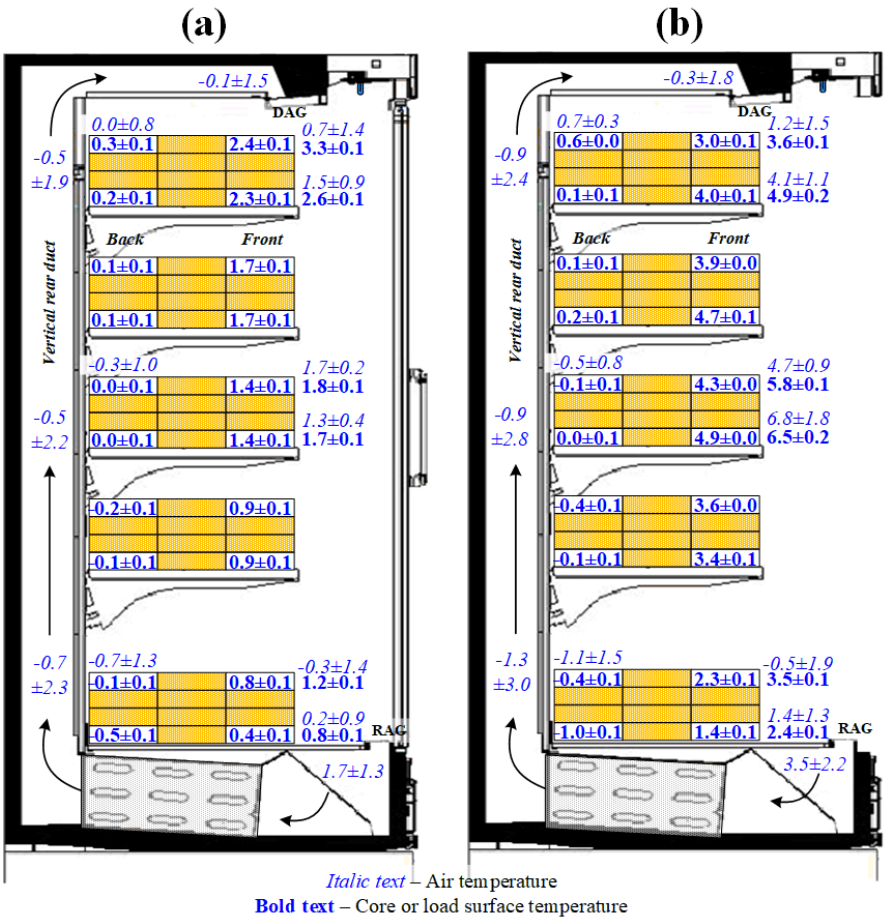


**Figure 3.9** Air velocity profiles in the closed display cabinet measured by a hot wire anemometer on the middle (z = 0 m) and right (z = +0.26 m) planes: (a) vertical flow direction and (b) horizontal flow direction

**Figure 3.9b** presents the average and standard deviations of product (core and surface) and air temperatures on the middle plane (z = -0.105 m) of the cabinet without doors during quasi-steady state. It was found that product and air temperatures at the front areas remarkably increased at all positions. Unlike the case with doors, there was external warm infiltration mixing with the air curtain. As a result, products at the middle shelf had highest temperature (core 4.9 °C and surface 6.5 °C). Due to higher percentage of perforation areas at the bottom shelf, the temperature of products on this shelf remained lowest (core 1.4 °C and surface 2.4 °C) compared to the other shelf. Indeed, highest product temperature is often found on the bottom shelf of most open display cabinets (Evans et al., 2007). Allowing high perforation percentage at this shelf seems to be an effective remedy for this issue.

Product temperature at the back of the cabinet without doors was slightly lower that of the cabinet with doors (maximum difference of -0.5 °C at the back of the bottom shelf). This is because higher refrigeration capacity is required to compensate additional heat loads due to warn air infiltration. As shown in **Figure 3.9a and b**, mean air temperature after the evaporator of the cabinet without doors (-1.3 °C) was lower that than of the one with doors (-0.7 °C). In opposite, the standard deviation was higher in the case without door (3.0 °C). Like the cabinet with doors, the product located at the back not only exchange heat with the supplied air from the PBP through convection but also exchange heat within and between the products themselves through conduction. As a result, the product temperature at the back was lower than that at the front of the cabinet.

Globally, higher temperature heterogeneity was observed in the storage space of the cabinet without doors, of which the temperature difference between the product at the front and at the back fell within the range of 2.7 – 4.9 °C. In case of the cabinet with doors, this value was less than 2.1 °C. The findings confirm that the closed display cabinet has better temperature performance compared to the open one.

### *3.3.3. Air velocity profile*

**Figure 3.10** presents time-averaged air velocity profiles in the closed display cabinet measured by a hot-wire anemometer. As shown in **Figure 3.10a**, the air velocity in the vertical flow direction (y-axis) varied from 0.01 $m \cdot s^{-1}$ to 0.59 $m \cdot s^{-1}$ in the middle plane (z = 0 m) and it was not significantly different from that of the right plane (z = +0.26 m). The highest velocity (≈ 0.59 $m \cdot s^{-1}$) was found near the discharge grille of the air curtain (x = 0.33 m, y = 0.065 m). At the y = 0.315 m position, the thickness of the air curtain increased because of the entrainment of neighboring air by the air jet. At the lower positions ($y \geq 0.565$ m), maximal velocity was located close to the door due to the adhesion of airflow to the door surface (Coanda effect). This maximum velocity remained almost constant near the door (about 0.40-0.50 $m \cdot s^{-1}$). As can be seen from its corresponding temperature presented in **Section 3.3.2**, the air is almost stagnant in the area beyond the air curtain under the DAG (x > 0.40 m, y = 0.065 m), resulting in a high temperature at this position (**Figure 3.8a**).

**Figure 3.10b** shows the profile of the horizontal component of air velocity between shelves. The low air velocity (0.0-0.10 $m \cdot s^{-1}$) on the top shelf compared with the others (0.10-0.20 $m \cdot s^{-1}$) can be explained by the lowest percentage of perforated area at this position (2.3%). As depicted in **Figure 3.10b,** the velocity changed from one position to another. This denotes that there is no plug flow from the PBP to the front but there is a more complex flow because of the interaction between the back-air stream and the air curtain. There was probably air recirculation to a small extent between shelves as observed in a refrigerator (Laguerre et al., 2007). It is to be emphasized that the results presented in **Figure 3.10b** should be interpreted cautiously because of the limitations of the hot wire anemometer in the measurement of low air velocity and complex flow. More advanced measurement techniques, for example Laser Doppler Velocimetry (LDV) and Particle Image Velocimetry (PIV), are preferable when dealing with such complex flow, and generate more accurate data. These techniques allow the investigation of the air flow not only in x and y directions but also in z direction (a sign of complex flow).

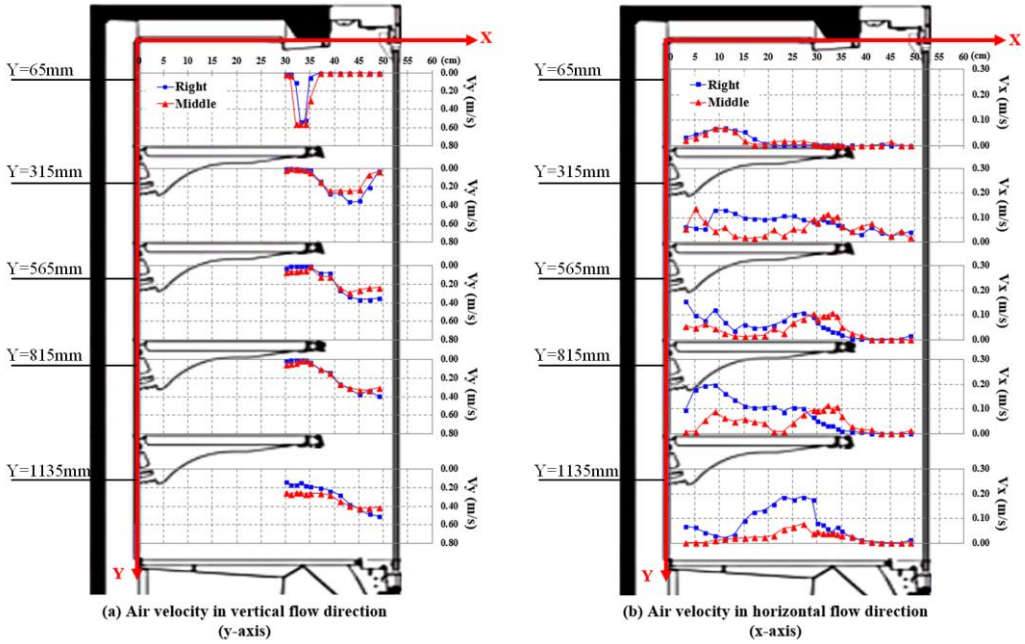


**Figure 3.10** Air velocity profiles in the closed display cabinet measured by a hot wire anemometer on the middle (z = 0 m) and right (z = +0.26 m) planes: (a) vertical flow direction and (b) horizontal flow direction

### *3.3.4. Airflow rate in the vertical rear duct*

The air velocity profiles across the width of the vertical rear duct on different planes (left, middle and right) and for three heights (H1, H4 and H6) are presented in **Figure 3.11a, b and c**. The average value for the nine measurement positions at each height are also presented in these figures. The average air velocity decreased from 1.16 $m \cdot s^{-1}$ (with a standard deviation of 0.40 $m \cdot s^{-1}$) upstream of the duct (H1) to 0.58 $m \cdot s^{-1}$ (with a standard deviation of 0.12 $m \cdot s^{-1}$) downstream of the duct (H6). This is because there is a perforated plate between the upstream and downstream of the rear duct which allows some air outflow to the food storage zone of the display cabinet. The standard deviation also decreased according to the height since the velocity variation among the three planes became smaller.

Because of the 90° elbow at the bottom of the duct and the high percentage of perforated area on the bottom shelf, the velocity profile across the duct width at the lowest level (H1) was not uniform: a lower velocity was observed near the perforated plate (x = -0.15 m), whereas a higher velocity was observed near the back wall of the cabinet (x = -0.45 m). However, it became more uniform at higher levels (H4 and H6) because of coarser perforated areas on the perforated plate and because of the well-developed flow at these levels. Indeed, the mean velocity of about 0.6 $m \cdot s^{-1}$ (Reynolds number, $\mathrm{Re} = \frac{\rho \bar{v}_a D_h}{\mu} \approx 5100$) observed at H4 and H6 leads to the conclusion that turbulent flow and almost uniform velocity profile can be expected inside the duct.

**Section 3.3.2** has shown that the temperature distribution in the display cabinet is asymmetric. Based on the velocity profile observed in the rear duct, this finding is confirmed. The air velocity on the left plane (z = -0.26 m) was markedly lower than those of the other two planes as depicted in **Figure 3.11b and c**. This can be explained by the effect of airflow maldistribution in the cooling duct located at the bottom of the display cabinet (from the fan discharge to downstream of the evaporator) because of the interaction between two air streams generated by fans which rotate in the same direction, leading to deviation of airflow on the same side of the channel and a slight asymmetric placement of the evaporator. In the present case, the flow streams mostly deviated to the right side of the cooling duct, and this explains the lower velocity on the left plane. This dissymmetry in flow was also

observed by Marinetti et al. (2012) and Marinetti et al. (2014) who performed experimental and numerical analysis of the flow distribution in a cooling duct model of a refrigerated display cabinet. They found a higher velocity in the right part of the duct.

**Figure 3.11d** presents the mean air velocity calculated on the basis of nine measurement positions on the cross-section of the rear duct at each height for different percentages of product-occupied volume (0%, 36% and 52%). Based on the results, the presence of packages in the cabinet volume did not have a significant impact on the air velocity in the vertical rear duct. The velocity at all heights remained the same, whatever the loading percentage. This infers that the impact of slot-perforated density is more significant than the package-occupied volume as illustrated in **Figure 3.12**. The airflow distribution percentage decreased significantly with height because of a lower percentage of perforated area, while it changed indistinctly (<5% difference) whatever the percentages of product-occupied volume. It should be kept in mind that with respect to the design of the studied cabinet, a 10-mm gap from the PBP is spared so that products will not be completely placed against it to avoid product freezing.

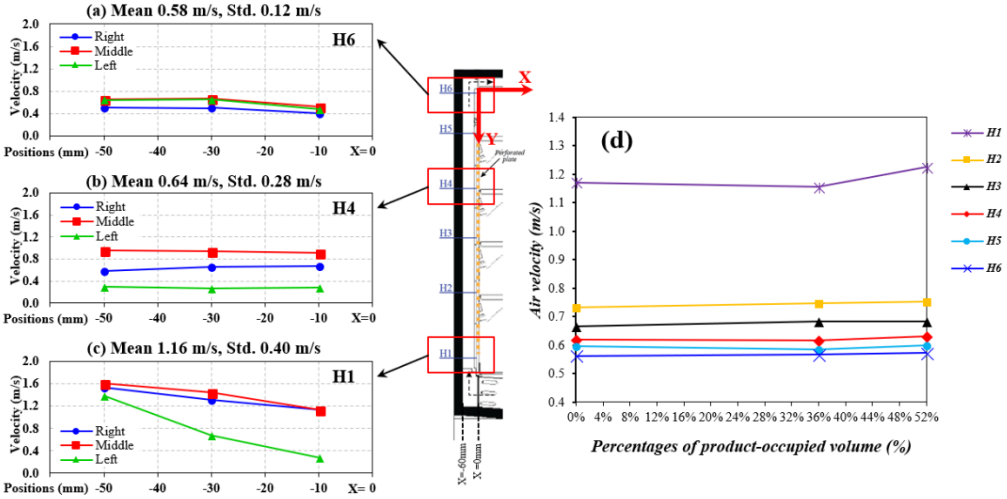


**Figure 3.11** Air velocity profiles on three different planes (a) left, (b) middle and (c) right at three heights along the vertical rear duct of the unloaded display cabinet, and (d) influence of percentages of product-occupied volume on the air velocity (average value of nine measurements at a given height)

Moreover, the flow distribution percentage from the DAG (air curtain) at the top was close to that from the PBP (about 50% in each case, i.e. a distribution ratio of 50%-50%). This ratio is lower than that recommended by Gray et al. (2008) and Wu et al. (2014) for an open display cabinet. According to these authors, a 70%-30% distribution of flow between the air curtain and the rear duct perforations was appeared to yield a high performance. The open display cabinet requires a higher airflow rate from the DAG to generate a sufficient and stable air curtain, since it is the only thermal barrier that protects the food storage zone from the environment compared with a closed display cabinet. Based on the results presented in **Section 3.3.2**, this ratio is acceptable.

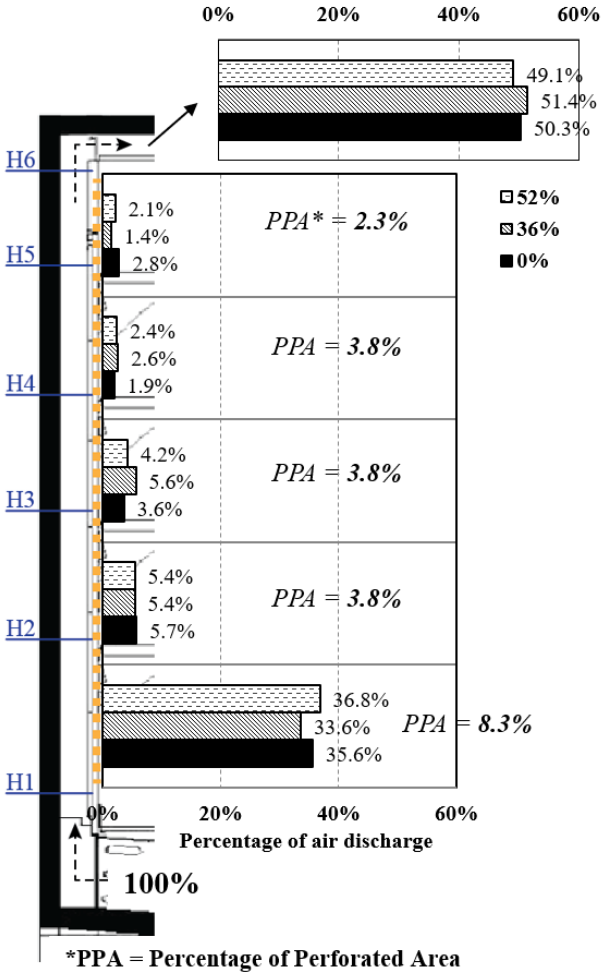


**Figure 3.12** Percentage of airflow distribution through the perforated back plate at the level of each shelf for different percentages of product-occupied volume (0%, 36%, and 52%)

## 3.4. Conclusions

The product and air temperature and velocity profiles in a closed display cabinet under unloaded and loaded conditions were experimentally investigated. The main objective was to analyze phenomena taking place during operation. The unloaded condition allows the principal understanding of thermal mechanisms in the equipment. Two periodic temperature fluctuations, small and large, were regularly observed, corresponding to the on/off compressor cycle and the defrosting cycle, respectively. The distribution of the time-averaged air temperature and its amplitude of fluctuation were analyzed at several positions. In the food storage zone under unloaded condition, the air temperature never exceeded 2 °C and the amplitude of fluctuation is tolerable (standard deviation of about 1 °C). At the back of the bottom shelf, a temperature below 0 °C (a mean temperature of about -0.4 °C) could lead to freezing problems. The observed trends could be qualitatively explained by heat losses and the thermal inertia of the elements of the display cabinet. Under the same room condition, lower mean air temperature and less temperature heterogeneity were observed in the storage zone of the closed display cabinet compared to the open one. Regarding the closed condition, the ambient temperature has an almost linear influence on the internal air temperature (when using the thermostat temperature as the reference). It also influences the energy consumption of the display cabinet.

A further study on the closed refrigerated display cabinet loaded with test products was experimentally investigated. The consistent temperature profiles were found under loaded and unloaded conditions. The front of the top shelf exposed to the highest temperature, whereas the back of the bottom shelf exposed to the lowest temperature. By comparing to the cabinet without doors, the result confirms that closed display cabinet can achieve better temperature performance.

The air velocity was measured by a hot wire anemometer; the results show that the air curtain is deviated toward the door by a Coanda effect. The flow between the shelves is far from plug flow because of the interaction between the air flowing through the PBP and the air curtain.

The occupied volume in the cabinet storage domain has no significant impact on the airflow rate from the PBP when a small gap is spared between the back products

and the PBP. The air distribution between the DAG and the perforated plate is found to be split into two equal airflow rates.

In future research, the influence of the operating conditions (door opening frequency, occupied volume, etc.) on the product and air temperatures as well as on the air velocity will be studied. Laser Doppler Velocimetry (LDV) and/or Particle Image Velocimetry (PIV) will be used to map the velocity profiles in the display cabinet to overcome the limitations of hot-wire anemometer measurements due to complex flows. These experimental results will then be used to validate a simplified heat transfer model based on a zonal approach which requires less computer resources and calculation time compared with Computation Fluid Dynamics (CFD) simulation. The developed model will be integrated into those already developed for other equipment such as a food production plant (Lecoq et al., 2016), a refrigerated truck (Hoang et al., 2012), a cold room (Laguerre et al., 2015) and a domestic refrigerator (Laguerre and Flick, 2010), and will make it possible to acquire knowledge of the product time-temperature history throughout the cold chain.

# Chapter IV

# Influence of operating conditions on the thermal performance

# Influences of operating conditions on the temperature performance of a closed refrigerated display cabinet

**Nattawut Chaomuang**, Alain Denis, Denis Flick and Onrawee Laguerre

Published in *International Journal of Refrigeration* (2019), 103, pages 32-41

**Abstract**

An experimental study was performed in order to investigate the effects of operating conditions, including door opening frequency, ambient air temperature and product-occupied volume, on the air and product temperature distributions inside a closed refrigerated display cabinet. The product position in the cabinet is a determining factor of its temperature: a high temperature was observed at the front, particularly at the top of the cabinet, and a low temperature was observed at the back. Air infiltration due to door openings caused a product temperature increase at the front and a temperature decrease at the back. At a higher door opening frequency (more than 60 openings per hour per door), the product temperature at the level of the front middle shelf was the most affected. Both the ambient temperature and occupied volume also affected product temperature variations in the closed display cabinet. In comparison to an open display cabinet, a closed display cabinet achieves lower product temperature and better temperature homogeneity, even with a high door-opening frequency. These findings indicate that the use of closed refrigerated display cabinets should be advocated in order to achieve better food preservation.

***Keywords*:** Closed refrigerated display cabinet; Door-opening frequency; Experimental study; Thermal performance; Temperature

**Nomenclature**

| | |
|---|---|
| $A$ | area [$m^{-2}$] |
| $H$ | opening height [m] |
| $T$ | temperature [°C] |
| $\overline{u}$ | mean air velocity [$m \cdot s^{-1}$] |
| $\delta_c$ | characteristic time [s] |
| $\theta$ | dimensionless temperature $= \frac{\overline{T}-\overline{T}_{th}}{T_e-\overline{T}_{th}}$ [-] |
| $\rho$ | density [$kg \cdot m^{-3}$] |

*Subscripts*

| | |
|---|---|
| $a$ | air |
| $e$ | external ambient |
| $init$ | initial |
| $jet$ | air curtain |
| $p$ | product/package |
| $th$ | thermostat |

*Abbreviations*

| | |
|---|---|
| DAG | Discharge Air Grille |
| OPH | Number of door Openings Per Hour |
| PBP | Perforated Back Panel |
| RAG | Return Air Grille |

## 4.1. Introduction

Poor temperature control is often observed in open refrigerated display cabinets which are widely used in retail stores (ASHRAE, 2010). In open cabinets, a stable and homogeneous storage temperature is difficult to maintain since an air curtain alone is used to protect food products from the ambient surroundings, resulting in significant infiltration of warm and humid air (Gaspar et al., 2011). Air infiltration is frequently cited as one of the major factors causing temperature heterogeneity (Laguerre et al., 2012) and high energy consumption (Tassou et al., 2011). Temperature variations of up to 5 °C between locations within the cabinet were observed (Willocx et al., 1994); the products in the front areas were usually exposed to a high temperature, whereas the products at the back were at lower temperatures (Evans et al., 2007). A great deal of research has been carried out using both experimental investigations (Chen and Yuan, 2005; Gray et al., 2008) and numerical simulations (Field and Loth, 2006; Moureh and Yataghene, 2016) in order to maximize the air curtain efficiency, thereby enhancing the overall

performance of open display cabinets. In addition to efforts designed to improve the air curtain efficiency, a novel short air curtain design was proposed (Hammond et al., 2016). In this study, multiple short air curtains used for each shelf provided enclosure of the front of the cabinet, rather than a single long air curtain. The experimental results showed that beyond potential energy savings, a more uniform temperature distribution can be achieved. A review of the current usage situation and attempts to improve the performance of refrigerated display cabinets can be found in Chaomuang et al. (2017). Despite many improvements over the last few decades, higher display cabinet efficiency remains a necessary research topic for sustainable retail refrigeration (Al-Sahhaf, 2011).

Installation of doors on open-front display cabinets has become an alternative designed to address the air infiltration issue. It has been proven that the closed display cabinet achieves several favorable outcomes including energy savings of 20-70% (Faramarzi, 1999; Fricke and Becker, 2010; Kauffeld, 2015; Navigant Consulting Inc., 2009), reductions in internal temperature heterogeneity (Chaomuang et al., 2019; Evans and Swain, 2010; Lindberg et al., 2010), and improved food quality (Atilio de Frias et al., 2015). Moreover, doors can also provide better thermal comfort in retail stores due to less cold air spillage from the display cabinet (Lindberg et al., 2017). Given these benefits, doors have been installed to an increasing extent in various countries. An agreement between the French authorities and the major supermarket stakeholders aims to replace open display cabinets by closed display cabinets, and to ensure that by 2020, 75% of all display cabinets in use will be closed models (RPF, 2016).

In contrast to the energy consumption aspect, the temperature performance of closed refrigerated display cabinets is seldom investigated, particularly in terms of spatial and temporal temperature variations. A comparative investigation conducted by Evans and Swain (2010) revealed that the temperature variations within closed cabinets were lower than those within open cabinets. Lindberg et al. (2010) demonstrated that an overall air temperature reduction of at least 2 °C was achieved when the display cabinet was retrofitted with doors. Atilio de Frias et al. (2015) observed a substantial decrease in the spatial temperature differences of almost 6 °C and underscored the better visual quality and lower decay rate of minimally-processed vegetables achieved by the installation of doors on display cabinets.

An experimental analysis of heat transfer and airflow in a closed refrigerated display cabinet under closed conditions was performed in our previous study (Chaomuang et al., 2019). The knowledge acquired provides an insight into the thermal exchange mechanisms taking place in the equipment. It was found that convection and conduction were the predominant heat transfer modes, while radiation was rather weak due to the presence of low-emissivity coating materials on the glass doors. In addition, the main causes of air and product temperature variations in closed display cabinets are air infiltration through the door gaps and the proximity to the cabinet lighting. The authors highlighted that closed display cabinets can achieve better temperature performance in comparison with open cabinets.

As much greater air infiltration occurs during door openings than through the door gaps when the cabinets are closed, the opening frequency plays an important role in the performance of closed display cabinets. Lindberg et al. (2010) found that when the opening frequency increased from 10 to 30 openings per hour (OPH), the heat extraction rate of the heat exchanger increased by 16%, while the difference between the maximum and minimum product temperatures ($\Delta T = T_{\max} - T_{\min}$) increased from 2.7 °C to 3.0 °C. Orlandi et al. (2013) numerically highlighted the influence of this factor on the energy consumption of the closed display cabinet. Their results showed that this factor becomes the predominant factor determining the refrigeration load when an opening frequency of 60 OPH is applied. To the best of our knowledge, the influence of the door-opening frequency on the temperature distribution (spatial and temporal) had rarely been studied.

The present study aims to investigate the influence of operating conditions, i.e. the frequency of door openings, ambient temperature and percentage of occupied volumes, on the thermal performance of a closed refrigerated display cabinet. This performance was evaluated using air and product data for design improvements and the practical handling of closed refrigerated display cabinets in supermarkets.

## 4.2. Material and methods

### *4.2.1. Closed refrigerated display cabinet*

The closed refrigerated display cabinet was placed in a test room in which the ambient temperature was controlled at 19.4 °C (with a standard deviation of 0.5 °C)

and the air humidity varied between 0.007 and 0.009 kg water/kg dry air. As shown in **Figure 4.1a**, the test room was equipped with 2 fans to homogenize the room temperature. To avoid the influence of airflow in the room on the measured value inside the cabinet, the rear of the display cabinet was located against these fans. **Figure 4.1b** depicts the closed refrigerated display cabinet (Offlip 2 Eco 125S, Costan) used in the study, which had external dimensions (width × length × height) of 650 mm × 1310 mm × 1980 mm and internal dimensions of 525 mm × 1250 mm × 1345 mm. The cabinet is an integral-type cabinet which is designed to meet the requirements of cabinet class M1 and climate class 3, i.e. product temperature varies between -1 °C and +5 °C for an ambient temperature of 25 °C and a relative humidity of 60% (EN ISO 23953-2, 2015). Two hinged doors (620 mm × 1330 mm) and the lateral walls are made of a double-glazed window with 22-mm thickness in which a 14-mm air gap filled with 90% argon gas is sandwiched between two panes of 4-mm tempered glass. The glass panes are also coated with a low-emissivity material to avoid the transmission of infrared radiation. There are 8-mm gaps between the door and the lateral wall of the cabinet to assist door openings.

There are five shelves from the top (Shelf 1) to bottom (Shelf 5) in the display cabinet. The space above Shelves 1 to 4 (350 mm in width × 1250 mm in length) is 225 mm, while that above Shelf 5 (475 mm × 1250 mm) is 345 mm (**Figure 4.1**). These spaces between shelves represent a total storage volume of about 0.60 $m^3$ in the display cabinet.

Different perforation patterns and percentages of the perforated back panel (PBP) are allocated to each shelf as illustrated **Figure 4.1**. The percentage of perforated area (PA) over Shelf 1 is the lowest (2.3%) as there is no perforation in the center. For the intermediate shelves (Shelves 2-4), the same percentage of 3.8% is applied, while more refined perforation is applied Shelf 5 with the highest percentage, 8.3%.

Air is cooled down and flows upwards along the vertical rear duct after flowing through a finned-tube heat exchanger by means of two propeller fans underneath the bottom shelf as schematically illustrated in **Figure 4.1**. Because of the different percentages of the PBP on each shelf, different air flow rates into the shelves-storage space were observed (Chaomuang et al., 2019). Another part of the air flows upward until it reaches a discharge air grille (DAG). Here, an air curtain homogenized using a honeycomb is established, providing protection of products

located at the front of the cabinet. Some of the air flowing from the PBP mixes with the air curtain and flows downward to a return air grille (RAG) to be cooled down and returned to the display cabinet.

### *4.2.2. Temperature measurement*

Test packages made of methylcellulose (width × length × height: 100 × 50 × 200 mm) were loaded in the display cabinet of which the total storage volume was 60% occupied (**Figure 4.1**). Calibrated T-type thermocouples (200 µm diameter, uncertainty of ±0.2 °C) were installed at various positions in the cabinet for the air temperature measurements. Some of them were inserted into the geometric center and/or attached onto the surface of the test packages using aluminum tape for product temperature measurements. Air and product temperatures were recorded using a data acquisition system (Agilent 34970A) at an interval of 10 seconds after the beginning of testing. The time-averaged temperature of both air and products was then calculated over a 5-hour (quasi)-steady state period in which the defrosting period was excluded from the calculation.

### *4.2.3. Door-opening regime*

#### *4.2.3.1. Automatic door opening*

Two cabinet doors are assigned to an automatic 12-hour door-opening regime by using a programmable apparatus to control the frequency of door openings. The baseline of the door-opening experiment consists in opening each door for three minutes to simulate stocking and replenishing activities as illustrated in **Figure 4.2**. Each door is then open in sequence with respect to a frequency of 10 openings per hour (OPH) with a full opening angle of 90° for a duration of 15 seconds (one second to open the door, 13 seconds holding time and one second to close the door). According to this defined frequency, the door opening takes place every 3 minutes, i.e. at 0 min. the right door is open, at 3 min. the left door is open, at 6 min. the right door is open, at 12 min. the left door is open and so on (see **Figure 4.2**). It is important to note that this door-opening regime is programmed as prescribed in the standard test (EN ISO 23953-2, 2015).

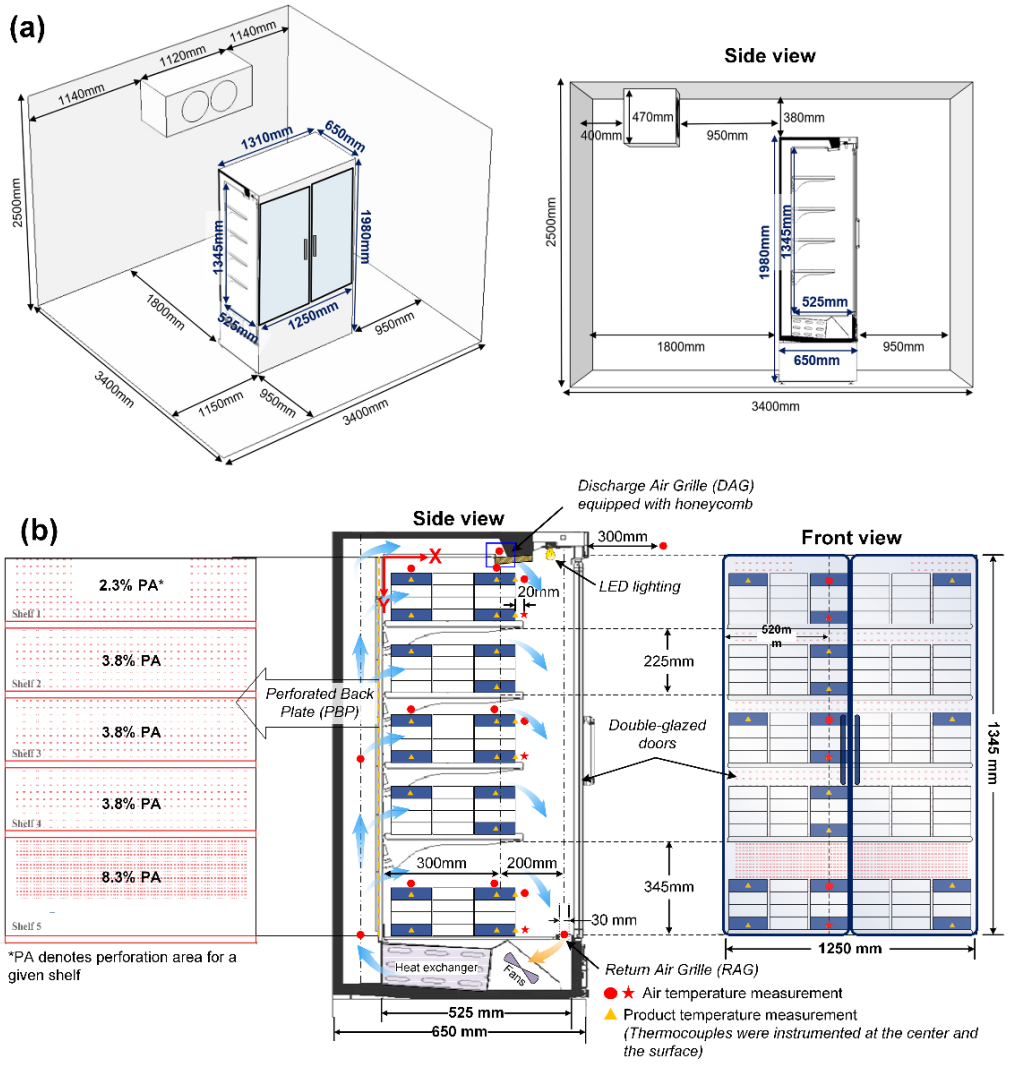


**Figure 4.1** (a) Location of the closed refrigerated display cabinet in the climate-controlled room (b) diagram showing the experimental setup for air and product temperature measurements inside the display cabinet

### *4.2.3.2. Experimental procedure*

After temperature stabilization, the closed display cabinet operated for three periods, each of a duration of 12 h. The display cabinet lighting and the room lighting were switched off for the first period. The lighting was then switched on and the automatic door-opening system was started for the second period. After the end of the door-opening experiment, the doors were closed while the lighting remained on. Air and product temperatures were recorded throughout the three periods, and the time-averaged values were calculated as described in **Section 4.2.2**.

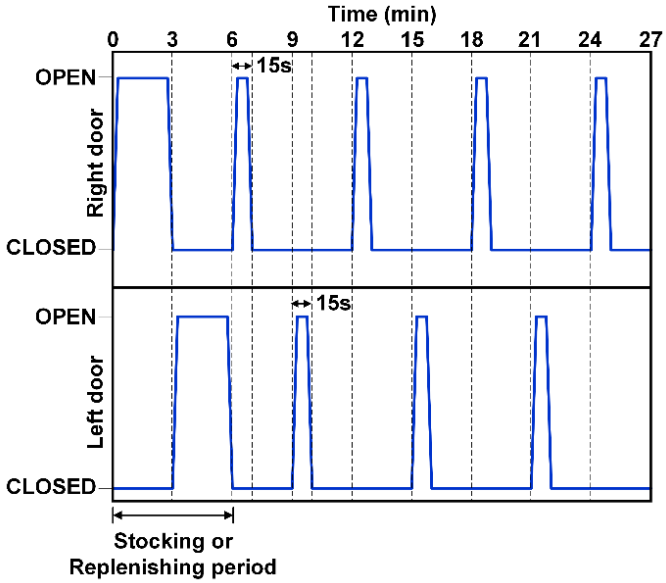


**Figure 4.2** Algorithm of automatic door openings

### *4.2.4. Variations in operating conditions*

Air and product temperature measurements were carried out in the closed refrigerated display cabinet. The operating conditions of these measurements are summarized in **Table 4.1**. The experiment carried out at an ambient temperature of 19.4 °C, with a door-opening frequency of 10 OPH, and 60% total occupied volume (considered as full load) was then assigned to be a baseline for analysis of the influence of operating conditions on the thermal performance of the closed refrigerated display cabinet. It should be emphasized that when the influence of one factor was studied (e.g. door-opening frequency), the other factors were fixed (ambient temperature 19.4 °C and 60% of total occupied volume).

#### *4.2.4.1. Door-opening frequency*

In addition to the permanently closed doors and permanently open doors (door-opening frequency of 0 and ∞ respectively), the frequency of 10, 20, 40 and 60 OPH was programmed to study its influence on the air and product temperature distributions inside the closed refrigerated display cabinet. The duration of 15 s with the full opening angle of 90° was applied for all door-opening frequencies and the same experimental procedure (**Section 4.2.3.2**) was applied to all experiments. Based on data available in the literature (Fricke and Becker, 2010) and information provided by a display cabinet manufacturer, the average frequency of door openings is, respectively 6.3 and 12.1 OPH. The frequency of 60 OPH was therefore set as

an extreme condition as it is rarely encountered in reality. Note that the doors were completely removed from the display cabinet for the permanently open condition.

*4.2.4.2. Ambient temperature*

In addition to the room temperature of 19.4 °C considered as a baseline, the test room was controlled at different temperatures of 14.6 °C, 24.3 °C and 28.2 °C (with a standard deviation of less than 0.5 °C for all temperatures) to investigate its influence on the air and product temperatures in the display cabinet. The water content of the air in the test room varied from 0.008 to 0.013 kg water/kg dry air, corresponding to the variation in the relative air humidity of 50% and 75%, respectively. This small variation in water content in the air exerted little influence on the temperature performance, but it does affect the energy performance because of frost formation on the evaporator (Chen and Yuan, 2005). The same experimental procedure (**Section 4.2.3.2**) was applied in all experiments.

*4.2.4.3. Occupied volume*

Two occupied volumes were used in the experiments: 30% (considered as half load) and 60% (considered as full load). The difference in these occupied volumes concerns the number of layers of test packages in height only, while the arrangement remained the same (6 columns in width and 3 columns in depth, see **Figure 4.1**). The same experimental procedure (**Section 4.2.3.2**) was applied to all experiments.

**Table 4.1** Operating conditions in a closed refrigerated display cabinet

| Experiment | Door-opening frequency | Ambient temperature (STD) | Percentage of occupied volume |
|---|---|---|---|
| | [OPH[(d)]] | [°C] | [%] |
| 1[(a)] | 10 | 19.4 (0.5) | 60 |
| 2[(b)] | 0 | | |
| 3 | 20 | | |
| 4 | 40 | | |
| 5 | 60 | | |
| 6[(c)] | ∞ | | |
| 7 | 10 | 14.6 (0.5) | 60 |
| 8 | | 24.3 (0.3) | |
| 9 | | 29.2 (0.3) | |
| 10 | 10 | 19.4 (0.5) | 30 |

[(a)] Baseline; [(b)] Permanently closed; [(c)] Permanently open; [(d)] Number of openings per hour per door

## 4.3. Results and discussion

### *4.3.1. Evolution of air and product temperatures*

**Figure 4.3** shows the evolution of the air and product (core and surface) temperatures in the center plane (520 mm from the left wall) of the closed refrigerated display cabinet over the 36-h operation comprising 12 h of closed-door and lights off conditions, 12 h of door openings with a frequency of 10 OPH and lights on, and 12 h of closed-door and lights on conditions. During the closed-door periods, the air temperature fluctuation was almost identical and followed the on/off regulation of the compressor (with a duration of about 10 min.) and the defrosting operation (every 6 h with a duration of about 25 min.) as shown in **Figure 4.3a**. During the door openings, a larger amplitude of fluctuation in the air temperature was observed at the front of the cabinet (A1, A3 and A5).

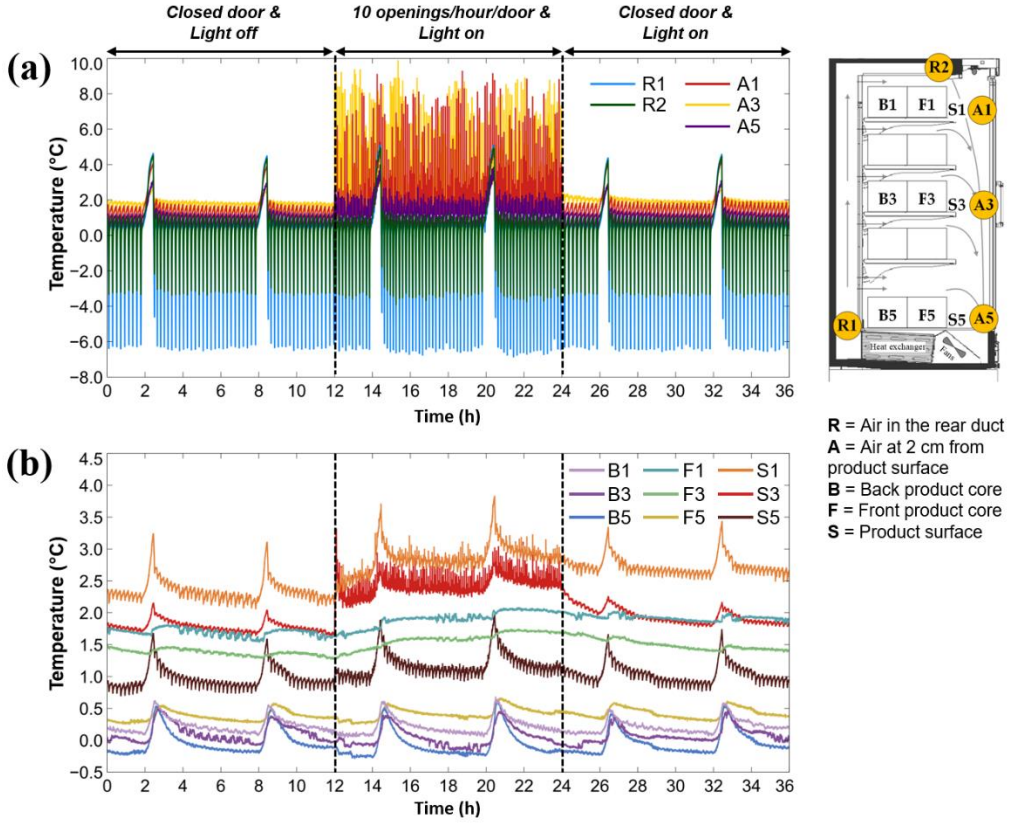


**Figure 4.3** Evolution of (a) air, and (b) product (core and surface) temperatures on the center plane of a closed refrigerated display cabinet over 36-hour operation for an ambient temperature of 19.4 °C.

The product temperature fluctuations during the closed-door periods were also subject to the on/off compressor and defrost operations; however, their amplitudes were much lower than that of the air (**Figure 4.3b**). During the door openings, the product surface temperature fluctuations became more pronounced on the top and middle shelves (S1 and S3). The surface temperature fluctuations on the bottom shelf (S5) and those of the core at the front (F1, F3 and F5) were less obvious despite a slight temperature increase. The door-opening frequency (10 OPH) exerted an insignificant effect on the average temperatures and the temperature fluctuations of the products at the back (B1, B3 and B5).

To ascertain the thermal phenomena during the door openings, additional air temperatures at the A1, A3 and A5 positions were recorded with more frequent data acquisition (a time interval of 1 s). After 24 h of temperature stabilization, recording of the door-opening cycles with a frequency of 10 OPH was undertaken for 12 h.

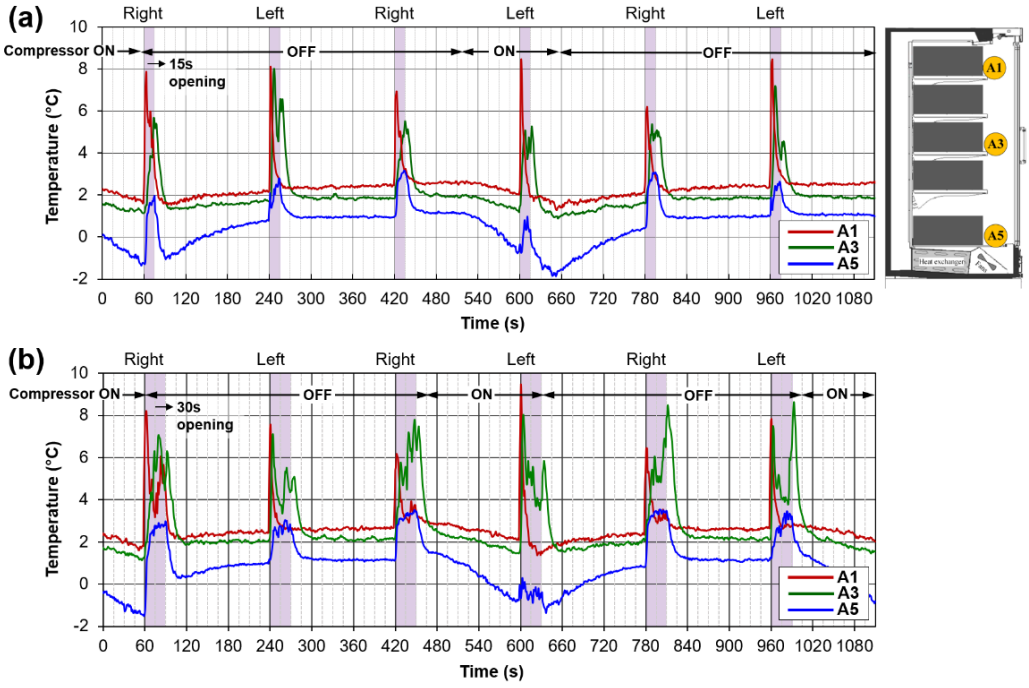


**Figure 4.4** Air temperature evolution at 2 cm from the front product surface on the center plane of the closed display cabinet during 6 door openings (10 OPH frequency) with (a) 15 s and (b) 30 s opening durations (acquisition interval of 1 s)

**Figure 4.4a and b** show the air temperature evolution during 6 door openings (3 openings for the right and left doors sequentially) with 15 s and 30 s opening durations, respectively. The effect of door openings can be observed during the second part of compressor "off" periods (240 < t < 420s and 780 < t < 960s in **Figure 4.4**) since the air temperature is rather constant when the door is closed. For both opening durations, the air temperature increased (from its initial value $T_{init}$) as soon as the door was opened, and then dropped gradually to the normal state (variation with the on/off compressor operation) when the door was closed. The magnitude of temperature increase ($\Delta T_{max} = T_{peak} - T_{init}$) and time to reach the peak ($T_{peak}$) vary with the position. On the top shelf (A1, red line in **Figure 4.4a and b**), after the door was opened, the air temperature rapidly reached a peak ($\Delta T_{max} \cong 6.5$ °C), then decreased to the normal state within a few seconds even though the door remained open. This is because the air curtain was destabilized during the door opening, then it tended rapidly to stabilize while the door was completely open. The time required for the air curtain to stabilize again (at the top shelf) is the same order of magnitude as the characteristic time which can be calculated from of the opening height of the cabinet ($H$ =1.3 m) and the air velocity at the DAG ($\overline{u}_{jet}$ = 0.60 m·s$^{-1}$), i.e. $\delta_c = \frac{H}{\overline{u}_{jet}}$ ($\delta_c$ = 2.2 s for the studied cabinet). When a perturbation occurs in front of the top shelf, this perturbation is convected up to the RAG and the time needed is approximately $\delta_c$.

At further downstream: on the middle shelf, after the left door was opened, the air temperature (A3, green line in **Figure 4.4a and b**) increased to the peak ($\Delta T_{max} \cong$ 6.3 °C) over a relatively longer time interval compared with the air at the level of the upper shelf (A1, closer to the DAG), then dropped. Nonetheless, after the door was closed, the air temperature increased again, and it took about 10 s to reach equilibrium. The second temperature increase can be explained by the door closure movement, which forces warm external air into the cabinet. Smooth door closings could reduce this temperature increase. A different air temperature evolution at this position (A3) was observed when the right door was opened. Based on the opening procedure of 15 s and 30 s, the air temperature tended to increase gradually and seemed not to decrease until the door was closed.

A gradual increase in the air temperature on the bottom shelf (A5, blue line in **Figure 4.4a and b**) was always observed ($\Delta T_{max} \cong 3.2$ °C), regardless of the door (left or right) which was opened. The air temperature decreased and reached the normal state only after the door had been closed. The longer the duration of the door opening (30 s, **Figure 4.4b**), the higher the air temperature at this position.

Time-averaged air and product (core and surface) temperatures were calculated over 5 h in the quasi-steady state (excluding the defrost period) of each operating period (closed door-lights off, open door with a frequency of 10 OPH-lights on, and closed door-lights on) and reported in **Figure 4.5**. It is noteworthy that the time-averaged temperatures during the door openings were calculated over 5 hours between two defrost cycles to respect the quasi-steady state condition (temperature during defrost cycles was excluded from the calculation).

On the whole, the average air and product temperatures at most positions were not significantly different between lights on and off conditions when the doors were closed (**Figure 4.5a and c**). The illumination effect is only significant at the front of the top shelf due to the proximity to the cabinet lighting.

During the door-opening period (**Figure 4.5b**), the average air temperature was slightly lower in the rear duct (about 0.1 °C) and higher at the front (up to 0.9 °C). External warm air infiltration into the cabinet during the door openings explained an increase in the air temperature at the front. According to the air temperature increase, the compressor working cycles became more frequent, thereby lowering the air temperature in the rear duct. Compared with the closed-door periods, the number of compressor working cycles during the door openings was approximately 18% greater. Each door opening caused an increase in product temperatures at the front and a decrease in those at the back (**Figure 4.5b**). This resulted in a greater temperature difference between the front and the back products on the shelf. Overall, the product temperature distribution in the closed display cabinet was consistent for every period. The highest temperature position was at the front of the top shelf and the lowest temperature position was at the back of the bottom shelf. The top shelf was also the position at which the front and the back products had the maximum temperature difference.

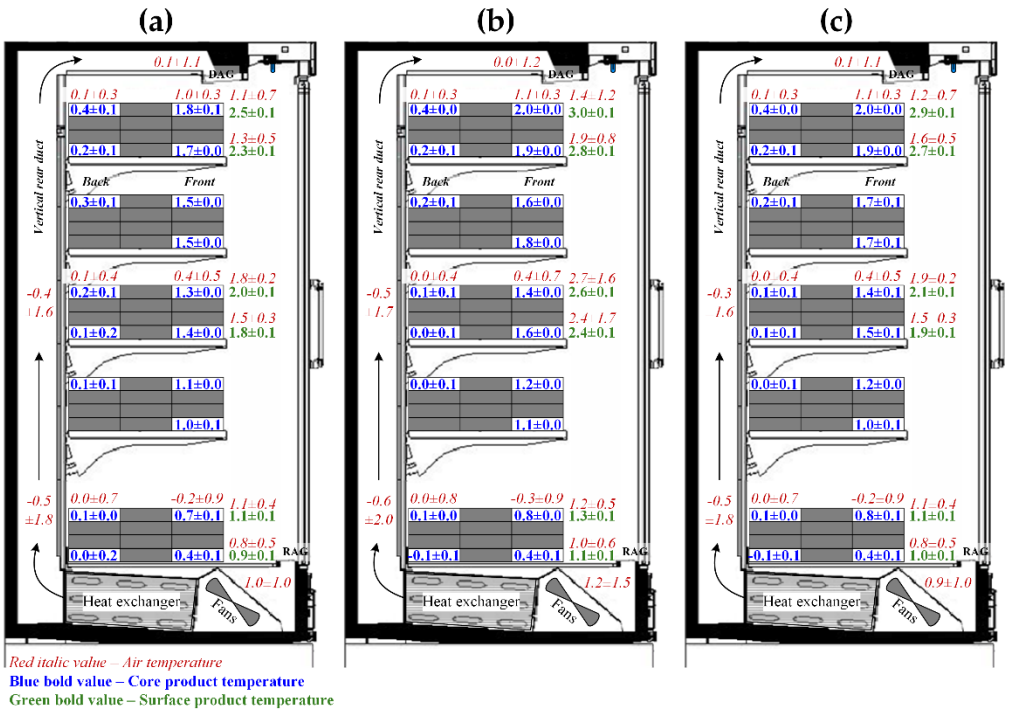


**Figure 4.5** Time-averaged (± standard deviation in °C) air and product temperatures in the closed refrigerated display cabinet for an ambient temperature of 19.4 °C during (a) closed door – light off, (b) open door with a frequency of 10 OPH – light on, and (c) closed door – light on conditions. Values are the average over 5 hours of quasi-steady state

Because there were additional heat losses through the lateral glass walls, the product core temperature at the sides was higher than that at the center (**Table 2**). It should be emphasized that the measurement of product core temperatures at the side was taken at a distance of 100 mm from the lateral wall since 1-kg test packages were used in the study. There will be a tendency to observe higher temperatures at the sides in the EN23953 test because 500-g test packages (width × length × height: 100 × 50 × 100 mm) are usually used and the measurement is performed at a distance of 50 mm from the wall.

**Table 4.2** Effect of lateral glass wall on the product core temperature in the closed display cabinet

| Plane | Time-averaged product core temperature† [°C] | | |
|---|---|---|---|
| | F1 | F3 | F5 |
| Left | 3.0 | 2.3 | 1.5 |
| Center | 2.0 | 1.4 | 0.8 |
| Right | 3.6 | 3.5 | 3.3 |

†Average (top package on the stack) over 5 h of quasi-steady state excluding the defrost period.

### *4.3.2. Effect of door-opening frequency*

Different door-opening frequencies were applied to the closed display cabinet to investigate their effects on the time-averaged temperatures at different locations in the cabinet. The air and product temperatures at any given position inside the display cabinet are influenced by the operating conditions. Theoretically, these temperatures should be high when the ambient temperature and the door opening frequency are high. However, in practice, under such conditions (high ambient temperature and high door opening frequency), the compressor operates at a greater frequency (shorter "off" cycle) to compensate for thermal loads in the cabinet to a greater extent. Thus, the time-averaged air temperature after the heat exchanger (where the thermostat sensor is located: $\overline{T}_{th}$) is lower, and this leads to lower air/product temperatures at the back and higher temperatures at the front. To overcome this complexity and to enable comparison of temperatures obtained from different operating conditions, the dimensionless temperature ($\theta_i$) was defined (**Eq. 4.1**) by taking the time-averaged temperatures of external ambient air ($\overline{T}_e$) and of supply air just after the heat exchanger ($\overline{T}_{th}$) as references. In this manner, the dimensionless temperature at a given position was not influenced by the ambient temperature and the supply air temperature which decreased when the door-opening frequency increased.

$$\theta_i = \frac{\overline{T}_i - \overline{T}_{th}}{\overline{T}_e - \overline{T}_{th}} \tag{4.1}$$

**Figure 4.6** shows the dimensionless product core temperatures ($\theta_p$) at the front and the back of the closed display cabinet for door-opening frequencies of 0, 10, 20, 40 and 60 OPH. The value ∞ represents the permanently open condition in which the doors were completely removed. As shown in **Figure 4.6a**, it was observed that $\theta_p$ at the front of all shelves increased with an increase in the door-opening frequency. When the door-opening frequency was less than 40 OPH, $\theta_p$ was the highest at the level of the top shelf (F1) and it was the lowest at the bottom (F5). Beyond this frequency, the door opening resulted in a relatively smaller increase in $\theta_p$ at the top shelf (F1), as compared to its effect on the product at the level of the lower shelves (F2 and F3) for which $\theta_p$ became the highest. This can be explained by the fact that the products at these positions (F2 and F3) are the most influenced by the introduction of external warm air when the door is open as observed in the open

display cabinet (Laguerre et al., 2012). Warm air infiltration during door openings is enhanced by the vortices which form in the mixing layer of the air curtain. At the level of the lower shelves (F4 and F5), $\theta_p$ remained relatively lower (**Figure 4.6a**) because there was more cold air flowing from the back through the PBP into these shelves.

The small effect of the door-opening frequency on $\theta_p$ was observed at the back **(Figure 4.6b)**. When the door-opening frequency varied from 0 to 40 OPH, $\theta_p$ at the back of all shelves increased slightly and was steady when the door-opening frequency increased from 40 to 60 OPH. However, when the doors were permanently open, $\theta_p$ at the back of Shelves 1-3 (B1, B2 and B3) tended to increase, while it seemed to change only slightly for the product at the level of the lower shelves (B4 and B5). This is because the back product mainly exchanges heat with the air flowing through the PBP, of which the temperature is practically uninfluenced by the external ambient temperature.

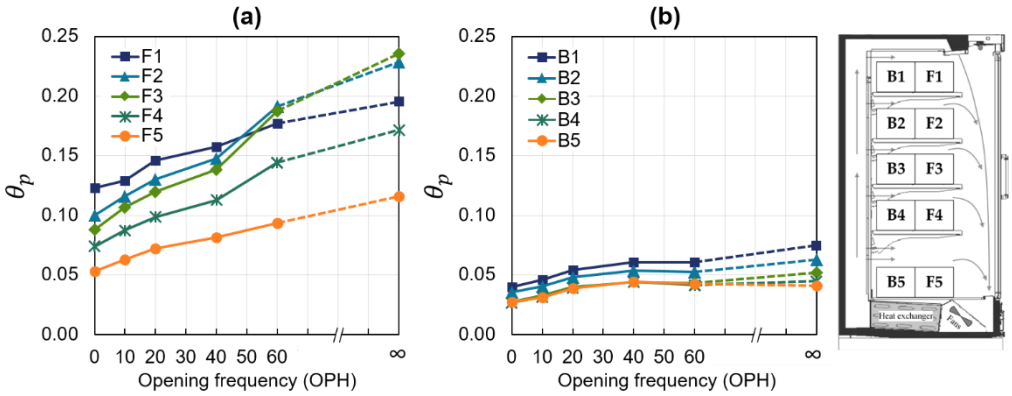


**Figure 4.6** Effect of door-opening frequency on the dimensionless product core temperature (a) at the front, and (b) at the back of the five shelves

Despite a very high door-opening frequency (60 OPH), the closed refrigerated display cabinet achieves somewhat better temperature homogeneity compared with the cabinet without doors (**Table 4.3**): the average product core temperatures both at the front and the back of the display cabinet where a door-opening frequency of 60 OPH was applied remained lower than those under permanently open conditions. This difference was more pronounced when the surface temperature was considered, particularly at the front of Shelf 3 (5.1 °C for 60 OPH and 8.7 °C for permanently open). Regarding the field investigation by Fricke and Becker (2010),

it was found that the daily mean door-opening frequency was only 6.3 OPH with a mean opening duration of 12 s (the most frequent duration was 5 s). Based on these findings, food preserved in closed refrigerated display cabinets would be maintained under better temperature conditions, thereby prolonging the shelf life and reducing food loss.

**Table 4.3** Time-averaged product temperature† (in °C) at the back and front of the display cabinet with a door- opening frequency of 60 OPH and permanently open (without doors) condition for an ambient temperature of 19.4 °C and occupied volume of 60%.

| Shelf no. | 60 OPH | | | Permanently open | | |
|---|---|---|---|---|---|---|
| | Back | Front | | Back | Front | |
| | Core | Core | Surface | Core | Core | Surface |
| 1 (top) | 0.0 | 2.4 | 3.6 | 0.2 | 2.7 | 4.7 |
| 2 | -0.2 | 2.7 | - | 0.0 | 3.4 | - |
| 3 | -0.4 | 2.6 | 5.1 | -0.3 | 3.6 | 8.7 |
| 4 | -0.4 | 1.7 | - | -0.4 | 2.2 | - |
| 5 (bottom) | -0.4 | 0.7 | 1.6 | -0.5 | 1.1 | 2.0 |

†Average (top and bottom packages on the stack) over 5 h of quasi-steady state excluding the defrost period; the standard deviation was 0.1 °C for all positions under both conditions.

In addition to the temperature performance, the closed refrigerated display cabinet also shows energy saving potential. Based on the total period of a complete compressor working cycle, the time fraction during the compressor "on" period increased from 23% for the closed-door condition to 25%, 32%, 37% and 44% for the door-opening frequencies of 10, 20, 40 and 60 OPH, respectively. The time fraction was 63% in the case of the cabinet without doors.

### *4.3.3. Effect of ambient temperature*

Air and product temperature measurements in the closed refrigerated display cabinet were conducted for four different ambient temperatures (see **Table 4.1**) while a door-opening frequency of 10 OPH and an occupied volume of 60% were applied in all experiments. The same dimensionless temperature ($\theta_p$) defined in the previous section was used, and the results are reported in **Figure 4.7**. It was observed that $\theta_p$ was almost independent of $\overline{T}_e - \overline{T}_{th}$ for the products at the front of the cabinet (**Figure 4.7a**), while it decreased a little for most products at the back (Shelf 2-5) when $\overline{T}_e - \overline{T}_{th}$ increased. This result is in agreement with that observed in our previous study (Chaomuang et al., 2019). Despite door openings, forced

convection and conduction, which are linear phenomena, heat transfer modes remain predominant in the closed display cabinet. Free convection and radiation from the external walls, which are non-linear phenomena, can explain the slight influence of $\overline{T}_e - \overline{T}_{th}$ on the dimension temperature. As reported in **Table 4.4**, when $\overline{T}_e - \overline{T}_{th}$ rose from 15.0 °C to 30.4 °C, on the average $\overline{T}_p - \overline{T}_{th}$ at the front and the back positions increased from 1.5 °C to 3.1 °C and from 0.5 °C to 0.9 °C, respectively. Under a door opening frequency of 10 OPH, the highest temperature position was at the front of the top shelf where $\overline{T}_{pf} - \overline{T}_{th}$ was approximately 14% of $\overline{T}_e - \overline{T}_{th}$. The lowest temperature occurred across the back of Shelf 3-5 where $\overline{T}_{pb} - \overline{T}_{th}$ was approximately 3% of $\overline{T}_e - \overline{T}_{th}$. These results highlight that the product temperature in a closed display cabinet is directly influenced by the external ambient temperature, and the front area is the position at which the products are the most exposed to a high temperature.

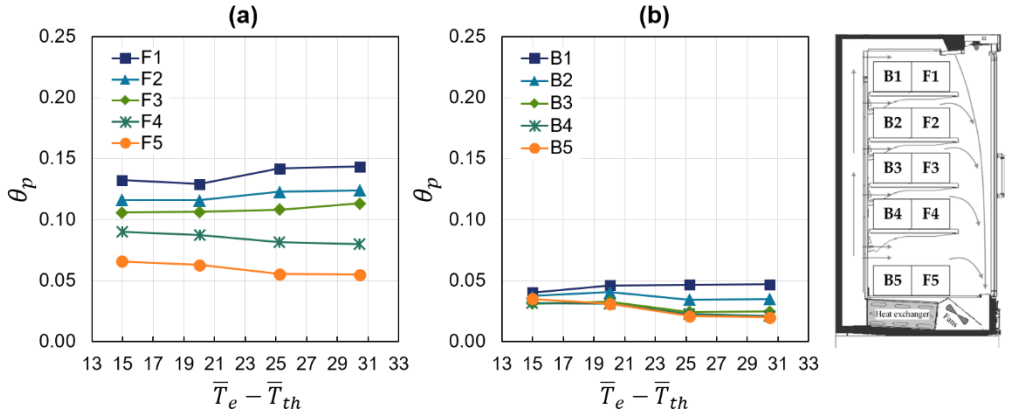


**Figure 4.7** Variation of dimensionless product core temperature ($\theta_p$) with the difference between the average of ambient air temperature $\overline{T}_e$ and of air temperature after the heat exchanger $\overline{T}_{th}$: (a) front products (b) back products (opening frequency of 10 OPH and occupied volume of 60%)

**Table 4.4** Effect of external ambient temperature ($\overline{T}_e$) on the product core temperature ($\overline{T}_p$) in the closed display cabinet.

| Temperature difference | $\overline{T}_e - \overline{T}_{th}$ | [°C] | 15.0 | 20.0 | 25.2 | 30.4 | Average |
|---|---|---|---|---|---|---|---|
| *Front product (pf)* | | | | | | | |
| Shelf 1 | $\overline{T}_{pf} - \overline{T}_{th}$ | [°C] | 2.0 | 2.6 | 3.6 | 4.4 | 3.1 |
| Shelf 2 | | | 1.7 | 2.3 | 3.1 | 3.8 | 2.7 |
| Shelf 3 | | | 1.6 | 2.1 | 2.7 | 3.4 | 2.5 |
| Shelf 4 | | | 1.3 | 1.7 | 2.1 | 2.4 | 1.9 |
| Shelf 5 | | | 1.0 | 1.3 | 1.4 | 1.7 | 1.3 |
| **Average** | | | **1.5** | **2.0** | **2.6** | **3.1** | **2.3** |
| *Back product (pb)* | | | | | | | |
| Shelf 1 | $\overline{T}_{pb} - \overline{T}_{th}$ | [°C] | 0.6 | 0.9 | 1.2 | 1.4 | 1.0 |
| Shelf 2 | | | 0.6 | 0.8 | 0.9 | 1.1 | 0.8 |
| Shelf 3 | | | 0.5 | 0.7 | 0.6 | 0.8 | 0.6 |
| Shelf 4 | | | 0.5 | 0.6 | 0.6 | 0.6 | 0.6 |
| Shelf 5 | | | 0.5 | 0.6 | 0.5 | 0.6 | 0.6 |
| **Average** | | | **0.5** | **0.7** | **0.8** | **0.9** | **0.7** |

The cabinet doors were periodically opened with a frequency of 10 OPH and with 60% occupied volume.

### *4.3.4. Effect of occupied volume*

Two percentages of occupied volume in the closed display cabinet were studied: 30% and 60%. A door-opening frequency of 10 OPH and an ambient temperature of 19.4 °C were applied to both experiments. The same dimensionless temperature ($\theta_p$) defined in Section 3.2 was also used for analysis so that the variation in the air temperature after the heat exchanger ($\overline{T}_{th}$) due to different thermal loads was eliminated. As shown in **Figure 4.8** higher percentage of occupied volume leads to a decrease in product temperature at all positions. When the cabinet volume was occupied to a greater extent, the space above the product top surface became smaller, resulting in higher air velocity flowing from the back. Cold exchange between the air and the products was therefore enhanced. By knowing the air mass flow rate ($\dot{m}_{a,i}$, Chaomuang et al., 2019) and the area above the product for each shelf ($A_i$), the mean air velocity flowing from the back ($\overline{u}_{a,i}$) was estimated by

$$\overline{u}_{a,i} = \frac{\dot{m}_{a,i}}{\rho_a A_i} \tag{4.2}$$

where $i$ is the number of the shelf ranging from 1 (top) to 5 (bottom) and $\rho_a$ is the air density (1.28 kg·m$^{-3}$ at 0 °C). As shown in **Figure 4.9**, the air velocity above the products on Shelves 1-4 in the display cabinet with a 60% occupied volume could

be about 5 times higher than that with a 30% occupied volume. It was about 1.7-fold in the case of the bottom shelf. It should be borne in mind that the air velocity presented in **Figure 4.9** was an average value supposing plug flow which is seldom observed in a real cabinet (Chaomuang et al. 2019).

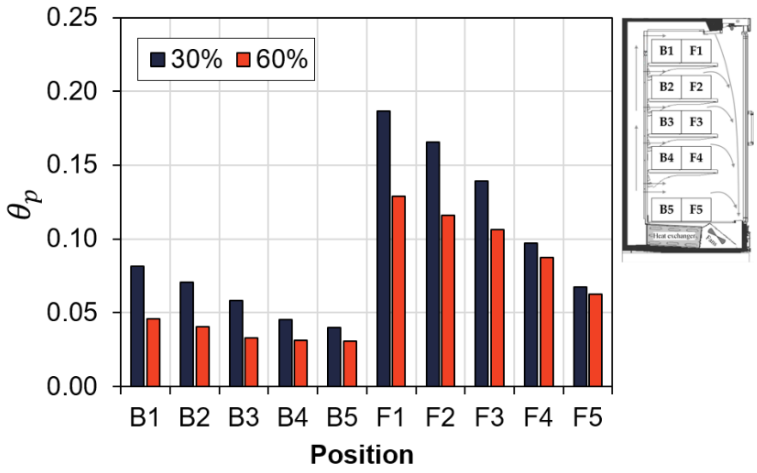


**Figure 4.8** Effect of occupied volume on the product temperature in the closed display cabinet (opening frequency of 10 OPH and ambient temperature of 19.4 °C)

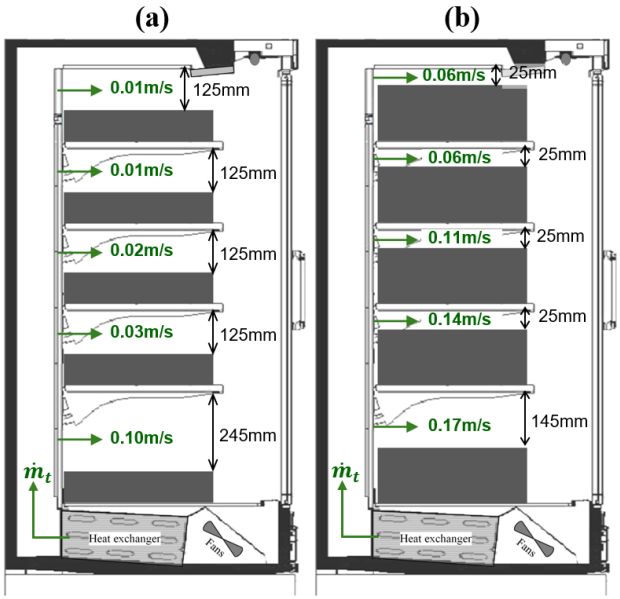


**Figure 4.9** Variation in air velocity above the products on different shelves in the closed display cabinet (1.25 m in length) for two occupied volumes: (a) 30%, (b) 60%.

## 4.4. Conclusions

Closed refrigerated display cabinets are increasingly used in retail stores because of their numerous advantages, particularly a considerable reduction in warm and

humid air infiltration, compared with open cabinets. In this study, air and product temperature measurements in the closed display cabinet were carried out under various operating conditions to evaluate the thermal performance of the cabinet including door-opening frequency, ambient air temperature and product-occupied volume. The product position in the cabinet is a determining factor of its temperature. The product at the front always had a higher temperature than that at the back, whatever the operating conditions, and that on the top shelf most often had the highest temperature. Higher door-opening frequency and/or higher ambient temperature result in a substantial increase in the product temperature at the front. The product temperature on the front middle shelf was the most affected when the door-opening frequency exceeded 60 OPH. On the other hand, each door opening causes a slight decrease in product temperature at the back because more refrigeration capacity was required to withstand higher thermal loads. Product-occupied volume also causes product temperature variations. A lower product temperature was observed at all positions when the cabinet volume was occupied to a greater extent. Overall, the closed refrigerated display cabinet fitted with doors provides better thermal performance, i.e. lower product temperature and more temperature homogeneity, as compared to the cabinet without doors despite a very high door opening frequency. Based on the time fraction of periods during which the compressor was operating, the closed refrigerated display cabinet also shows energy saving potential.

# Chapter V

# Airflow characterization using PIV and CFD techniques

# Experimental and numerical characterization of airflow in a closed refrigerated display cabinet using PIV and CFD techniques

**Nattawut Chaomuang**, Alain Denis, Denis Flick and Onrawee Laguerre

Submitted to *Journal of Food Engineering* (submitted)

A part of this work was also submitted to *Revue Générale du Froid*

---

**Abstract**

Air velocity measurements were carried out using the Particle Image Velocimetry (PIV) technique in a display cabinet under two configurations: closed and open doors. Two conditions (refrigeration system turned "on" and turned "off") were studied in the closed configuration. The airflow pattern was almost the same for both conditions. The air curtain was quite stable. In the upper part of the cabinet, air recirculation occurred, and this phenomenon induces external air infiltration through the door gaps. The air curtain in the open configuration (refrigeration system turned "off") was less stable than the closed configuration. Large unsteady eddies developed in the mixing layers, thereby promoting greater external air infiltration. A two-dimensional computational fluid dynamic (2D-CFD) model was developed and showed the ability to reproduce the main flow phenomena observed in the experiment. The trend of predicted product temperature profile was also in agreement with the experimental values, despite slight under-estimation.

***Keywords:*** Closed display cabinet; Air velocity; Experimental study; PIV; CFD

**Nomenclature**

| | |
|---|---|
| $A$ | area [$m^{-2}$] |
| $C_p$ | specific heat [$J \cdot kg^{-1} \cdot K^{-1}$] |
| $d_p$ | particle diameter [m] |
| $e$ | thickness [m] |
| $g$ | gravitational acceleration [$m \cdot s^{-2}$] |
| $k$ | turbulent kinetic energy [$m^2 \cdot s^{-2}$] |
| $\dot{m}$ | mass flow rate [$kg \cdot s^{-1}$] |
| $Pr$ | Prandtl number = $\frac{\mu C_p}{\lambda}$ [-] |
| $\dot{Q}$ | heat generation rate due to light absorption [$W \cdot m^{-2}$] |
| $Re$ | Reynolds number = $\frac{\rho_a \overline{V}_0 w_{\mathrm{DAG}}}{\mu_a}$ [-] |
| $Ri$ | Richardson number = $\frac{(\rho_e - \rho_a) g w_{DAG}}{\rho_e \overline{V}_0^2}$ [-] |
| $S$ | source term |
| $T$ | temperature [°C or K] |
| $V$ | velocity magnitude [$m \cdot s^{-1}$] |
| $\overline{V}$ | mean velocity magnitude [$m \cdot s^{-1}$] |
| $u, v$ | air velocity in $x$ and $y$ directions, respectively [$m \cdot s^{-1}$] |
| $u_p$ | settling velocity of particles = $\frac{g d_p^2 (\rho_p - \rho_a)}{18 \mu_a}$ [$m \cdot s^{-1}$] |
| $U$ | heat transfer coefficient [$W \cdot m^{-2} \cdot K^{-1}$] |
| $w$ | width [m] |
| | |
| *Greek symbols* | |
| $\Gamma$ | diffusivity coefficient [$m^2 \cdot s^{-1}$] |
| $\varepsilon$ | dissipation rate of $k$ [$m^2 \cdot s^{-3}$] |
| $\lambda$ | thermal conductivity [$W \cdot m^{-1} \cdot K^{-1}$] |
| $\mu$ | dynamic viscosity [Pa·s] |
| $\rho$ | density [$kg \cdot m^{-3}$] |
| $\sigma$ | dimensionless diffusion parameter [-] |
| $\upsilon$ | kinematic viscosity [$m^2 \cdot s^{-1}$] |
| $\phi$ | generalized variable |
| | |
| *Subscripts* | |
| $a$ | air |
| $ar$ | argon |
| $cli$ | cabinet light |
| $d$ | door |
| $e$ | external ambient |
| $eq$ | equivalent |
| $gap$ | gap |

| | |
|---|---|
| $gl$ | glass |
| $p$ | particle |
| $rli$ | room light |
| $rms$ | root-mean-square |
| $T$ | turbulent |

*Abbreviations*

DAG Discharge Air Grille
RAG Return Air Grille
PBP Back Perforated Panel

## 5.1. Introduction

About 66-77% of the total heat load of open refrigerated display cabinets used in supermarkets were attributed to the entrainment of ambient warm and humid air into the system (Gaspar et al., 2011; Tassou et al., 2011). To address this issue, numerous studies have been carried out using both experimental and numerical approaches. Chen and Yuan (2005) conducted experiments to evaluate the effects of several important parameters on the performance of an open display cabinet and proposed the thermal entrainment factor to characterize the air curtain efficiency. This factor was correlated to the Reynolds (*Re*) and Richardson (*Ri*) numbers which indicate the importance of momentum (depending on the discharge air velocity of the air curtain) and buoyancy effects, respectively. It was found that air entrainment was promoted when the momentum effect increased whereas it became less pronounced when the buoyancy effect was dominant. Because of the non-intrusive aspect and high spatial resolution accuracy, PIV measurement has become a technique used to study flow structures in various applications (Adrian, 2005). Field et al. (2002) implemented the PIV technique together with a hot wire anemometer to examine the entrainment characteristics of air curtains with an $Re$ range of 1500–8500 and an $Ri$ range of 0.13–0.58. The entrainment of ambient air was found to be dominated by eddies that engulfed the ambient air entering the air curtain and the development of these eddies was related to $Re$. The authors suggested that a decrease in $Re$ could reduce the amount of entrained air as long as the integrity of the air curtain was preserved. The effectiveness of the air curtain can also deteriorate as a result of external disturbances (Heidinger et al., 2015). Kaffel et al. (2015) performed experiments using both PIV and Laser Doppler

velocimetry (LDV) techniques to demonstrate the effect of external lateral airflow on the effectiveness of the air curtain in a reduced-scale model of a display cabinet.

Because of the difficulties involved in experimental implementation, several numerical studies on open display cabinets have been carried out (Cortella et al., 2001; D'Agaro et al., 2006; Laguerre et al., 2012a; Moureh and Yataghene, 2016). Ge and Tassou (2001) numerically studied the influence of design parameters and operating conditions on the air curtain performance: the width and length of the air jet, initial jet velocity (and turbulence), the position/dimensions of the return air grille (RAG). Foster et al. (2005) used a 3D-CFD model to study the airflow in an open refrigerated display cabinet. These authors found that the inclination of the discharge air grille (DAG) has a significant effect on the air curtain performance to protect food in storage zone and the optimum angle depends on the width and the air velocity of the curtain. Navaz et al. (2005) combined both experimental (PIV and LDV) and numerical (CFD Fluent) approaches to determine the effect of design parameters on the air entrainment across the air curtain of an open display cabinet. The turbulence intensity, the shape of the velocity profile at the DAG and $Re$ were found to be the most significant parameters influencing the amount of air entrainment. Based on these studies, optimal jet characteristics should be attained in order to maintain the insulating capacity of the air curtain. In addition to efforts designed to optimize air curtain efficiency, Hammond et al. (2016) proposed a new design featuring multiple short air curtains for each shelf rather than a single long air curtain and reported a reduction in electricity consumption of 35.9% and a smaller range of maximum and minimum product temperatures (a difference of 9.5 °C for the conventional design and 3.1 °C for the short air curtain design).

Display cabinets retrofitted with doors constitute an energy saving alternative because they reduce the infiltration of external warm/humid air. Several studies have shown that a closed display cabinet generates 23-73% energy savings (Evans, 2014; Fricke and Becker, 2010; Lindberg et al., 2010; Navigant Consulting Inc., 2009) and the presence of doors was found to have no impact on the sales volume (Fricke and Becker, 2010). Given these advantages, display cabinets with doors have become default specification for new stores opened by various major retailers in Europe (EIA, 2017) and will account for about 75% of total display cases in French supermarkets by 2020 (RPF, 2016). Faramarzi et al. (2002) reported that

retrofitting a display cabinet with glass doors reduced the total cooling load by 68% and the average product temperature by 0.2 °C. To the best of the authors' knowledge, the study of airflow in a closed display cabinet is rare even though door installation can affect the airflow pattern in display cabinets, which in turn influences the heat transfer and product temperatures (Faramarzi et al, 2002).

A review of the literature on experimental and numerical investigations of the performance of display cabinets was carried out by the authors (Chaomuang et al., 2017). An experimental study of heat transfer in a closed display cabinet was conducted and the effect of operating conditions on the product temperature was highlighted: room temperature, door-opening frequency and percentage of occupied volume (Chaomuang et al., 2019a, 2019b). In order to build on our previous studies, the objectives of this study were:

※ To conduct air velocity measurement in a display cabinet using the PIV technique. It is to be emphasized that the originality of our study is the measurement of unstable and low air velocity ($0 < V_a < 0.7$ m·s$^{-1}$) in closed and open cavities. Thus, several difficulties associated with implementation had to be overcome.

※ To analyze the airflow pattern of a closed display cabinet and to compare it with the airflow pattern in an open display cabinet. Thermal aspects based on the results obtained from the previous studies (Chaomuang et al., 2019a, 2019b) were discussed.

※ To develop a 2D-CFD model of a closed display cabinet in order to investigate the phenomena which could not be observed by the experiment.

The experimental and numerical methodologies developed in this study can be useful to scientists for understanding the phenomena and for the industry in order to improve the design under various operating conditions.

## 5.2. Materials and methods

### *5.2.1. Refrigerated display cabinet*

A closed refrigerated display cabinet (Offlip 2 Eco 125S, Costan) equipped with a single-band air curtain and two double-glazed glass doors was installed in a test room in which the temperature was controlled at 19 °C (**Figure 5.1**). The storage

space was composed of five shelves on which test product packages (made of methylcellulose) occupied about 60% of the total storage volume. Two propeller fans located under the bottom shelf provided air circulation within the display cabinet. After passing through an evaporator (situated behind the fans), air was blown along a vertical rear duct up to a discharge air grille (DAG) at which level the air curtain was located. This air curtain descends and covers the entire front area of the display cabinet. A perforated back panel (PBP) allowed horizontal airflow from the back to join the air curtain at the front. At the bottom of the display cabinet, the air was driven through a RAG, thus completing the airflow circuit. The characteristics of the cabinet and its components are given in **Table 5.1**.

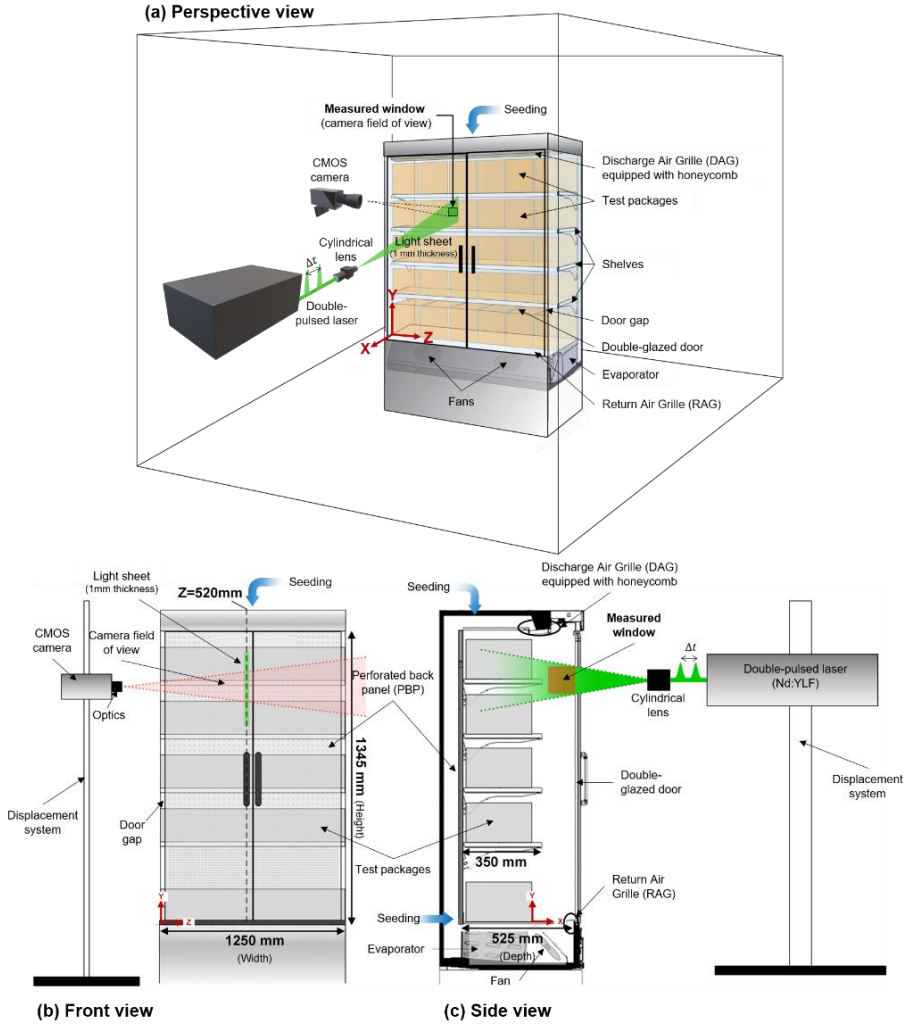


**Figure 5.1** Experimental setup for PIV measurement in a closed refrigerated display cabinet: (a) perspective view; (b) front view; and (c) side view

**Table 5.1** Characteristics of the closed refrigerated display cabinet used in the study

| | |
|---|---|
| Dimensions of the storage space (width × height × depth) | 1250 mm × 1345 mm × 525 mm |
| Dimensions of shelves<br>Shelves 1-4<br>Shelf 5 | <br>1250 mm × 25 mm ×350 mm<br>1250 mm × 25 mm × 475 mm |
| Dimensions of a test product package | 200 mm × 50 mm × 100 mm |
| Dimensions of a double-glazed door | 620 mm × 1330 mm × 22 mm |
| Discharge air grille width | 50 mm |
| Return air grille width | 30 mm |
| Dimensions of the perforated back panel (width × height × thickness) | 1250 mm × 1345 mm × 3 mm |
| Perforation percentage of the back panel (based on total panel area) | Shelf 1: 2.8%<br>Shelves 2-4: 3.8%<br>Shelf 5: 8.3% |
| Number of propeller fans | 2 |

To characterize experimentally the airflow pattern inside a closed display cabinet, two conditions were studied: the refrigeration system was turned "off" and "on", while the cabinet fans operated continuously under both conditions. In such a manner, the influence of fans alone (the first condition) and combined fans/refrigeration (the second condition) on airflow can be highlighted. In addition, the experiment was conducted in the display cabinet with the doors open, and the refrigeration system was turned off.

### *5.2.2. PIV measurements*

The air velocity measurement was performed using a two-dimensional PIV system (LaVision, FlowMaster 2D). The PIV system is composed of a double-pulsed Nd:YLF laser (527 nm wavelength, 10 mJ pulse energy, 0.2-20 kHz repetition rate), a 12-bit CMOS camera (HighSpeedStar 4G, 1024 × 1024 pixels in resolution) equipped with a lens (Sigma, 105 mm, f/1:2.8) and a programmable timing unit for the synchronization of the device. To achieve light scattering, fine droplets of distilled water generated by a fogging system (Areco, model OD V7, with a median droplet diameter of 7 µm) were injected at the top and the back of the display cabinet. The overall experimental setup is illustrated in **Figure 5.1**. PIV measurement was conducted on a center plane (z = 520 mm, **Figure 5.1b**) along the air curtain of the display cabinet. Image acquisition and post-processing were conducted using a software package, DaVis 10.0.5.

#### *5.2.2.1. Principle of PIV measurement*

The principle of PIV measurement involves the analysis of images of tracer particles present in a thin light sheet illuminated by a double-pulsed laser beam. The light scattered by these particles is captured by a high-resolution digital camera positioned perpendicular to the light sheet and synchronized with the two laser impulsions. For air velocity evaluation, each of recorded images of the first and second illuminations is divided into small areas, called interrogation windows. The local particle displacement between these two successive illuminations is then evaluated by a cross-correlation statistical method at the level of each interrogation window. Given the time delay between the two illuminations, an instantaneous velocity vector field can be calculated. This operation was repeated iteratively for all interrogation areas to obtain a whole flow field across the recorded image. The calculation process of velocity vectors is summarized in Keane and Adrian (1992). A comprehensive and more detailed explanation of the PIV measurement is widely available in the literature (Prasad, 2000; Raffel et al., 2018).

#### *5.2.2.2. Measurement procedure*

An entire measurement plane (z = 520 mm, **Figure 5.1**) was covered with 36 measured windows (112 mm × 112 mm) with a partial overlap between them. Because of the opaque door frame, the measurement was performed at 30 mm from the bottom shelf. The camera and the laser were mounted on a displacement system allowing the position of the measured windows to be changed (precision of displacement ±1 mm). For each measured window, 1200 pairs of images were recorded at a frequency of 0.5 kHz. A reliable representation of mean velocity and other statistical information were verified. It is to be emphasized that a preliminary sensitivity study was conducted in order to determine the optimum number of pairs of images. A multi-pass algorithm with decreasing interrogation area was used to process instantaneous vector calculation. Two passes were used with interrogation dimensions of 64 × 64 pixels and 32 × 32 pixels, respectively. Both passes were defined with 50% overlap. Given the interrogation dimensions of the second pass, the spacing between two calculated velocity vectors was 16 pixels (about 3.5 mm) in both the horizontal and vertical directions. Any region near high reflection surface in the images (e.g. DAG, RAG, shelf edges and test packages) was always masked out and not included in the vector calculation. Referring to the guideline

proposed by Keane and Adrian (1992), a time delay between two laser illuminations of 500 µs was the optimum for a good velocity estimation in our case since it allowed a mean particle displacement of less than 25% of the width of the interrogation window. After the mean velocity fields of all 36 measured windows were obtained, the entire measurement plane was established with the DaVis software by connecting all the windows together.

#### *5.2.2.3. Measurement accuracy*

There are various sources of errors in a PIV measurement (Wilson and Smith, 2013). Typically, errors are classified into systematic (bias) and random errors (Coleman and Steele, 2018). Based on a recent implementation of a processing algorithm in DaVis 10.0.5, it is possible to quantify the measurement uncertainties of instantaneous velocity components by using a correlation statistics method (Sciacchitano and Wieneke, 2016). This method accounts for most parameters that cause random errors from the vector computation process e.g. particle image disparity, particle background image noise and out-of-plane particle motion (Sciacchitano et al., 2015). Nevertheless, the systematic error due to the so-called peak-locking effect is not taken into account since the magnitude of this error is relatively small, compared with the random error (Wieneke, 2015). To minimize this systematic error, a particle image diameter of at least two pixels is recommended (Prasad, 2000), and this diameter was approximately 3-4 pixels in our case. The settling velocity ($u_p$) of the water droplets used in the experiment was also negligible (~ 0.0015 $m \cdot s^{-1}$) compared with the air velocity in the display cabinet ($0 < V < 0.7$ m $s^{-1}$). Thus, the particle velocity can be considered as representative of the airflow. Overall, the uncertainty of the measurement varied between 0.1 and 0.3% in most regions of interest and was slightly higher (0.6%) in the mixing or shear layers and at the level of the bottom shelf, particularly near the RAG because of higher turbulence levels.

## 5.3. Experimental results

### *5.3.1. Closed display cabinet*

**Figure 5.2a, b and c** show respectively the mean air velocity profiles, root-mean-square (rms) velocity fluctuations and velocity vector fields at the middle plane (z = 520 mm) of the display cabinet running only with fans (refrigeration system

turned "off"). **Figure 5.2d, e and f** show the same parameters for the display cabinet running with fans and the refrigeration system turned "on". Because of high spatial resolution, only one of the eight vectors (in both x and y directions) is depicted in the velocity vector fields (**Figure 5.2c and f).** For better visibility of the flow pattern, some large arrows were manually superimposed on the fields.

Note that the mean air velocity ($\overline{V}$) and the rms velocity fluctuation ($V_{rms}$) are given by

$$\overline{V} = \frac{1}{N}\sum_{i=1}^{N}\sqrt{u_i^2 + v_i^2} \tag{5.1}$$

$$V_{rms} = \sqrt{\frac{1}{N}\sum_{i=1}^{N}[(u_i - \overline{u})^2 + (v_i - \overline{v})^2]} \tag{5.2}$$

where $N$ is the total number of measured windows (1200 in our experiment); $u_i$ and $v_i$ are the air velocities in $x$ and $y$ directions measured at the instant *i*, respectively [m·s$^{-1}$]

When the refrigeration system was turned "off" **(Figure 5.2a)**, the inlet mean velocity magnitude of the jet normal to the DAG was approximately 0.57 m·s$^{-1}$, corresponding to a Reynolds number of about 2000 (based on the DAG width of 50 mm). This $Re$ value was low compared with that of a typical open display cabinet (4200 and 8000, Field and Loth, 2006). From the DAG to the top shelf, the jet slightly accelerated because it was deviated by the test packages at the front. The jet then spread out and the velocity gradually decelerated due to the diffusion process – i.e. entrainment of neighboring air by the air jet. According to the discharge angle of the DAG (about 8° relative to the vertical axis), the air flowed toward the door. Under the top shelf level (y < 1120 mm), the velocity profile showed a Coanda effect (jet adhesion to the wall) which caused relatively high velocity close to the door surface. The air velocity increased progressively when it flowed downward because of additional air flowing from the back through the PBP at each shelf, thereby enhancing the momentum flux along the flow path. Because of a higher percentage of perforated area on the PBP over the bottom shelf, higher air velocity can be clearly observed at this position. When it approached the RAG, the airflow was accelerated again by the cabinet fans.

High-velocity fluctuations were observed in two regions: the top and bottom parts of the cabinet (**Figure 5.2b)**. In the top parts near the DAG, high-velocity fluctuations can be explained by the development of eddies on both sides of the jet, i.e. in the mixing layers where high velocity gradient leads to large turbulent kinetic energy production. The fluctuations were further amplified because of the edge of the top shelf and the presence of the door which triggered air recirculation once air approached it. In the bottom part, fluctuations resulted from mixing between the back flow and the air curtain. Here, the flow was also turbulent in the air space above the test packages at the level of the bottom shelf and air recirculation also emerged near the front of the packages. Apart from these regions, small velocity fluctuations were observed. The vector field depicted in **Figure 5.2c** shows the downward flow with recirculation at the front of the top shelf.

A similar airflow pattern was observed in the display cabinet with the refrigeration system turned "on" (**Figure 5.2d, e and f)** compared with the case in which the refrigeration system was turned "off" (**Figure 5.2a, b and c)** despite slight discrepancies. The Coanda effect was less pronounced when refrigeration was applied because the air in the vicinity of the door surface had a relatively higher temperature, and thus an upward buoyancy force impeded downward flow for $y <$ 1000 mm. As shown in **Figure 5.2d**, the velocity was relatively lower at the door when the refrigeration system of the display cabinet operated and reached its maximum near the shelf edges. **Figure 5.2e** shows the same regions with relatively high velocity fluctuations in the case of the refrigeration system turned "off" (top and bottom parts), but higher turbulence was generated by interaction between the air curtain and the shelf edges. The vector field depicted in **Figure 5.2f** shows similar flow patterns as in the case of the refrigeration system turned "off", with the exception of slightly more pronounced recirculation (upward flow) in the top part and the local maximum velocity situated at a greater distance from the door.

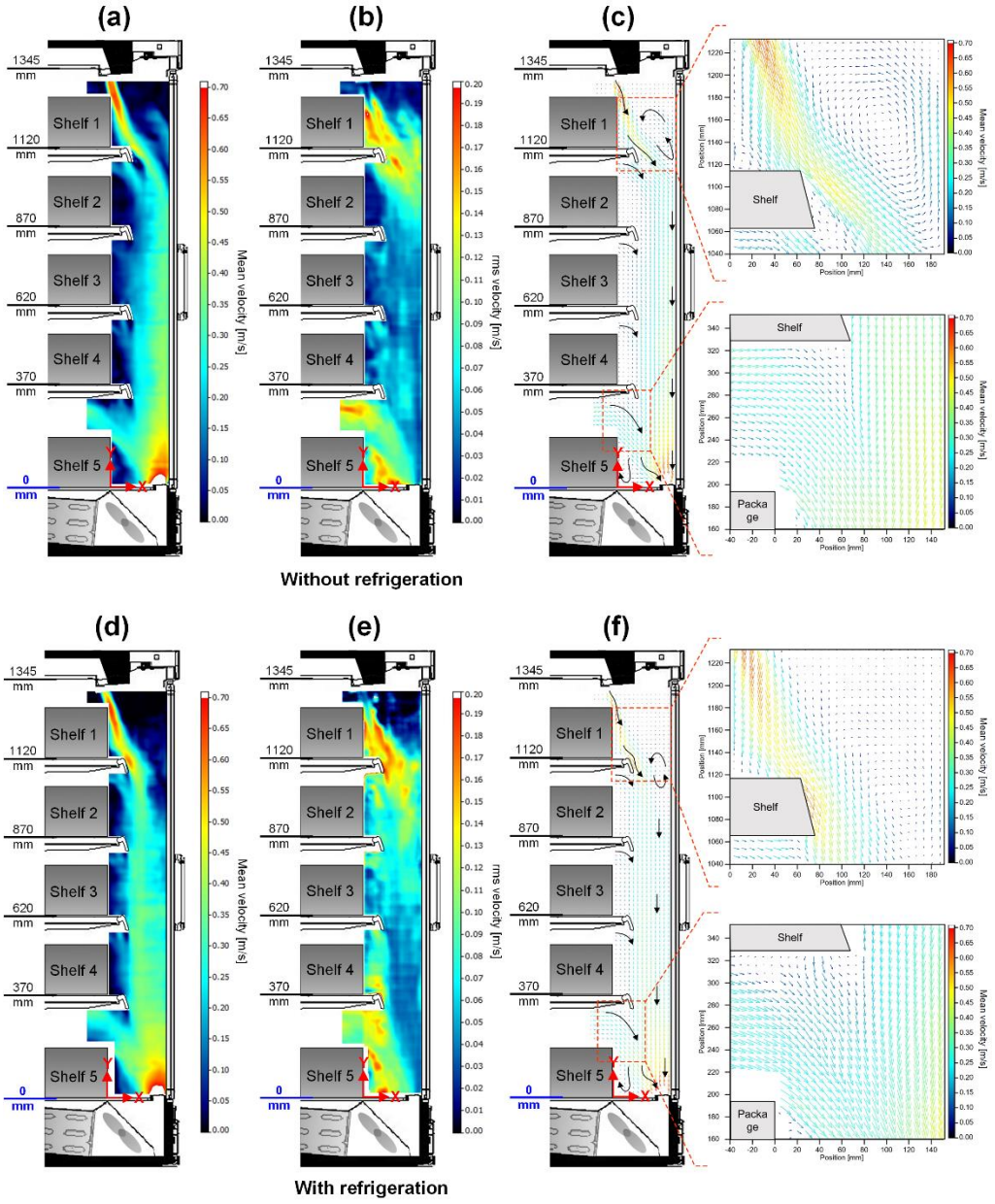


**Figure 5.2** Mean air velocity profiles (a); velocity fluctuations (b); and velocity vector fields (c); along the air curtain of a closed display cabinet running with fans only (refrigeration system "off"). Mean air velocity profiles (d); velocity fluctuations (e); and velocity vector fields (f); along the air curtain of a closed display cabinet running with fans and the refrigeration system "on".

### *5.3.2. Comparison between closed and open display cabinets*

The doors of the display cabinet were open with an opening angle of 90° and the PIV measurement was carried out with the same procedure as described in **Section 5.2.2**. The performing of measurements in the open display cabinet was particularly troublesome because it proved difficult to control the particle density. Particles

always flowed out to the ambient during the experiment, resulting in insufficient seeding to disperse the light. Because of this technical constraint, only the experiment with the refrigeration system turned "off" was carried out. **Figure 5.3** shows the air velocity profiles, the velocity fluctuations and the corresponding vector fields of the closed and open display cabinets. Note that the velocity profile, the velocity fluctuations and the vector field presented in **Figure 5.3a, c and d** are the same as those presented in **Figure 5.2a, b and c**, respectively. They are repeated here for the purposes of comparison with the open display cabinet.

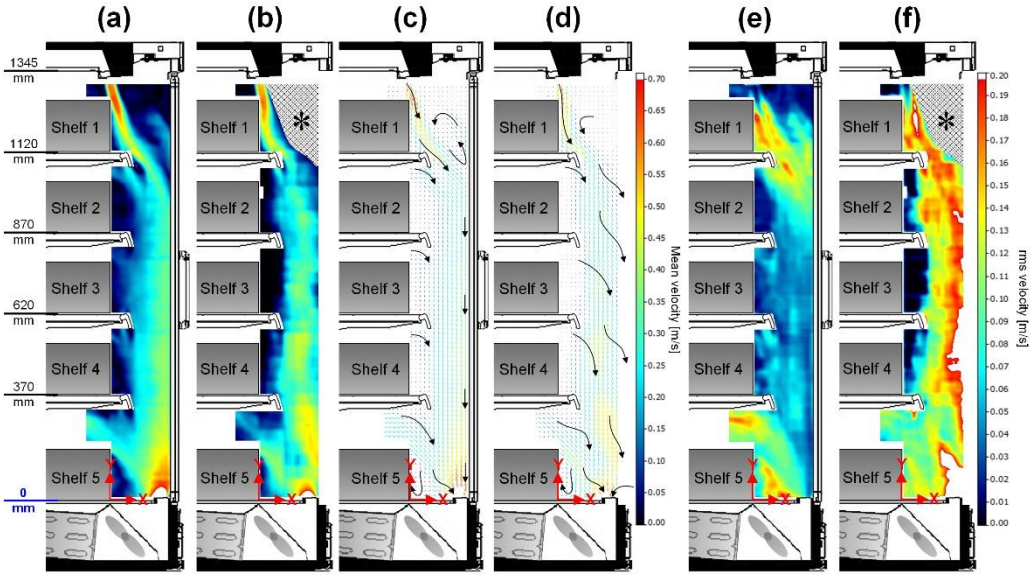


**Figure 5.3** Velocity profiles, velocity fluctuations and vector fields on the middle plane of the closed (a, c and e) and open (b, d and f) display cabinets. The asterisk (∗) represents a zone without signals (absence of particles in the external ambient air).

As shown in **Figure 5.3a and b**, the inlet mean velocity magnitude of the jet normal to the DAG under the open-door condition was almost the same as the closed-door value. When the doors were open, a large amount of external ambient air entered at the level of the top shelf level (y > 1050 mm) by the entrainment process of the discharged air jet. Despite an average air outflow in a great deal of the opening height (100 mm < y < 1050 mm, **Figure 5.3f**), large unsteady structures (eddies) were always observed (**Figure 5.4**), resulting in a wide region of mixing layers before approaching the RAG. It can be observed that the velocity fluctuations were much greater on the outer side of the air curtain ($V_{rms}$ > 0.2 m·s$^{-1}$ for y < 1000 mm, **Figure 5.3d**) than for the closed cabinet ($V_{rns}$≈ 0.05 m·s$^{-1}$, **Figure 5.3c**) where the

air curtain was more stable. Very near to the RAG (y < 100 mm, **Figure 5.3f**), there was also large air inflow.

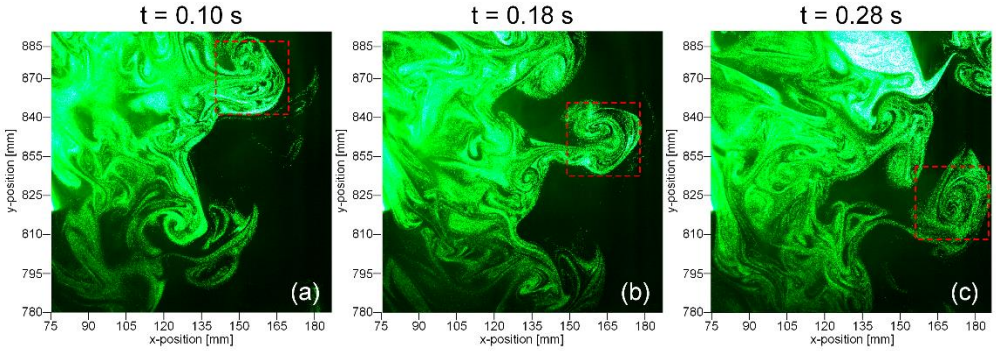


**Figure 5.4** Example of large unsteady eddy development at three consecutive instants (780 mm < y < 892 mm): (a) 0.10 s; (b) 0.18 s; and (c) 0.28 s.

Air inflow and outflow through the gaps along the door edges of the closed display cabinet were observed in our previous study (Chaomuang et al., 2019a). A PIV measurement was additionally conducted in the middle of the left door gap to quantify the volumetric air infiltration rate through the gaps (8 mm in width). By integration of the positive horizontal velocity component ($u$) over the height of the door, the volumetric air infiltration rate through the gaps was estimated to be approximately 0.0029 $m^3 \cdot s^{-1}$. It was assumed that the amount of outflow air was replaced by the ambient air infiltration and the rates of the air infiltration through the door gaps on the left and the right sides were the same. This result suggested that air infiltration under closed-door conditions accounted for about 8% of the supply air from the DAG, which is much less than the case of open display cabinets (~30-40%, Amin et al., 2009).

From a thermal point of view for the closed display cabinet, there is a small amount of convective exchange with the external ambient air through the gaps. The conduction and radiation exchanges through the doors are limited by the presence of double-glazing windowpanes coated with low-infrared emissivity materials. In addition, the low velocity fluctuations near the door reduce the convective heat transfer between the inner side of the door and the air curtain. The air entrained by the air jet at the top shelf level comes mainly from air recirculation near the door and it is, therefore, fairly cold. On the contrary, for the open display cabinet, the air entrained by the air jet is warm ambient air which mixes with the cold air in the outer mixing layer. While on the average air flows out at the intermediate height

(100 mm < y < 1050 mm), ambient air is engulfed by the air curtain via the large unsteady eddies. Moreover, there is no radiation shield between the external walls and the products located at the front of the shelves. These findings explain the better thermal performance observed in closed display cabinets, compared with open ones (Chaomuang et al., 2019a).

## 5.4. CFD modeling

A two-dimensional CFD model was developed to investigate the airflow and its influence on the temperature distribution in the closed display cabinet. The main objective is not to simulate precisely all the flow and transfer details. Instead, the aim was to examine the capability of a 2D k-ε model to reproduce the main phenomena and to predict the product temperatures in the display cabinet with acceptable accuracy. An example of more precise models with a three-dimensional large-eddy simulation (LES) can be found in Moureh and Yataghene (2017). The prediction of velocity profiles (with the refrigeration system turned "off" and "on") was compared with the results obtained from the PIV measurements presented in **Section 5.3**. The results of temperature measurements conducted in our previous study (Chaomuang et al., 2019a) were used to compare with the numerical prediction of temperature distributions in the present study (refrigeration system turned "on"). According to Chaomuang et al. (2019a), the air and product temperatures were measured by using calibrated thermocouples (±0.2ºC accuracy) in the middle section of a closed refrigerated display cabinet which operated under closed-door conditions and at a room temperature of 19 °C (humidity ratio of 0.003–0.004 kg of water vapor/kg of dry air). Timed-averaged temperatures were calculated over 5 h of quasi-steady state during which the defrosting period was excluded.

### *5.4.1. Geometry and mesh details*

The dimensions used for the 2D model were those of the real closed display cabinet (**Table 5.1**) and only the internal storage space of the cabinet was considered in the computational domain (**Figure 5.5**). The domain consisted of fluid and solid regions, representing airflow and products in the cabinet, respectively. An incompressible ideal gas was used for the fluid region while the thermal properties of methylcellulose were specified for the solid region (density = 1071 kg·m$^{-3}$;

thermal conductivity = 0.510 $W \cdot m^{-1} \cdot K^{-1}$; heat capacity = 3372 $J \cdot kg^{-1} \cdot K^{-1}$, Icier and Ilicali, 2005). Both unstructured and structured meshes were used for the entire domain. Much finer meshes were particularly defined at the areas close to the DAG and the RAG. Several models with different mesh sizes (M1-3, **Figure 5.6**) were preliminarily tested for the grid independence study so that numerical accuracy was ensured. It was found that the mesh M2 with 134,968 nodes and 97,693 elements was satisfactory since the numerical results did not change when the mesh size was reduced. As a result, this mesh was used in all calculations.

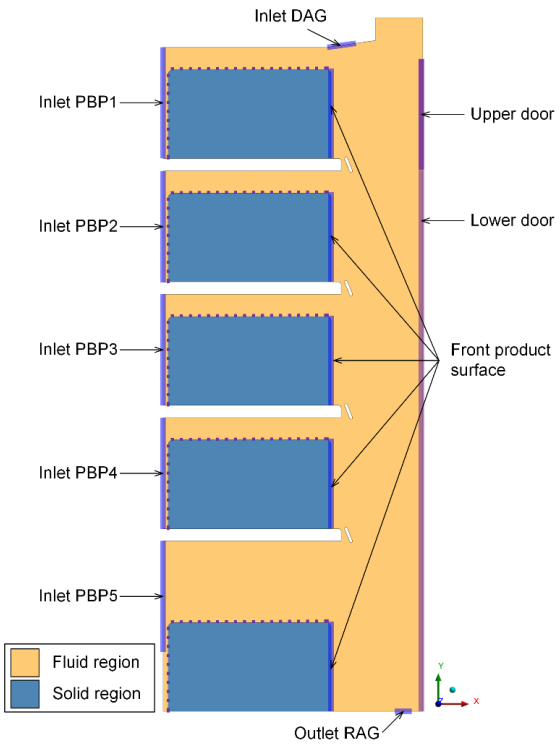


**Figure 5.5** The computational domain of the 2D-CFD model for a closed display cabinet and the locations of boundary conditions.

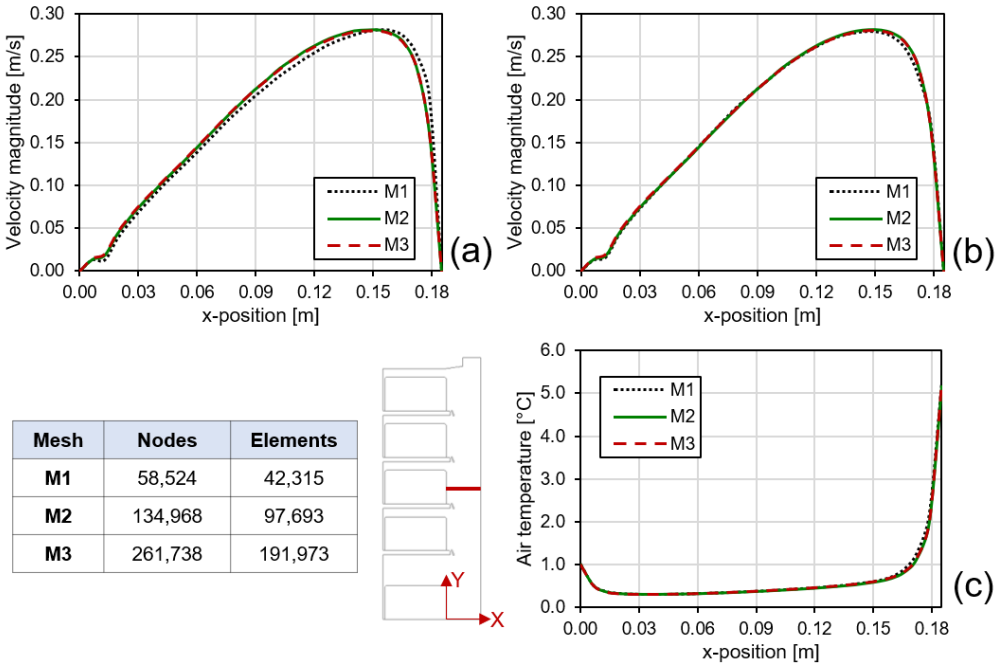


| Mesh | Nodes | Elements |
|---|---|---|
| **M1** | 58,524 | 42,315 |
| **M2** | 134,968 | 97,693 |
| **M3** | 261,738 | 191,973 |

**Figure 5.6** Velocity profiles without (a) and with (b) energy equation and temperature profile (c) in front of Shelf 3 for different meshes.

### *5.4.2. Mathematical description*

The CFD model in steady state was developed by using commercial ANSYS Code Fluent 17.2 software. The model is based on solving the governing equations which consist of the conservation of mass, momentum and energy equations (Versteeg and Malalasekera, 2007). Since the flow is turbulent, these governing equations are time-averaged (Reynolds-averaged Navier-Stokes, RANS) and the standard k-ε turbulence model was used together with these equations. Note that turbulence was firstly modeled with other k-ε turbulence models (i.e. Renormalization Group (RNG) and Realizable) and the results obtained were found to be almost identical. The standard k-ε turbulence model was therefore used as it was the best compromise between accuracy and reasonable computational time. The model also used an enhanced wall treatment function in conjunction with the turbulence model to take into account viscous effects near the walls. For 2D, steady-state and incompressible fluid flow, the general form of the governing equations can be written as

$$\frac{\partial(\rho u\phi)}{\partial x}+\frac{\partial(\rho v\phi)}{\partial y}=\frac{\partial}{\partial x}\left(\rho\Gamma_\phi\frac{\partial\phi}{\partial x}\right)+\frac{\partial}{\partial y}\left(\rho\Gamma_\phi\frac{\partial\phi}{\partial y}\right)+S_\phi \qquad (5.3)$$

where $\phi$ is a generalized transport variable, $\Gamma_\phi$ and $S_\phi$ are respectively the diffusion coefficient and the source term for the corresponding transport variable

$\phi$ as presented in **Table 5.2**. Note that the energy equation as a function of temperature was activated only for the case of the refrigeration system turned "on".

**Table 5.2** General form of the governing equations[(a)]

| Equation | Mass | Momentum | | Energy | k | ε |
|---|---|---|---|---|---|---|
| | | x-direction | y-direction | | | |
| $\phi$ | 1 | $u$ | $v$ | $T$ | $k$ | $\varepsilon$ |
| $\Gamma_\phi$ | 0 | $\upsilon + \upsilon_T$ | $\upsilon + \upsilon_T$ | $\frac{\upsilon}{Pr} + \frac{\upsilon_T}{Pr_T}$ | $\frac{\upsilon_T}{\sigma_k}$ | $\frac{\upsilon_T}{\sigma_\varepsilon}$ |
| $S_\phi$ | 0 | $S_u$ | $S_v$ | $S_T$ | $S_k$ | $S_\varepsilon$ |

[(a)]The complete description of these equations can be found in Tu et al. (2018).

### *5.4.3. Boundary conditions*

**Figure 5.5** shows the locations of boundary conditions imposed in the computational domain. Values used for boundary conditions were taken from the experimental data presented in this present study and in our previous work (Chaomuang et al., 2019a).

#### *5.4.3.1. Inlet boundary conditions*

Six velocity inlet boundary conditions were imposed in the computational domain: one inlet for the flow at the DAG and the other five inlets for the flow from the PBP at the levels of different shelves (**Figure 5.5**). Uniform velocity profile and a direction normal to the inlet were assumed under all inlet boundary conditions. The velocity inlet at the DAG was the mean velocity magnitude obtained from the PIV measurement. The velocities at the PBP inlets were estimated based on the air distribution percentages (Chaomuang et al., 2019a) for each shelf. They represent the airflow rate averaging through the PBP at a given shelf divided by the total flow rate in the display cabinet. Given the velocity magnitude at the DAG, the corresponding velocities over these shelves were determined. In the case with the refrigeration system turned "on", thermal boundary conditions were activated, and the measured temperatures were applied. All the inlet boundary condition values are summarized in **Table 5.3**.

**Table 5.3** Inlet boundary conditions

| Parameter | Unit | DAG | PBP | | | | |
|---|---|---|---|---|---|---|---|
| | | | Shelf 1 | Shelf 2 | Shelf 3 | Shelf 4 | Shelf 5 |
| Air distribution percentage[(a)] | % | 50 | 2 | 2 | 3 | 5 | 38 |
| Velocity | $m \cdot s^{-1}$ | 0.57 | 0.005 | 0.005 | 0.008 | 0.013 | 0.096 |
| Temperature[(a)] | °C | -0.1 | -0.5 | -0.5 | -0.5 | -0.6 | -0.7 |
| Turbulent intensity[(b)] | % | 3 | 5 | 5 | 5 | 5 | 5 |
| Length scale[(c)] | m | 0.002 | 0.005 | 0.005 | 0.005 | 0.005 | 0.005 |

[(a)]taken from the experimental data of Chaomuang et al. (2019a)
[(b)]lower turbulent intensity at the DAG was assumed due to the effect of the honeycomb.
[(c)]estimated from the honeycomb characteristics for the DAG and the hydraulic diameter of a slot for the PBP

*5.4.3.2. Wall boundary conditions*

Wall boundary conditions were used to confine the fluid and solid regions and non-slip boundary conditions were considered to be present at all walls. When the refrigeration system was turned "on", the thermal boundary conditions were defined at the walls considered in the heat transfer calculation. The walls in contact with fluid and solid regions were defined as coupled thermal interfaces (dotted lines in **Figure 5.5**). Although installation of doors can significantly reduce thermal radiation from the ambient by up to 94% (Faramarzi et al, 2002), a lot of heat generation due to visible radiation still occurs. Therefore, in addition to the coupled thermal interface, heat generation due to the absorption of visible radiation from the room and cabinet lights were applied directly at the front product surface level for all shelves (**Figure 5.5**). The heat dissipated from the room light ($\dot{Q}_{rli}$, the same for all shelves) was estimated from the lighting power density of 1.0 $W \cdot m^{-2}$, which is equivalent to a luminous intensity of 650 lux (an average value used in supermarkets, IESNA, 1991). The heat dissipated from the cabinet light ($\dot{Q}_{cli}$) was estimated from its power (10 W, manufacturer's data) with respect to the view factor for the different shelves.

For calculations concerning the door, the heat flux was calculated from the room temperature of 19 °C (experimental data) and the heat transfer coefficient of the door ($U_d$). The latter was determined by a thermal resistance method (**Eq. (5.4)**). Based on the characteristics of the door (manufacturer's data), which is composed

of two panes of tempered glass (4-mm thickness each) split by an argon gap (14-mm thickness), we obtained

$$U_d = \frac{1}{\frac{2e_{gl}}{\lambda_{gl}} + \frac{e_{ag}}{\lambda_{ag}}} = 1.13 \text{ W·m}^{-2}\text{·K}^{-1} \quad (5.4)$$

Since there was an inflow of warm air through the upper part of the door gaps ($\dot{m}_{gap} \cong 0.0036$ kg·s$^{-1}$, experimental data), an equivalent heat transfer coefficient ($U_{d,eq}$) was distinctly defined **(Eq. (5.5))** for this part of the door (250 mm in height).

$$U_{d,eq} = U_d + \frac{\dot{m}_{gap} C_p}{A_d} = 12.7 \text{ W·m}^{-2}\text{·K}^{-1} \quad (5)$$

where $A_d$ is the area of the upper part of the door (**Figure 5.5**).

The other walls were considered as adiabatic.

*5.4.3.3. Numerical calculation*

The model was solved iteratively with a SIMPLE algorithm for the coupling of pressure-velocity. The convection terms were estimated based on the second order upwind scheme. The default values of relaxation factors in Fluent software were applied for all variables. A numerical convergence criterion of $1 \times 10^{-6}$ was used for the residuals of components of velocity, turbulence kinetic energy, turbulent dissipation and energy equations and $2 \times 10^{-4}$ for the continuity equation. The simulation was driven using a computer server (Dell, Precision 3620, 64-bit operating system) with Intel Xeon E3-1240 Quad Core running at 3.50 GHz (8 Mb internal cache) and 64 Gb RAM. The computational time was four hours for the mesh used (M2, **Figure 5.6**).

## 5.5. Numerical results

*5.5.1. Air velocity profile*

The air velocity profiles of the closed display cabinet with the refrigeration system turned "off" and "on" are shown in **Figure 5.7a and b**, respectively. The air curtain formed at the DAG was deviated to the door as it descended to the RAG. A large air recirculation region was observed in the upper part of the cabinet and some small recirculation regions were also detected around product packages. Near the DAG, the edge effect of the package on the top shelf caused a slight increase in the jet

velocity. The diffusion process at the shear layer between the air curtain and the adjacent air caused a velocity decrease when flowing downward. Beyond the mid-height between Shelves 1 and 2, the air velocity was maintained because the air curtain momentum was strengthened by the air flowing from the PBP. Unlike the open display cabinet, the thickness of the air curtain in the closed display cabinet was limited by the presence of the doors. Thus, flow integrity was preserved. In the case where the refrigeration system was turned "off" (**Figure 5.7a**), the maximum velocity was close to the door due to the Coanda effect. However, the higher air temperature near the door deflected the maximum velocity slightly further from the door in the case where the refrigeration system was turned "on" (**Figure 5.7b**). Since the mass flow rate gradually increased along the flow path, relatively high velocity was observed in the vicinity of the RAG. In comparison with the experimental results (**Section 5.3**), the developed model is capable of reproducing the main phenomena of the flow distributions in the closed display cabinet in both cases.

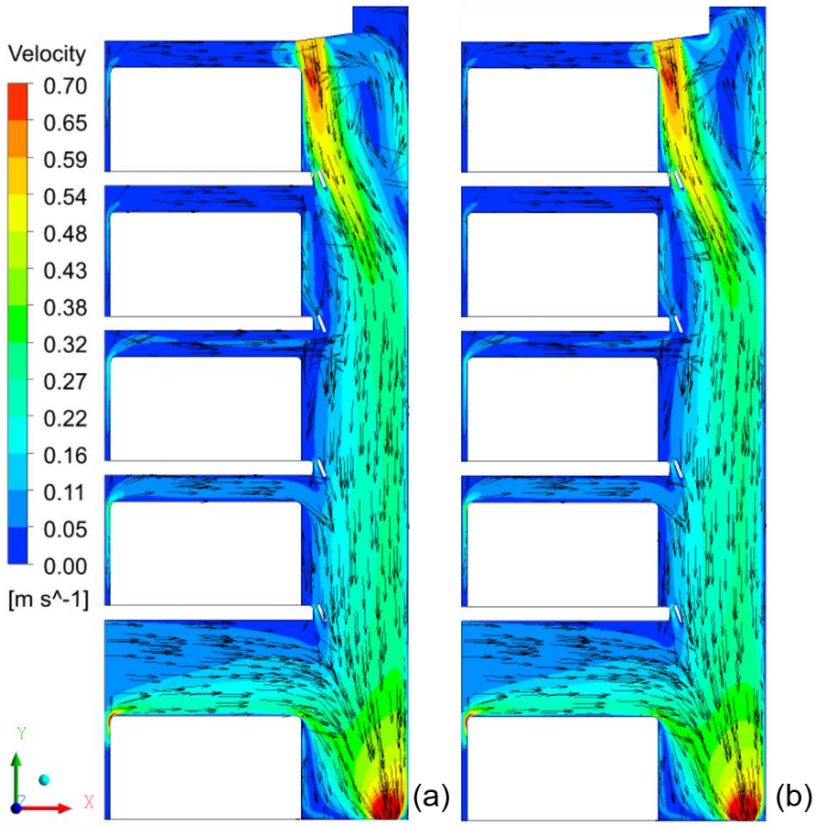


**Figure 5.7** Air velocity profiles in a closed display cabinet (a) refrigeration system turned "off"; and (b) refrigeration system turned "on".

*5.5.2. Air and product temperature distributions*

**Figure 5.8a and b** depict the results of air and product temperature distributions obtained from the experiment and the numerical prediction (with the refrigeration system turned "on"), respectively.

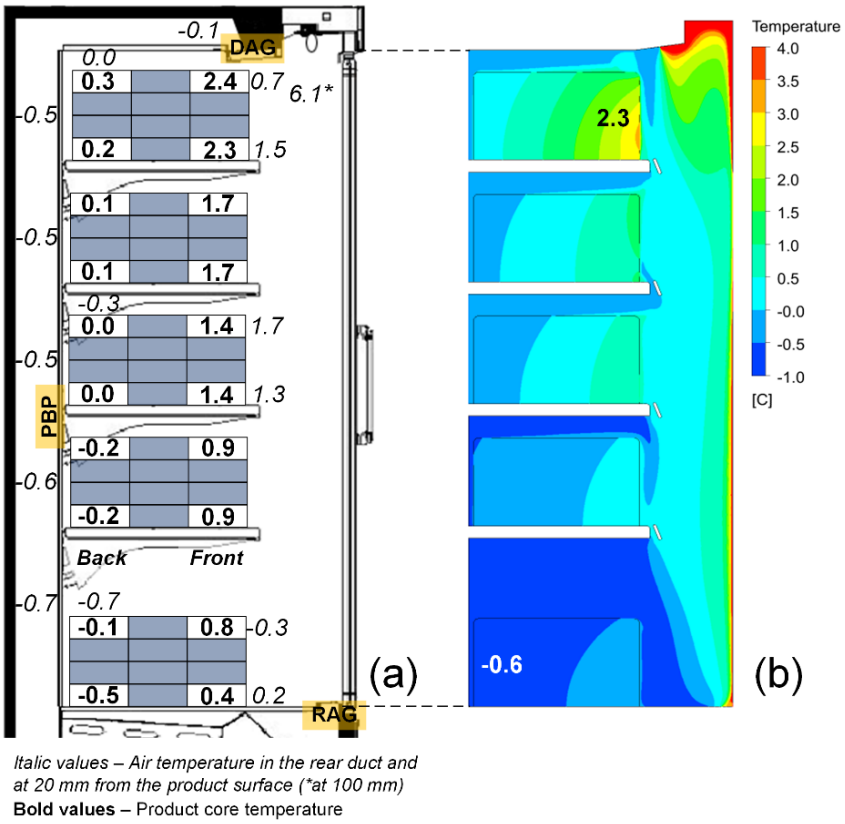


**Figure 5.8** Air and product temperature distributions in a closed refrigerated display cabinet: (a) experiment (Chaomuang et al., 2019a); and (b) numerical prediction.

Overall, the predicted air and product temperature distributions showed relatively good agreement with the experimental data. For both experimental and numerical results, the air temperature was lower than 2.0 °C everywhere, except in the upper part beyond the air curtain where the temperature recorded at a measurement point was 6.1 °C (the simulation under-estimated by 4 °C). The air recirculation mixed with the warm air infiltration through the door gaps can explain the high air temperature at this position. Spatial temperature heterogeneity was observed between products located at the front and the back of the shelves. The higher product temperature at the front resulted from the heat exchanges with the air curtain which was warmer than the air coming from the PBP and (visible) radiation

absorption due to the lights. Due to the proximity to the cabinet lights, the product at the front of the top shelf was the product with the highest temperature. The lowest product temperature was at the back of the bottom shelf because heat exchange was mainly governed by convection with the cold air from the PBP and conduction within the products. Since the cold air flowed from the PBP into the bottom shelf with a relatively higher mass flow rate (highest perforation percentage), the product at the back of the bottom shelf had the lowest temperature. In agreement with results published by Faramarzi et al. (2002), these findings showed that the installation of doors could reverse the product temperature distribution in display cabinets since the highest product temperature was mostly located at the front of the bottom shelf of the cabinets without doors (Evans et al., 2007). Nevertheless, closed refrigerated display cabinets still provide a better thermal performance (i.e. lower product temperature with small temperature variations between positions), compared with open ones (Chaomuang et al., 2019a).

## 5.6. Conclusions

Air velocity measurements using the PIV technique were conducted in a closed display cabinet. Two configurations were studied: closed- and open-door with a 90° opening angle. The measurements were carried out under two conditions (refrigeration system turned "off" and "on") for the closed configuration and under only one condition (refrigeration system turned "off") for the open one. According to the studied closed display cabinet, the $Re$ (based on the DAG width) was approximately 2000. In the closed configuration, similar flow phenomena were observed in the case of the refrigeration system turned "off" or "on" despite small discrepancies. The air curtain deviated to the door through a Coanda effect (maximum velocity near the door surface). However, it was less pronounced in the case of the refrigeration system turned "on" for which the upward buoyancy force impeded the downward flow. The air curtain was quite stable in most regions, with the exception of the top and the bottom of the cabinet where relatively high velocity fluctuations occurred. At the top of the cabinet, air recirculation occurred and could have promoted external ambient air infiltration through the door gaps. In the open configuration, the air curtain was less stable. In the outer mixing layers of the air curtain, large unsteady eddies developed, causing the ambient air to be entrained in

the curtain. Comparison between the flow patterns in the closed and open configurations leads to the conclusion that products would be better protected in closed display cabinets.

A steady-state 2D-CFD model with the standard k-ε turbulence model was also developed in this study to investigate the airflow and its influence on the thermal distributions in a closed display cabinet. Qualitatively, good agreement was found between numerical predictions and experimental results. Despite its simplifications, the model has shown the ability to reproduce the main flow phenomena observed by the experiments. The predicted product temperature profile trend also agreed with the experimental data. In future studies, the developed model will be used to examine the influences of unexplored design parameters and the operating conditions on the air and product temperature distributions, e.g. airflow rate, air temperature at the DAG and product occupied volume.

Even though a specific display cabinet was used, the results provide general information on the phenomena taking place in the display cabinet. The presence of doors causes air recirculation which could induce the infiltration of external warm air through the gaps along the door frames. Sealing these gaps would certainly mitigate this issue. Nonetheless, the design of closed display cabinets should probably be revisited. For example, the air curtain might not be necessary due to the replacement of the physical barriers.

# Chapter VI

# Simplified heat transfer modeling in steady state

# Simplified heat transfer modelling of a closed refrigerated display cabinet: Part I – Static model development and validation

**Nattawut Chaomuang**, Onrawee Laguerre and Denis Flick

Submitted to *Applied Thermal Engineering* (submitted)

The work of Part I was also presented in the 25th IIR International Congress of Refrigeration (ICR2019), Montreal, Canada

---

**Abstract**

Installation of doors on open refrigerated display cabinets is one of the simple and effective methods to improve the cabinet performance because it can reduce the warm and humid air infiltration into the cabinets. However, their presence can change airflow pattern and temperature distribution. It is, thus, necessary to understand these thermal phenomena. To describe the evolution of product and air temperatures at different zones in the closed refrigerated display cabinet, a simplified heat transfer model was developed based on a zonal approach. Part I of this study shows how the developed model allows the prediction of time-averaged air and load temperatures at various positions in the cabinet. The predicted values were compared with measured air and load temperatures for three ambient temperatures. Good agreement was found between the predicted and measured temperatures with the maximum difference of less than 0.5 °C for every studied position and the overall mean absolute error of 0.2 °C. In Part II, the dynamic aspects of model will be presented allowing the prediction of the temperature fluctuations according to the "on/off" compressor working cycle and defrosting process.

***Keywords:*** Closed refrigerated display cabinet; Simplified model; Heat transfer; Temperature; Numerical study; Static simulation

**Nomenclature**

| | |
|---|---|
| $C_{eq}$ | Equivalent thermal conductance [W·K$^{-1}$] |
| $C_p$ | Heat capacity [J·kg$^{-1}$·K$^{-1}$] |
| $e$ | Thickness [m] |
| $h$ | Convective heat transfer coefficient [W·m$^{-2}$·K$^{-1}$] |
| $\dot{m}$ | Mass flow rate [kg·s$^{-1}$] |
| $q$ | Heating power [W] |
| $Q$ | Cooling load [W] |
| $RH$ | Relative humidity [%] |
| $S$ | Exchange area [m$^2$] |
| $T$ | Temperature [°C or K] |
| $t$ | Time [s] |
| $U$ | Overall heat transfer coefficient [W·m$^{-2}$·K$^{-1}$] |

*Greek letters*

| | |
|---|---|
| $\alpha, \beta$ | Exponential dimensionless heat transfer coefficient $= \exp\left(-\frac{US}{\dot{m}C_p}\right)$ |
| $\delta, \gamma$ | Air distribution coefficient |
| $\theta$ | Dimensionless average temperature |
| $\lambda$ | Thermal conductivity [W·m$^{-1}$·K$^{-1}$] |
| $\rho$ | Density [kg·m$^{-3}$] |
| $\tau$ | Period of one complete compressor working cycle [s] |
| $\varphi$ | Phase shift [rad] |
| $\phi$ | Mass fraction of water vapor [kg·kg$^{-1}$] |
| $\omega$ | Angular frequency $= \frac{2\pi}{\tau}$ [rad·s$^{-1}$] |
| $\Delta H_f$ | Heat of fusion of water [kJ·kg$^{-1}$] |
| $\Delta H_v$ | Heat of vaporization of water [kJ·kg$^{-1}$] |

*Subscripts*

| | |
|---|---|
| $a$ | air |
| $ag$ | argon |
| $a\ell$ | aluminum |
| $c$ | ceiling |
| $d$ | door |
| $del$ | delay |
| $exp$ | experimental |
| $ext$ | external |
| $f$ | frost |
| $gap$ | gap |
| $gl$ | glass |

| | |
|---|---|
| $i, j, k$ | index numbers |
| $\ell$ | latent |
| $l$ | load |
| $lb$ | back load |
| $lf$ | front load |
| $li$ | lighting |
| $ll$ | load to load |
| $num$ | numerical |
| $ov$ | overall |
| $pl$ | perforated back plate |
| $pu$ | polyurethane |
| $rd$ | rear duct |
| $s$ | sensible |
| $sat$ | saturated |
| $sh$ | shelf |
| $t$ | total |
| $th$ | thermostat |
| $w$ | wall |

*Abbreviations*

| | |
|---|---|
| DAG | Discharge Air Grille |
| MAE | Mean Absolute Error |
| PBP | Perforated Back Panel |
| RAG | Return Air Grille |

## 6.1. Introduction

Temperature is a well-known factor in determining food quality and safety across the logistic cold chain from production to final consumption. Failure in temperature control at any stage can trigger food quality deterioration, thus shortening food shelf life and consequently increasing consumers' health risk. Several field investigations have shown that temperature control in retail display cabinets is often subject to temperature abuse because food products are stored out of their recommended temperature limits (Derens-Bertheau et al., 2015; Lundén et al., 2014). About half of the total retail display cabinet line-ups in a typical supermarket are open refrigerated display cabinets, of which the chilled-space storage is protected from the ambient surroundings by cold air curtain (ASHRAE, 2010). Warm and humid air infiltration is a primary cause of the heterogeneity of temperature distribution in the equipment (Evans et al., 2007; Gaspar et al., 2011; Laguerre et al., 2012b). This draws a lot of attention with the view to minimize the air infiltration particularly

through the enhancement of air curtain efficiency as highlighted in a recent review by Chaomuang et al. (2017). Despite the immense efforts in both academic and industrial research levels, the issue of air infiltration remains problematic.

Installation of doors on the open front of the display cabinets becomes a viable alternative. It has been proven to be an effective solution to mitigate the air infiltration problem – achieving potential energy savings (Fricke and Becker, 2010; Lindberg et al., 2010), improving temperature homogeneity (Chaomuang et al., 2019; Evans and Swain, 2010) as well as promoting food quality (Atilio de Frias et al., 2015). In addition, the thermal comfort in the retail stores can be enhanced, which can be possibly translated into a positive sales impact (Lindberg et al., 2017). These advantages encourage the implementation of closed refrigerated display cabinets in many retail stores. For instance, it will account for about 75% of all display cabinets in French supermarkets by the end of 2020 (RPF, 2016).

Due to a reduction of cooling load after door installation, some modifications of the refrigeration system can be made. Lindberg et al. (2010) exhibited that the performance of closed display cabinet was enhanced when refrigerant inlet temperature was increased. Faramarzi et al. (2002) suggested to reduce the size of thermostatic expansion valves to avoid a hunting effect. In addition, the presence of doors can modify flow pattern and temperature distribution inside the closed display cabinets. In concordance with our previous study (Chaomuang et al., 2019a), the position of the warmest product temperature was different (temperature at the front of the upper shelf became higher than that of the bottom shelf in closed cabinets, in opposite to open ones). An understanding of mechanism of heat transfer and airflow in the equipment becomes necessary since it can demonstrate if these modifications will compromise the quality and safety of food products. An experimental investigation is therefore necessary to determine real conditions occurring within the display cabinet. However, such investigation is both costly and labor-intensive. For this reason, a numerical simulation with Computational Fluid Dynamics (CFD) model is complementary as one can see it is widely used in various refrigerated food applications (Norton and Sun, 2006; Smale et al., 2006). Two main advantages of the CFD numerical approach were emphasized by Laguerre et al. (2015). Firstly, it enables the knowledge of local parameters (temperature, humidity and velocity) that allows the understanding of the

phenomena. Secondly, it permits the prediction of influence of operating conditions and equipment design, which is rather cost-inefficient or impractical to perform by experiments. Extensive studies applied such model to open refrigerated display cabinets (Cortella, 2002; Gaspar et al., 2012; Ge and Tassou, 2001; Yu et al., 2009), whereas little research associated with closed display cabinets has been carried out. Orlandi et al. (2013) developed a three-dimensional CFD transient model to quantify incoming energy due to air infiltration during door openings. The model developed better understanding of the physical mechanisms of energy transport with various operating conditions (i.e. frequency of door openings) and equipment design (i.e. hinged or sliding doors). D'Agaro et al. (2006) developed a CFD model of the water condensation and evaporation processes on the glass doors of a low-temperature (frozen food) closed display cabinet. This study aimed to understand the fogging and defogging mechanisms taking place during door openings since this incident is a very important issue for this cabinet type.

Although the CFD model is a powerful tool, there are limitations because of the calculation time and computational resource requirements. Simplified heat transfer models based on a zonal approach become a complementary approach. Laguerre et al. (2012a) developed a model based on this approach in an open refrigerated display cabinet. This model was successful to predict load temperatures at different zones in the equipment with short calculation time. It also enabled the study of the influence of operating conditions. Further work by Ben-abdallah et al. (2018) proposed a similar heat transfer model in transient state under Modelica simulation environment through which the dynamic behavior of air and product temperatures in the open display cabinet can be investigated. Moreover, demand response strategies during on- and off-peak periods for electricity usage can be devised with the model. Some authors in our team also proposed simplified heat and/or mass transfer models for other refrigerating equipment in the cold chain: production plant (Lecoq et al., 2016), refrigerated vehicle (Hoang et al., 2012), cold room (Laguerre et al., 2015) and domestic refrigerator (Laguerre, 2010). Nevertheless, to the best of our knowledge, such a model for a closed refrigerated display cabinet is not available.

The objective of the study is to develop a simplified heat transfer model of a closed refrigerated display cabinet based on a zonal approach. This development is divided

into two parts: Part I proposes a steady state heat transfer model, which allows the prediction of time-averaged air and load temperatures in the closed display cabinet. Details of overall model conceptualization, static model development, determination of model input parameters as well as model validation by comparing with experimental data were discussed. Part II presents the model development in transient state, which allows the prediction of the temperature fluctuations according to the on/off working cycles of the compressor operation and to the defrosting operation.

The acquired information of the simulation enables the identification of the critical zones, i.e. too warm and too cold, which can lead to food quality deterioration and chilling injury, respectively. The influence of compressor operation on the load temperature fluctuation can also be evaluated with the dynamic model. In fact, the quality of the food products is affected not only by the average level of temperature but also by the temperature fluctuation (Cai et al., 2006; Tano et al., 2007).

Closed refrigerated display cabinets will be soon a new component of the series of refrigeration equipment in the food cold chain. To take into account this evolution, this developed simplified heat transfer model will be further integrated with the other models already developed by our teams for several refrigerating equipment. By this mean, it allows the prediction of time-temperature history of food products from a production plant to a household refrigerator. Furthermore, an evaluation tool for consumer risk can be also established when these models are linked with predictive microbiological and/or quality models (Duret et al., 2015).

## 6.2. Experimental study

Temperature measurement in a closed refrigerated display cabinet was carried out; the obtained result was then used for the model validation. The display cabinet was installed in a test room in which the ambient temperature was controlled at 14.6±0.4 °C, 19.5±0.6 °C, and 24.4±0.4 °C. The water content of the air in the test room varied from 0.008 to 0.012 kg water/kg dry air, corresponding to a variation in the relative air humidity between 60% and 75%. This small variation in water content in the air showed little influence on the temperature performance, but more impact on the energy performance because of the condensation and frost formation on the evaporator (Chen and Yuan, 2005). As depicted in **Figure 6.1**, the closed display

cabinet was loaded with test product packages made of methylcellulose (dimensions in width × height × length: 100 × 50 × 200 mm). Calibrated thermocouples (T-type, accuracy ±0.2 °C) were placed at various positions in the display cabinet for air temperature measurement (Fig.1, red stars): in the vertical rear duct from the duct upstream to the discharge air grille (DAG) and at 20 mm from the surface of the test packages. Some thermocouples were also instrumented at the core (**Figure 6.1**, blue circles) and the surface (**Figure 6.1**, green triangles) of the packages for load temperature measurement. Noting that each thermocouple was calibrated in a thermostatic oil bath (Fluke, model 7340, temperature stability of ±0.005 °C) with setting temperatures of -5, 0, 10, 20 and 30 °C and the precision of ±0.2 °C was determined.

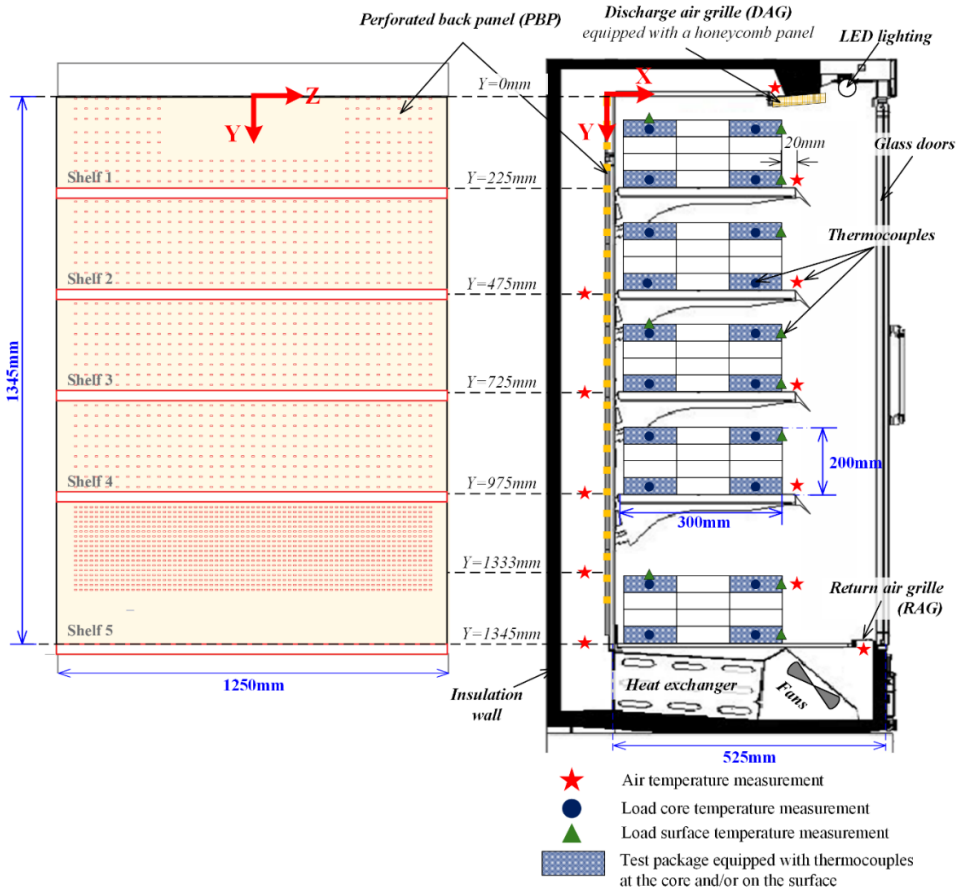


**Figure 6.1** Characteristics of a closed display cabinet and schematic view of experimental setup for the temperature measurement

Air and product temperatures were recorded every 10 s for at least 24 h with a data acquisition system (Agilent 34970A). The time-averaged values were then calculated over 3 h of the quasi-steady state in which the average over one "on/off"

cycle of compressor regulation remained the same. The defrosting period emerging every 6 h for a duration of 30 min was also excluded from the calculation. The lights in the test room and in the display cabinet were switched on to represent the real use condition in supermarkets and the cabinet doors were always closed during the experiment. Perforation pattern of the back panel (PBP) of the studied cabinet is also depicted in Fig.1. According to the total panel area over each shelf, there are 2.3% of holes at the top shelf, 8.3% at the bottom shelf and 3.8% at all intermediate shelves.

The airflow pattern in the closed display cabinet is schematically illustrated in **Figure 6.2a**. At the discharge air grille (DAG), an air curtain is established and provides cooling capacity for the loads in the cabinet. It flows downwards to return air grille (RAG). Due to the fans underneath the bottom shelf, air from the RAG is driven through a heat exchanger to be cooled down and then flows vertically along a rear duct to complete the circulation at the DAG once again. A part of the cold air also flows horizontally from the back through the perforated back panel (PBP) towards the front of the cabinet and mixes with the air curtain.

The presence of gaps along the doorframes allows the accommodation of door openings; however, it induces warm ambient air infiltration into the cabinet. As shown in **Figure 6.2b**, visualization of air flow at the front of the top shelf of the studied display cabinet using smoke and a laser beam permits better understanding of the phenomena. At this position, a part of the air curtain recirculates and then mixes with the external warm air coming through the door gaps. This leads to an increase of temperature in the air curtain.

**Figure 6.2a** also presents time-averaged air and load temperatures and their standard deviations in the closed display cabinet for the ambient temperature of 19.5 °C. Because of the heat losses through the cabinet walls, the time-averaged air temperature in the rear duct successively increased from -0.8 °C after the heat exchanger to -0.2 °C at the DAG. On the other hand, the stabilization due to the thermal inertia of these walls caused a moderate decrease of the standard deviation (from 2.3 °C to 1.6 °C). The highest load temperature was observed at the front of the top shelf (average 2.3 °C). In fact, the load located at this position was not only subject to heat exchanges with the air curtain but also to heat generation due to

(visible) light absorption because of its proximity to cabinet lighting. As a result, the load temperature was higher than that of the neighboring air.

Despite the heat loss through the glass doors, the air and load temperatures decreased from the top (air 1.5 °C, load 2.4 °C) to the bottom shelves (air -0.2 °C, load 0.4 °C). This is because more cold air is flowing from the back at the lower shelves over which the percentage of perforation area is higher than that over the top shelf (**Figure 6.1**).

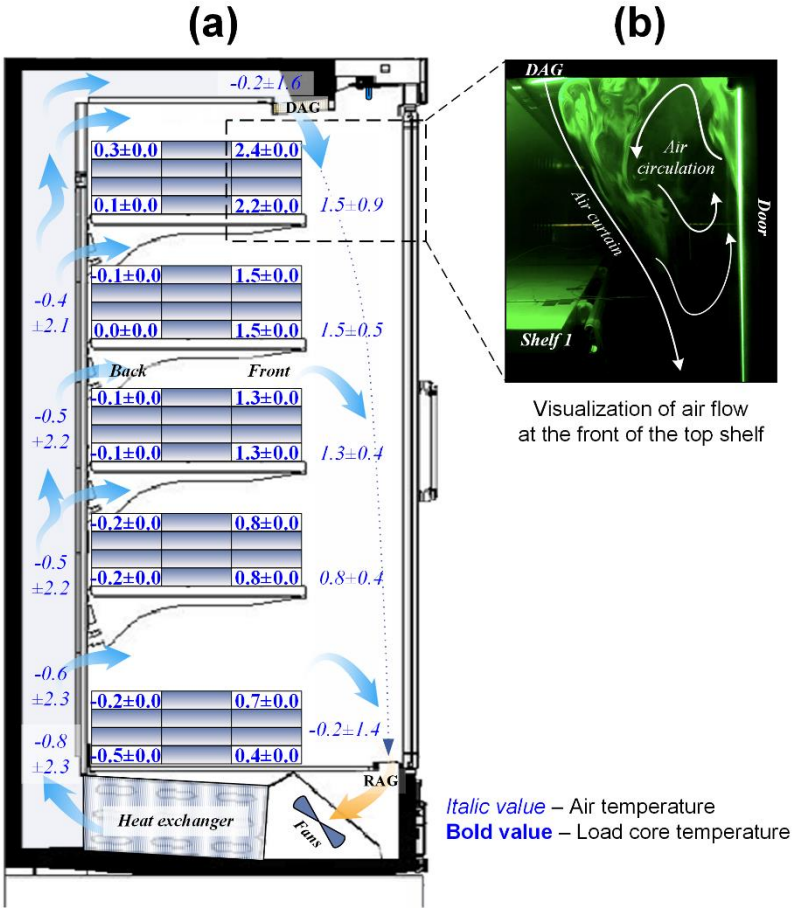


**Figure 6.2** (a) Experimental mean air and product core temperatures and the standard deviations during (quasi) steady state at various positions in a closed display cabinet for room temperatures of 19.5 °C (b) visualization of air flow at the front of the top shelf.

Forced convection and conduction, main heat transfer modes in the closed display cabinet, explain the load temperature difference between the front and the back. This difference is the most significant at the top shelf (ΔT~2.1 °C). Because the glass doors are shielded with low-emissivity coating materials, thermal radiation between the loads and the surroundings is restricted. Faramarzi et al. (2002) showed

that glass doors can reduced radiation into the cabinet by 94%. Natural convection is also limited because the doors of the display cabinet were always closed during the experiment resulting in insignificant difference between the highest and coldest internal air temperatures ($\Delta T_a < 5$°C).

## 6.3. Model development

### *6.3.1. Model conceptualization*

A simplified heat transfer model in a closed refrigerated display cabinet was developed in this study with a zonal approach. This model allows the prediction of both air and load temperatures at various positions in the display cabinet. The model was developed with static and dynamic aspects. The static aspect of the model is to predict the time-averaged air and load temperatures under steady state condition, while the dynamic aspect is to predict fluctuations in the temperatures due to the compressor working cycles (unsteady state condition). **Figure 6.3** shows an example of the temperature fluctuations at 3 positions (DAG, top/front and bottom/rear) in the display cabinet.

For the sake of simplicity for presentation, the evolution of the temperatures is firstly assumed to follow a sinusoidal variation:

$$T_i(t) = \overline{T}_i + \Delta T_i \cos(\omega t + \varphi_i) = \overline{T}_i + \Delta T_i \cos(\omega(t - t_{del,i})) \qquad (6.1)$$

where $T_i(t)$ is the temperature evolution at a given position $i$ and at time $t$ in the display cabinet; $\overline{T}_i$ is the time- averaged temperature at that position; $\Delta T_i$ is the amplitude of temperature fluctuation defined as $(T_{i,max} - T_{i,min})/2$ ; $\omega$ is the angular frequency defined as $2\pi/\tau$ where $\tau$ is the period of one complete compressor cycle and $\varphi_i$ is the phase shift related to the delay time $t_{del,i}$ (due to the effects of inertia) at which the temperature at the position $i$ reaches its maximum value. The static model presented in this paper (Part I) allows the prediction of the time-averaged air and load temperatures. The dynamic model for the prediction of these temperature fluctuations will be presented in another part of the study (Part II). It is to be emphasized that the sinusoidal temperature variation in **Eq. (6.1)** is only to present the concept of the model development in a simple manner since the real temperature variation is periodic and not sinusoidal (**Figure 6.3**). For the model calculation, the temperature profile of the supply air ($T_{th}$, input parameter) is

decomposed by using Discrete Fourier Transform. The temperature variations at other positions in the display cabinet are in response to this input temperature profile. This topic will be further discussed in more detail in Part II of the study.

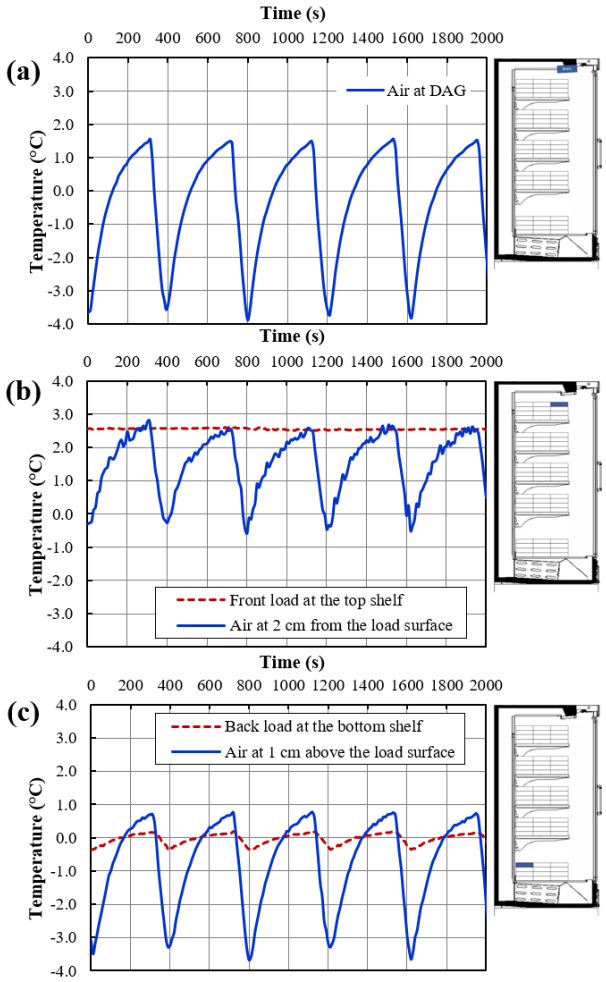


**Figure 6.3** Experimental time-temperature profiles (a) air at the discharge air grille (DAG) (b) front load (core) at the top shelf and air at 2 cm from the load surface and (c) back load (core) at the bottom shelf and air at 1 cm above the load surface

### *6.3.2. Zone definition*

Based on the zonal approach, heat exchange zones at different positions in the display cabinet were schematically presented in **Figure 6.4**. There are two main domains; each one is decomposed into several zones. The first domain (Domain I) represents the heat transfer in the vertical rear duct where cold air exchanges heat with the external ambient air through the rear wall and the ceiling of the cabinet. The second domain (Domain II) represents the heat transfer in the shelf space. In

every zone in the domains, algebraic and ordinary differential equations describe the heat transfers (by mean of thermal resistances) and energy balances.

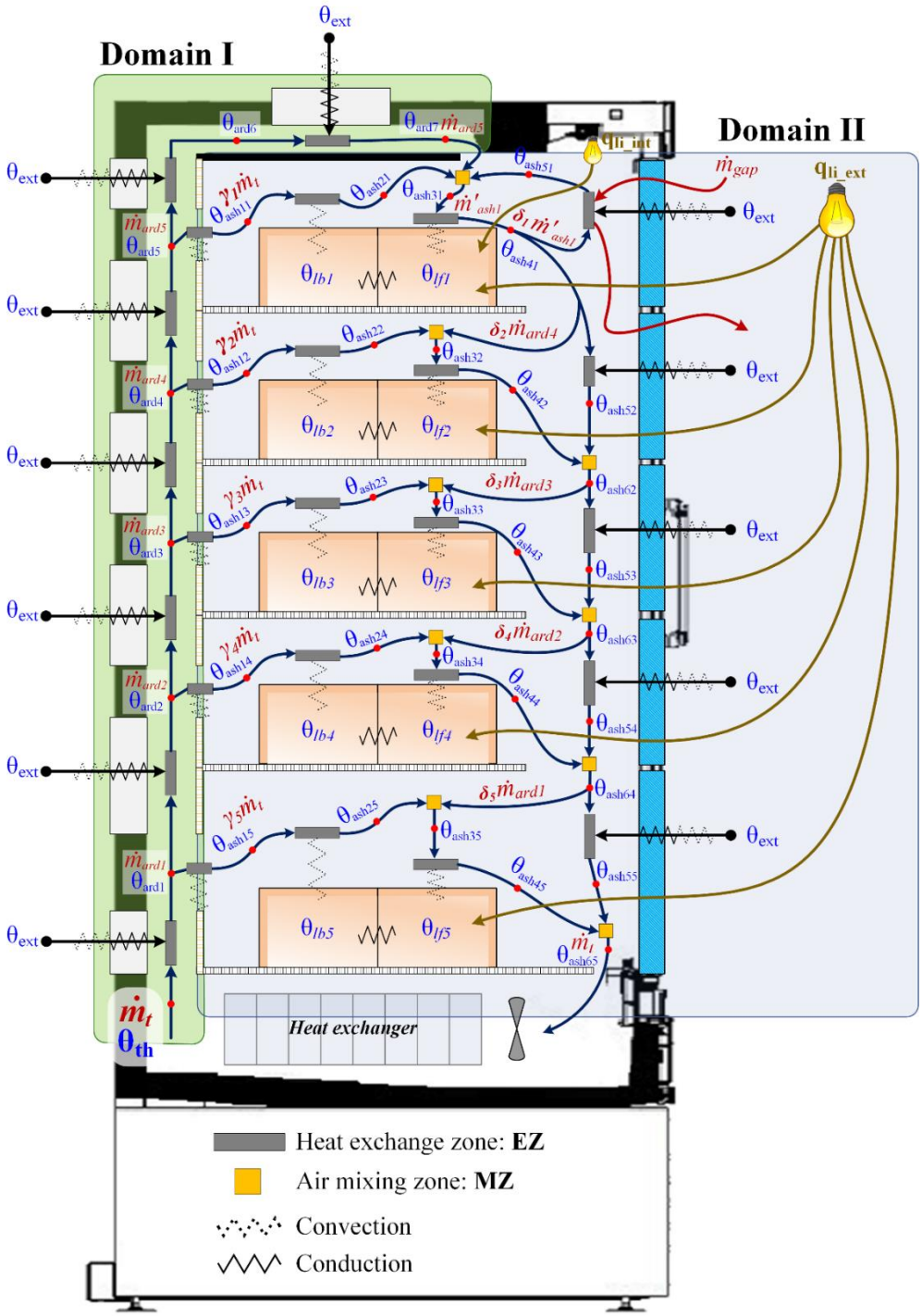


**Figure 6.4** Schematic view of the simplified model composed of two domains: Domain I heat losses through the vertical rear duct and the cabinet ceiling and Domain II heat exchange in the shelves-space storage.

Symbols and indexes are established for the model development. As depicted in **Figure 6.4**, heat exchange zone (denoted as EZ) and air mixing zone (denoted as MZ) are represented by rectangular and square symbols, respectively. Two indexes are assigned in the Domain I, e.g. EZ [1, 1]. The first index in the brackets indicates the selected domain (Domain I in this example) and the second index indicates the position in that domain (Position 1 in this example). Unlike Domain I, there are three indexes in the Domain II, e.g. EZ [2, 1, 1] or MZ [2, 1, 1]. An additional (third) index is added in this domain to indicate the shelf number which ranges from 1 (top) to 5 (bottom) of the display cabinet.

### *6.3.3. Static model development*

Static model is first developed to predict the time-averaged air and load temperatures under steady state condition, for which the following assumptions are established:

- All temperatures are constant with respect to time. In practice, the temperatures vary due to compressor working and defrosting cycles, night/day period etc.
- Air temperature just after the heat exchanger where the thermostat sensor is located ($T_{th}$) and the external ambient air ($T_{ext}$) are also constant and they are the input parameters.
- There are two loads of the same volume on each shelf (back and front) and the temperature of each load is considered homogeneous.

Dimensionless temperature ($\theta_i$) based on the time-averaged thermostat temperature ($\overline{T}_{th}$) and the external ambient air temperature ($T_{ext}$) is defined (**Eq. (6.2)**) to generalize the model, and it will be used throughout the development.

$$\theta_i = \frac{\overline{T}_i - \overline{T}_{th}}{T_{ext} - \overline{T}_{th}} \quad \text{for} \begin{cases} T_{th} = \overline{T}_{th} \\ T_{ext} \neq \overline{T}_{th} \end{cases} \tag{6.2}$$

In fact, all heat transfer phenomena involved in the display cabinet (i.e. forced convection and conduction) are linear with respect to temperature difference. Therefore, the properties of the dynamic linear system can be used: the time-averaged output ($\overline{T}_i$) for a fluctuating input ($T_{th}$) is equal to the response for the

time-averaged input ($\overline{T}_{th}$). Moreover, the defined dimensionless temperature $\theta_i$ is also independent of $T_{ext} - \overline{T}_{th}$ due to the linearity between the internal and external temperatures. As previously mentioned in **Section 6.2**, free convection and radiation from the external walls, which are non-linear phenomena, are limited because the display cabinet was closed with doors coated with low-emissivity materials.

*6.3.3.1. Heat losses through the rear wall and the cabinet ceiling (Domain I)*

In Domain I, the heat balance is established into seven zones from the upstream of the vertical rear duct to the DAG. Zones 1 to 6, i.e. EZ [1, 1…6], correspond to the heat exchange on the rear wall (exchange area, $S_w$). It is assumed that a part of supply air is flowing through the PBP at the mid height of each shelf (with air distribution coefficient, $\gamma$). In this way, the exchange areas of Zone 1 and 6 correspond to a half of the shelf height while the ones of Zone 2 to 5 correspond to two halves of the shelf height. Zone 7, i.e. EZ [1, 7], represents the heat exchange on the cabinet ceiling (exchange area, $S_c$).

Considering EZ [1, 1] (**Figure 6.5a**), the supply air (total mass flow rate, $\dot{m}_t$), after being cooled down by the heat exchanger, is assumed to be at the temperature at the thermostat sensor ($\theta_{th}$) which is located there. Flowing upward in the vertical rear duct, the supply air exchanges heat with the external air ($\theta_{ext}$) through the rear wall by conduction and by convection (overall heat transfer coefficient, $U_{ovw}$). The air temperature is then increased from $\theta_{th}$ to $\theta_{ard1}$. As by integration along a part of the rear duct (**Figure 6.5b**), the heat balance equation of EZ [1, 1] is given by

$$\dot{m}_t C_{pa} d\theta_a = U_{ovw}(\theta_{ext} - \theta_a) dS_w \Longrightarrow \frac{\theta_{ext} - \theta_{ard1}}{\theta_{ext} - \theta_{th}} = \exp\left(-\frac{U_{ovw} S_{w1}}{\dot{m}_t C_{pa}}\right)$$

$$\theta_{ard1} = \alpha_{rd1}\theta_{th} + (1 - \alpha_{rd1})\theta_{ext} \tag{6.3}$$

where $\alpha_{rd1} = \exp\left(-\frac{U_{ovw} S_{w1}}{\dot{m}_t C_{pa}}\right)$, $\theta_{th} = 0$ and $\theta_{ext} = 1$

A part of air flows into the shelf space while the other part (mass flow rate, $\dot{m}_{ard1}$) continues flowing upward along the rear duct until it reaches the DAG. The heat balance of EZ [1, 2…7] was carried out in the same manner as that of EZ [1, 1].

Because of the heat transfer from external air through the rear wall and the ceiling of the cabinet, the supply air temperature increased successively from $\theta_{th}$ to $\theta_{ard7}$.

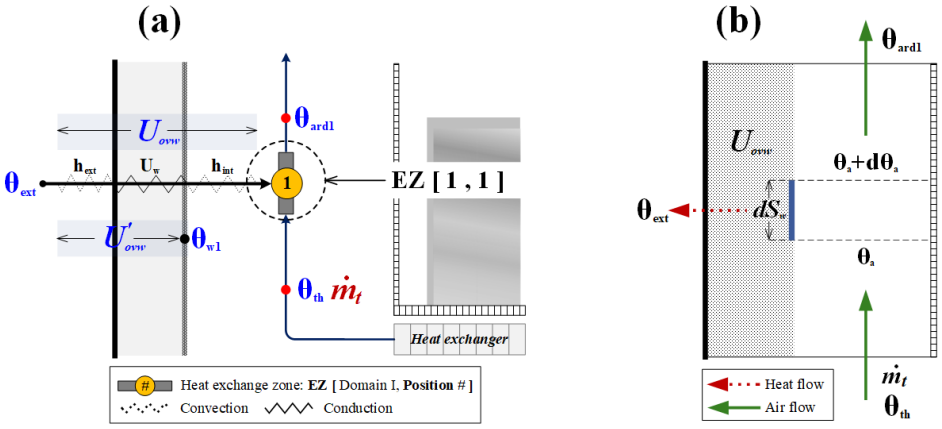


**Figure 6.5** Heat balance in Domain I at the position after the heat exchanger in the vertical rear duct denoted as EZ [1, 1]: (a) schematic view (b) mathematical view

*6.3.3.2. Heat transfer on the shelf space (Domain II)*

Domain II is composed of five cabinet shelves as shown in **Figure 6.4**. Each shelf has four heat exchange zones (EZ [2, 1…4, 1…5]) and one or two air mixing zones (MZ [2, 1…2, 1…5]). The heat transfer mechanism on the top shelf (Shelf 1) is different from the other shelves (Shelf 2 to 5) because there are additional heat loads due to the external ambient air infiltration through the door gaps and the cabinet lighting. For this reason, the heat balance equations at EZ [2, 1…4, 1] were individually developed and there is only one air mixing zone on this shelf (MZ [2, 1, 1]). It is to be emphasized that cold air leakage through the gap is assumed to occur between Shelf 1 and 2. In reality, this leakage spreads over the height of the door. Nevertheless, this simplification is acceptable because the external warm air infiltration has more impact on the internal temperature than the leakage of cold air.

*6.3.3.2.1. Heat exchange between air and the perforated back panel (interface between Domain I and II)*

Considering EZ [2, 1, 1] (**Figure 6.6a**), a part of the air (mass flow rate, $\dot{m}_{ash1} = \gamma_1 \dot{m}_t$ and temperature, $\theta_{ard5}$) flows horizontally from the back to the front at the mid height of Shelf 1. At steady state, the air temperatures before and after passing through the PBP are the same:

$$\theta_{ash11} = \theta_{ard5} \tag{6.4}$$

A similar equation applies for all shelves.

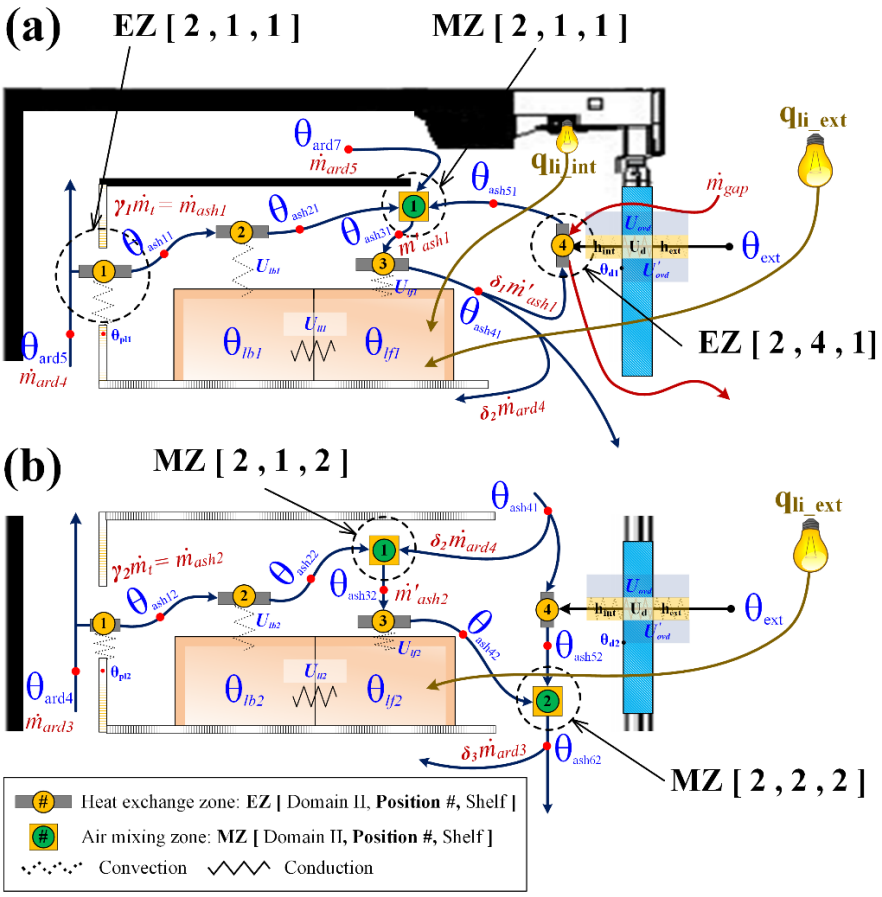


**Figure 6.6** Examples of heat and mass balances in Domain II: (a) Shelf 1 and (b) Shelf 2

*6.3.3.2.2. Heat exchange between the air and the back load*

For Shelf 1 (i.e. EZ [2, 2, 1], **Figure 6.6a**), the supply air from the back (mass flow rate, $\dot{m}_{ash1}$ and temperature, $\theta_{ash11}$) exchanges heat by convection (heat transfer coefficient, $U_{lb1}$) with the back load of temperature $\theta_{lb1}$. This results in the air temperature rise from $\theta_{ash11}$ to $\theta_{ash21}$.

$$\dot{m}_{ash1} C_{pa} d\theta_a = U_{lb1}(\theta_{lb1} - \theta_a) dS_l \Rightarrow \ln\left(\frac{\theta_{lb1} - \theta_{ash21}}{\theta_{lb1} - \theta_{ash11}}\right) = -\frac{U_{lb1} S_{l1}}{\dot{m}_{ash1} C_{pa}}$$

$$\theta_{ash21} = \alpha_{sh11}\theta_{ash11} + (1 - \alpha_{sh11})\theta_{lb1} \tag{6.5}$$

where $\alpha_{sh11} = \exp\left(-\frac{U_{lb1} S_{l1}}{\dot{m}_{ash1} C_{pa}}\right)$

In addition to this convective exchange with air, the back load also exchanges heat with the front load by conduction (heat transfer coefficient, $U_{ll1}$). At steady state, the heat balance equation for the back load is

$$U_{ll1}S_{ll1}(\theta_{lb1} - \theta_{lf1}) + \dot{m}_{ash1}C_{pa}(\theta_{ash21} - \theta_{ash11}) = 0$$

$$\theta_{ash21} = \theta_{ash11} + \beta_{sh11}(\theta_{lf1} - \theta_{lb1}) \quad (6.6)$$

where $\beta_{sh11} = \frac{U_{ll1}S_{ll1}}{\dot{m}_{ash1}C_{pa}}$

An analogous analysis of heat balance at this zone was applied for all shelves, i.e. EZ [2, 2, 1…5].

*6.3.3.2.3. Heat exchange between the mixed air and the front load for Shelf 1*

The air above the front load at Shelf 1 is a mix of three air streams as depicted in **Figure 6.6a**. This mixing zone, MZ [2, 1, 1] includes air from the DAG (mass flow rate, $\dot{m}_{ard5}$ and temperature, $\theta_{ard7}$), air from the PBP (mass flow rate, $\dot{m}_{ash1}$ and temperature, $\theta_{ash21}$) and a part of the recirculating air (mass flow rate, $\delta_1\dot{m}'_{ash1}$ and temperature, $\theta_{ash51}$). After mixing, the air mass flow rate and temperature becomes $\dot{m}'_{ash1}$ and $\theta_{ash31}$, respectively.

Mass balance:

$$\dot{m}'_{ash1} = \dot{m}_{ard5} + \dot{m}_{ash1} + \delta_1\dot{m}'_{ash1} \implies \dot{m}'_{ash1} = \frac{\dot{m}_{ash1}+\dot{m}_{ard5}}{1-\delta_1} \quad (6.7)$$

Energy balance:

$$\dot{m}'_{ash1}\theta_{ash31} = \dot{m}_{ard5}\theta_{ard7} + \dot{m}_{ash1}\theta_{ash21} + \delta_1\dot{m}'_{ash1}\theta_{ash51} \quad (6.8)$$

Then, this mixed air exchanges heat with the front load, EZ [2, 3, 1], and its temperature becomes $\theta_{ash41}$ (the integration along the exchange surface is the same as for **Eq (6.3)** and **(6.5)**).

$$\theta_{ash41} = \alpha_{sh21}\theta_{ash31} + (1 - \alpha_{sh21})\theta_{lf1} \quad (6.9)$$

where $\alpha_{sh21} = \exp\left(-\frac{U_{lf1}S_{l1}}{\dot{m}'_{ash1}C_{pa}}\right)$

In addition to this convective exchange with the air, the front load also exchanges heat with the back load by conduction (heat transfer coefficient, $U_{ll1}$) and receives

heat from the conversion of supermarket and display cabinet lighting powers ($q_{li1}$). At steady state:

$$U_{ll1}S_{ll1}(\theta_{lb1} - \theta_{lf1}) + q'_{li1} = \dot{m}'_{ash1}C_{pa}(\theta_{ash41} - \theta_{ash31})$$

$$\theta_{ash41} = \theta_{ash31} + \beta_{sh21}(\theta_{lb1} - \theta_{lf1}) + q''_{li1} \quad (6.10)$$

where $\beta_{sh21} = \frac{U_{ll1}S_{ll1}}{\dot{m}'_{ash1}C_{pa}}$, $q'_{li1} = \frac{q_{li1}}{T_{ext} - \bar{T}_{th}}$ and $q''_{li1} = \frac{q'_{li1}}{\dot{m}'_{ash1}C_{pa}}$

*6.3.3.2.4. Heat exchange between the mixed air and the front load for Shelves 2-5*

Unlike Shelf 1, different analysis of heat balance is applied to the other shelves. The heat transfer mechanism on Shelf 2 was selected as a case sample of the model development and it is illustrated in **Figure 6.6b**. Here, there are two air streams involved at the mixing zone, MZ [2, 1, 2], including the air from the PBP (mass flow rate, $\dot{m}_{ash2}$ and temperature, $\theta_{ash22}$) and a part of the air curtain (mass flow rate, $\delta_2\dot{m}_{ard4}$ and temperature, $\theta_{ash41}$).

Mass balance:

$$\dot{m}'_{ash2} = \dot{m}_{ash2} + \delta_2\dot{m}_{ard4} \quad (6.11)$$

Energy balance:

$$\dot{m}'_{ash2}\theta_{ash32} = \dot{m}_{ash2}\theta_{ash22} + \delta_2\dot{m}_{ard4}\theta_{ash41} \quad (6.12)$$

The mixed air then exchanges heat with the front load, EZ [2, 3, 2], and its temperature becomes $\theta_{ash42}$.

$$\theta_{ash42} = \alpha_{sh22}\theta_{ash32} + (1 - \alpha_{sh22})\theta_{lf2} \quad (6.13)$$

where $\alpha_{sh22} = \exp\left(-\frac{U_{lf2}S_{l2}}{\dot{m}'_{ash2}C_{pa}}\right)$

The load located at the front of Shelf 2 is subjected to the convection with the mixed air, the conduction with the adjacent load at the back (heat transfer coefficient, $U_{ll2}$) and the heat conversion of visible radiation from the supermarket lighting power ($q_{li2}$). At steady state:

$$U_{ll2}S_{ll2}(\theta_{lb2} - \theta_{lf2}) + q'_{li2} = \dot{m}'_{ash2}C_{pa}(\theta_{ash42} - \theta_{ash32})$$

$$\theta_{ash42} = \theta_{ash32} + \beta_{sh22}(\theta_{lb2} - \theta_{lf2}) + q''_{li2} \quad (6.14)$$

where $\beta_{sh22} = \frac{U_{ll2} S_{ll2}}{\dot{m}'_{ash2} C_{pa}}$, $q'_{li2} = \frac{q_{li2}}{T_{ext} - \bar{T}_{th}}$ and $q''_{li2} = \frac{q'_{li2}}{\dot{m}'_{ash2} C_{pa}}$

An analogous analysis of mass balance at MZ [2, 1, 2] and heat transfer at EZ [2, 3, 2] was applied to Shelf 3 to 5.

*6.3.3.2.5. Heat losses through the door for Shelf 1*

The heat exchange through the door in front of Shelf 1, EZ [2, 4, 1], is different from the other shelves (**Figure 6.6a**). The heat balance equation was specifically developed. Based on the experimental study, there was a formation of air recirculation at the front door of the display cabinet (see **Figure 6.2b**). This air recirculation involves a part of the air curtain (mass flow rate, $\delta_1 \dot{m}_{ash1}$ and temperature, $\theta_{ash41}$) which interacts with the air flowing through the door gaps (mass flow rate, $\dot{m}_{gap}$), and it is submitted to heat losses through the glass doors (overall heat transfer coefficient, $U_{ovd}$). These exchanges result in an increase of air temperature to be $\theta_{ash51}$. To simplify the model, an equivalent thermal conductance ($C_{eq}$) was determined to take into account the effect of overall heat transfer coefficient through the glass door and the mass flow rate of the air infiltration through the gaps defined as

$$C_{eq} = U_{ovd} S_{d1} + \dot{m}_{gap} C_{pa} \tag{6.15}$$

At steady state:

$$\theta_{ash51} = \alpha_{sh31} \theta_{ash41} + (1 - \alpha_{sh31}) \theta_{ext} \tag{6.16}$$

where $\alpha_{sh31} = \exp\left(-\frac{C_{eq}}{\delta_1 \dot{m}'_{ash1} C_{pa}}\right)$

*6.3.3.2.6. Heat losses through the door for Shelf 2-5 (development on Shelf 2 as a* case *sample)*

As mentioned earlier (**Section 6.3.3.2**), it was assumed that there is no air infiltration/leakage through the gaps located in front of the other shelves. The air curtain from the top shelf is split into two parts. The first part (mass flow rate, $\delta_2 \dot{m}_{ard4}$ and temperature, $\theta_{ash41}$) is mixed with the air flowing from the back of Shelf 2 and exchanges heat with the front load as described in Subsection iv. The second part (mass flow rate, $(1 - \delta_2) \dot{m}_{ard4}$ and temperature, $\theta_{ash41}$) continues flowing downwards and exchanges heat with the external ambient air through the

glass doors (overall heat transfer coefficient, $U_{ovd}$ ), and consequently its temperature increases to be $\theta_{ash52}$.

$$\theta_{ash52} = \alpha_{sh32}\theta_{ash41} + (1 - \alpha_{sh32})\theta_{ext} \tag{6.17}$$

where $\alpha_{sh32} = \exp\left(-\frac{U_{ovd}S_{d2}}{(1-\delta_2)\dot{m}_{ard4}C_{pa}}\right)$

In the mixing zone (i.e. MZ [2, 2, 2], **Figure 6.6b**), this air mixes with the air which exchanged heat with the load located at the front of the shelf (mass flow rate, $\dot{m}'_{ash2}$ and temperature, $\theta_{ash42}$). The air temperature becomes $\theta_{ash62}$.

Mass balance:

$$\dot{m}_{ard3} = \dot{m}'_{ash2} + (1 - \delta_2)\dot{m}_{ard4} \tag{6.18}$$

Energy balance:

$$\dot{m}_{ard3}\theta_{ash62} = \dot{m}'_{ash2}\,\theta_{ash42} + (1 - \delta_2)\dot{m}_{ard4}\theta_{ash52} \tag{6.19}$$

An analogous analysis of heat and mass balances at these zones, i.e. EZ [2, 4, 2] and MZ [2, 2, 2], was applied to Shelf 3 to 5.

*6.3.3.3. Equations in matrix form*

In Domain I, the air temperature in the vertical rear duct is successively calculated and the equations can be generalized in the following form:

$$\theta_{ard,i} = \alpha_{rd,i} \cdot \theta_{ard,i-1} + \left(1 - \alpha_{rd,i}\right) \cdot \theta_{ext} \text{ for } i = 1, 2, \dots, 7 \tag{6.20}$$

Note that the air temperature of $i = 0$ refers to the temperature near the thermostat sensor ($\theta_{ard0} = \theta_{th}$).

Equation in a matrix form is used to summarize the heat balance equations in Domain II. Because of the difference of heat transfer phenomena, the equation of Shelf 1 (top shelf, $j = 1$) is separately formulated:

$$\bar{\bar{A}} \cdot \vec{\theta}_1 = \vec{B} \cdot \theta_{ard7} + \vec{C} \cdot \theta_{ash1,1} + \vec{D} \cdot \theta_{ext} + \vec{E} \cdot q''_{li1} \tag{6.21}$$

where

$$\bar{\bar{A}} = \begin{bmatrix} 1 & 0 & 0 & 0 & -(1-\alpha_{sh1,1}) & 0 \\ 1 & 0 & 0 & 0 & \beta_{sh1,1} & -\beta_{sh1,1} \\ \dot{m}_{ash,1} & -\dot{m}'_{ash1} & 0 & -\delta_m \dot{m}'_{ash1} & 0 & 0 \\ 0 & \alpha_{sh2,1} & -1 & 0 & 0 & (1-\alpha_{sh2,1}) \\ 0 & 1 & -1 & 0 & \beta_{sh2,1} & -\beta_{sh2,1} \\ 0 & 0 & -\alpha_{sh3,1} & 1 & 0 & 0 \end{bmatrix}$$

$$\vec{\theta}_1 = \begin{bmatrix} \theta_{ash2,1} \\ \theta_{ash3,1} \\ \theta_{ash4,1} \\ \theta_{ash5,1} \\ \theta_{lb,1} \\ \theta_{lf,1} \end{bmatrix}; \vec{B} = \begin{bmatrix} 0 \\ 0 \\ -\dot{m}_{ard5} \\ 0 \\ 0 \\ 0 \end{bmatrix}; \vec{C} = \begin{bmatrix} \alpha_{sh1,1} \\ 1 \\ 0 \\ 0 \\ 0 \\ 0 \end{bmatrix}; \vec{D} = \begin{bmatrix} 0 \\ 0 \\ 0 \\ 0 \\ 0 \\ (1-\alpha_{sh3,1}) \end{bmatrix} \text{ and } \vec{E} = \begin{bmatrix} 0 \\ 0 \\ 0 \\ 0 \\ -1 \\ 0 \end{bmatrix}$$

The equations of Shelf 2 to 5 ( $j = 2 \dots 5$ ) are generalized as follows:

$$\theta_{ash1,j} = \theta_{ard,6-j} \tag{6.22}$$

$$\bar{\bar{F}} \cdot \vec{\theta}_j = \vec{G} \cdot \theta_{ash,k,j-1} + \vec{H} \cdot \theta_{ash1,j} + \vec{I} \cdot q''_{li,j} \begin{cases} \text{if } j = 2 \rightarrow k = 4 \\ \text{if } j = 3,4,5 \rightarrow k = 6 \end{cases} \tag{6.23}$$

where

$$\bar{\bar{F}} = \begin{bmatrix} 1 & 0 & 0 & -(1-\alpha_{sh1,j}) & 0 \\ 1 & 0 & 0 & \beta_{sh1,j} & -\beta_{sh1,j} \\ \dot{m}_{ash,j} & -\dot{m}'_{ash,j} & 0 & 0 & 0 \\ 0 & \alpha_{sh2,j} & -1 & 0 & (1-\alpha_{sh2,j}) \\ 0 & 1 & -1 & \beta_{sh2,j} & -\beta_{sh2,j} \end{bmatrix}$$

$$\vec{\theta}_j = \begin{bmatrix} \theta_{ash2,j} \\ \theta_{ash3,j} \\ \theta_{ash4,j} \\ \theta_{lb,j} \\ \theta_{lf,j} \end{bmatrix}; \vec{G} = \begin{bmatrix} 0 \\ 0 \\ -\delta_j \dot{m}_{ard,6-j} \\ 0 \\ 0 \end{bmatrix}; \vec{H} = \begin{bmatrix} \alpha_{sh1,j} \\ 1 \\ 0 \\ 0 \\ 0 \end{bmatrix} \text{ and } \vec{I} = \begin{bmatrix} 0 \\ 0 \\ 0 \\ -1 \\ 0 \end{bmatrix}$$

and

$$\theta_{ash5,j} = \alpha_{sh3,j}\theta_{ash,k,j-1} + \left(1-\alpha_{sh3,j}\right)\theta_{ext} \tag{6.24}$$

$$\theta_{ash6,j} = \left(\dot{m}'_{ash,j}\theta_{ash4,j} + \left(1-\delta_j\right)\dot{m}_{ard,6-j}\theta_{ash5,j}\right) / \dot{m}_{ard,5-j} \tag{6.25}$$

### *6.3.4. Estimation of model input parameters*

Input parameters used in the developed model were obtained from several sources: physical measurement, calculation based on literature and material properties (**Table 6.1**) and model fitting.

**Table 6.1** Thermal properties of materials

| Materials | Density [kg·m$^{-3}$] | Heat capacity [J·kg$^{-1}$·K$^{-1}$] | Thermal conductivity [W·m$^{-1}$·K$^{-1}$] | Reference |
|---|---|---|---|---|
| Air (at 0 °C) | 1.287 | 1006 | 0.024 | (Bergman et al., 2011) |
| Aluminium | 2700 | 910 | 237 | |
| Polyurethane foam | 70 | 1045 | 0.026 | |
| Glass pane | 2500 | 750 | 1.4 | |
| Methylcellulose | 1071 | 3372 | 0.510 | (Icier and Ilicali, 2005) |
| Argon gas (at 20 °C) | | | 0.017 | (Annaratone, 2010) |

#### *6.3.4.1. Air flow rate*

The air flow rate at the upstream of the vertical rear duct ($\dot{m}_t$) and the proportion of the air flowing through the PBP at different shelves (represented by the air distribution coefficient $\gamma_i$) are input parameters of the model. The measurement of the air velocity in the rear duct was thus carried out by using a hot-wire anemometer (Testo 435-4) (Chaomuang et al., 2019), which was previously calibrated in the range of 0-2 m·s$^{-1}$ (uncertainty 0.02 m·s$^{-1}$). Three holes were drilled in the rear wall of the cabinet (at z = -260, 0, and +260 mm) at six height levels (at y = 15, 215, 465, 715, 965 and 1335 mm) to introduce the instrument. The flow perturbation due to the intrusive feature of the test probes can be considered negligible because the sensor is very small (7.5 mm in diameter) compared to the space in the rear duct (60 mm in width). There were nine measurement positions (three positions for each hole) across the cross-sectional area of the duct. At each position, the air velocity was recorded every second for 5 min. and its time-averaged value was then calculated. The mass flow rate and the proportion of the air flowing through the PBP at different heights were then estimated based on the average value obtained at the nine positions. The results are reported in **Table 6.2**. Given the proportion of the air flowing over the entire PBP, the mass flow rate at the DAG was attributed to about half of the total mass flow rate. In addition to the temperature measurements, the air velocity at the front of display cabinet (for different heights)

from the discharge to return air grille was also measured by a hot wire anemometer and the shape of the curtain was presented (Chaomuang et al., 2019a).

**Table 6.2** Values of input parameters used in the heat transfer model of a closed refrigerated display cabinet

| Parameters | Value | Unit | Reference |
|---|---|---|---|
| Mass flow rate | | | |
| Rear duct upstream ($\dot{m}_t$) | 0.1120 | kg·s$^{-1}$ | Measurement |
| Gaps ($\dot{m}_{gap}$) | 0.0051 | kg·s$^{-1}$ | Model fitting |
| Air distribution coefficients† | | | |
| Air supply from PBP ($\gamma_{1..5}$) | (0.02, 0.02, 0.04, 0.05, 0.36) | - | Measurement |
| Air supply at the air curtain ($\delta_{1..5}$) | (0.90, 0.70, 0.70, 0.70, 0.70) | - | Model fitting |
| Heat transfer coefficients | | | |
| Convection | | | |
| Back load ($U_{lb}$) | 15 | W·m$^{-2}$·K$^{-1}$ | Model fitting |
| Front load ($U_{lf}$) | 24 | W·m$^{-2}$·K$^{-1}$ | Model fitting |
| Conductive | | | |
| Between the two loads ($U_{ll}$) | 3.4 | W·m$^{-2}$·K$^{-1}$ | Calculation |
| Overall | | | |
| Rear wall and ceiling ($U_{ovw}$) | 0.77 | W·m$^{-2}$·K$^{-1}$ | Calculation |
| Door ($U_{ovd}$) | 1.02 | W·m$^{-2}$·K$^{-1}$ | Calculation |
| Equivalent thermal conductance ($C_{eq}$) | 17.6 | W·m$^{-2}$·K$^{-1}$ | Calculation |
| Exchange areas (for a cabinet with 1.25 m in length) | | | |
| Rear walls ($S_w$) | | | |
| $S_{w1}$ | 0.216 | m$^2$ | Measurement |
| $S_{w2...5}$ | 0.313 | m$^2$ | Measurement |
| $S_{w6}$ | 0.156 | m$^2$ | Measurement |
| Ceiling | | | |
| $S_c$ | 0.500 | m$^2$ | Measurement |
| Doors ($S_d$) | | | |
| $S_{d1...4}$ | 0.313 | m$^2$ | Measurement |
| $S_{d5}$ | 0.431 | m$^2$ | Measurement |
| Loads ($S_l$) | | | |
| $S_{l1...5}$ | 0.438 | m$^2$ | Measurement |
| $S_{ll1...5}$ | 0.250 | m$^2$ | Measurement |
| Lightings | | | |
| $q_{li1}$ | 10 | W | Calculation |
| $q_{li2...5}$ | 0.25 | W | Calculation |

*6.3.4.2. Conductive heat transfer coefficient between two adjacent loads*

The conductive heat transfer coefficient between the back and front loads was calculated using a thermal resistance concept and it was supposed to have the same value for every shelf. In our study, the load was made of methylcellulose of which the thermal conductivity is about 0.51 $W \cdot m^{-1} \cdot K^{-1}$ (Icier and Ilicali, 2005) and the distance between adjacent loads (core to core) is 0.15 m.

$$U_{ll1} = U_{ll2} = U_{ll3} = U_{ll4} = U_{ll5} = \frac{\lambda}{e} = 3.4 \text{ W} \cdot \text{m}^{-2} \cdot \text{K}^{-1}$$

The air space between two adjacent loads was considered negligible since the test packages were fully loaded in the display cabinet.

*6.3.4.3. Overall wall heat transfer coefficient*

The overall heat transfer coefficients due to the heat loss through the rear wall, ceiling and door of the display cabinet were also estimated based on the thermal resistance concept. Natural convection between the external air and the outer wall/door ($h_{ext}$~10 $W \cdot m^{-2} \cdot K^{-1}$, Laguerre et al., 2012a), conduction within the wall/door ($U_w$ or $U_d$) and forced convection between the supply air and the inner wall/door ($h_{int}$~20 $W \cdot m^{-2} \cdot K^{-1}$, Laguerre et al., 2012a) were taken into account.

The rear wall and the ceiling were composed of an insulation layer made of polyurethane foam (30-mm thickness) and an aluminum sheet (0.5-mm thickness), manufacturer data.

$$U_{ovw} = U_{ovc} = \frac{1}{\frac{1}{h_{ext}} + \frac{1}{U_w} + \frac{1}{h_{int}}} = \frac{1}{\frac{1}{h_{ext}} + \frac{e_{al}}{\lambda_{al}} + \frac{e_{pu}}{\lambda_{pu}} + \frac{1}{h_{int}}} = 0.77 \text{ W} \cdot \text{m}^{-2} \cdot \text{K}^{-1}$$

The door of the cabinet is a double-glazing window made of two panes of tempered glass (4-mm thickness each) split by an argon gap (14-mm thickness), manufacturer data.

$$U_{ovd} = \frac{1}{\frac{1}{h_{ext}} + \frac{1}{U_d} + \frac{1}{h_{int}}} = \frac{1}{\frac{1}{h_{ext}} + \frac{2e_{gl}}{\lambda_{gl}} + \frac{e_{ag}}{\lambda_{ag}} + \frac{1}{h_{int}}} = 1.02 \text{ W} \cdot \text{m}^{-2} \cdot \text{K}^{-1}$$

*6.3.4.4. Exchange area for the display cabinet in length of 1.25 m*

The exchange area of the rear wall and door was split with respect to the shelf height: 0.25 m for Shelf 1 to 4 and 0.345 m for Shelf 5. The values are reported in

**Table 6.2**. The exchange area between the loads located at the back and the front and the surrounding air was estimated as:

$$S_l = S_{lb} = S_{lf} = (0.2 + 0.15) \times 1.25 = 0.4375 \text{ m}^2$$

The exchange area between the back and the front loads by conduction was estimated as:

$$S_{ll} = 0.2 \times 1.25 = 0.25 \text{ m}^2$$

*6.3.4.5. Heat absorption due to the supermarket and display cabinet lightings*

The illuminance level in a supermarket where refrigerated display cabinets are installed ranges from 300 to 1000 lux (IESNA, 1991) depending on types of designed activity areas. On average, the value of 650 lux (which is equivalent to lighting power density of about 1.0 $\text{W}\cdot\text{m}^{-2}$) was used and dispersed equally to the front loads at all shelves.

$$q_{li\_ext} = q_{li2\ldots5} = (1.0 \text{ W} \cdot \text{m}^{-2})(0.25 \text{ m}^2) = 0.25 \text{ W}$$

Light-Emitting Diodes (LED) with input power of 13 W (manufacturer data) are used in the studied display cabinet. Due to its proximity to the cabinet lighting, the load at Shelf 1 would receive most of the heat dissipated from this lighting. The remainder lighting may be received by the loads on the other shelves and even escapes from the cabinet, which is difficult to quantify. As a first approach, 75% of the cabinet lighting power was only applied to the front load at Shelf 1.

$$q_{li\_int} = (0.75)(13 \text{ W}) = 9.75 \text{ W}$$

According to both the supermarket and display cabinet lightings, the following value was used:

$$q_{li1} = q_{li\_ext} + q_{li\_int} = 10 \text{ W}$$

*6.3.4.6. Model fitting*

There are five input parameters which are difficult to be quantified with physical experiment: the parameter of air circulation at Shelf $1(\delta_1)$, the air distribution coefficients at the other shelves ($\delta_{2-5}$), the mass flow rate of the air infiltration through the door gaps $(\dot{m}_{gap})$ and the convective heat transfer coefficients between the load surface and the surrounding air (back load $U_{lb}$ and front load $U_{lf}$). A model

fitting based on full factorial design was then performed to determine a plausible combination of these input parameters. The combination providing the minimum error between the calculated and the measured values of the air and load temperatures was applied to the developed model. The mean absolute error (MAE) based on 20 temperature measurements in the closed display cabinet for the ambient temperature of 19.5 °C was used to evaluate this model fitting. The twenty temperature positions were composed of ten positions of air temperature (five positions in the rear duct and five positions at 2 cm from the front loads at five shelves, stars in **Figure 6.1**) and ten positions of load temperature (five positions at the back and five positions at the front, circle in **Figure 6.1**). The load temperature is the averaged value of the one at the top and the bottom layers. These positions were chosen as they allow the prediction of air temperature along the rear duct, along the air curtain and of load temperature at every shelf. The same twenty temperature positions were also used for the model validation at other ambient temperatures.

$$\mathrm{MAE} = \frac{1}{N}\sum_{i=1}^{N}\left|T_{num,i} - T_{exp,i}\right| \tag{6.26}$$

The range of 0.1 to 0.9 (interval of 0.1) was applied for the air distribution coefficients of the air curtain. As the airflow characteristic at Shelf 1 is different from the other shelves, the air distribution coefficient of the air circulation $(\delta_1)$ was individually estimated while the same value of the coefficient $(\delta_{2\ldots5})$ was applied to the other shelves. The mass flow rate of the air infiltration through the door gaps $(\dot{m}_{gap})$ was estimated based on the airflow ratio $\delta_{gap} = \frac{\dot{m}_{gap}}{\dot{m}_{DAG}}$ where $\dot{m}_{DAG}$ is the mass flow rate of the air flowing from the DAG. The value was assumed to be between 5% and 20% (interval of 1%). The range used to evaluate the values of the convective heat transfer coefficients is based on the values measured by Laguerre et al. (2012b). The convective heat transfer coefficient $\left(U_{lf}\right)$ between the loads located at the front of the open display cabinet and the air were reported in the range of 18-26 $W{\cdot}m^{-2}{\cdot}K^{-1}$. Because the back loads are not exposed to the air curtain, the heat transfer coefficient $(U_{lb})$ was assumed to be slightly lower than for the front load: values in the range of 15-20 $W{\cdot}m^{-2}{\cdot}K^{-1}$ (interval of 1) were tested. Based on the specified ranges and intervals of the parameter values, 69984 combinations were studied in total. The values of the top ten combinations of these input

parameters providing the minimum MAE are reported in **Table 6.3** and the first combination was selected and applied to the model. A sensitivity study was performed by using these values of fitting parameters as a reference. As shown in **Figure 6.7**, a 20-percent increase/decrease of the air flow ratio ($\delta_{gap}$) caused the warmest load temperature to be increased/decreased up to 0.2 °C while it is less than 0.1 °C for other parameters.

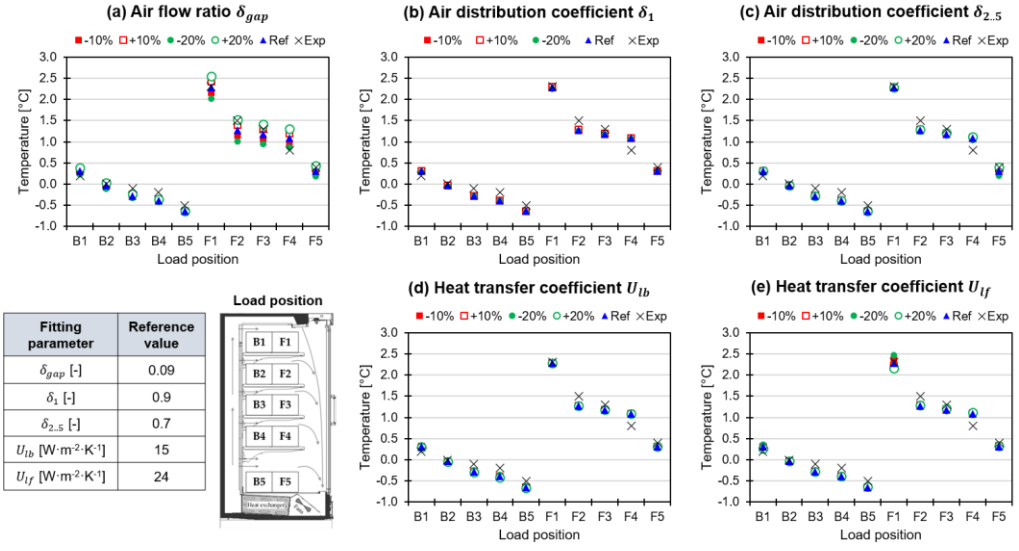


| Fitting parameter | Reference value |
|---|---|
| $\delta_{gap}$ [-] | 0.09 |
| $\delta_1$ [-] | 0.9 |
| $\delta_{2..5}$ [-] | 0.7 |
| $U_{lb}$ [W·m$^{-2}$·K$^{-1}$] | 15 |
| $U_{lf}$ [W·m$^{-2}$·K$^{-1}$] | 24 |




**Figure 6.7** Sensibility study showing the variation in load temperatures with respect to the fitting parameters: air flow ratio (a), air distribution coefficients at Shelf 1 (b), air distribution coefficients at Shelf 2 to 5 (c), heat transfer coefficients over the back loads (d) heat transfer coefficients over the front loads (e).

**Table 6.3** Values of the first top ten combinations of the input parameters with the mean absolute error (MAE) for the model fitting

| Parameter | Unit | 1† | 2 | 3 | 4 | 5 | 6 | 7 | 8 | 9 | 10 |
|---|---|---|---|---|---|---|---|---|---|---|---|
| $\delta_1$ | - | 0.9 | 0.9 | 0.8 | 0.8 | 0.9 | 0.9 | 0.8 | 0.9 | 0.3 | 0.9 |
| $\delta_{2-5}$ | - | 0.7 | 0.7 | 0.7 | 0.7 | 0.7 | 0.7 | 0.7 | 0.7 | 0.7 | 0.7 |
| $U_{lb}$ | $W \cdot m^2 \cdot K^{-1}$ | 15 | 15 | 15 | 15 | 15 | 16 | 15 | 15 | 15 | 15 |
| $U_{lf}$ | $W \cdot m^2 \cdot K^{-1}$ | 24 | 25 | 23 | 24 | 26 | 24 | 25 | 27 | 22 | 23 |
| $\delta_{gap}$ | - | 0.09 | 0.09 | 0.09 | 0.09 | 0.09 | 0.09 | 0.09 | 0.09 | 0.1 | 0.09 |
| MAE | °C | 0.1472 | 0.1476 | 0.1478 | 0.1479 | 0.1481 | 0.1483 | 0.1484 | 0.1484 | 0.1485 | 0.1486 |

†*The combination of parameters used in the developed model in this study*

## 6.4. Static model validation

For model validation purposes, measurements of air and load temperatures at various positions in the closed display cabinet were carried out for three ambient temperatures (14.6 °C, 19.5 °C and 24.4 °C). As shown in **Figure 6.8**, the air temperature just after the heat exchanger decreased when the external ambient air temperature increased because the refrigeration system is required to provide more cooling capacity to compensate the additional heat gain. For this reason, different time-averaged air temperatures at the thermostat sensor ($\overline{T}_{th}$) corresponding to the ambient temperature were applied to the model.

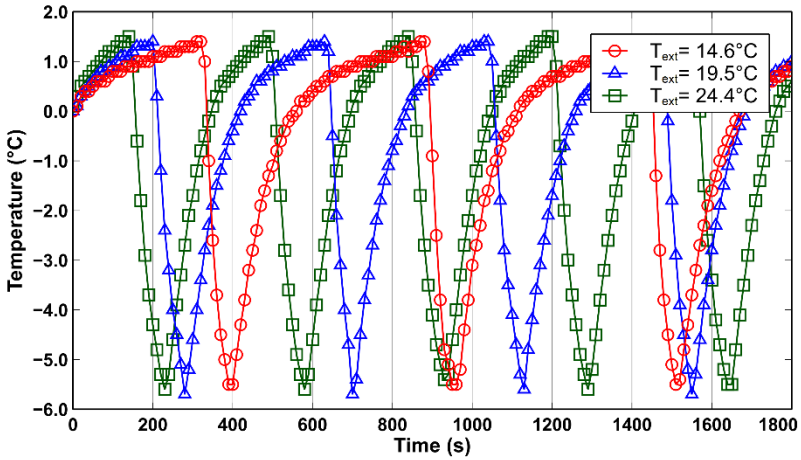


**Figure 6.8** Temperature variation of the air after the heat exchanger (T_th) for three ambient temperatures.

The results of calculated and measured air and load temperatures for three ambient temperatures were illustrated in **Figure 6.9**. Temperature of the air in the vertical rear duct progressively increased due to heat losses through the rear wall. As the rear duct wall adjacent to the shelf space is perforated, some cold air is permitted to cool down the load at the back of the cabinet. As a result, the temperature of the load located at the back tended to decrease from the top to the bottom shelf. Similarly, the temperature of load located at the front also decreased from the top to the bottom shelves, but with higher temperature. This is because there were additional heat loads including heat losses through the glass door, the air infiltration through the door gap and the heat absorption corresponding to the cabinet lighting. In addition, the temperature was affected by the different percentages of perforation

area of the back panel on each shelf: lowest at the top and highest at the bottom. These findings showed that the highest and lowest temperature positions in this closed display cabinet were respectively at the front of the top shelf and the back of the bottom shelf. Overall, both air and load temperatures in the closed display cabinet increased with an increase of external ambient temperature at all positions in the shelves-space storage (**Table 6.4**).

As depicted in **Figure 6.10**, comparative results provide a good agreement between the calculated and measured air and load temperatures even for the two external temperatures (14.6 °C and 24.4 °C) which were not used for the model fitting. The overall mean absolute error based on 60 paired-data of three ambient temperatures was about 0.2 °C ($R^2 = 0.96$, **Table 6.5**). Mostly, the air temperature at the front of the shelves was slightly over-estimated. The measurement position should be mentioned as a possible source of uncertainty because a single point measurement may not be representative of the air at the front. Nevertheless, the model is likely to well represent the load temperature. The maximum difference of the calculated and measured load temperatures was less than 0.5 °C for every studied position. Besides, the differences between the highest and the coldest load temperatures obtained from the experimental and the numerical data were less than 14% for all studied ambient temperatures.

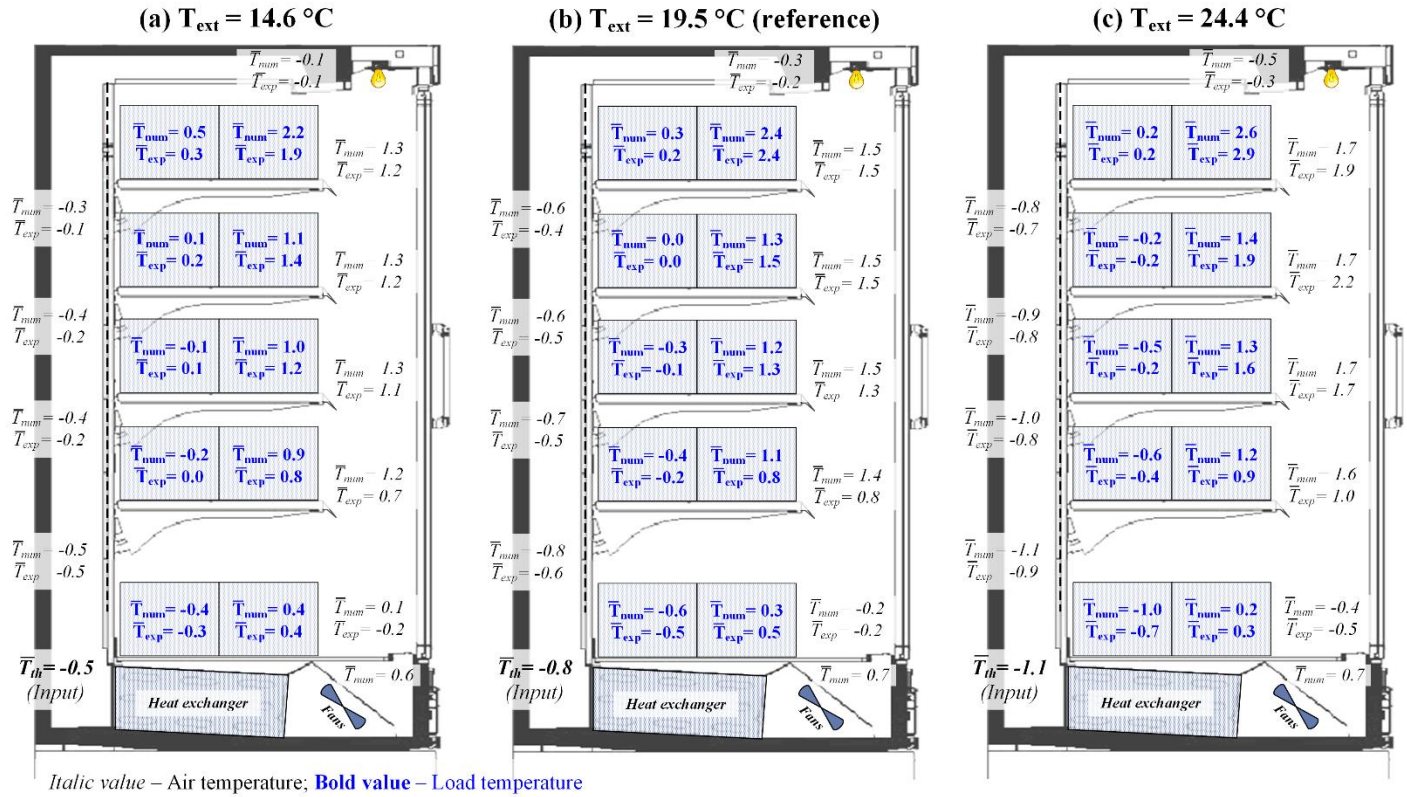


**Figure 6.9** Comparison between numerical and experimental results of air and load temperatures (in °C) in a closed display cabinet for three ambient temperatures: (a) 14.6 °C, (b) 19.5 °C and (c) 24.4 °C. (Experimental values indicated for load temperature are the averages of the top and bottom layers)

**Table 6.4** Effect of ambient temperature on load temperature at various positions in a closed refrigerated display cabinet

| $T_{ext}$ [°C] | $\overline{T}_{th}$ [°C] | $\overline{T}_{l\_exp} - \overline{T}_{th}$ [°C] | | | | | | $\overline{T}_{l\_num} - \overline{T}_{th}$ [°C] | | | | | |
|---|---|---|---|---|---|---|---|---|---|---|---|---|---|
| | | Back | | | Front | | | Back | | | Front | | |
| | | 1 | 3 | 5[(a)] | 1[(b)] | 3 | 5 | 1 | 3 | 5[a] | 1[b] | 3 | 5 |
| 14.6 | -0.5 | 0.8 | 0.6 | 0.2 | 2.4 | 1.7 | 0.9 | 0.9 | 0.4 | 0.1 | 2.6 | 1.5 | 0.9 |
| 19.5 | -0.8 | 1.0 | 0.7 | 0.3 | 3.1 | 2.1 | 1.2 | 1.1 | 0.5 | 0.2 | 3.1 | 2.0 | 1.1 |
| 24.4 | -1.1 | 1.3 | 0.9 | 0.4 | 4.0 | 2.7 | 1.5 | 1.3 | 0.6 | 0.2 | 3.6 | 2.4 | 1.3 |

*[(a)]Lowest temperature position*

*[(b)]Highest temperature position*

**Table 6.5** Error of air and load temperatures calculated from the developed model for different ambient temperatures compared to the measured values

| $T_{ext}$ [°C] | Mean absolute error [°C] | | | Coefficient of determination[†], $R^2$ [-] | | |
|---|---|---|---|---|---|---|
| | Both | Load | Air | Both | Load | Air |
| 14.6 | 0.14 | 0.13 | 0.15 | 0.95 | 0.96 | 0.95 |
| 19.5 | 0.15 | 0.14 | 0.16 | 0.96 | 0.97 | 0.97 |
| 24.4 | 0.24 | 0.24 | 0.23 | 0.96 | 0.96 | 0.96 |
| Overall | 0.17 | 0.18 | 0.17 | 0.96 | 0.96 | 0.95 |

*[†]The coefficient of determination is defined as* $R^2 = \frac{\left[\sum_{i=1}^{N}(T_{num,i}-\overline{T}_{num})(T_{exp,i}-\overline{T}_{exp})\right]^2}{\sum_{i=1}^{N}(T_{num,i}-\overline{T}_{num})^2 \sum_{i=1}^{N}(T_{exp,i}-\overline{T}_{exp})^2}$

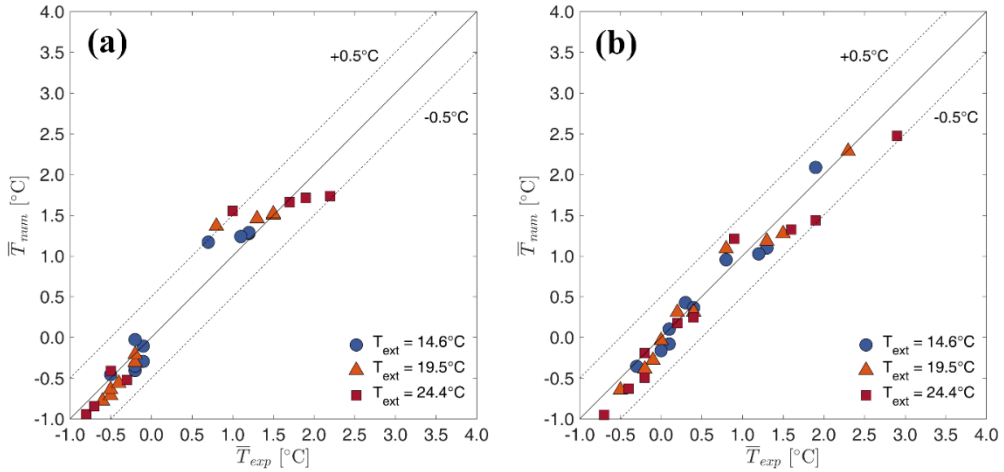


**Figure 6.10** Calculated and measured time-averaged temperatures of (a) air and (b) load in a closed display cabinet for ambient temperatures of 14.6, 19.5 and 24.4 °C.

## 6.5. Discussions

### *6.5.1. Effect of air infiltration through the door gaps*

In this part, the model was used to investigate the effect of the air infiltration through the door gaps on the load temperature in the closed display cabinet. This effect on the energy consumption was also studied and the numerical results are presented hereafter.

Based on the results at the ambient temperature of 19.5 °C, it was found that load temperatures could be notably decreased (up to 0.7 °C) when the air infiltration through the door gap reduced by half as shown in **Figure 6.11**. This suggested that the temperature performance of closed refrigerated display cabinets could be improved by minimizing the air infiltration through door gaps of the cabinets.

### *6.5.2. Effect of ambient air humidity*

The influence of ambient humidity on the load temperature was considered as nonsignificant because of low water content in air (about 0.008 to 0.012 kg water/kg dry air) (Chen and Yuan, 2005). However, the cooling load of the refrigeration system of the display cabinet is highly influenced by this humidity. The present model was further used to estimate the frost formation on the evaporator surface and the total cooling load of the refrigeration system by taking both sensible and latent heat loads into account.

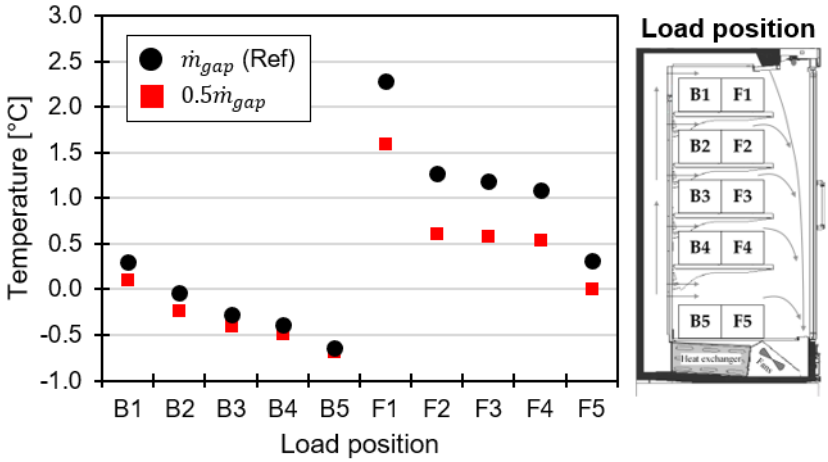


**Figure 6.11** Numerical result showing the variation of load temperatures with air infiltration rate through the door gaps

The external air infiltrates through the door gaps ($\dot{m}_{gap}$) with the mass fraction of water vapor of external air $\phi_{ext} = RH_{ext}\phi_{sat}T_{ext}$. The same quantity of air flows out with a lower water vapor mass fraction and the value of this fraction is close to that after the evaporator ($\phi_{th}$). Hence, the frost formation on the evaporator ($m_f$) can be approximately estimated by

$$\frac{dm_f}{dt} = \dot{m}_{gap}(\phi_{ext} - \phi_{th}) \tag{6.27}$$

The closed display cabinet operated at the ambient temperature of 19.5 °C and 65%RH ($\phi_{ext}$ = 0.009 kg·kg$^{-1}$) was used to illustrate this model application. The air after the evaporator can be assumed to be almost saturated i.e. $\phi_{th} \cong \phi_{sat}T_{th}$. In our case $T_{th}$ = -0.8 °C, thus $\phi_{th}$ = 0.003 kg·kg$^{-1}$, and the air infiltration rate through door gaps was $\dot{m}_{gap} = 0.0051$ kg·s$^{-1}$. For this example, the rate of frost formation on the evaporator was approximately 0.031 g·s$^{-1}$ ≈ 100 g·h$^{-1}$.

The total cooling load ($Q_t$) is the sum of the energy used to cool down the air from $T_{RAG}$ to $T_{th}$with the total mass flow rate and to convert the water vapor in the air into frost.

$$Q_t = Q_s + Q_\ell = \dot{m}_t C_p(T_{RAG} - T_{th}) + \dot{m}_{gap}(\phi_{ext} - \phi_{th})(\Delta H_v + \Delta H_f) \tag{6.28}$$

Given the total mass flow rate $\dot{m}_t = 0.1120$ kg·s$^{-1}$, the total cooling load was about 249 W ($Q_s$ = 169 W and $Q_\ell$ = 80 W). When the external air infiltration through the door gaps decreased by half, the rate of frost formation on the evaporator was

reduced to 0.016 g·s$^{-1}$ (≈ 58 g·h$^{-1}$) and the total cooling load to 162 W ($Q_s$ = 122 W and $Q_\ell$ = 40 W). Based on this calculation, the total cooling load of the refrigeration system would be reduced by 35%.

### *6.5.3. Generalization of the model for other closed display cabinets*

The simplified model proposed in this study was developed based on a closed refrigerated display cabinet of which the specific geometry is determined. The model is therefore applicable to closed display cabinets with similar configurations as described in Section 2 (i.e. the location of the heat exchanger and fans are underneath the bottom shelf, the lighting is at the top front of the cabinet, etc.). Among all parameters, the number of shelves equipped in the display cabinet shows the main limitation to the model applicability because the percentage of perforation area of the back panel over each shelf is different, resulting in different corresponding air distribution coefficients ($\gamma_i$). For different patterns of the PBP and different shelf numbers, additional measurements or CFD simulations have to be conducted to obtain these coefficients. To apply the developed model to other closed display cabinets, all required input parameters are presented in **Figure 6.12**.

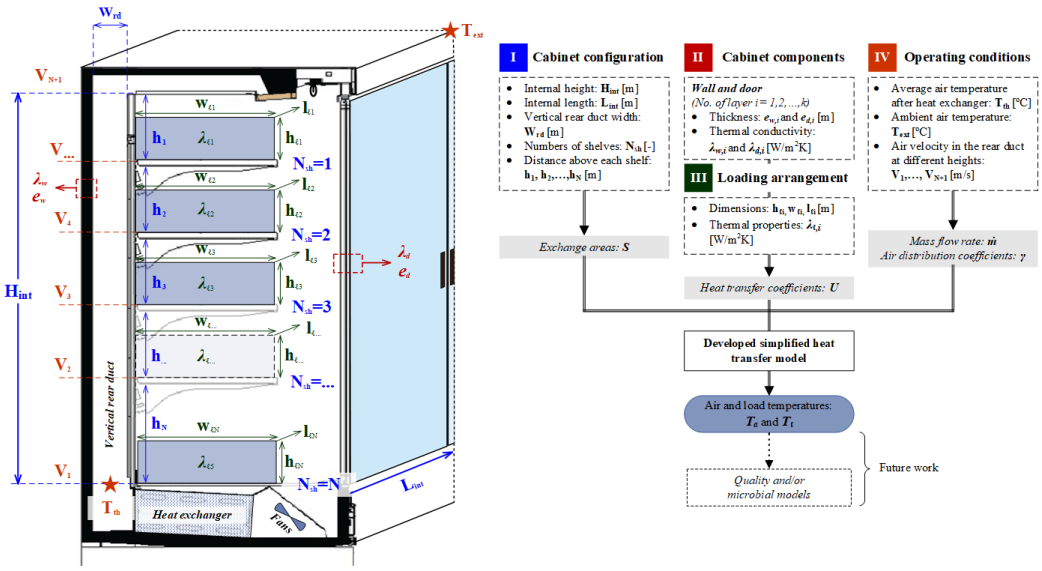


**Figure 6.12** Input parameters required for application to another closed display cabinet

### *6.5.4. Air infiltration during door openings*

The developed model does not take into account the air infiltration due to door openings because the airflow during door openings is too complex to be predicted by the simplified model. CFD model is more appropriate to cope with this phenomenon. To keep the model simplicity, a simple way to include the air infiltration during door openings could be done by introducing a higher value of $\dot{m}_{gap}$. Otherwise, some model modifications are required to be more realistic i.e. subtraction of air recirculation zone and introduction of external air infiltration at a given mixing zone (e.g. MZ [2,1,1…5]).

## 6.6. Conclusions

In Part I of this study, a simplified heat transfer model in steady state was developed for a closed refrigerated display cabinet. Based on a zonal approach, the display cabinet was decomposed into various heat exchange zones allowing the prediction of air and load temperatures at different positions. Five parameters ($\delta_1, \delta_{2..5}, \dot{m}_{gap}, U_{lf}$ and $U_{lb}$) were adjusted to fit the time-averaged temperatures for the external ambient temperature of 19.5 °C in the static model. For the other external ambient temperatures (14.6 °C and 24.4 °C), good agreement between the predicted and measured time-averaged temperatures were obtained without any adjustment. The overall mean absolute error based on 60 paired-data (air/load temperatures) for three ambient temperatures was less than 0.2 °C, and the maximum difference of the calculated and measured load temperatures never exceeds 0.5 °C for every studied position. In the shelves-space storage, time-averaged load temperatures at 10 positions (front and back of the five shelves) were predicted and compared with the experimental results. It was observed that the load temperatures were well represented by the model whereas the air temperature in the air curtain was slightly less well represented. Possible explanation of the discrepancy between the model and the experiment is that the air temperature at a given height was measured only at one position, which may not be representative of the average air curtain temperature. Nevertheless, the load temperature ranges and trends in the closed display cabinet are well represented by the proposed model with a short calculation time (less than 1 s). The model also showed its applicability

to investigate the effect of the air infiltration through the door gaps on the performance of the closed display cabinet in both thermal and energy aspects.

Air and load temperatures vary according to the compressor working cycle of the refrigeration system. In Part II of the study, this dynamic aspect will be integrated in the developed model. All input parameters determined in Part I will be further used in the dynamic model. The model will be also used to investigate temperature increase during defrost operation.

It is worth to remind that the developed model does not take into account the air infiltration due to door openings because the airflow during door openings is too complex to be predicted by the simplified model. CFD model is then more appropriate to cope with the phenomena. Nevertheless, suggestions were provided to include this phenomenon by both simple and more realistic manners. Besides, the main objective of the proposed model is to predict load temperatures in the equipment in short calculation time so that the model can be further integrated with others models already developed in the similar manner by the same research team (production plant, refrigerated truck, cold room, open display cabinet and domestic refrigerator). By this way, the integrated model will make it possible to acquire knowledge of the product time-temperature history across the entire food cold chain. By linking with quality and microbiological predictive models, the developed model can also be used as an evaluation tool of consumers' risk and can somewhat assist food operators to manage the logistic plan resulting in food loss reduction.

# Chapter VII

# Simplified heat transfer modeling in unsteady state

# Simplified heat transfer modeling of a closed refrigerated display cabinet: Part II – Dynamic model development and application

**Nattawut Chaomuang**, Onrawee Laguerre and Denis Flick

Submitted to *Applied Thermal Engineering* (submitted)

**Abstract**

This study proposes a simplified heat transfer model of a closed refrigerated display cabinet using a zonal approach, and it is divided into two parts. Part I presents the development of the model in the static regime allowing the prediction of time-averaged air and load temperatures. In Part II, the model in the dynamic regime was developed and solved with a spectral approach to predict the temperature fluctuations according to "on/off" compressor regulation. The thickness from the load surface in which its temperature significantly fluctuates was estimated in function of the compressor working frequency. The air temperature fluctuations are damped each time when the air exchanges heat with solid surfaces (e.g. walls, load) and with the ambient air (e.g. through the doors). Only the first effect depends on the frequency. Despite the exposure to large air temperature fluctuation (up to 5 °C), the surface load temperature was not much fluctuating ($\Delta T_l \leq 0.5$ °C). Good agreement was found between the predicted and the measured temperature fluctuations. The model also demonstrates the capability to predict the air and load temperature increases during the defrost operation.

***Keywords:*** Closed refrigerated display cabinet; Simplified model; Heat transfer; Temperature fluctuation; Spectral approach

**Nomenclature**

| | |
|---|---|
| $Bi$ | Biot number $= \frac{Ue}{\lambda}$ |
| $C_{eq}$ | equivalent thermal conductance [W· K$^{-1}$] |
| $C_p$ | heat capacity [J·kg$^{-1}$·K$^{-1}$] |
| $e$ | thickness [m] |
| $Fo$ | Fourier number $= \frac{\kappa\tau}{e^2}$ |
| $\mathbf{G}$ | transfer function |
| $h, U$ | heat transfer coefficient [W·m$^{-2}$·K$^{-1}$] |
| $L$ | length [m] |
| $m$ | solid mass [kg] |
| $\dot{m}$ | mass flow rate [kg·s$^{-1}$] |
| $q$ | heating power [W] |
| $S$ | exchange area [m$^2$] |
| $T$ | temperature [°C or K] |
| $t$ | time [s] |
| $u$ | velocity [m·s$^{-1}$] |
| $w$ | width [m] |

*Greek letters*

| | |
|---|---|
| $\alpha, \beta$ | exponential dimensionless heat transfer coefficient $= \exp\left(-\frac{US}{\dot{m}C_p}\right)$ |
| $\delta, \eta, \gamma$ | air distribution coefficient |
| $\theta$ | dimensionless average temperature |
| $\theta'$ | dimensionless temperature fluctuation |
| $\kappa$ | thermal diffusivity $= \frac{\lambda}{\rho C_p}$ [m$^2$·s$^{-1}$] |
| $\lambda$ | thermal conductivity [W·m$^{-1}$·K$^{-1}$] |
| $\mu$ | dynamic viscosity [N·s·m$^{-2}$] |
| $\xi$ | characteristic time $= \frac{(mC_p)_{solid}}{(\dot{m}C_p)_{fluid}}$ [s] |
| $\rho$ | density [kg·m$^{-3}$] |
| $\tau$ | period of a compressor working cycle [s] |
| $\varphi$ | phase shift [rad] |
| $\Psi$ | pulsation independent effect |
| $\omega$ | angular frequency $= \frac{2\pi}{\tau}$ [rad·s$^{-1}$] |
| $\Theta$ | dimensionless half amplitude of temperature variation |

*Subscripts*

| | |
|---|---|
| $a$ | air |
| $ag$ | argon |
| $a\ell$ | aluminum |

| | |
|---|---|
| $c$ | ceiling |
| $d$ | door |
| $dc$ | display cabinet |
| $del$ | delay |
| $df$ | defrost |
| $dy$ | dynamic |
| $exp$ | experimental |
| $ext$ | external |
| $gap$ | gap |
| $gl$ | glass |
| $l$ | load |
| $lb$ | back load |
| $lf$ | front load |
| $li$ | lighting |
| $ll$ | load to load |
| $num$ | numerical |
| $ov$ | overall |
| $pl$ | perforated back plate |
| $pu$ | polyurethane |
| $rd$ | rear duct |
| $sh$ | shelf |
| $sdy$ | shelf (dynamic model) |
| $t$ | total |
| $th$ | thermostat |
| $w$ | wall |

*Abbreviations*

| | |
|---|---|
| DAG | Discharge Air Grille |
| PBP | Perforated Back Panel |
| RAG | Return Air Grille |

## 7.1. Introduction

Among all risk factors associated with quality and safety of food products, temperature is of the utmost importance. All refrigerating equipment should be able to keep food products at the recommended temperature within a narrow fluctuation range across the cold chain to assure the food quality and safety (East et al., 2013; Jol et al., 2006; Platenius, 1939; Tano et al., 2007). Nevertheless, periodical temperature fluctuation is unavoidable because of automatic "on/off" cycles of compressor operation of refrigeration system. Knowledge of spatial and temporal

temperature fluctuations inside refrigerating equipment would provide useful information for appropriate temperature control.

Retail display is often pointed out as the hotspot for temperature abuse in the cold chain (Baldera Zubeldia et al., 2016; Derens-Bertheau et al., 2015; Mercier et al., 2017). Air infiltration through the frontal opening of refrigerated display cabinets is the main cause of this issue. Dealing with it by closing the front of the display cabinets with doors become one of the simple and effective solutions because of better temperature performance (Chaomuang et al., 2019; Evans et al., 2007; Lindberg et al., 2010). As a result, the use of closed refrigerated display cabinets increases in retail stores (EIA, 2014), and approximately 75% of total display cabinets in French supermarkets will be closed with doors by 2020 (RPF, 2016).

This work on a closed refrigerated display cabinet is a continuity of the previous study (Part I) with the objective to present a simplified heat transfer model based on a zonal approach. Such a model is complementary to Computational Fluid Dynamics (CFD) model because less computational time and resources are required (Laguerre et al., 2014). The static model presented in Part I allows the prediction of time-averaged air and load temperatures at different positions in the closed display cabinet. Part II presents the development of the dynamic model which predicts the air and load temperature fluctuations according to the "on/off" regulation of compressor working cycles. Simplified models of open refrigerated display cabinets were already developed by our teams (Ben-abdallah et al., 2018; Laguerre et al., 2012). To our best knowledge, the development of a simplified model for a closed refrigerated display cabinet taking into account both the static and dynamic regimes is new.

Most of dynamic models for refrigerating equipment are usually developed with the component sub-models of vapor compression systems (i.e. compressor, condenser, expansion device and evaporator) (Zsembinszki et al., 2017). A comprehensive review of dynamic modeling for the vapor compression systems is provided in the two-part article of Rasmussen (2012) in which both physics-based (e.g. lumped parameter, moving boundary, finite control volume,…) and data-based (e.g. linear, time-series,…) models for each system components are presented. Examples of the physics-based models can be found in numerous studies for different refrigerating equipment including cold-storage plants (Eames et al., 2012; Hasse et al., 1996;

Lovatt et al., 1998), refrigerated trucks (Rachek et al., 2010) and domestic refrigerators (Borges et al., 2011; Borges et al., 2015; Chen and Lin, 1991; Hermes and Melo, 2008). Nevertheless, these studies are dedicated to the dynamic response of the refrigerating equipment to enhance overall system energy efficiency (Azzouz et al., 2008), whilst bulk air/product temperatures in the equipment are often considered as heat reservoir. Despite very much higher computational time, the CFD approach is more appropriate choice for the analysis of spatiotemporal temperature fluctuations in high resolutions (Alfaro-Ayala et al.; Ambaw et al., 2016; Gruyters et al., 2018; Wang et al., 2015). A balance between simplicity and fidelity to select suitable modeling approach is therefore important.

In the present study, a simplified dynamic model was developed based on the zonal approach and solved with a spectral method by using Fourier transform and transfer functions. The model did not include the refrigeration components, but formulated supply air temperature profile from the experimental data during a transient cycle of compressor regulation with Discrete Fourier Transform. The dynamic response of air/load temperature was readily determined by the transfer functions specified at different positions. By this way, the model not only allows the prediction of temperature fluctuations in the display cabinet but also shows the influence of different parameters on the damping of the temperature fluctuations with quick calculation. Moreover, this study proposes the estimation of the thickness at the surface of the load in which the temperature fluctuation can be observed. This thickness varies with the compressor working frequency while the dynamic models available in the literature often assume uniform load temperature, which is not realistic.

## 7.2. Model development

This section deals with the development of the model in the dynamic aspect. Based on the zonal approach, two domains of heat exchange zones in the display cabinet were defined and they are the same as the ones presented in Part I of the study. The first domain corresponds to the heat exchange in the vertical rear duct and the second one corresponds to the heat exchange in the storage space of the display cabinet. **Figure 7.1** presents an example of one position of heat exchange zone in Domain I and heat exchange zones at Shelf 1 and 2 in Domain II. The descriptions

of the symbols and indexes are also the same as those in Part I. Since the dynamic model was solved with the spectral method, transfer functions were defined at all positions of heat exchange zones.

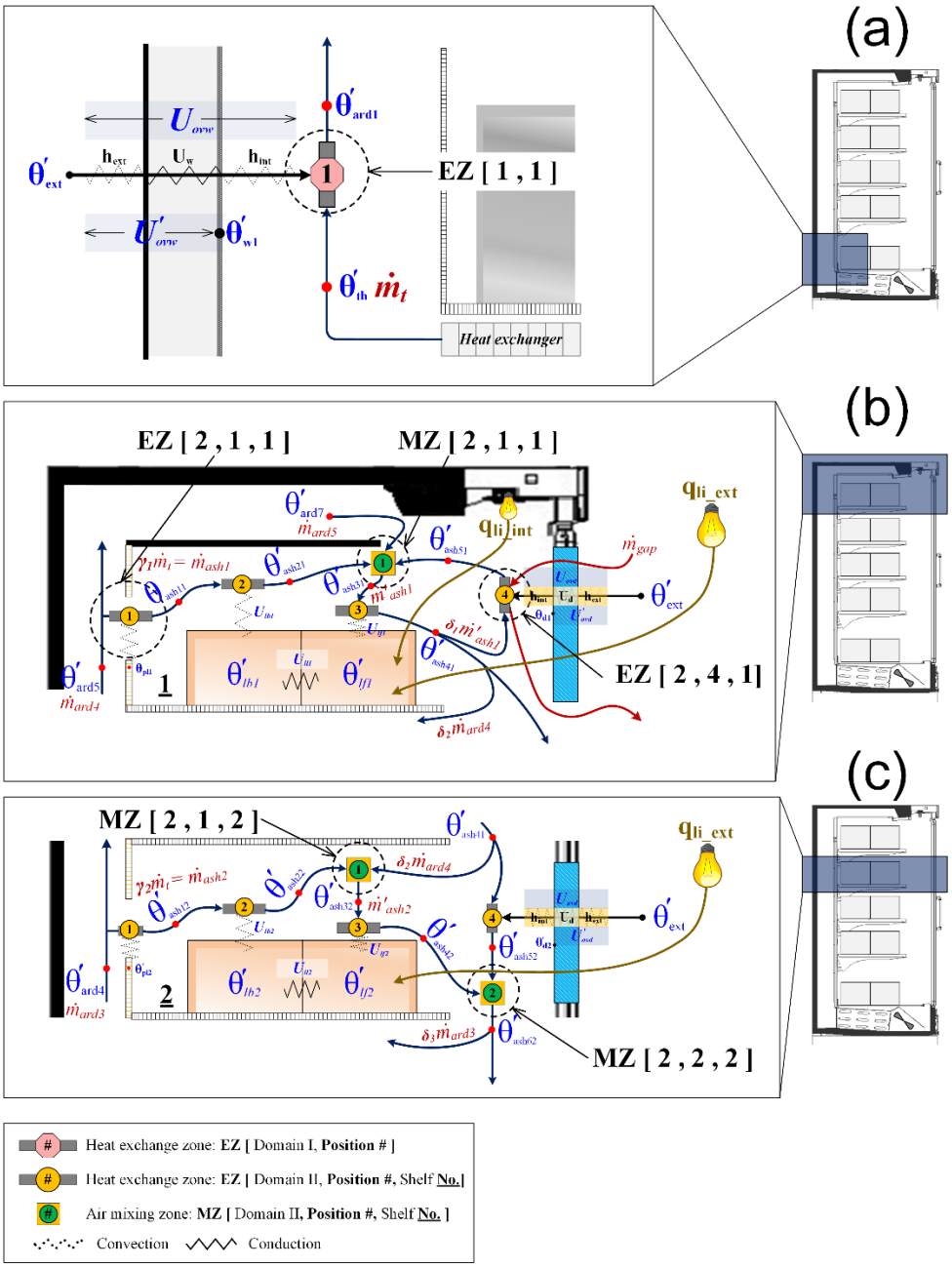


**Figure 7.1** Schematic view of the simplified model: (a) heat exchange in Domain I at the position after the heat exchanger in the vertical rear duct denoted as EZ [1, 1], (b) heat exchanges in Domain II on Shelf 1 and (c) Shelf 2.

*7.2.1. Model description*

As described in Part I of the study, the air and load temperatures in the closed refrigerated display cabinet vary according to the compressor on/off cycle. As an input to the model, the temperature evolution of the air just after the heat exchanger at which the thermostat sensor is located ($T_{th}$) is first assumed to be sinusoidal:

$$T_{th}(t) = \overline{T}_{th} + \Delta T_{th} \cos(\omega t) \tag{7.1}$$

Both air and load temperatures at any position in the cabinet are in response to the air temperature after the heat exchanger ($T_{th}$) as well as the external ambient air temperature ($T_{ext}$). Because all associated heat transfer phenomena in the display cabinet (i.e. forced convection and conduction) satisfy linear relationship with temperature difference, the properties of the dynamic linear systems can be employed for thermal analysis of the display cabinet. It is to be emphasized that free convection and thermal radiation from the external walls, which are non-linear phenomena, are limited because the doors were coated with low-emissivity materials (readers are referred to Part I of this study for more details). Therefore, the evolution of the temperature at a given position $i$ also follows a sinusoidal variation:

$$T_i(t) = \overline{T}_i + \Delta T_i \cos(\omega t + \varphi_i) = \overline{T}_i + \Delta T_i \cos(\omega(t - t_{del,i})) \tag{7.2}$$

where $\overline{T}_i$ is the time-averaged temperature at a position $i$ in the display cabinet and $\Delta T_i$ is the amplitude of the temperature fluctuation at that position. From the superposition theorem, the temperature evolution at a given position is given by

$$T_i(t) = \overline{T}_{th} + \left(T_{ext} - \overline{T}_{th}\right) \cdot \theta_i + \Delta T_{th} \cdot \theta_i' \tag{7.3}$$

where $\theta_i$ and $\theta_i'$ are respectively the dimensionless static and dynamic temperatures. They are defined as follow:

For the problem where $T_{th} = \overline{T}_{th}$, $T_{ext} \neq \overline{T}_{th}$ and $q_{li} \neq 0$

$$\theta_i = \frac{\overline{T}_i - \overline{T}_{th}}{T_{ext} - \overline{T}_{th}} \tag{7.4}$$

For the problem where $T_{th} = \overline{T}_{th} + \Delta T_{th} \cos(\omega t)$, $T_{ext} = \overline{T}_{th}$ and $q_{li} = 0$

$$\theta_i' = \frac{T_i - \overline{T}_i}{\Delta T_{th}} \tag{7.5}$$

The solutions of **Eq. (7.4)** can be obtained from the static aspect of the model of which the detail was presented in Part I of the study. The dynamic aspect is now integrated to obtain the solutions of **Eq. (7.5)** in the following form:

$$\theta_i' = \Theta_i \cos(\omega t + \varphi_i) = \mathrm{Re}(\mathbf{G}_i e^{i\omega t}) \text{ with } \Theta_i = \frac{\Delta T_i}{\Delta T_{th}} \tag{7.6}$$

where $\mathbf{G}_i$ is the transfer function at a position $i$; $\Theta_i$ and $\varphi_i$ are the magnitude and the phase shift of $\mathbf{G}_i$, respectively.

$$\Theta_i = |\mathbf{G}_i| \tag{7.7}$$

$$\varphi_i = Arg(\mathbf{G}_i) \tag{7.8}$$

It needs to be emphasized that the sinusoidal temperature variation in **Eq. (7.1)** is only to present the concept of the model development in a simple manner since the real temperature variation is periodic and not sinusoidal (**Figure 7.2**). For the model calculation, the temperature profile of the supply air ($T_{th}$, input parameter) was decomposed by using Discrete Fourier Transform and the temperature variations at other positions in the display cabinet were in response to this input temperature profile. More detail is given in **Section 7.2.3**.

### *7.2.2. Dynamic model development*

Based on **Eq (7.5)** and **(7.6)**, the dimensionless air temperature fluctuation after the heat exchanger becomes:

$$\theta_{th}' = \cos(\omega t) = \mathrm{Re}(e^{i\omega t}) \tag{7.9}$$

Since homogeneous boundary condition $\left(T_{ext} = \overline{T}_{th}\right)$ is assumed for the dynamic problem:

$$\theta_{ext}' = 0 \tag{7.10}$$

#### *7.2.2.1. Attenuation of temperature fluctuation due to heat exchange with the rear wall (Domain I)*

In unsteady state condition, the temperature of the inner side of the rear wall of the display cabinet changes with time because it is exposed to fluctuating temperature of cold air. Considering EZ [1, 1] (**Figure 7.1**), the heat balance equation is given by

$$m_{w1}C_{pw}\frac{d\theta'_{w1}}{dt} = U'_{ovw}S_{w1}(\theta'_{ext} - \theta'_{w1}) - \dot{m}_t C_{pa}(\theta'_{ard1} - \theta'_{th}) \quad (7.11)$$

The first term on the right side corresponds to the heat loss (overall heat transfer coefficient between inner wall and external ambient air, $U'_{ovw}$). The second term corresponds to the heat exchange with the supply air.

Because the thermal inertia of the air is very much lower than that of the wall, the heat balance equation for air along the inner side of the wall is given by

$$\dot{m}_t C_{pa} d\theta'_a = h_{int}(\theta'_w - \theta'_a)dS_w \Longrightarrow \ln\left(\frac{\theta'_{w1}-\theta'_{ard1}}{\theta'_{w1}-\theta'_{th}}\right) = -\frac{h_{int}S_{w1}}{\dot{m}_t C_{pa}}$$

$$\theta'_{ard1} = \alpha_{dy1}\theta'_{th} + (1-\alpha_{dy1})\theta'_{w1} \quad (7.12)$$

where $\alpha_{dy1} = \exp\left(-\frac{h_{int}S_{w1}}{\dot{m}_t C_{pa}}\right)$

From **Eq. (7.11) and (7.12)**, the heat transfer equation at EZ [1, 1] becomes:

$$m_{w1}C_{pw}\frac{d\theta'_{w1}}{dt} = U'_{ovw}S_{w1}(\theta_{ext} - \theta'_{w1}) + \dot{m}_t C_{pa}(1-\alpha_{dy1})(\theta'_{th} - \theta'_{w1}) \quad (7.13)$$

Since

$\theta'_{th} = \mathrm{Re}(e^{i\omega t})$

$\theta'_{w1} = \mathrm{Re}(\mathbf{G}_{w1}e^{i\omega t})$

$\theta'_{ard1} = \mathrm{Re}(\mathbf{G}_{ard1}e^{i\omega t})$

**Eq. (7.13)** is reduced to

$$m_{w1}C_{pw}\frac{d}{dt}(\mathbf{G}_{w1}e^{i\omega t}) = -U'_{ovw}S_{w1}(\mathbf{G}_{w1}e^{i\omega t}) + \dot{m}_t C_{pa}(1-\alpha_{dy1})(e^{i\omega t} - \mathbf{G}_{w1}e^{i\omega t})$$

thus,

$$\mathbf{G}_{w1} = \frac{1}{(1+\Psi_{dy1})+i\omega\xi_{dy1}} \quad (7.14)$$

where $\Psi_{dy1} = \frac{U'_{ovw}S_{w1}}{\dot{m}_t C_{pa}(1-\alpha_{dy1})}$ and $\xi_{dy1} = \frac{m_{w1}C_{pw}}{\dot{m}_t C_{pa}(1-\alpha_{dy1})}$

Replacing **Eq. (7.14)** into **Eq. (7.12)** yields

$$\mathbf{G}_{ard1} = \frac{(1-\alpha_{dy1})}{(1+\Psi_{dy1})+i\omega\xi_{dy1}} + \alpha_{dy1} \quad (7.15)$$

Similar equations were derived for all heat exchange zones in Domain I.

The implication of **Eq. (7.15)** shows that a part of the fluctuation of $\theta'_{th}$ (fraction $\alpha_{dy1}$) is not attenuated whereas the remaining part (fraction $1-\alpha_{dy1}$) is damped with a pulsation independent effect $(\Psi_{dy1})$ and a pulsation dependent effect $(\xi_{dy1})$. The attenuated fraction $(1-\alpha_{dy1})$ increases with the air/wall heat exchange intensity and decreases with the air flow rate.

The pulsation independent effect $(\Psi_{dy1})$ is related to the increase of heat loss with a constant ambient temperature. The pulsation dependent effect, corresponding to the characteristic time $(\xi_{dy1})$, is proportional to the thermal inertia of the wall. This effect increases if the compressor on/off period decreases (i.e. $\omega$ increases).

*7.2.2.2. Attenuation of temperature fluctuation in the shelves-space storage (Domain II)*

*7.2.2.2.1. Heat exchange between the transversal air flow and the PBP (interface between Domain I and II)*

A part of the air flows into the shelf space through the perforated back panel (PBP) of which the thermal inertia leads to a pulsation dependent attenuation of the air temperature fluctuation. The heat balance equation is developed in a similar manner to the heat exchange in the vertical rear duct, except that there is no exchange with the external ambient air; therefore, there is no pulsation independent attenuation.

Considering EZ [2, 1, 1], the heat balance equations are given by

$$m_{pl1}C_{ppl}\frac{d\theta'_{pl1}}{dt} = \dot{m}_{ash1}C_{pa}(\theta'_{ard5} - \theta'_{ash11}) \quad (7.16)$$

$$\theta'_{ash11} = \alpha_{sdy11}\theta'_{ard5} + (1-\alpha_{sdy11})\theta'_{pl1} \quad (7.17)$$

where $\alpha_{sdy11} = \exp\left(-\frac{h_{int}S_{pl1}}{\dot{m}_{ash1}C_{pa}}\right)$

**Eq. (7.16) and (7.17)** yield

$$\mathbf{G}_{pl1} = \mathbf{G}_{ard5} \cdot \left(\frac{1}{1+i\omega\xi_{sdy11}}\right) \quad (7.18)$$

$$\mathbf{G}_{ash11} = \mathbf{G}_{ard5} \cdot \left( \frac{1-\alpha_{sdy11}}{1+i\omega\xi_{sdy11}} + \alpha_{sdy11} \right) \quad (7.19)$$

where $\xi_{sdy11} = \frac{m_{pl1} C_{ppl}}{\dot{m}_{ash1} C_{pa} (1-\alpha_{sdy11})}$

Similar equations of the heat exchange at this zone were derived for all shelves.

*7.2.2.2.2. Heat exchange between the air and the back load*

In fact, temperature fluctuation in a solid structure steadily decreases along the distance from the surface due to its thermal inertia (Carslaw and Jaeger, 1959). To simplify the model, the temperature fluctuation is assumed to be the same from the load surface to a specific depth (equivalent thickness, $e_{eq}$), while the temperature fluctuation is neglected for the rest of the load (core); more details are presented in **Section 7.3**.

Considering EZ [2, 2, 1], the heat balance equations are given by

$$m'_{lb1} C_{pl} \frac{d\theta'_{lb1}}{dt} = \dot{m}_{ash1} C_{pa} (\theta'_{ash11} - \theta'_{ash21}) \quad (7.20)$$

where $m'_{lb1} = \rho_l S_l e_{eq}$

$$\theta'_{ash21} = \alpha_{sh11} \theta'_{ash11} + (1 - \alpha_{sh11}) \theta'_{lb1} \quad (7.21)$$

where $\alpha_{sh11} = \exp\left( -\frac{U_{lb1} S_{l1}}{\dot{m}_{ash1} C_{pa}} \right)$

**Eq. (7.20) and (7.21)** yield

$$\mathbf{G}_{lb1} = \mathbf{G}_{ash11} \cdot \left( \frac{1}{1+i\omega\xi_{sdy21}} \right) \quad (7.22)$$

$$\mathbf{G}_{ash21} = \mathbf{G}_{ash11} \cdot \left( \frac{1-\alpha_{sh11}}{1+i\omega\xi_{sdy21}} + \alpha_{sh11} \right) \quad (7.23)$$

where $\xi_{sdy21} = \frac{m'_{lb1} C_{pl}}{\dot{m}_{ash1} C_{pa} (1-\alpha_{sh11})}$

*7.2.2.2.3. Air mixing above the front load*

For Shelf 1, there are three air streams mixing above the front load including air from the DAG (mass flow rate, $\dot{m}_{ard5}$), air from the back (mass flow rate, $\dot{m}_{ash1}$) and a part of the recirculating air (mass flow rate, $\delta_1 \, m'_{ash1}$). Considering MZ [2, 1, 1], the heat balance equation is given by

$$m'_{ash1}\mathbf{G}_{ash31} = \dot{m}_{ard5}\mathbf{G}_{ard7} + \dot{m}_{ash1}\mathbf{G}_{ash21} + \delta_1\, m'_{ash1}\mathbf{G}_{ash51} \quad (7.24)$$

For Shelf 2-5, there are only two air streams mixing above the front load including the air from the back (mass flow rate, $\dot{m}_{ash2}$) and a part of the air curtain (mass flow rate, $\delta_2\dot{m}_{ard4}$). Considering MZ [2, 1, 2], the heat balance equation is given by

$$m'_{ash2}\mathbf{G}_{ash32} = \dot{m}_{ash2}\mathbf{G}_{ash22} + \delta_2\dot{m}_{ard4}\mathbf{G}_{ash41} \quad (7.25)$$

Analogous analysis of heat balance at MZ [2, 1, 2] was applied to Shelf 3 to 5.

*7.2.2.2.4. Heat exchange between the mixed air and the front load*

The heating due to light is constant and it does not contribute to temperature fluctuations. The heat balance at EZ [2, 3, 1] is reduced to

$$m'_{lf1}C_{pl}\frac{d\theta'_{lf1}}{dt} = \dot{m}'_{ash1}C_{pa}(\theta'_{ash31} - \theta'_{ash41}) \quad (7.26)$$

$$\theta'_{ash41} = \alpha_{sh21}\theta'_{ash31} + (1 - \alpha_{sh21})\theta'_{lf1} \quad (7.27)$$

where $\alpha_{sh21} = \exp\left(-\frac{U_{lf1}S_{l1}}{\dot{m}'_{ash1}C_{pa}}\right)$

$$\mathbf{G}_{lf1} = \mathbf{G}_{ard31} \cdot \left(\frac{1}{1+i\omega\xi_{sdy31}}\right) \quad (7.28)$$

$$\mathbf{G}_{ash41} = \mathbf{G}_{ash31} \cdot \left(\frac{1-\alpha_{sh21}}{1+i\omega\xi_{sdy31}} + \alpha_{sh21}\right) \quad (7.29)$$

where $\xi_{sdy31} = \frac{m'_{lf1}C_{pl}}{\dot{m}'_{ash1}C_{pa}(1-\alpha_{sh21})}$

Analogous analysis of the heat balance was applied to all shelves.

*7.2.2.2.5. Heat exchange with the door*

The heat balance equation in this zone was developed in a similar manner to the heat exchange in the vertical rear duct (**Section 7.2.2.1**) which takes into account the attenuation due to the pulsation independent and dependent effects. For Shelf 1, i.e. EZ [2, 4, 1], the heat balance equation is given by

$$m_{d1}C_{pd}\frac{d\theta'_{d1}}{dt} = C'_{eq}(\theta'_{ext} - \theta'_{d1}) - \delta_1\dot{m}'_{ash1}C_{pa}(\theta'_{ash41} - \theta'_{ash51}) \quad (7.30)$$

$$\theta'_{ash41} = \alpha_{sdy21}\theta'_{ash51} + \left(1 - \alpha_{sdy21}\right)\theta'_{d1} \quad (7.31)$$

where $\alpha_{sdy21} = \exp\left(-\frac{h_{int}S_{d1}}{\delta_1 \dot{m}'_{ash1} C_{pa}}\right)$ and $C'_{eq} = U'_{ovd}S_{d1} + \dot{m}_{gap}C_{pa}$

$$\mathbf{G}_{d1} = \mathbf{G}_{ash41} \cdot \left(\frac{1}{(1+\Psi_{sdy1})+i\omega\xi_{sdy41}}\right) \tag{7.32}$$

$$\mathbf{G}_{ash51} = \mathbf{G}_{ash41} \cdot \left(\frac{(1-\alpha_{sdy21})}{(1+\Psi_{sdy1})+i\omega\xi_{dy41}} + \alpha_{sdy21}\right) \tag{7.33}$$

where $\Psi_{sdy1} = \frac{C'_{eq}S_{d1}}{\delta_1 \dot{m}'_{ash1} C_{pa}(1-\alpha_{sdy21})}$ and $\xi_{dy41} = \frac{m_{d1}C_{pd}}{\delta_1 \dot{m}'_{ash1} C_{pa}(1-\alpha_{sdy21})}$

For Shelf 2, i.e. EZ [2, 4, 2], the heat balance equation is given by

$$m_{d2}C_{pd}\frac{d\theta'_{d2}}{dt} = U'_{ovd}S_{d2}(\theta'_{ext} - \theta'_{d2}) - (1-\delta_2)\dot{m}_{ard4}C_{pa}(\theta'_{ash41} - \theta'_{ash52}) \tag{7.34}$$

$$\theta'_{ash52} = \alpha_{sdy22}\theta'_{ash41} + (1-\alpha_{sdy22})\theta'_{d2} \tag{7.35}$$

where $\alpha_{sdy22} = \exp\left(-\frac{h_{int}S_{d2}}{(1-\delta_2)\dot{m}_{ard4}C_{pa}}\right)$

$$\mathbf{G}_{d2} = \mathbf{G}_{ash41} \cdot \left(\frac{1}{(1+\Psi_{sdy2})+i\omega\xi_{sdy42}}\right) \tag{7.36}$$

$$\mathbf{G}_{ash52} = \mathbf{G}_{ash41} \cdot \left(\frac{(1-\alpha_{sdy22})}{(1+\Psi_{sdy2})+i\omega\xi_{dy42}} + \alpha_{sdy22}\right) \tag{7.37}$$

where $\Psi_{sdy2} = \frac{U'_{ovd}S_{d2}}{(1-\delta_2)\dot{m}_{ard4}C_{pa}(1-\alpha_{sdy22})}$ and $\xi_{dy42} = \frac{m_{d2}C_{pd}}{(1-\delta_2)\dot{m}_{ard4}C_{pa}(1-\alpha_{sdy22})}$

Analogous analysis (**Eq. (7.34) - (7.37)**) was applied to Shelf 3 to 5.

*7.2.2.2.6. Air mixing between the air flowing from the back and the air curtain*

This incident emerges at all shelves except Shelf 1. Heat balance equation is therefore developed for these shelves. Considering MZ [2, 2, 2], the heat balance equation is given by

$$\dot{m}_{ard3}\mathbf{G}_{ash62} = \dot{m}'_{ash2}\mathbf{G}_{ash42} + (1-\delta_2)\dot{m}_{ard4}\mathbf{G}_{ash52} \tag{7.38}$$

*7.2.3. Temperature variation of the air after the heat exchanger*

In the study, the temperature of supply air after the heat exchanger is considered to be equal to the air temperature at the thermostat sensor ($T_{th}$) which is located there. **Figure 7.2** shows the air temperature profiles obtained from the measurements with calibrated thermocouples during a period of the compressor operation ($\tau$) for three

ambient temperatures (14.6, 19.5 and 24.4 °C). It was observed that the duration of the compressor being "off" was affected by the ambient temperature: it decreased with an increase of the ambient temperature. This incident shows the implication of higher demand of cooling load from the refrigeration system (more frequency of the compressor operation). On the other hand, the "on" period of the compressor operation is rather consistent ($\tau_{ON}$ ~ 90-100 s) due to the cooling capacity of the refrigeration system used in the studied display cabinet. To predict the temperature fluctuation in the closed display cabinet for different ambient temperatures, an air temperature profile with respect to the external temperature was applied to the developed model (**Figure 7.2**).

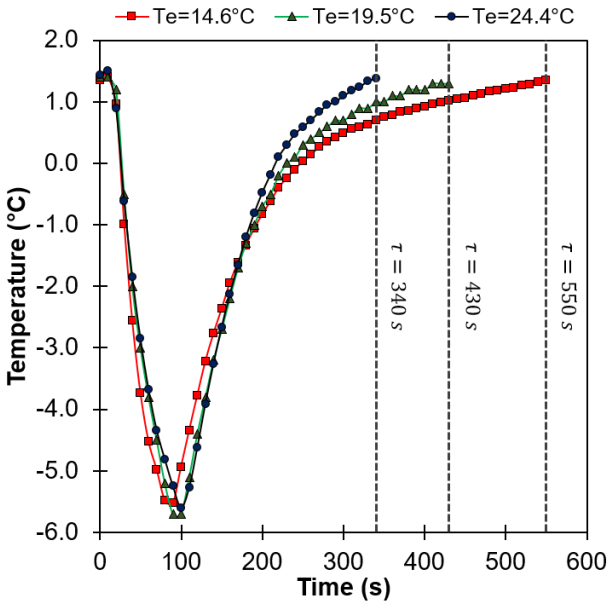


**Figure 7.2** Experimental temperature profiles of air after the heat exchanger for different ambient temperatures.

Referring to the earlier assumption, the temperature variation at any position was supposed to be in response to a sinusoidal temperature variation of the air after the heat exchanger ($T_{th}$). However, in reality this temperature variation is not sinusoidal, but only periodic (**Figure 7.2**). Discrete Fourier Transform was therefore applied to decompose the temperature profile of the supply air in the following form:

$$T_{th}(t) = \overline{T}_{th} + \sum_{k=1}^{N/2} |\Delta T_{th,k}| \cos(k\omega t + \varphi_{th,k}) \quad (7.39)$$

$|\Delta T_{th,k}|$ and $\varphi_{th,k}$ are the magnitude and the phase shift related to the *k-th* complex Fourier's transform coefficient. *N* is the number of measured data during a period of the compressor operation $(\tau)$. The coefficient $k = 1$ represents the fundamental pulsation while the other coefficients $k = 2, 3, \dots, \frac{N}{2}$ represent the harmonic pulsations.

Based on **Eq. (7.39)**, the temperature variations at other positions in the closed display cabinet can be estimated by

$$T_i(t) = \overline{T}_i + \sum_{k=1}^{N/2} \Theta_{i,k} \cdot |\Delta T_{th,k}| \cos\left(k\omega t + \varphi_{th,k} + \varphi_{i,k}\right) \qquad (7.40)$$

where $\overline{T}_i$ is the average temperature at a given position $i$ retrieved from the static aspect of the model (presented in Part I) and $\Theta_{i,k}$ and $\varphi_{i,k}$ is the magnitude and the phase shift of that position obtained from the solution of the dynamic aspect explained in **Section 7.2.2**.

In addition to the identification of influential parameters on the damping of the temperature fluctuations, the spectral method also permits quick calculation. 2-4 harmonics ($k$) are often enough to describe the supply air temperature profile $T_{th}$. This method needs only to solve a limited number of algebraic complex equations, instead of ordinary differential equations. It is worth noting that the same model developed in this study could also be solved by temporal discretization (e.g. Runge-Kutta).

## 7.3. Estimation of the equivalent depth in which temperature fluctuations occur in the product

For the dynamic model development in the present study, temperature gradients within the load cannot be neglected since the internal resistance to conduction within the load is much higher than external resistance to convection (Bergman et al., 2011) i.e. the Biot number $Bi = \frac{U_{lb} e_l}{\lambda_l} = \frac{U_{lf} e_l}{\lambda_l} \gg 0.1$. Given the thermal properties of the methylcellulose (thickness $e_l$ = 200 mm; density $\rho_l$ = 1071 kg·m$^{-3}$; thermal conductivity $\lambda_l$ = 0.51 W·m$^{-1}$·K$^{-1}$ and specific heat $C_{pl}$ = 3372 J·kg$^{-1}$·K$^{-1}$, (Icier and Ilicali, 2005)) and the estimated convective heat transfer coefficients $U_{lb}$= 15 W·m$^{-2}$·K$^{-1}$ and $U_{lf}$= 24 W·m$^{-2}$·K$^{-1}$ (Part I of the study), $Bi$ = 5.9 and $Bi$ = 9.4 are determined for

the back and front loads, respectively. Based on the characteristic time of an "on/off" cycle of compressor regulation ($340s < \tau < 550s$, **Fig. 2**), the Fourier number for the load given by $Fo = \frac{\kappa_l \tau}{e_l^2}$ varied between $1.2\times10^{-3}$ and $1.9\times10^{-3}$ ($\kappa_l = \frac{\lambda_l}{\rho_l C_{pl}}$ is the thermal diffusivity of the load). This very small $Fo$ indicates that heat is far to penetrate up to the core of the load during the "on/off" compressor working cycle. Since $Fo < 0.2$ (Bergman et al., 2011), the load of thickness $e_l$ can be considered as a semi-infinite solid hereafter for the analytical model development of temperature fluctuation in the solid.

In real condition, periodic air temperature fluctuation provides temperature fluctuation in the load where the maximum amplitude is located at the load surface ($x = 0$, **Figure 7.3a**). Considering the load as a semi-infinite solid with constant thermal conductivity, the temperature fluctuation within the load decays exponentially with respect to the distance from the surface. Far from the surface, the amplitude of temperature fluctuation becomes null as schematically illustrated in **Figure 7.3a**. Since 1D discretization of the load would require many additional state variables, two layers of different thermal conductivities are assumed in our model for its simplicity (**Figure 7.3b)**. A thin layer at the surface characterized by an equivalent thickness ($e_{eq}$) is assumed to have a very high thermal conductivity ($\lambda = \infty$) whereas the rest of the load (core) is assumed to have a very low thermal conductivity ($\lambda = 0$, perfect insulation). The equivalent thickness is chosen so that the temperature fluctuation at the surface predicted by the simplified model is the same as for a semi-infinite solid.

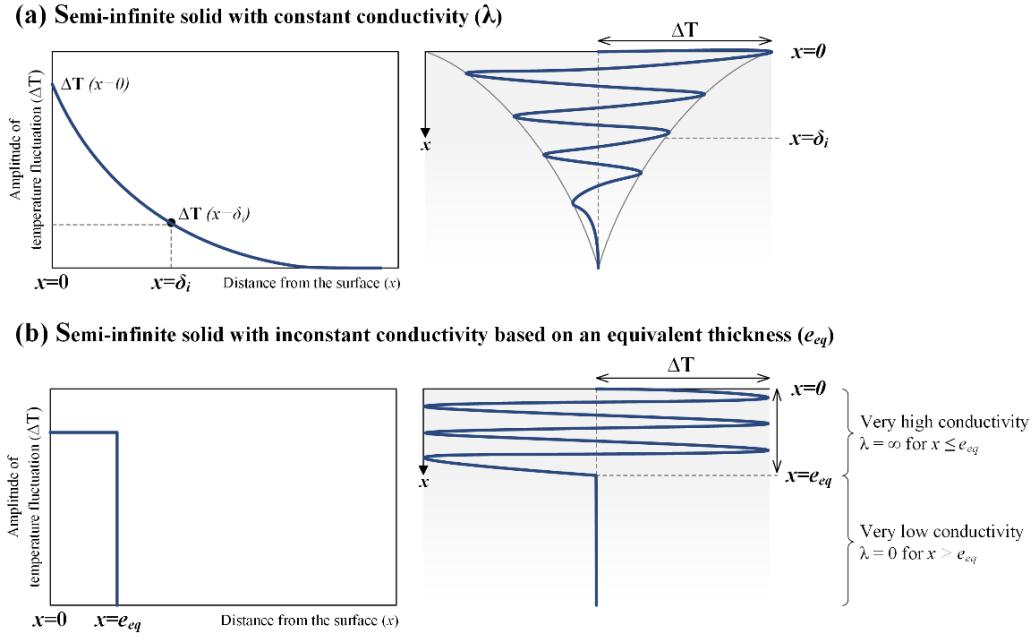


**Figure 7.3** Illustration curves of temperature fluctuations in a solid (a) with constant conductivity (real condition) and (b) with inconstant conductivity split at the equivalent thickness (simplified condition).

### *7.3.1. Development of temperature fluctuation model in a solid*

Two analytical models were used to determine the equivalent thickness of which the solutions have to satisfy the same temperature fluctuations at the surface. For the first model, the heat transfer in the load with perfect conduction in the range of the equivalent thickness ($0 < x < e_{eq}$) is considered (Model I). The second model involves the heat transfer in the load with constant conductivity with respect to the distance from the surface (Model II).

The solution of the Model I depends on the heat transfer rate between the load and its surrounding air:

$$m_l C_{pl} \frac{dT_l}{dt} = h_a S_l (T_a - T_l) \iff \rho_l e_{eq} C_{pl} \frac{dT_l}{dt} = h_a (T_a - T_l) \qquad (7.41)$$

Let $\Phi = \frac{\rho_l e_{eq} C_{pl}}{h_a}$, **Eq. (7.41)** is reduced to

$$\frac{dT_l}{dt} + \frac{T_l}{\Phi} = \frac{T_a}{\Phi} \qquad (7.42)$$

Considering the temperature fluctuation of the surrounding air as a sinusoidal variation $(T_a = e^{i\omega t})$, the solution of Model I can be calculated from

$$\frac{\Delta T_l}{\Delta T_a} = \frac{1}{(1+\omega^2\Phi^2)^{1/2}} \tag{7.43}$$

For Model II, the solution is given by considering the conduction heat transfer rate in a semi-infinite solid with constant properties for which the heat balance equation is given by

$$\frac{\partial T_l}{\partial t} = \kappa_l \frac{\partial^2 T_l}{\partial x^2} \tag{7.44}$$

At the load surface ($x = 0$), the heat transfer by convection between the load and air is defined as:

$$-\lambda_l \frac{\partial T_l}{\partial x} = h_a(T_l - T_a) \tag{7.45}$$

Taking into account **Eq. (7.44) and (7.45)**, the solution of the temperature fluctuation at the surface of the load can be calculated from (Carslaw and Jaeger, 1959):

$$\frac{\Delta T_l}{\Delta T_a} = \frac{1}{\left[\left(1+\frac{\sqrt{\lambda_l\rho_l C_{pl}\omega/2}}{h_a}\right)^2 + \frac{\lambda_l\rho_l C_{pl}\omega}{2h_a^2}\right]^{1/2}} \tag{7.46}$$

Let the temperature fluctuations obtained from the solutions of the two models (**Eq. (7.43) and (7.46)**) have the same amplitude, the equivalent thickness can be estimated by

$$e_{eq} = \left[\frac{h_a}{\rho_l C_{pl}\omega}\sqrt{\frac{\lambda_l/2}{\rho_l C_{pl}\omega}} + \frac{\lambda_l}{\rho_l C_{pl}\omega}\right]^{1/2} \tag{7.47}$$

This equation shows that the equivalent thickness ($e_{eq}$) depends not only on the thermal diffusivity ($\kappa_l$) and the angular frequency ($\omega$) but also the convective heat transfer coefficient between the load surface and the air ($h_a$). For the sake of simplicity, it can be assumed that $\frac{\sqrt{\lambda_l\rho_l C_{pl}\omega}}{h_a} \gg 1$ or $\mathrm{E}\sqrt{\omega} \gg h_a$ where $\mathrm{E} = \sqrt{\lambda_l\rho_l C_{pl}}$ is the thermal effusivity or heat penetration coefficient. Based on a period of compressor working cycle ($340s < \tau < 550s$) and the thermal properties of the methylcellulose, the order of magnitude of $\mathrm{E}\sqrt{\omega}$ is about 145-185 $W\cdot m^{-2}\cdot K^{-1}$ which is high compared to the estimated convective heat transfer coefficients (15 $W\cdot m^{-}$

$^{2}\cdot K^{-1}$ and 24 $W\cdot m^{-2}\cdot K^{-1}$ for the back and front loads, respectively). Therefore, the equivalent thickness can be simply calculated from the following equation:

$$e_{eq} = \left[\frac{\lambda_l}{\rho_l C_{pl}\omega}\right]^{1/2} = \sqrt{\kappa_l/\omega} \tag{7.48}$$

and the ratio of the temperature fluctuation between load surface and air is given by

$$\frac{\Delta T_l}{\Delta T_a} = \frac{h_a}{\sqrt{\lambda_l \rho_l C_{pl}\omega}} \tag{7.49}$$

Based on the compressor period and the material thermal properties mentioned earlier, the temperature fluctuation ratio calculated from **Eq. (7.49)** was approximately 0.09 for the back load.

### *7.3.2. Case study*

To verify the accuracy of the estimation of the equivalent thickness by using **Eq. (7.48)**, temperature measurement was carried out at different depths of the test package located at the back of the bottom shelf in the studied display cabinet as depicted in **Figure 7.4a**. The test package of methylcellulose located at this position was selected because it is the most exposed to air temperature fluctuation. Calibrated thermocouples (0.2 mm in diameter) were placed carefully in the test package at different depths from the surface to the core ($x$ = 0, 2, 5, 15, 25 mm) after making an insert hole with a small needle. A thermocouple was also placed at 10 mm above the test package surface for the air temperature measurement. Because of the small diameter of sensor wires, the real condition in the display cabinet was not disturbed. The experimental result as illustrated in **Figure 7.4b** showed the decay of the temperature fluctuations in the load from the surface to the core. It should be emphasized that the amplitude of temperature fluctuation is the difference between the maximal and minimal temperatures over one cycle of the compressor operation: $\Delta T_l = T_{\max} - T_{\min}$. It is obvious that the maximum temperature fluctuation in the load is located at the surface ($x = 0$ mm, $\Delta T_l \simeq 0.55$°C) and it exponentially decreases toward the core ($x = 25$ mm, $\Delta T_l \simeq 0.03$ °C).

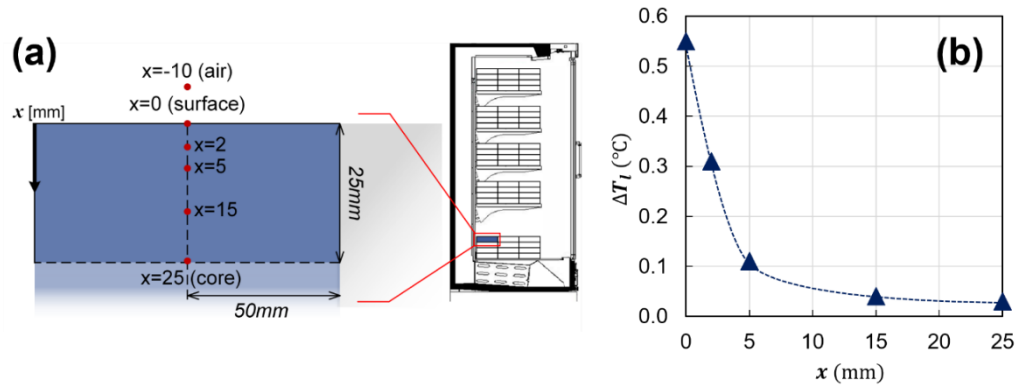


**Figure 7.4** (a) Schematic of temperature measurement for the test package located at the back row (top layer) on the bottom shelf at different depths from the surface (x=0 mm) to the core (x=25 mm) and for the air at 10 mm above. (b) Decay of temperature fluctuations in the load from the surface to the core

**Figure 7.5** shows the temperature evolutions of the air and the load at the different depths during the quasi-steady state. As shown in **Figure 7.5a**, the temperature fluctuation in the air above the load surface was around 4.10 °C and it was 0.55 °C at the load surface which corresponds to the temperature fluctuation ratio $\frac{\Delta T_l}{\Delta T_a} \simeq 0.13$. This measured temperature fluctuation ratio shows the same order of magnitude with the calculated one. Accordingly, the **Eq. (7.48)** is a satisfactory approximation for the equivalent thickness, which is then used to calculate the weight of the load $(m_l')$ of which the temperature fluctuates in the dynamic aspect of the model. For the methylcellulose package ($\kappa = 1.41 \times 10^{-7}$ m$^2$·s$^{-1}$) and for $\tau$ varying between 340 s and 550 s (**Figure 7.2**), the equivalent thickness ($e_{eq}$) ranges between 2.8 mm and 3.5 mm.

The weights of the wall and the door in contact with the air circulating in the display cabinet were estimated from their inner layers of aluminum sheet ($e_{a\ell} = 0.5$ mm, manufacturing data) and glass pane ($e_{gl} = 4$ mm, manufacturing data), respectively. The weight of the PBP is estimated from the plate thickness ($e_{pl} = 3$ mm, manufacturing data) and the total plate area subtracted by the perforation area. All estimated values of the weights of solid materials are summarized in **Table 7.1**.

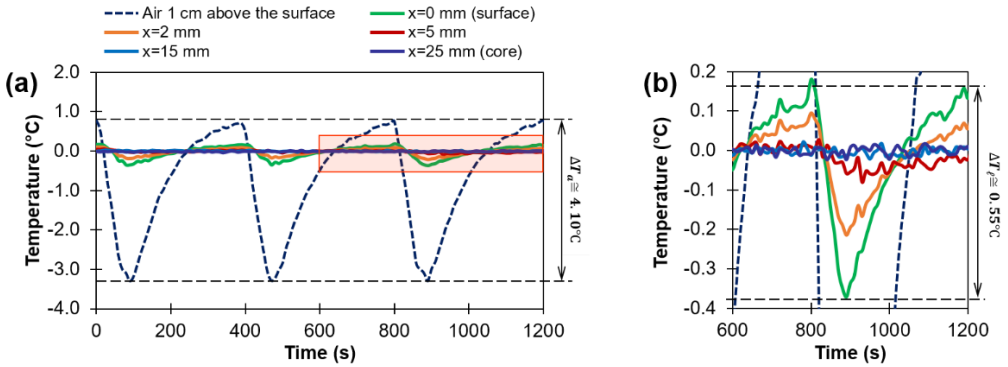


**Figure 7.5** Experimental temperature evolutions of the air (10 mm above the load) and of the back load on the bottom shelf at the different depths from the surface (x=0 mm) to the core (x=25 mm): (a) overall view and (b) enlarged scale on the highlighted area

**Table 7.1** Weights and thermal mass of the load and the solid components of the display cabinet used in the model

| Components | Weight | Thermal mass | References |
|---|---|---|---|
| | kg | J·K$^{-1}$ | |
| Load $(m_l)$ | | | |
| $m'_{lf} = m'_{lb}$ | 1.44 | 4855.7 | Calculation |
| Rear walls $(m_w)$ | | | |
| $m_{w1}$ | 0.29 | 263.9 | Calculation |
| $m_{w2} = m_{w3} = m_{w4} = m_{w5}$ | 0.42 | 382.2 | Calculation |
| $m_{w6}$ | 0.21 | 191.1 | Calculation |
| Ceiling | | | |
| $m_c$ | 0.68 | 618.8 | Calculation |
| Doors $(m_d)$ | | | |
| $m_{d1} = m_{d2} = m_{w3} = m_{d4}$ | 3.13 | 2347.5 | Calculation |
| $m_{d5}$ | 4.31 | 3232.5 | Calculation |
| Perforated back panel $(m_{pl})$ | | | |
| $m_{pl1}$ | 2.47 | 2247.7 | Calculation |
| $m_{pl2} = m_{pl3} = m_{pl4}$ | 2.43 | 2211.3 | Calculation |
| $m_{pl5}$ | 3.20 | 2912.0 | Calculation |

## 7.4. Results and discussion

### *7.4.1. Air and load temperature fluctuations in a closed refrigerated display cabinet*

After the integration of the dynamic regime, the simplified heat transfer model was employed to simulate the temperature evolutions of the air and the loads inside the

closed refrigerated display cabinet. The predicted and measured results for the external ambient temperature of 19.5 °C are shown in **Figure 7.6**. The temperature fluctuation of the supply air decreased from the position just after the heat exchanger ($\Delta T_{th} = 7.3$ °C, **Figure 7.2** Experimental temperature profiles of air after the heat exchanger for different ambient temperatures.) to the DAG ($\Delta T_{DAG} = 5.4$ °C, **Figure 7.6a**) by 1.9 °C. While traveling to the DAG, a part of the air also flows horizontally into the shelve space through the PBP. The air temperature fluctuation at the back of the bottom shelf (**Figure 7.6d**) was more pronounced than that of the upper shelves (**Figure 7.6b-c**). This can be explained by the higher air flow rate through the PBP at the lower shelf and a higher air temperature fluctuation of this air ($\Delta T_a$ decrease along the rear duct). At the front of the shelves, the highest air temperature fluctuation is at the top shelf (**Figure 7.6e**). The high temperature fluctuation at this position resulted from the high temperature fluctuation of the air curtain from the DAG. Despite the exposure to high air temperature fluctuation, the load surface temperatures at all positions were not much fluctuating ($\Delta T_l \leq 0.5$ °C). It was found that the ratio of the load to its surrounding air temperature fluctuation ($\frac{\Delta T_l}{\Delta T_a}$) was approximately 0.1. However, both air and load temperatures at the front of the shelves were fluctuating around higher average temperature, compared to the ones at the back of the same shelves. This result implies that food quality and safety would be more influenced by the average temperature than the temperature fluctuation in the closed display cabinet in this case where massive products were considered (methylcellulose packages). In the case of product packages offering a high exchange surface and a low thermal inertia (e.g. vacuum-packed sliced ham) particularly when the product thickness is smaller than $e_{eq}$ (**Eq. (7.48)**), higher product temperature fluctuations are expected. More investigations should be carried out to study the influence of such temperature fluctuation on food quality and safety.

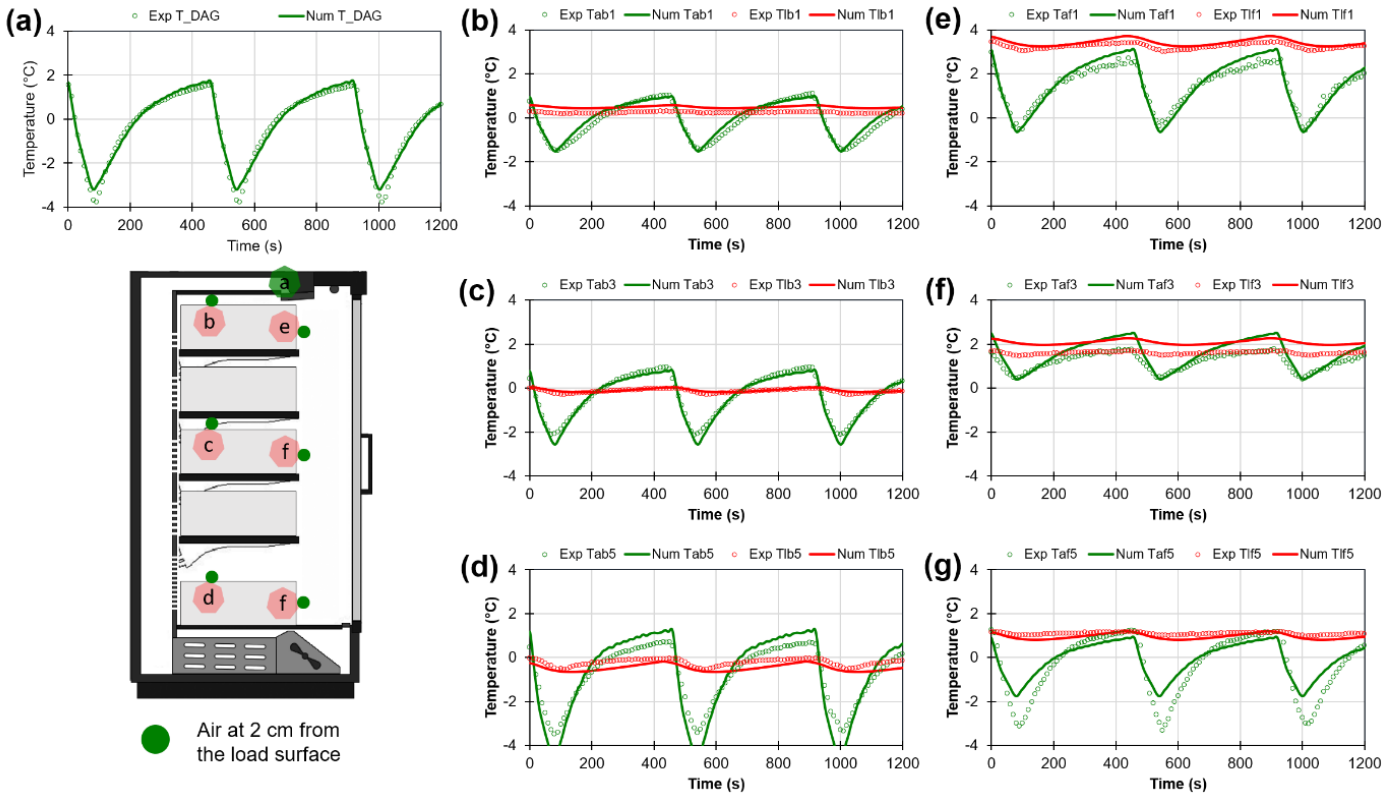


**Figure 7.6** Temperature evolution of the air and the load surface at different positions inside the closed display cabinet for the ambient temperature of 19.5 °C. (a) air at the discharge air grille (DAG), (b-d) back and (e-g) front loads with the surrounding air on the top, middle and bottom shelves, respectively (the time-averaged load temperature at the front was extrapolated from the core temperatures between the back and the front loads).

### *7.4.2. Dynamic model validation*

**Figure 7.7** shows a comparison between the predicted and measured temperature fluctuations of the air and the load (surface) at different positions in the closed refrigerated display cabinet. As shown in **Figure 7.7a**, the air temperature fluctuations were properly represented by the model at most positions (maximum difference of 0.5 °C). For certain positions, the air temperature fluctuations were slightly over/underestimated. The measurement position is possibly a source of the discrepancies between the predicted and measured air temperature fluctuations at that position. On the bottom shelf, a single point measurement may not be representative of the air temperature because mixing between the back flow and the air curtain occurs, thus generating high spatial air velocity fluctuations. The model clearly represents the load temperature fluctuations (**Figure 7.7b**). The maximum difference between the measured and predicted results was around 0.1 °C. Overall, the simplified heat transfer model developed in this study is acceptable for the prediction of temperature distributions in a closed refrigerated display cabinet under periodic working conditions.

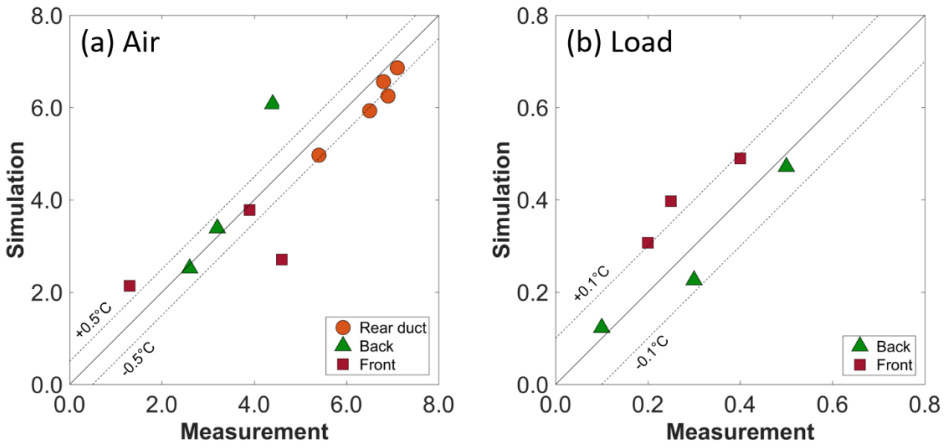


**Figure 7.7** Comparison between the simulation and the measurement of temperature fluctuations of (a) air and (b) loads inside the closed refrigerated display cabinet. Data based on the external ambient temperature of 19.5 °C

### *7.4.3. Temperature evolution during the defrost operation*

Frost formation on the surface of evaporator coils is inherent in all refrigeration systems. An increase of frost thickness causes a reduction of heat transfer and air flow rates, which ultimately deteriorates the overall display cabinet performance.

Therefore, periodic defrost operation is always required to maintain the display cabinet performance. It is well known that the food quality and safety can be affected by temperature raise during the defrost operation which can sometimes exceed the desired limit (Lawrence and Evans, 2008). The validated simplified model was further used to simulate the air and load temperature evolutions during the defrosting process in the closed display cabinet. For this simulation, the Fourier transform was applied to the air temperature after the heat exchanger ($T_{th}$) for a period of 6.5 h: 3 h before and after the defrost operation which lasts for 30 mins (**Figure 7.8**). Note that this input air temperature profile was selected based on the setting time for the defrost operation which takes place every 6 h (i.e. 4 cycles per day) for the studied display cabinet.

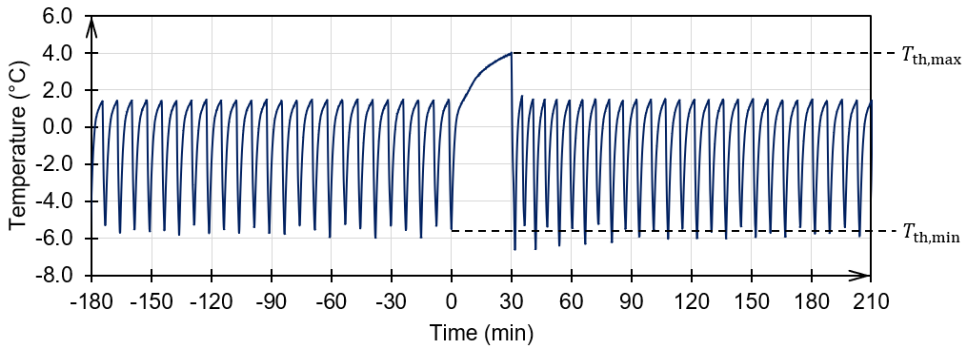


**Figure 7.8** Input temperature profile of the air after the heat exchanger ($T_{th}$)

Based on our assumption, the equivalent thickness ($e_{eq}$) of the load is influenced by the frequency of the air temperature fluctuation. During defrosting period ($\tau_{df} =$ 30 min), $T_{th}$ increases approximately like a sine function of pulsation $\omega' = \frac{\pi}{2\tau_{df}}$. As a result, an equivalent thickness of 12.8 mm was estimated from **Eq. (7.48)**.

**Figure 7.9 and 7.10** respectively show the air and the load temperature evolutions during defrosting period at different positions (back and front of the top, middle and bottom shelves) in the closed refrigerated display cabinet for the external ambient temperature of 19.5 °C. Based on the experimental data, the air temperature increase ($\Delta T = T_{max} - T_{min}$) at these positions was between 2 and 6 °C (**Figure 7.9**) while the surface load temperature increased by only 0.5 - 1.0 °C (**Figure 7.10**). The highest air and load temperature increases were observed at the front of the top shelf (**Figure 7.9d and 7.10d**).

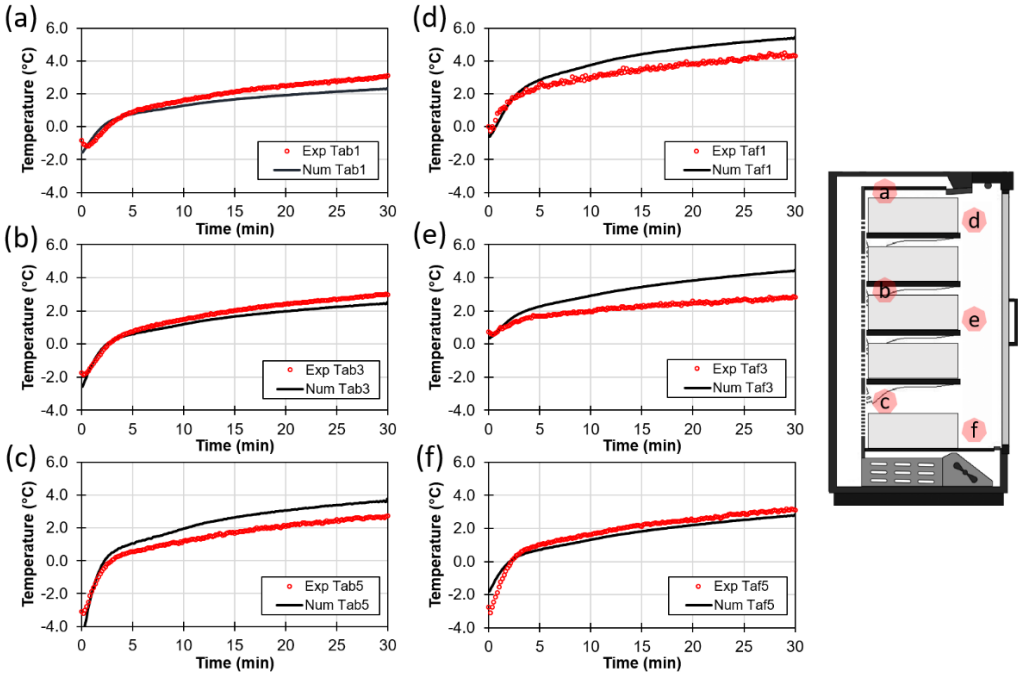


**Figure 7.9** Air temperature evolution at various position in a closed refrigerated display cabinet during the defrost operation ($T_{ext}$ = 19.5°C)

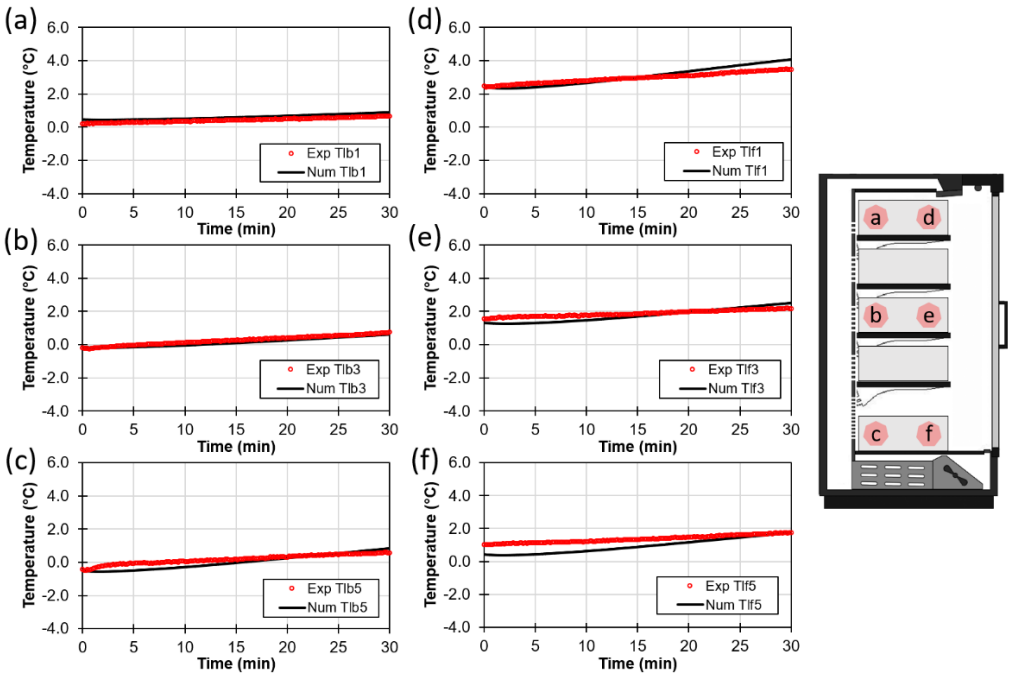


**Figure 7.10** Load temperature evolution at various position in a closed refrigerated display cabinet during the defrost operation ($T_{ext}$ = 19.5°C)

As shown in **Figure 7.11a and b**, the air and load temperature increase obtained from the simulation was in relatively good agreement with the experimental data. The model well represented the area of large air temperature increase at the back of the cabinet (**Figure 7.9a-7.9c**), whereas it was likely to overestimate in the area of low air temperature increase at the front (**Figure 7.9e-7.9f**). These findings showed that the model prediction was more accurate in the zone with less interaction between the cold air from the back and the heat entering the cabinet at the front. The overestimation was also observed for the load surface temperature increase. This discrepancy can be explained by the approximation of the equivalent load thickness with **Eq. (48)** which assumed $E\sqrt{\omega'} \gg h_a$. The precision would be improved if the more complex equation (**Eq. (47)**) was applied. Nevertheless, the over-estimated temperature increase by the model can be considered as the worst scenario that may happen in real use condition. Note that the air and load temperature increase was calculated based on the maximum and minimum temperatures from the beginning to the end of the defrost operation as shown in **Figure 7.8** as an example.

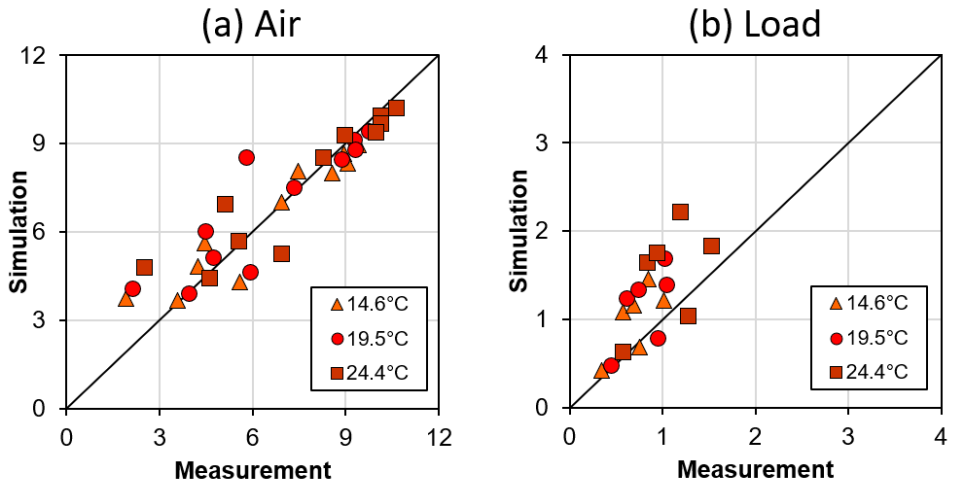


**Figure 7.11** Comparison between the simulation and the measurement of temperature increase ($T_{max} - T_{min}$) during defrosting period of (a) air and (b) load inside the closed refrigerated display cabinet for three external ambient temperatures

## 7.5. Conclusions

In Part II of this study, a simplified heat transfer model based on zonal approach was developed in transient state for a closed refrigerated display cabinet. The dynamic aspect of the model solved by a spectral approach (using transfer function and Fourier transform) allows the prediction of the air and load temperature fluctuations according to the "on/off" compressor operation at different positions. This solving approach also permits the identification of influential parameters on the damping of the temperature fluctuations with quick calculation. Since 2-4 harmonics (k) are usually enough to describe the supply air temperature profile, this approach only needs to solve a limited number of algebraic complex equations, instead of ordinary differential equations. To take into account the temperature variation within the load, the load thickness in which the temperature fluctuates with the same order as at the surface was estimated in function of on/off compressor working frequency. Given the input parameters used in the static model (without any adjustment), a relatively good agreement between the experimental and numerical results for the air and load temperature fluctuations was observed: maximum difference of 0.5 °C and 0.1 °C for the air and load, respectively. The results show the air temperature fluctuation progressively decreases from the rear duct entrance to the DAG. Accordingly, the air temperature fluctuations at the lower shelf were greater than that of the upper one. Despite the exposure to the high air temperature fluctuation, the load temperature was not much fluctuating in the closed refrigerated display cabinet ($\Delta T_l \leq 0.5$ °C). This would be the same for all products so long as the product thickness is smaller than the equivalent thickness.

The model was further used to investigate the evolution of the air and load temperatures during defrost operation. It was found that the increase in temperature depends on the position in the display cabinet. The predicted temperature increase during the defrosting period was in a relatively good agreement with the experimental data, but with an overestimation at some locations.

Although the proposed model was developed based on a specific closed display cabinet, it can be generalized to other display cabinets as addressed in Part I of the study. It needs to be emphasized that the air infiltration due to door openings is not considered in the developed model because of its complex airflow. This aspect

could be integrated in a future work. The model will be further linked with others models already developed in similar manner by the same research team for different refrigerating equipment in the cold chain, i.e. production plant, refrigerated truck, cold room, open display cabinet and domestic refrigerator. By such a way, the prediction of the evolution of the product time-temperature across the entire food cold chain can be established. The developed models can then be used to evaluate the consumers' risk by integrating with quality and/or microbiological predictive models.

# Chapter VIII

# General conclusions and perspectives

## 8.1. General conclusions

Closed refrigerated display cabinets are becoming increasingly used in supermarkets because of potential energy savings compared to open ones. This growing trend has contributed to an expanding research in the area of commercial refrigeration. However, most studies focused on improvements of energy efficiency after door installation while the influence of the presence of doors and the frequency/duration of door openings on product temperatures are much less studied. Like many refrigerating equipment, forced convection is usually a primary heat transfer mode in closed display cabinets; therefore, the temperature and its homogeneity are directly governed by the airflow patterns. A study on this matter becomes necessary to improve understanding of the main mechanism of these transport phenomena. Following this rationale, the work presented in this thesis was an attempt to bridge this research gaps by implementing both experimental and numerical approaches to characterize the airflow and heat transfer in a closed refrigerated display cabinet.

### *8.1.1. Experimental study*

A number of experiments were conducted in a closed refrigerated display cabinet under various operating conditions to study their influences on food temperature in the equipment. Thermocouples were distributed throughout the display cabinet to ascertain the internal air and the product temperature profiles. The implementation of an automatic door opening system made it possible to observe the air and product temperature evolutions according to different opening frequencies and durations. The use of a hot-wire anemometer and Particle Image Velocimetry (PIV) allowed to characterize the airflow pattern. It enables the knowledge of the velocity profile of the air curtain from the discharge air grille (DAG) to the return air grille (RAG), the airflow rate in the rear duct and the proportion of the air flowing from the perforated back panel (PBP) to the storage compartment at different shelves. The main results from the experimental study are summarized as follows:

*8.1.1.1. Airflow characteristic of a closed refrigerated display cabinet*

※ About 50%-50% airflow ratio between the DAG and the PBP was observed in the studied display cabinet. The variation in the occupied-volume percentages has insignificant effect on the airflow ratio.

※ The presence of doors caused the air recirculation at the upper part of the closed display cabinet where the warm ambient air infiltration through the door gaps was also observed leading to an increase in the air curtain temperature. Based on the air velocity measurement in the middle of the door gaps using the PIV technique, the air infiltration under the permanently closed-door condition accounted for about 8% of the supply air from the DAG.

※ At the lower part of the cabinet (from the top shelf level to the RAG), the presence of doors caused the air curtain to deviate toward the doors through a Coanda effect (maximum velocity observed near the door surface). This effect depends on the air temperature near the door surface; higher temperature enhances the upward flow because of higher buoyancy force.

※ Overall, the air curtain was quite stable in most regions of the closed display cabinet, except for the top (neat the DAG) and the bottom (near the RAG) of the cabinet where relatively high velocity fluctuations occurred.

*8.1.1.2. Thermal characteristic of a closed refrigerated display cabinet*

<u>I. Closed-door condition</u>

※ The overall thermal transmission coefficient of the studied closed display cabinet was measured. Compared with domestic refrigerators, the insulating capacity of the closed display cabinet was relatively lower. The gaps at the door edges and the thermal bridges were found to be the most significant contributor (~ 70%) of the overall thermal transmission of the studied display cabinet.

※ Two temporal air temperature variations periodically emerge in the closed display cabinet: one according to the "on/off" cycles of compressor regulation and the other one according to the compressor "off" period during the defrost operation.

※ The air temperature at the front-top shelf takes the longest time to reach the quasi-steady state (about an hour since the display cabinet started up). This

indicates the minimum duration for the air temperature stabilization before product loadings. A quasi-steady state is confirmed when the time-averaged temperature over one "on/off" cycle of compressor regulation remains the same.

※ Despite large air temperature fluctuations in the rear duct up to the DAG during the quasi-steady state ($\Delta T_a$ ~ 8-9 °C), the air temperature fluctuations in the storage compartment were relatively low ($\Delta T_a$ ~ 2-4 °C) because of the thermal inertia of solid cabinet components (e.g. rear wall, ceiling and PBP). This resulted in much lower fluctuations in the product temperatures ($\Delta T_p$ < 0.6 °C). The ratio of the product to its surrounding air temperature variation ($\Delta T_p/\Delta T_a$) was approximately 0.1. A reduction in the amplitude of the compressor regulation for the studied cabinet may be unnecessary, thereby prolonging the lifespan of the compressor.

※ Defrosting process causes drastic air and product temperature increases. The ratio of product to supply air temperature increase was between 0.05 and 0.10, depending on the product position in the closed display cabinet.

※ Both air and product temperatures vary spatially in the closed display cabinet. Based on the temperature profile at the center of the cabinet (symmetry plane), the front areas contribute to higher temperature, whereas the rear areas are at lower temperature. The front of the top shelf and the back of the bottom shelf are respectively the highest and lowest temperature positions in the cabinet. The temperature distribution at the sides of the cabinet has the same trend as that at the center, but the temperature at the sides is slightly higher because of additional heat losses through the lateral glass walls.

※ Forced convection and conduction are the predominant heat transfer modes in the closed display cabinet. This explains an almost linear relationship between the ambient temperature and the internal air temperature. Thermal radiation from the external walls is restricted by the glass doors shielded with low-emissivity coatings. However, visible radiation from the room and cabinet lightings still occurs and induces heat generation in the products, particularly at the front of the cabinet top shelf. When the cabinet doors are closed, free convection is insignificant in the cabinet because of small difference between the highest and coldest internal air temperatures ($\Delta T_a$ < 5 °C).

II. Periodic door-opening condition

※ Spatial and temporal air and product temperature distributions under the periodic door-opening condition has the same trend as that under closed-door condition. The product at the front always has a higher temperature than that at the back.

※ The air temperature evolution during the opening, holding and closing periods depends on its position in the cabinet. The nearer to the DAG, the quicker the air temperature stabilization after the door is opened. However, the air temperature is unstable at a certain distance from the DAG (i.e. from the middle shelf in this study). Due to this instability, the air temperature increases progressively during door openings and decreases after the door is closed.

※ An additional heat load due to higher door-opening frequency and/or higher ambient temperature resulted in a substantial increase in the product temperature at the front. The product temperature on the front middle shelf was the most affected when the opening frequency exceeded 40 openings per hour per door (OPH). This additional heat load also caused a slight decrease in the product temperature at the back because of more cooling capacity was needed (the average air temperature after the evaporator was lower). It is to be noticed that the highest temperature position was at the front-top shelf under closed-door condition.

※ Under periodic door-opening (10 OPH) condition, lower product temperature at all positions when the storage compartment was more occupied could be explained by higher convective heat transfer coefficient (higher velocity in the air space over the products).

*8.1.1.3. Comparison between the closed and open configurations*

I. Unloaded display cabinet (permanently closed and permanently open doors)

The air temperature profile was similar during permanently closed and permanently open-door (doors of the studied cabinet were completely removed) conditions. As the case of loaded display cabinet, the front of the top shelf and the back of the bottom shelf are respectively the highest and lowest temperature positions. However,

※ Lower air temperature level at all positions in the closed configuration was observed: maximum difference of 3.1 °C at the middle shelf.

※ Lower spatial air temperature variations on the same shelf: the air temperature difference between the front and the back was less than 1 °C in the closed configuration, while it was about 2-3 °C in the open one.

※ Less heat load on the evaporator in the closed configuration: the air temperature difference between the RAG and the DAG was less than 1.3 °C, while it was about 5.9 °C in the open one. Therefore, the time fraction during compressor "on" period decreased from 49% (open configuration) to 24% (closed configuration), about 50% reduction.

II. Loaded display cabinet (permanently closed, periodic door openings and permanently open doors)

Slightly different air and product temperature profiles were observed during permanently closed and permanently open door conditions. For the permanently open-door condition, the air and product temperatures were highest at the front of the middle shelf, while the lowest temperature positions remained at the back of the bottom shelf. The same trend of the temperature profiles was observed when the periodic door openings were applied. The closed refrigerated display cabinet provides better temperature performance despite a very high door-opening frequency (i.e. 60 OPH), compared to the case of permanently open doors (or without doors). The following information was obtained for the closed display cabinet:

※ Lower air and product temperature levels at all positions. The air and product temperatures respectively decreased up to 5.1 °C and 2.5 °C under permanently closed-door condition in comparison with permanently open-door condition. Under the opening frequency of 60 OPH, the product temperatures remained at least 1.0 °C lower than the ones under permanently open-door condition.

※ More uniform temperature distribution. The temperature difference between the highest and the lowest product (core) temperatures decreased from 4.0 °C (permanently open) to 2.0 °C (permanently closed) and 3.0 °C (opened with the frequency of 60 OPH).

※ Energy saving potential. The time fraction during the compressor "on" period decreased from 65% (permanently open) to 44% for the door-opening frequencies of 60 OPH and to 23% for permanently closed doors.

### *8.1.2. Numerical modeling*

Numerical tools were developed in the thesis by both Computational Fluid Dynamics (CFD) simulation and a simplified model based on a zonal approach.

#### *8.1.2.1. CFD simulation*

A steady-state 2D-CFD model with the standard k-ε turbulence model was developed to investigate the airflow and its influence on the air and product temperature distributions in a closed display cabinet. Two conditions (refrigeration system turned "off" or "on") were considered. Despite the simplified hypothesis, the developed model has shown the ability to reproduce the main flow phenomena observed by the experiments. The zone of air recirculation (where the ambient air infiltration through the door gaps causes an increase in the air curtain temperature) was identified at the front of the top shelf level. This phenomenon was more pronounced when the refrigeration system was turned "on". The model was then used to explore the influence of the airflow pattern on the temperature distribution. The trend of predicted product temperature profile was in a relatively good agreement with the experimental data.

#### *8.1.2.2. Simplified heat transfer model based on the zonal approach*

A simplified heat transfer model was developed based on a zonal approach to describe the evolution of product and air temperatures at different zones in the closed refrigerated display cabinet. The simplified model was developed in static and dynamic aspects, which permits, respectively, the predictions of both time-averaged air and product temperatures and the temperature fluctuations according to the on/off working cycles of the compressor regulation.

According to the zonal approach, the display cabinet was divided into various zones, the heat transfers in each zone are described by algebraic and ordinary differential equations, corresponding to energy balances.

The input parameters were obtained by several manners: measurement (presented in the experimental study), calculation from correlations reported in literature and

model fitting with the experimental time-averaged temperatures. Five input parameters were estimated by model fitting (for the ambient temperature of 19.5 °C) because of the difficulty to measure them: air circulation parameter at the top shelf, air distribution coefficients at the other shelves, air infiltration rate through the door gaps and convective heat transfer coefficients between the load surface and the surrounding air. The sensitivity study showed that the air infiltration rate through the door gaps is the most influencing parameter on the load temperatures. A 20% increase/decrease of this fitted parameter caused the warmest load temperature at the front-top shelf to be increased/decreased up to 0.2 °C while it is less than 0.1 °C for other parameters.

I. Static model

Without any adjustment to the fitting input parameters, the predicted and measured time-averaged temperatures were in a good agreement for the other external ambient temperatures (14.6 °C and 24.4 °C). The overall mean absolute error based on 60 paired data (air/load temperatures) for three ambient temperatures was less than 0.2 °C. The maximum difference of the calculated and measured load temperatures never exceeds 0.5 °C for every studied position. Moreover, the differences between the highest and the coldest load temperatures obtained from the experimental and the numerical data differed less than 14% for all studied ambient temperatures.

In the storage compartment, the model represented well the load temperatures, whereas it over-estimated the air temperature in the air curtain. Possible explanation of the discrepancy between the model and the experiment is that the air curtain temperature was measured only at one position of a given height, which may not be representative. However, the load temperature ranges and trends in the closed display cabinet are well represented by the proposed model with a short calculation time (less than 1 s).

The model showed its ability to investigate the effect of the air infiltration through the door gaps on the performance of the closed display cabinet in both thermal and energy aspects. Based on the numerical simulation, a reduction of the air infiltration through the door gaps by half could lead to decreases in the load temperatures of up to 0.7 °C and in the total cooling load of the refrigeration system by 35%.

II. Dynamic model

A spectral method was used to solve the dynamic model in the study. The supply air temperature profile (air after the evaporator where the thermostat sensor situated) from the experimental data during a transient cycle of compressor regulation was formulated by using Discrete Fourier Transform (DFT). The dynamic response of air/load temperature was readily determined by the transfer functions specified at all positions of heat exchange zones. By solving with the spectral method, the model allows not only the prediction of air/load temperature fluctuations in the display cabinet but also the identification of different influencing parameters on the damping of the temperature fluctuations. Moreover, this solving method also permits a quick calculation since only 2-4 harmonics for the DFT are enough to describe the supply air temperature profile $T_{th}$. This method needs only to solve a limited number of algebraic complex equations, instead of ordinary differential equations.

The estimation of the equivalent load thickness in which the temperature fluctuates with the same order as at the surface was derived in function of on/off compressor working frequency. This proposed method of estimation allows to take the temperature variation within the load into account in a simple manner compared to one-dimensional discretization of the load.

The numerical results of the air and load temperature fluctuations under periodic working conditions were in a good agreement with the experimental data: maximum difference of 0.5 °C for air and 0.1 °C for load. The high discrepancy at some positions in the storage compartment can be explained by the oversimplified assumptions concerning the flow distributions.

Based on the simulation during the compressor "on" and "off" regulation, the amplitude of the supply air temperature fluctuations progressively decreased when the air flowed in the rear duct and in the storage compartment. Despite the large surrounding air temperature fluctuations ($\Delta T_a$ ~ 2-5 °C), the load temperature was not much fluctuating ($\Delta T_l$ < 0.5 °C). This would be the same for all product types so long as the product thickness is larger than the equivalent thickness.

The air/load temperature fluctuations within the cabinet are very small compared to the supply air temperature fluctuations after the evaporator during the "on/off"

cycles of compressor. Damping of temperature fluctuation is a result of heat loss with a constant ambient temperature (pulsation independent effect), and thermal inertia of the wall and product (pulsation dependent effect, increasing when the compressor on/off period decreases).

The model also showed its ability to investigate the temperature increase of the air and the loads during the defrost operation. Comparison between the predicted and measured temperature increases during the defrosting period showed good agreement, with a small overestimation at some locations. For the air, the model prediction was more accurate in the rear zone because of less interaction between the cold air from the back and the heat entering the cabinet at the front. For the load, the precision would be improved if a more complex equation was applied to estimate the equivalent load thickness.

## 8.2. Perspectives

### *8.2.1. Experimentation*

Extensive experiments were carried out in the present study to characterize the airflow and temperature distributions in the closed display cabinet. The thermal cabinet performance under different operating conditions together with the comparison between the closed and open configurations was also examined. However, there are some other aspects not taken into considerations because of technical and time constraints. The suggestion for future work is listed below:

#### *8.2.1.1. Effect of air humidity in a test room on product temperature*

During the experimental study, the air temperature and air velocity can be controlled in the test room, but it is technically not possible to control the air humidity. The measurement of the air characteristics (dry-bulb air temperature and %relative humidity) was undertaken with a thermo-hygrometer (Testo 174H, accuracy ±3%RH). Then, the air humidity ratio (kg of water vapor/kg of dry air) was calculated using a psychrometric chart. The experimental results reported by Chen and Yuan (2005) showed the moderate effect of the ambient air humidity variations on the temperature distributions inside the display cabinet (open type in their study), but the significant effect on the refrigeration load. The ambient air humidity effect would be less in the closed display cabinets; however, no justification is available in literature.

#### *8.2.1.2. Effect of air humidity in a closed display cabinet on product quality*

For unwrapped products such as fruits and vegetables displayed in the cabinet, air humidity is a determining factor of their quality (freshness, color, etc.). High ambient humidity allows better food preservation; however, it leads to more frost formation on the evaporator, thus, less energy efficiency. Optimization of these two criteria should be undertaken by modification of design and operating conditions.

#### *8.2.1.3. Effect of air humidity in a test room on energy consumption*

The scope of the present study was to address the thermal performance of closed refrigerated display cabinets. The frequency of "on/off" compressor regulation was only used as an indicator of energy performance. Measurements of electrical energy consumption along with temperature measurements under different operating conditions would provide additional useful information.

#### *8.2.1.4. Air infiltration rate during door openings*

Air infiltration during door openings is an important factor determining the overall performance of closed refrigerated display cabinets. Implementation of a tracer gas technique to quantify the air infiltration rate for different opening frequencies would provide additional useful information, which can be further used in numerical simulations and design improvements.

### *8.2.2. Modeling*

A 2D-CFD and a simplified heat transfer models based on a zonal approach were developed in the closed-door condition i.e. the air infiltration due to door openings was not considered. Because of this limitation, suggestions are therefore proposed for future work.

#### *8.2.2.1. CFD simulation*

A 3D-CFD model in transient state with dynamic meshing is more appropriate to deal with the phenomena during door openings. The selection of turbulence model is also necessary. Because of calculation time in 3D-CFD simulation, a 2D-CFD model in steady state could be used to investigate the temperature distribution during door openings by substituting the door boundary condition with a velocity inlet (inflow) at the upper part and an outlet (outflow) at the lower part. Additional

measurements of air velocity at the door during openings need to be carried out for model input.

*8.2.2.2. Simplified heat transfer model based on the zonal approach*

The air infiltration due to door openings was not considered in the simplified model because the airflow during door openings is relatively complex. To keep the model simplicity, the air infiltration during door openings could be included by introducing a higher value of the air infiltration rate through the door gaps. Otherwise, some model modifications are required to be more realistic i.e. subtraction of air recirculation zone and introduction of external air infiltration rate at a given mixing zone. Additional experiments should be carried out to quantify the air infiltration rate during the door openings for model input.

The transient effect of intermittent heat load cannot be simulated by the spectral method because periodicity is assumed for the dynamic model. To include the heat load during the door openings, a temporal discretization could be used to solve the model (e.g. Runge-Kutta).

Finally, the experimental and numerical methodologies developed in this thesis can be applied to other types of closed display cabinet i.e. horizontal air curtain, more or less shelves and doors with some additional experiments and equations.

# Reference


Adrian, R. J. (2005). Twenty years of particle image velocimetry. *Experiments in Fluids, 39*(2), 159-169.

Al-Sahhaf, A. A. (2011). Investigation of the entrainment and infiltration rates through air curtains of open low-front refrigerated display cabinet. (Degree of Doctor of Philosophy), Brunel University, London, England.

Alfaro-Ayala, J. A., Uribe-Ramírez, A. R., Minchaca-Mojica, J. I., Ramírez-Minguela, J. d. J., Alvarado-Alcalá, B. U., & López-Núñez, O. A. (2017). Numerical prediction of the unsteady temperature distribution in a cooling cabinet. *International Journal of Refrigeration, 73*, 235-245.

Alzuwaid, F., Ge, Y. T., Tassou, S. A., Raeisi, A., & Gowreesunker, L. (2015). The novel use of phase change materials in a refrigerated display cabinet: An experimental investigation. *Applied Thermal Engineering, 75*, 770-778.

Alzuwaid, F. A., Ge, Y. T., Tassou, S. A., & Sun, J. (2016). The novel use of phase change materials in an open type refrigerated display cabinet: A theoretical investigation. *Applied Energy, 180*, 76-85.

Ambaw, A., Bessemans, N., Gruyters, W., Gwanpua, S. G., Schenk, A., De Roeck, A., . . . Nicolai, B. M. (2016). Analysis of the spatiotemporal temperature fluctuations inside an apple cool store in response to energy use concerns. *International Journal of Refrigeration, 66*, 156-168.

Amin, M., Dabiri, D., & Navaz, H. K. (2009). Experimental Investigation of the Effect of Various Parameters on the Infiltration Rates of Single Band Open Vertical Refrigerated Display Cases with Zero Back Panel Flow. *ASHRAE Transactions, 115*(2), 255-265.

Amin, M., Dabiri, D., & Navaz, H. K. (2009). Tracer gas technique: A new approach for steady state infiltration rate measurement of open refrigerated display cases. *Journal of Food Engineering, 92*(2), 172-181.

Amin, M., Navaz, H., Dabiri, D., & Faramarzi, R. (2008). Air curtains of open refrigerated display cases revisited: a new technique for infiltration rate measurements. *WIT Trans. Eng. Sci, 61*, 179-190.

Annaratone, D. (2010). *Engineering heat transfer*: Springer Science & Business Media.

ASHRAE. (2010). Retail food store refrigeration and equipment *ASHRAE Handbook: Refrigeration*. Atlanta, GA: American Society of Heating, Refrigerating and Air-Conditioning Engineers.

Atilio de Frias, J., Luo, Y., Kou, L., Zhou, B., & Wang, Q. (2015). Improving spinach quality and reducing energy costs by retrofitting retail open refrigerated cases with doors. *Postharvest Biology and Technology, 110*, 114-120.

Audits International. (1999). *U.S. Cold temperature evaluation design and study summary*.

Axell, M., Fahlén, P., & Tuovinen, H. (1999). *Influence of air distribution and load arrangement in display cabinets*. Paper presented at the 20th International Congress of Refrigeration, Sydney, Australia.

Axell, M., & Lindberg, U. (2005). *Field measurements in supermarkets*. Paper presented at the Proceedings of the IIF-IIR Meeting ‘Commercial Refrigeration', Vicenza, Italy.

Azzouz, K., Leducq, D., & Gobin, D. (2008). Performance enhancement of a household refrigerator by addition of latent heat storage. *International Journal of Refrigeration, 31*(5), 892-901.

Badia-Melis, R., Mc Carthy, U., Ruiz-Garcia, L., Garcia-Hierro, J., & Robla Villalba, J. I. (2018). New trends in cold chain monitoring applications - A review. *Food Control, 86*(Supplement C), 170-182.

Baldera Zubeldia, B., Nieto Jiménez, M., Valenzuela Claros, M. T., Mariscal Andrés, J. L., & Martin-Olmedo, P. (2016). Effectiveness of the cold chain control procedure in the retail sector in Southern Spain. *Food Control, 59*, 614-618.

Ben-abdallah, R., Leducq, D., Hoang, H. M., Pateau, O., Ballot-Miguet, B., Delahaye, A., & Fournaison, L. (2018). Modeling and experimental investigation for load temperature prediction at transient conditions of open refrigerated display cabinet using Modelica environment. *International Journal of Refrigeration, 94*, 102-110.

Bergman, T. L., Incropera, F. P., DeWitt, D. P., & Lavine, A. S. (2011). *Fundamentals of heat and mass transfer* (7 ed.): John Wiley & Sons.

Bertrand, M. (1993). Consommation et lieux d'achat des produits alimentaires en 1991. *INSEE-Consommation, modes de vie*(No. 54-55), 299.

Bøgh-Sorensen, L. (1980). *Product temperatures in chilled cabinets*. Paper presented at the 26th European Meeting of Meat Research Workers, Colorado Springs, CO, USA.

Bøgh-Sørensen, L., & Olsson, P. (Eds.). (1990). *The chill chain*. London: Elsevier Applied Science.

Borges, B. N., Hermes, C. J. L., Gonçalves, J. M., & Melo, C. (2011). Transient simulation of household refrigerators: A semi-empirical quasi-steady approach. *Applied Energy, 88*(3), 748-754.

Brown, W., Ryser, E., Gorman, L., Steinmaus, S., & Vorst, K. (2016). Temperatures experienced by fresh-cut leafy greens during retail storage and display. *Acta Horticulturae, 1141*, 103-108.

Cai, J., Risum, J., & Thybo, C. (2006). *Quality model of foodstuff in a refrigerated display cabinet*. Paper presented at the International Refrigeration and Air Conditioning Conference, West Lafayette, IN, USA.

Cao, Z., Gu, B., Mills, G., & Han, H. (2010). A novel strategy for predicting the performance of open vertical refrigerated display cabinets based on the MTF model and ASVM algorithm. *International Journal of Refrigeration, 33*(7), 1413-1424.

Carslaw, H., & Jaeger, J. (1959). *Conduction of heat in solids* (2 ed. Vol. 1). England: Clarendon Press, Oxford.

Carson, J. K., & East, A. R. (2018). The cold chain in New Zealand – A review. *International Journal of Refrigeration, 87*, 185-192.

Chaomuang, N., Flick, D., Denis, A., & Laguerre, O. (2019). Experimental analysis of heat transfer and airflow in a closed refrigerated display cabinet. *Journal of Food Engineering, 244*, 101-114.

Chaomuang, N., Flick, D., & Laguerre, O. (2017). Experimental and numerical investigation of the performance of retail refrigerated display cabinets. *Trends in Food Science & Technology, 70*(Supplement C), 95-104.

Chen, Y.-G. (2009). Parametric evaluation of refrigerated air curtains for thermal insulation. *International Journal of Thermal Sciences, 48*(10), 1988-1996.

Chen, Y.-G., & Yuan, X.-L. (2005). Experimental study of the performance of single-band air curtains for a multi-deck refrigerated display cabinet. *Journal of Food Engineering, 69*(3), 261-267.

Chen, Z.-j., & Lin, W.-h. (1991). Dynamic simulation and optimal matching of a small-scale refrigeration system. *International Journal of Refrigeration, 14*(6), 329-335.

Coleman, H. W., & Steele, W. G. (2018). *Experimentation, validation, and uncertainty analysis for engineers*: John Wiley & Sons.

Cortella, G. (2002). cfd-aided retail cabinets design. *Computers and Electronics in Agriculture, 34*(1–3), 43-66.

Cortella, G., Manzan, M., & Comini, G. (2001). CFD simulation of refrigerated display cabinets. *International Journal of Refrigeration, 24*(3), 250-260.

D'Agaro, P., Cortella, G., & Croce, G. (2006). Two- and three-dimensional CFD applied to vertical display cabinets simulation. *International Journal of Refrigeration, 29*(2), 178-190.

D'Agaro, P., Croce, G., & Cortella, G. (2006). Numerical simulation of glass doors fogging and defogging in refrigerated display cabinets. *Applied Thermal Engineering, 26*(16), 1927-1934.

Derens-Bertheau, E., Osswald, V., Laguerre, O., & Alvarez, G. (2015). Cold chain of chilled food in France. *International Journal of Refrigeration, 52*, 161-167.

Derens, E., Palagos, B., & Guilpart, J. (2006, September 17-21, 2006). *The cold chain of chilled products under supervision in France*. Paper presented at the 13th World Congress of Food Science & Technology, Nantes, France.

Duret, S., Gwanpua, S. G., Hoang, H.-M., Guillier, L., Flick, D., Laguerre, O., . . . Geeraerd, A. (2015). Identification of the significant factors in food quality using global sensitivity analysis and the accept-and-reject algorithm. Part II: Application to the cold chain of cooked ham. *Journal of Food Engineering, 148*, 58-65.

Eames, I. W., Brown, T., Evans, J. A., & Maidment, G. G. (2012). Description and validation of a computer based refrigeration system simulator. *Computers and Electronics in Agriculture, 85*, 53-63.

East, A. R., Smale, N. J., & Trujillo, F. J. (2013). Potential for energy cost savings by utilising alternative temperature control strategies for controlled atmosphere stored apples. *International Journal of Refrigeration, 36*(3), 1109-1117.

EIA. (2014). *Chilling Facts VI: Closing the door on HFCs*. Environmental Investigation Agency.

EIA. (2017). Chilling Facts VII: Are Europe's supermarkets ready to quit HFCs? Environmental Investigation Agency.

EN ISO 23953-2. (2015). Refrigerated Display Cabinets *Part 2: Classification, requirements and test conditions*.

Evans, J. A. (2010). *Retail display*. Paper presented at the 1st IIR Conference on Sustainability and the Cold Chain, Cambridge, UK.

Evans, J. A. (2014). *Are Doors on Fridges the Best Environmental Solution for the Retail Sector?* The Institute of Refrigeration.

Evans, J. A., Scarcelli, S., & Swain, M. V. L. (2007). Temperature and energy performance of refrigerated retail display and commercial catering cabinets under test conditions. *International Journal of Refrigeration, 30*(3), 398-408.

Evans, J. A., & Swain, M. V. L. (2010). *Performance of retail and commercial refrigeration systems*. Paper presented at the IIR International Cold Chain Conference, Cambridge, UK.

Faramarzi, R. T. (1999). Efficient display case refrigeration. *ASHRAE Journal, 41*(11), 46-54.

Faramarzi, R. T., Coburn, B. A., & Sarhadian, R. (2002). Performance and energy impact of installing glass doors on an open vertical deli/dairy display case. *ASHRAE Transactions, 108*, 673.

Field, B. S., & Loth, E. (2006). Entrainment of refrigerated air curtains down a wall. *Experimental Thermal and Fluid Science, 30*(3), 175-184.

Field, B. S., Loth, E., & Hrnjak, P. (2002). *Entrainment in refrigerated air curtains*. Air Conditioning and Refrigeration Center. University of Illinois at Urbana-Champaign.

Foster, A. M., Madge, M., & Evans, J. A. (2005). The use of CFD to improve the performance of a chilled multi-deck retail display cabinet. *International Journal of Refrigeration, 28*(5), 698-705.

Fricke, B., & Becker, B. (2010). *Energy use of doored and open vertical refrigerated display cases.* Paper presented at the International Refrigeration and Air Conditioning Conference, West Lafayette, IN, USA.

Gaspar, P. D., Carrilho Gonçalves, L. C., & Pitarma, R. A. (2011). Experimental analysis of the thermal entrainment factor of air curtains in vertical open display cabinets for different ambient air conditions. *Applied Thermal Engineering, 31*(5), 961-969.

Gaspar, P. D., Gonçalves, L., & Pitarma, R. (2012). Detailed CFD modelling of open refrigerated display cabinets. *Modelling and Simulation in Engineering, 2012*, 1-17.

Ge, Y. T., & Tassou, S. A. (2001). Simulation of the performance of single jet air curtains for vertical refrigerated display cabinets. *Applied Thermal Engineering, 21*(2), 201-219.

Ge, Y. T., Tassou, S. A., & Hadawey, A. (2010). Simulation of multi-deck medium temperature display cabinets with the integration of CFD and cooling coil models. *Applied Energy, 87*(10), 3178-3188.

Gill, C. O., Jones, T., Houde, A., LeBlanc, D. I., Rahn, K., Holley, R. A., & Starke, R. (2003). The temperatures and ages of packs of beef displayed in multi-shelf retail cabinets. *Food Control, 14*(3), 145-151.

Gogou, E., Katsaros, G., Derens, E., Alvarez, G., & Taoukis, P. S. (2015). Cold chain database development and application as a tool for the cold chain management and food quality evaluation. *International Journal of Refrigeration, 52*, 109-121.

Gray, I., Luscombe, P., McLean, L., Sarathy, C. S. P., Sheahen, P., & Srinivasan, K. (2008). Improvement of air distribution in refrigerated vertical open front remote supermarket display cases. *International Journal of Refrigeration, 31*(5), 902-910.

Gruyters, W., Verboven, P., Delele, M., Gwanpua, S. G., Schenk, A., & Nicolaï, B. (2018). A numerical evaluation of adaptive on-off cooling strategies for energy savings during long-term storage of apples. *International Journal of Refrigeration, 85*, 431-440.

Hadawey, A. F., Jaber, T. J., Ghaffar, W. A., & Hasan, A. (2012). Air curtain design optimization of refrigerated vertical display cabinet using CFD. *International Journal of Scientific Engineering and Technology, 1*(4), 76-88.

Hammond, E. (2011, August 21 - 26, 2011). *Investigation of return air grille width on the efficiency of recirculated air curtains*. Paper presented at the 23rd International-Institute-of-Refrigeration(IIR) International Congress of Refrigeration, Prague, Czech Republic.

Hammond, E., Marques, C., & Ketteringham, L. (2016). *Application of short air curtain in retail display refrigerators*. Paper presented at the 4th IIR Conference on Sustainability and the Cold Chain, Auckland, New Zealand.

Hasse, H., Becker, M., Grossmann, K., & Maurer, G. (1996). Top-down model for dynamic simulation of cold-storage plants. *International Journal of Refrigeration, 19*(1), 10-18.

Heidinger, G., Nascimento, S., Gaspar, P., & Silva, P. (2013). *Impact of environmental conditions on the performance of open multideck display case evaporators*. Paper presented at the 2nd IIR International Conference on Sustainability and the Cold Chain, Paris, France.

Heidinger, G., Nascimento, S., Gaspar, P., & Silva, P. (2015). *Experimental study of the influence of consumers' movement parallel to the frontal opening of a multideck display case on the evaporator's thermal performance*. Paper presented at the Proceedings of the 24th IIR International Congress of Refrigeration, Yokohama, Japan.

Hermes, C. J. L., & Melo, C. (2008). A first-principles simulation model for the start-up and cycling transients of household refrigerators. *International Journal of Refrigeration, 31*(8), 1341-1357.

Hoang, H. M., Raoult, F., & Leducq, D. (2016, May 18-20, 2016). *Potential use of phase change materials in a display cabinet: development of a dynamic modelling approach*. Paper presented at the 11th IIR Conference on Phase Change Materials and Slurries for Refrigeration and Air Conditioning, Karlsruhe, Germany.

Hoang, M. H., Laguerre, O., Moureh, J., & Flick, D. (2012). Heat transfer modelling in a ventilated cavity loaded with food product: Application to a refrigerated vehicle. *Journal of Food Engineering, 113*(3), 389-398.

Howell, R., Pascua, R., Wooles, L., & Goebel, S. (1999). *Spatial and temporal variation of relative humidity and temperature in supermarkets*. Paper presented at the Proceedings of Twentieth International Congress of Refrigeration, Sydney, Australia.

Howell, R., Rosario, L., Riiska, D., & Bondoc, M. (1999). *Potential savings in display case energy with reduced supermarket relative humidity*. Paper presented at the 20th International Congress of Refrigeration, Sydney, Australia.

Hunter, M. (2017). *We don't need to double world food production by 2050 – here's why.* The Conversation.

Icier, F., & Ilicali, C. (2005). The use of tylose as a food analog in ohmic heating studies. *Journal of Food Engineering, 69*(1), 67-77.

Illuminating Engineering Society of North America. (1991). Recommended Practice for Lighting Merchandising Areas: A Store Lighting Guide Y1. *Journal of the Illuminating Engineering Society, 20*(1), 161-222.

International Institute of Refrigeration (2009). *The role of refrigeration in worldwide nutrition*. 5th Informatory Note on Refrigeration and Food. International Institute of Refrigeration.

Jol, S., Kassianenko, A., Wszol, K., & Oggel, J. (2006). Issues in time and temperature abuse of refrigerated foods. *Food Safety Magazine, 11*.

Jouhara, H., Nannou, T., Ghazal, H., Kayyali, R., Tassou, S., & Lester, S. (2017). Temperature and energy performance of open refrigerated display cabinets using heat pipe shelves. *Energy Procedia, 123*, 273-280.

Kaffel, A., Moureh, J., Harion, J.-L., & Russeil, S. (2015). Experimental investigation of a plane wall jet subjected to an external lateral flow. *Experiments in Fluids, 56*(5), 1-19.

Kauffeld, M. (2009). Comparative Assessment of the Climate Relevance of Supermarket Refrigeration Systems and Equipment: Dessau-Roßlau: German Federal Environment Agency.

Kauffeld, M. (2015). Current and Future Carbon- saving Options for Retail Refrigeration. In J. A. Evans & A. M. Foster (Eds.), *Sustainable Retail Refrigeration* (pp. 125-158). Malaysia: Wiley Blackwell.

Keane, R. D., & Adrian, R. J. (1992). Theory of cross-correlation analysis of PIV images. *Applied Scientific Research, 49*, 191-215.

Kou, L., Luo, Y., Ingram, D. T., Yan, S., & Jurick, W. M. (2015). Open-refrigerated retail display case temperature profile and its impact on product quality and microbiota of stored baby spinach. *Food Control, 47*, 686-692.

Koutsoumanis, K., Pavlis, A., Nychas, G.-J. E., & Xanthiakos, K. (2010). Probabilistic model for Listeria monocytogenes growth during distribution, retail storage, and domestic storage of pasteurized milk. *Applied and environmental microbiology, 76*(7), 2181-2191.

Laguerre, O. (2010). Heat Transfer and Air Flow in a domestic refrigerator. In M. F. Mohammed (Ed.), *Mathematical Modeling of Food Processing* (pp. 445-474): CRC Press.

Laguerre, O., Ben Amara, S., Moureh, J., & Flick, D. (2007). Numerical simulation of air flow and heat transfer in domestic refrigerators. *Journal of Food Engineering, 81*(1), 144-156.

Laguerre, O., & Chaomuang, N. (2019). Closed Refrigerated Display Cabinets: Is It Worth It for Food Quality? In P. D. Gaspar & P. D. Silva (Eds.), *Novel Technologies and Systems for Food Preservation*: IGI Global.

Laguerre, O., Duret, S., Hoang, H. M., & Flick, D. (2014). Using simplified models of cold chain equipment to assess the influence of operating conditions and equipment design on cold chain performance. *International Journal of Refrigeration, 47*, 120-133.

Laguerre, O., Duret, S., Hoang, H. M., Guillier, L., & Flick, D. (2015). Simplified heat transfer modeling in a cold room filled with food products. *Journal of Food Engineering, 149*, 78-86.

Laguerre, O., & Flick, D. (2004). Heat transfer by natural convection in domestic refrigerators. *Journal of Food Engineering, 62*(1), 79-88.

Laguerre, O., & Flick, D. (2010). Temperature prediction in domestic refrigerators: Deterministic and stochastic approaches. *International Journal of Refrigeration, 33*(1), 41-51.

Laguerre, O., Hoang, H. M., & Flick, D. (2013). Experimental investigation and modelling in the food cold chain: Thermal and quality evolution. *Trends in Food Science & Technology, 29*(2), 87-97.

Laguerre, O., Hoang, M. H., & Flick, D. (2012). Heat transfer modelling in a refrigerated display cabinet: The influence of operating conditions. *Journal of Food Engineering, 108*(2), 353-364.

Laguerre, O., Hoang, M. H., Osswald, V., & Flick, D. (2012). Experimental study of heat transfer and air flow in a refrigerated display cabinet. *Journal of Food Engineering, 113*(2), 310-321.

Lawrence, J. M. W., & Evans, J. A. (2008). Refrigerant flow instability as a means to predict the need for defrosting the evaporator in a retail display freezer cabinet. *International Journal of Refrigeration, 31*(1), 107-112.

Lecoq, L., Flick, D., Derens, E., Hoang, H. M., & Laguerre, O. (2016). Simplified heat and mass transfer modeling in a food processing plant. *Journal of Food Engineering, 171*, 1-13.

Li, X., Zhu, D., Wang, N., & Zeng, X. (2007). *Influence of door opening on temperature fluctuation and energy consumption of refrigerated display cabinet*. Paper presented at the 22nd International Congress of Refrigeration, Beijing, China.

Ligthart, F. A. T. M. (2007). *Closed supermarket refrigerator and freezer cabinets: a feasibility study* (ECN-E-07-098).

Likar, K., & Jevšnik, M. (2006). Cold chain maintaining in food trade. *Food Control, 17*(2), 108-113.

Lindberg, U., Axell, M., & Fahlén, P. (2010). *Vertical display cabinets without and with doors–a comparison of measurements in a laboratory and in a supermarket*. Paper presented at the 1st IIR International Conference on Sustainability and the Cold Chain, Cambridge, United Kingdom.

Lindberg, U., Fahlén, P., Axell, M., & Fransson, N. (2017). Thermal comfort in the supermarket environment – multiple enquiry methods and simultaneous measurements of the thermal environment. *International Journal of Refrigeration, 82*, 426-435.

Lindberg, U. M., Axell, M., Fahlaen, P., & Fransson, N. (2008). *Supermarkets, indoor climate and energy efficiency-Field measurements before and after installation of doors on refrigerated cases*. Paper presented at the International Refrigeration and Air Conditioning Conference, West Lafayette, IN, USA.

Lovatt, S. J., Loeffen, M. P. F., & Cleland, A. C. (1998). Improved dynamic simulation of multi-temperature industrial refrigeration systems for food chilling, freezing and cold storage. *International Journal of Refrigeration, 21*(3), 247-260.

Lu, Y. L., Zhang, W. H., Yuan, P., Xue, M. D., Qu, Z. G., & Tao, W. Q. (2010). Experimental study of heat transfer intensification by using a novel combined shelf in food refrigerated display cabinets (Experimental study of a novel cabinets). *Applied Thermal Engineering, 30*(2–3), 85-91.

Lundén, J., Vanhanen, V., Myllymäki, T., Laamanen, E., Kotilainen, K., & Hemminki, K. (2014). Temperature control efficacy of retail refrigeration equipment. *Food Control, 45*, 109-114.

Madireddi, S., & Agarwal, R. K. (2005). *Computation of three-dimensional flow field and heat transfer inside an open refrigerated display case with an air curtain*. Paper presented at the IIR International Conferences, Vicenza, Italy.

Marinetti, S., Cavazzini, G., Fedele, L., De Zan, F., & Schiesaro, P. (2012). Air velocity distribution analysis in the air duct of a display cabinet by PIV technique. *International Journal of Refrigeration, 35*(8), 2321-2331.

Marinetti, S., Cavazzini, G., Lauri, I., Testa, S., & Minetto, S. (2014). Numerical and experimental analysis of the air flow distribution in the cooling duct of a display cabinet. *International Journal of Refrigeration, 42*, 8-13.

Mariquele, B. E. (2012). *"Critical" Quality Points in fresh-cut vegetables supply chain*. (Master Food Quality Management), Wageningen University.

McKellar, R. C., LeBlanc, D. I., Rodríguez, F. P., & Delaquis, P. (2014). Comparative simulation of Escherichia coli O157:H7 behaviour in packaged fresh-cut lettuce distributed in a typical Canadian supply chain in the summer and winter. *Food Control, 35*(1), 192-199.

Melo, C., Da Silva, L. W., & Pereira, R. H. (2000). *Experimental evaluation of the heat transfer through the walls of household refrigerators*. Paper presented at the International Refrigeration and Air Conditioning Conference, West Lafayette, IN, USA.

Mercier, S., Mondor, M., Villeneuve, S., & Marcos, B. (2018). The Canadian food cold chain: A legislative, scientific, and prospective overview. *International Journal of Refrigeration, 88*, 637-645.

Mercier, S., Villeneuve, S., Mondor, M., & Uysal, I. (2017). Time–Temperature Management Along the Food Cold Chain: A Review of Recent Developments. *Comprehensive Reviews in Food Science and Food Safety, 16*(4), 647-667.

Morelli, E., Noel, V., Rosset, P., & Poumeyrol, G. (2012). Performance and conditions of use of refrigerated display cabinets among producer/vendors of foodstuffs. *Food Control, 26*(2), 363-368.

Moureh, J., & Yataghene, M. (2016). Numerical and experimental study of airflow patterns and global exchanges through an air curtain subjected to external lateral flow. *Experimental Thermal and Fluid Science, 74*, 308-323.

Moureh, J., & Yataghene, M. (2017). Large-eddy simulation of an air curtain confining a cavity and subjected to an external lateral flow. *Computers & Fluids, 152*, 134-156.

Murmann, D., & Häger Kuhlung, O. (1987). von Hackfleisch im SB-Angebot. *Fleischwirtschaft, 67*, 245-248.

Navaz, H. K., Faramarzi, R., Gharib, M., Dabiri, D., & Modarress, D. (2002). The application of advanced methods in analyzing the performance of the air curtain in a refrigerated display case. *Journal of Fluids Engineering, 124*(3), 756-764.

Navaz, H. K., Henderson, B. S., Faramarzi, R., Pourmovahed, A., & Taugwalder, F. (2005). Jet entrainment rate in air curtain of open refrigerated display cases. *International Journal of Refrigeration, 28*(2), 267-275.

Navigant Consulting Inc. (2009). *Energy Savings Potential and R&D Opportunities for Commercial Refrigeration Final Report*.

Ndraha, N., Hsiao, H.-I., Vlajic, J., Yang, M.-F., & Lin, H.-T. V. (2018). Time-temperature abuse in the food cold chain: Review of issues, challenges, and recommendations. *Food Control, 89*, 12-21.

Norton, T., & Sun, D.-W. (2006). Computational fluid dynamics (CFD) – an effective and efficient design and analysis tool for the food industry: A review. *Trends in Food Science & Technology, 17*(11), 600-620.

Nunes, M. C. N., Emond, J. P., Rauth, M., Dea, S., & Chau, K. V. (2009). Environmental conditions encountered during typical consumer retail display affect fruit and vegetable quality and waste. *Postharvest Biology and Technology, 51*(2), 232-241.

Olsson, P. (Ed.) (1990). *Chilled cabinet surveys* (Vol. 3). London: Elsevier Applied Science Publishers.

Orlandi, M., Visconti, F., & Zampini, S. (2013). *CFD assisted design of closed display cabinets.* Paper presented at the 2nd IIR International Sustainability and the Cold Chain Conference, Paris, France.

Platenius, H. (1939). Effect of temperature on the rate of deterioration of fresh vegetables. *Journal of Agricultural Research, 59*(1), 41-58.

Prasad, A. K. (2000). Particle image velocimetry. *Current Science, 79*(1), 51-60.

Rachek, A., Sartre, V., & Bonjour, J. (2010, 2010-03-29). *Dynamic simulation of the refrigerated compartment of a truck coupled with its refrigeration system*.

Paper presented at the 1rst international cold chain and sustainability conference, Cambridge, United Kingdom.

Raffel, M., Willert, C. E., Scarano, F., Kähler, C. J., Wereley, S. T., & Kompenhans, J. (2018). *Particle image velocimetry: a practical guide*: Springer.

Rasmussen, B. P. (2012). Dynamic modeling for vapor compression systems—Part I: Literature review. *HVAC&R Research, 18*(5), 934-955.

Rediers, H., Claes, M., Peeters, L., & Willems, K. A. (2009). Evaluation of the cold chain of fresh-cut endive from farmer to plate. *Postharvest Biology and Technology, 51*(2), 257-262.

Rhiemeier, J., Harnisch, J., Ters, C., Kauffeld, M., & Leisewitz, A. (2009). *Comparative assessment of the climate relevance of supermarket refrigeration systems and equipment*. Environmental Research of the Federal Ministry for the Environment, Nature Conservation and Nuclear Safety.

Robertson, G. (2015). *Trial retrofit of doors on open refrigerated display cabinets*.

Rolfsman, L., & Borgqvist, M. (2014). *Changes of the refrigeration system in the dairy section of a Supermarket-Field measurements*. Paper presented at the 3rd IIR International Conference on Sustainability and the Cold Chain, London, United Kingdom.

Rossetti, A., Minetto, S., & Marinetti, S. (2015). Numerical modelling and validation of the air flow maldistribution in the cooling duct of a horizontal display cabinet. *Applied Thermal Engineering, 87*, 24-33.

Rossetti, A., Minetto, S., & Marinetti, S. (2015). A simplified thermal CFD approach to fins and tube heat exchanger: Application to maldistributed airflow on an open display cabinet. *International Journal of Refrigeration, 57*, 208-215.

RPF. (2016). Fermeture des meubles réfrigérés: du positif pour les clients. *La Revue Pratique du Froid et du Conditionnement d'Air*, 26-28.

Sagoo, S., Little, C., Allen, G., Williamson, K., & Grant, K. (2007). Microbiological safety of retail vacuum-packed and modified-atmosphere-packed cooked meats at end of shelf life. *Journal of food protection, 70*(4), 943-951.

Sciacchitano, A., Neal, D. R., Smith, B. L., Warner, S. O., Vlachos, P. P., Wieneke, B., & Scarano, F. (2015). Collaborative framework for PIV uncertainty

quantification: comparative assessment of methods. *Measurement Science and Technology, 26*(7), 074004.

Sciacchitano, A., & Wieneke, B. (2016). PIV uncertainty propagation. *Measurement Science and Technology, 27*(8), 084006.

Smale, N. J., Moureh, J., & Cortella, G. (2006). A review of numerical models of airflow in refrigerated food applications. *International Journal of Refrigeration, 29*(6), 911-930.

Tano, K., Oulé, M. K., Doyon, G., Lencki, R. W., & Arul, J. (2007). Comparative evaluation of the effect of storage temperature fluctuation on modified atmosphere packages of selected fruit and vegetables. *Postharvest Biology and Technology, 46*(3), 212-221.

Tassou, S. A., Datta, D., & Marriott, D. (2001). Frost formation and defrost control parameters for open multideck refrigerated food display cabinets. Proceedings of the Institution of Mechanical Engineers, Part A: *Journal of Power and Energy, 215*(2), 213-222.

Tassou, S. A., Ge, Y., Hadawey, A., & Marriott, D. (2011). Energy consumption and conservation in food retailing. *Applied Thermal Engineering, 31*(2–3), 147-156.

The Food Safety Authority of Ireland. (2003). *Microbiological quality/safety of pre-packed cooked sliced ham*.

The Grocery Trader. (2013). *The case for glass doors on refrigerated display cabinets is closed.* The grocery Trader.

Tu, J., Yeoh, G. H., & Liu, C. (2018). *Computational fluid dynamics: a practical approach*: Butterworth-Heinemann.

Food Code, 3-202.11 C.F.R. (2013).

United Nations. (2017). *World Population Prospects: The 2017 Revision, Key Findings and Advance Tables*.

Valin, H., Sands, R. D., Van der Mensbrugghe, D., Nelson, G. C., Ahammad, H., Blanc, E., . . . Havlik, P. (2014). The future of food demand: understanding differences in global economic models. *Agricultural Economics, 45*(1), 51-67.

Vallée, C. (2015, August 16-22, 2015). *Energy saving potential at partial load for vertical glass door refrigerated display cabinets.* Paper presented at the 24th IIR International Congress of Refrigeration, Yokohama, Japan.

Versteeg, H. K., & Malalasekera, W. (2007). *An introduction to computational fluid dynamics: the finite volume method*: Pearson education.

Wang, L., Zhang, L., & Lian, G. (2015). A CFD Simulation of 3D Air Flow and Temperature Variation in Refrigeration Cabinet. *Procedia Engineering, 102*, 1599-1611.

Wells, J. H., & Singh, R. (1989). A quality- based inventory issue policy for perishable foods. *Journal of Food Processing and Preservation, 12*(4), 271-292.

Wieneke, B. (2015). PIV uncertainty quantification from correlation statistics. *Measurement Science and Technology, 26*(7), 074002.

Willocx, F., Hendrick, M., & Tobback, P. (1994). A preliminary survey into the temperature conditions and residence time distribution of minimally processed MAP vegetables in Belgian retail display cabinets. *International Journal of Refrigeration, 17*(7), 436-444.

Wilson, B. M., & Smith, B. L. (2013). Uncertainty on PIV mean and fluctuating velocity due to bias and random errors. *Measurement Science and Technology, 24*(3), 035302.

Wu, X., Chang, Z., Yuan, P., Lu, Y., Ma, Q., & Yin, X. (2014). The optimization and effect of back panel structure on the performance of refrigerated display cabinet. *Food Control, 40*, 278-285.

Wu, X., Chang, Z., Zhao, X., Li, W., Lu, Y., & Yuan, P. (2015). A multi-scale approach for refrigerated display cabinet coupled with supermarket HVAC system – Part I: Methodology and verification. *International Journal of Heat and Mass Transfer, 87*, 673-684.

Wu, X., Li, W., Wang, Y., Chang, Z., Wang, C., & Ding, C. (2017). Experimental investigation of the performance of cool storage shelf for vertical open refrigerated display cabinet. *International Journal of Heat and Mass Transfer, 110*, 789-795.

Yu, K.-z., Ding, G.-l., & Chen, T.-j. (2007). Simulation of air curtains for vertical display cases with a two-fluid model. *Applied Thermal Engineering, 27*(14–15), 2583-2591.

Yu, K.-z., Ding, G.-l., & Chen, T.-j. (2008). Modified two-fluid model for air curtains in open vertical display cabinets. *International Journal of Refrigeration, 31*(3), 472-482.

Yu, K.-z., Ding, G.-l., & Chen, T.-j. (2009a). A correlation model of thermal entrainment factor for air curtain in a vertical open display cabinet. *Applied Thermal Engineering, 29*(14–15), 2904-2913.

Yu, K.-z., Ding, G.-l., & Chen, T.-j. (2009b). Experimental investigation on a vertical display cabinet with central air supply. *Energy Conversion and Management, 50*(9), 2257-2265.

Zhang, L., Fujinawa, T., & Saikawa, M. (2017). Theoretical study on a frost-free refrigerated display cabinet. *International Journal of Refrigeration, 74*, 95-104.

Zhijuan, C., Xuehong, W., Yanli, L., Qiuyang, M., & Wenhui, Z. (2013). Numerical simulation on the food package temperature in refrigerated display cabinet influenced by indoor environment. *Advances in Mechanical Engineering, 5*, 708785.

Zsembinszki, G., de Gracia, A., Moreno, P., Rovira, R., Ángel González, M., & Cabeza, L. F. (2017). A novel numerical methodology for modelling simple vapour compression refrigeration system. *Applied Thermal Engineering, 115*, 188-200.

**Thesis title:** Experimental characterization and modeling of airflow and heat transfer in a closed refrigerated display cabinet


## Abstract

The use of closed refrigerated display cabinets in supermarkets has been increased steadily because of the potential energy savings compared to open ones. This growing trend has contributed to the necessity to expand research in the field of retail refrigeration. Most studies in literature, however, focused on the improvements of energy efficiency after door installation while studies on the mechanism of heat transfer and airflow within closed display cabinets are still limited. In fact, airflow pattern influences the heat exchange between air and products, thus, product temperature. This PhD thesis aims to gain an insight into the mechanism of airflow and heat transfer in closed refrigerated display cabinets by the implementation of experimental and numerical approaches.

Experimental investigations were conducted in a closed refrigerated display cabinet (an integral type with a single band air curtain and two double-glazing doors) located in a controlled-temperature test room. Air/product temperatures and air velocity are the main parameters taken into investigations. Eighty calibrated thermocouples distributed throughout the cabinet made it possible to observe the spatial and temporal evolutions of the air and product temperatures under different operating conditions. These conditions were ambient air temperature (15, 19, 24 and 29 °C), product-occupied volume (unloaded, half-loaded and full-loaded with test packages made of methylcellulose), door-opening frequency (0 - permanently closed, 10, 20, 40, 60 Openings Per Hour - OPH) and opening duration (15s and 30s). An automatic door opening system was developed and allowed to apply the opening regime as prescribed in the standard test (EN ISO 23953-2, 2015). The experiment was also conducted in an open configuration of the cabinet (doors were completely removed) to determine the benefits of the doors on the temperature performance. The results showed that when the doors were permanently closed, the temperature distribution in the cabinet was similar whatever the ambient temperatures and occupied-volume percentages – the highest temperature position at the front-top shelf and the lowest temperature position at the rear-bottom shelf.

The temperature distribution changed when the doors were periodically or permanently open – the front of the middle shelf became the highest temperature position while the lowest temperature position remained at the rear-bottom shelf. However, the air and product temperatures in the cabinet with doors remained lower despite a very high door-opening frequency (i.e. 60 OPH, product temperatures at least 1.0 °C lower), compared to the case without doors.

Air velocity measurement using a hot-wire anemometer at the front of the cabinet from the discharge to the return air grilles allowed to observe the shape of the air curtain, while the measurement in the rear duct allowed to quantify the air flow distribution over the perforated back panel of different shelves. The use of a Particle Image Velocimetry (PIV) technique allowed the characterization of the air curtain with higher spatial resolution and accuracy. The result showed a zone of air recirculation at the upper part of the cabinet where warm ambient air infiltration through the door gaps was also observed, leading to an increase in the air curtain temperature. A 2D-CFD k-ε turbulence model was developed to reproduce the main flow phenomena observed by PIV so that its influence on the internal temperature distribution can be examined.

Finally, a simplified heat transfer model was developed based on a zonal approach in both static and dynamic regimes which permits, respectively, the predictions of time-averaged air and product temperatures and temperature fluctuations according to the on/off cycle of the compressor regulation. The dynamic model was solved with a spectral approach, thus the influence of different parameters on the damping of the temperature fluctuations can be identified.

**Keywords:** closed refrigerated display cabinet, airflow, heat transfer, temperature distribution, door openings, Particle Image Velocimetry, simplified model, temperature fluctuation, CFD model

**Titre de la thése :** Caractérisation expérimentale et modélisation des écoulements d'air et transferts thermiques dans un meuble frigorifique fermé


**Résumé**

En France, dans le cadre des économies d'énergie, un accord a été signé entre les Ministères et la Fédération du commerce et de l'Industrie afin d'obtenir dans la grande distribution 75% de meubles fermés en 2020. La généralisation des meubles fermés pour produits réfrigérés entraîne la nécessité d'élargir les connaissances scientifiques concernant ce type de meuble.

La plupart des études de la littérature ont porté sur l'amélioration de l'efficacité énergétique suite à l'installation des portes, tandis que les études sur les mécanismes de transfert de chaleur dans les meubles frigorifiques fermés sont rares. De plus, il convient d'étudier également la circulation d'air car elle influence les échanges de chaleur entre l'air et les produits, donc leur température. Cette thèse a pour objectif de mieux comprendre les phénomènes d'écoulement d'air et de transfert de chaleur dans les meubles frigorifiques fermés par la mise en œuvre d'approches expérimentales et numériques.

Des investigations expérimentales ont été menées sur un meuble frigorifique fermé avec un rideau d'air simple et des portes à double vitrage, placé dans une cellule d'essai à température contrôlée. Des thermocouples calibrés répartis dans le meuble ont permis d'observer les évolutions spatio-temporelles des températures de l'air et des produits dans différentes conditions de fonctionnement. Nous avons fait varier la température de l'air ambiant, le volume occupé par le produit et la fréquence d'ouverture des portes. Des expériences ont également été réalisées dans une configuration ouverte du meuble frigorifique (portes complètement retirées) afin de déterminer les avantages des portes sur les performances thermiques.

Les résultats ont montré que lorsque les portes étaient fermées en permanence, les champs de température étaient similaires, quelle que soit la température ambiante et le pourcentage de volume occupé ; la température la plus élevée se situe à l'avant de l'étagère supérieure. Cette répartition change lorsque les portes sont périodiquement ou définitivement ouvertes ; la position où la température est la plus élevée migre vers

l'avant de l'étagère du milieu. Même pour une fréquence très élevée d'ouverture des portes (60 ouvertures par heure), les températures de l'air et des produits dans le meuble fermé sont restées plus basses d'au moins 1,0 °C par rapport au meuble sans portes.

Des mesures de vitesse d'air par anémométrie à fil chaud au niveau du rideau d'air ont permis d'observer son allure générale tandis que les mesures effectuées dans le conduit arrière ont permis de quantifier la répartition du flux d'air à travers le plaque arrière perforée au niveau des différentes étagères. L'utilisation d'une technique de vélocimétrie par image de particules (PIV) a permis de caractériser le rideau d'air avec une résolution et une précision spatiale supérieures. Les résultats ont notamment montré l'existence d'une zone de recirculation de l'air dans la partie supérieure du meuble où l'on observe également une infiltration d'air ambiant chaud par les fentes présentes autour des portes, ce qui induit une augmentation de la température du rideau d'air. Des simulations numériques bidimensionnelles d'écoulement (CFD Computational Fluid Dynamics) avec le modèle de turbulence k-ε ont permis de reproduire les principaux phénomènes d'écoulement observés par PIV et de voir leur influence sur la distribution de température dans le meuble.

Enfin, un modèle simplifié des transferts de chaleur a été développé par une approche zonale en régime permanent et en régime transitoire ce qui permet de prévoir les températures moyennes de l'air et du produit et les fluctuations de température en fonction des cycles marche/arrêt du compresseur. Le modèle transitoire a été résolu avec une approche spectrale. L'influence de différents paramètres sur les niveaux de température et l'amortissement des fluctuations peut ainsi être identifiée par un calcul beaucoup plus rapide que par CFD.

**Mots clés :** meuble frigorifique fermé, écoulements d'air, transferts thermiques, distribution de la température, ouverture des portes, Vélocimétrie par image de particules, modèle simplifié, fluctuation de température, Modèle CFD